Author:
Hailes, Rebekah

Title:
Metallopolymers of Cobalt, Nickel, and Gold

Synthesis, Properties, and Applications

Metallopolymers of Cobalt, Nickel, and Gold: Synthesis, Properties, and Applications

Rebekah Lillian Naomi Hailes

A dissertation submitted to the University of Bristol in accordance with the requirements for award of the degree of Doctor of Philosophy in the School of Chemistry, Faculty of Science.

April 2019

Word count: 66,863

Abstract

The research discussed in this thesis involves the synthesis, characterisation, and properties of σ-bound metallopolymers containing nickel or cobalt, alongside supramolecular polymers containing cobalt or gold.

Chapter 1 gives context to the results presented in this thesis by broadly discussing a variety of polymerisation techniques. This introduction also aims to highlight relevant metallocene-containing and metallosupramolecular polymer examples.

Chapter 2 describes the synthesis and ROP of [*n*]nickelocenophanes to produce polynickelocenes with silicon and carbon main-chain spacers. To access soluble high molar mass materials, copolymerisations of the various monomers were performed. Characterisation of the magnetic properties of the [*n*]nickelocenophanes and homopolymers by SQUID magnetometry is also described.

Chapter 3 evaluates the thermodynamic parameters for ROP of the [*n*]nickelocenophanes described in Chapter 2 using DFT calculations. The syntheses of various other [*n*]nickelocenophanes and their propensity to ROP are also described. Finally, the effect on the thermodynamic parameters for ROP of adding a subsistent to the *ansa* bridge of tricarba[3]nickelocenophane was explored.

Chapter 4 encompasses two projects: firstly, the application of poly(cobaltoceniumethylene) materials in the protection of β-lactam antibiotics. Additionally, the syntheses of novel cobaltocenium-containing polymers is described, including both traditional σ-bound polymetallocenes as well as supramolecular cobaltocenium-containing polymers.

Chapter 5 describes the synthesis and supramolecular self-assembly of three gold(I)-containing complexes with subtle core structural differences. The energy landscapes of polymerisation were determined, and rationalised with reference to the extent of core conjugation.

Chapter 6 presents ongoing projects and potential avenues for future work, based on the results detailed in Chapters 2–5.

Acknowledgements

Firstly, I would like to express my sincere gratitude to Ian Manners for his guidance and support over the course of my PhD, and the opportunity to complete this piece of research as part of such an encouraging and diverse group of scientists. I would also like to thank George Whittell, whose contributions have been immeasurable, ranging from scientific advice to buoying my sprits when I needed it most.

I would like to extend my thanks to all of the members of the Manners group, past and present, as there are too many people to name here individually. I am particularly lucky to have worked with Rebecca Musgrave, Queen of Phane and an invaluable source of knowledge, whose encouragement throughout this process has been incredible. In addition, I must acknowledge Liam MacFarlane, Alex Oliver, and Elena Bussell for their advice and assistance, but more importantly, for their kindness and their friendship. I wish to thank the following people with whom I have had the fortunate opportunity to work closely with: Matt Robinson, Theresa Dellerman, and Charlie Jarrett-Wilkins. I am also grateful for my housemates throughout my time in Bristol: Bethany Russell, Zoe Adams, and in particular, Jon Davies. My gratitude is extended to Vince Annibale, Marius Arz, Diego Resendiz Lara, Nicola Oldroyd, Sam Pearce, Saurabh Chitnis, Paul Choi, Madeleine Iafrate, David Heard, Alastair Knights, Horatio He, John Finnegan, Tomoya Fukui, Laura Beckett, Steven Street, and everyone else who has made my time in Bristol an enjoyable and unforgettable experience.

More than anyone else though, I need to thank my family. Words cannot express how grateful I am for the tireless love and support of my parents, Helen and Steve, and my brother, Sam, not only throughout my PhD, but at every stage in life. A separate thank you must also be made to my dad for teaching me how to write an essay and for gently correcting my attempts, a foundation upon which I have relied whilst writing this thesis. Last, but never least, I thank my partner in life, Tom, for his patience, kindness, warmth, and love throughout the experiences we have shared.

Declaration

I declare that the work in this dissertation was carried out in accordance with the requirements of the University's Regulations and Code of Practice for Research Degree Programmes and that it has not been submitted for any other academic award. Except where indicated by specific reference in the text, the work is the candidate's own work. Work done in collaboration with, or with the assistance of, others, is indicated as such. Any views expressed in the dissertation are those of the author.

Rebekah Lillian Naomi Hailes

University of Bristol

April 2019

Table of Contents

List of Schemes

List of Figures

List of Tables

List of Abbreviations

°	degrees
°C	degrees centigrade
1D	one-dimensional
^{1}H NMR	proton nuclear magnetic resonance
2D	two-dimensional
3D	three-dimensional
Å	angstrom
a.u.	atomic units
AFM	atomic force microscopy
AIBN	azobisisobutyronitrile
anal.	analysis
arb. u.	arbitrary unit
atm	atmosphere
-*b*-	block
2,2′-bipy	2,2′-bipyridine
br	broad
°C	degrees centigrade
C_6D_6	d_6-benzene
Calcd	calculated
CD	circular dichroism
$CDCl_3$	chloroform-*d*
CDSA	crystallisation-driven self-assembly
cfu	colony-forming units
cm	centimetre
conc.	concentration
Cp	cyclopentadienyl
Cp_{cent}	cyclopentadienyl ring centroid
Cp_{ipso}	cyclopentadienyl ipso-carbon atom
δ	chemical shift
ΔG	free energy change
ΔH	enthalpy change
ΔS	entropy change
D_2O	deuterium oxide

Da	dalton
DFT	density functional theory
DIC	*N*,*N*′-diisopropylcarbodiimide
DIPEA	*N*,*N*-diisopropylethylamine
DLS	dynamic light scattering
DMAP	4-dimethylaminopyridine
DMPU	1,3-dimethyl-3,4,5,6-tetrahydro-2(1H)-pyrimidinone
DNA	deoxyribonucleic acid
DP_n	number-average degree of polymerisation
DSC	differential scanning calorimetry
E. coli	*Escherichia coli*
EDC	*N*-(3-dimethylaminopropyl)-*N*′-ethylcarbodiimide hydrochloride
eq.	equivalents
ESI	electrospray ionisation mass spectrometry
Fc	ferrocenyl, $(\eta^5\text{-}C_5H_5)Fe(\eta^5\text{-}C_5H_4)$-
FcH	ferrocene, $Fe(\eta^5\text{-}C_5H_5)_2$
FT-IR	fourier-transform infrared spectroscopy
g	gram
GPC	gel permeation chromatography
h	hours
HATU	1-[bis(dimethylamino)methylene]-1*H*-1,2,3-triazolo[4,5-*b*]pyridinium 3-oxid hexafluorophosphate
HOBt	hydroxybenzotriazole
HOMO	highest occupied molecular orbital
Hz	hertz
IC_{90}	inhibitory concentration
IL	intraligand
J	joule
K	kelvin
k_e	elongation rate constant
k_n	nucleation rate constant
k_p	rate of propagation
λ	wavelength
λ_{ex}	excitation wavelength

λ_{max}	wavelength of maximum absorbance
L_n	number-average contour length
L_w	weight-average contour length
L_w/L_n	length dispersity
LUMO	lowest unoccupied molecular orbital
μ_B	Bohr magneton
μ_{eff}	effective magnetic moment
μm	micrometre
m	multiplet
M	molar concentration
m/z	mass over charge
MALDI-TOF	matrix-assisted laser desorption/ionization time-of-flight
$[M]_c$	equilibrium monomer concentration
MCH	methylcyclohexane
Me	methyl
mg	milligram
MHz	megahertz
MIC	minimal inhibitory concentration
min	minute
mL	millilitre
MLCT	metal-to-ligand charge transfer
mm	millimetre
mmol	millimole
M_n	number average molecular weight
mol	moles
MO	molecular orbital
MRSA	methicillin-resistant *Staphylococcus aureus*
MS	mass spectrometry
M_w	weight average molecular weight
N_A	Avogadro constant
*n*Bu	normal butyl (C_4H_9)
NDM	New Delhi metallo
nm	nanometre
NMR	nuclear magnetic resonance

PEG	poly(ethylene glycol)
PDI	polydispersity index
PFS	poly(ferrocenylsilane)
Ph	phenyl
ppm	parts per million
PSS	poly(sodium 4-styrenesulfonate)
py	pyridine
R	8.314 J K^{-1} mol^{-1}
R_h	hydrodynamic radius
ROP	ring-opening polymerisation
s	singlet
S	total spin angular momentum
sec	seconds
SQUID	superconducting quantum interference device
θ	Weiss constant
t	triplet
*t*Bu	tertiary butyl (C_4H_9)
T_C	Curie temperature
T_c	ceiling temperature
T_f	floor temperature
T_g	glass transition temperature
T_m	melting temperature
TEM	transmission electron microscopy
TGA	thermal gravimetric analysis
THF	tetrahydrofuran
tht	tetrahydrothiophene
tmeda	*N*,*N*,*N*′,*N*′-tetramethylethylenediamine
TS	transition state
UV	ultraviolet
UV/Vis	ultra violet/visible
v/v	volume by volume
VE	valence electrons
w	concentration as weight fraction
WAXS	wide-angle X-ray scattering

1 Introduction

Metal centres play a crucial role in the functions of biological polymers and many solid state compounds, such as electrical conductors and superconductors, magnetic materials used in data storage, electrochromic materials, sensors, and catalysts.[1] Metal-containing polymers (metallopolymers) have long been regarded as desirable targets, as they take advantage of the beneficial properties of both traditional organic polymers (easy to process, flexible) and the metal centre. Since the mid 1990s, this field has seen rapid progress and metallopolymers now play an increasingly important role in terms of complementing the vast and impressive array of functional organic polymers that are available. This is primarily due to the development of new synthetic approaches (e.g. ring-opening polymerisation, polycondensation, electropolymerisation) and increased access to characterisation tools (ESI-MS, MALDI-TOF, electron microscopy etc.). After Lehn and coworkers demonstrated that hydrogen bonds can be used to prepare 'polymeric' materials,[2] the term 'metallopolymers' has expanded to encompass metal-containing supramolecular polymers, formed by non-covalent interactions in the main chain. As metal-containing polymers cover such a broad area of research including many important discoveries, a wide variety of topics and fundamental principles will be discussed in this section, but selected examples have been chosen based on their relevance to this thesis.

1.1 Ring-Opening Polymerisation

Ring-opening polymerisation (ROP) is an important synthetic route to macromolecules, and in most cases can be considered as a chain polymerisation (although some examples are more complex). A myriad of polymers have been prepared via ROP of alkene, ester, imide, phosphorus, and silicon containing monomers to name a few, including those of industrial importance such as nylon-6,6, poly(ethylene oxide), and poly(dimethylsiloxane).[3] A number

of reaction mechanisms can be invoked for ROP, including coordination, covalent, ionic (anionic or cationic), radical, and enzymatic polymerisation.

For a cyclic monomer to polymerise, ROP must be permissible both thermodynamically and kinetically, i.e. monomer-polymer equilibrium must favour the macromolecule, and an appropriate mechanism of polymerisation must exist (Scheme 1.1). Formally, the thermodynamic criterion requires Gibbs energy of polymerisation to be favourable (negative).

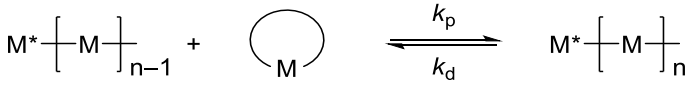

Scheme 1.1. The ROP of cyclic monomers, where k_p and k_d are the rate constant of propagation/depropagation, respectively, and M* is the active species.

The driving force for the majority of ROPs is manifested in the ring strain (as angular, conformational, and/or transannular strain), for which the associated standard enthalpy of polymerisation (ΔH^0_{ROP}) functions as a convenient measure.[3] The strain in cyclic monomers is especially high for three- and four-membered rings, due to large distortions from optimum bond lengths and angles, but the strain decreases suddenly for five-, six-, and seven-membered rings in which angular distortion is minimal but torsional strain arises from eclipsed ring substituents.[4] Strain increases for 8–13 membered rings due to transannular strain arising from repulsive interactions between ring substituents, and then decreases again for larger rings as they become able to accommodate substituents without transannular repulsions.

Temperature has a significant effect on the position of monomer-polymer equilibrium, such that limits exist, above (or below) which a given polymerisation is not thermodynamically feasible. For example, in exoentropic systems as the temperature of polymerisation increases, $T\Delta S$ becomes of greater importance; this favours an increase in monomer concentration until above the 'ceiling temperature' (T_c), polymerisation is not favoured. For

example, THF will not polymerise above 84 °C.[5] In rare cases, such as eight-membered inorganic rings (cyclooctasulphur,[6] cyclooctaselenium,[7] and octamethylcyclotetrasiloxane[8]) ROP is entropy-driven, i.e. ΔS is positive due to the increase in conformational freedom of the polymer compared to that of the cycles. In these unusual examples, depolymerisation is favoured with decreasing temperature, and a 'floor temperature' (T_f) exists, below which polymerisation is thermodynamically disfavoured (for cyclooctasulfur T_f = 159 °C).[6, 9]

In addition to the organic and main group examples discussed thus far, metallocycles can also readily undergo ROP reactions. For instance, silicon-bridged [1]ferrocenophanes undergo ROP to produce polyferrocenylsilanes (PFSs), due to their inherent ring strain that results from tilting of cyclopentadienyl (Cp) rings about the iron centre (Scheme 1.2). Enthalpic values for ROP of [*n*]ferrocenophanes range from ~12 kJ mol^{-1} for carbaphospha[2]ferrocenophane[10] to ~130 kJ mol^{-1} for thia[1]ferrocenophane,[11] with the enthalpic value for the ROP of the well-known dimethylsila[1]ferrocenophane ~80 kJ mol^{-1},[12] as estimated by differential scanning calorimetry (DSC). Although polymerisation to give PFSs has been the subject of extensive study, ROP of [*n*]metallocenophanes has generally proved an instrumental method to access macromolecules based on a variety of transition metals, and will thus be reviewed in depth.

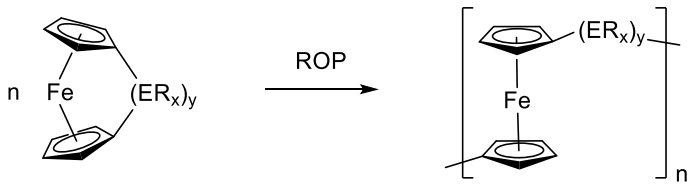

Scheme 1.2. Ring-opening polymerisation of a general [*n*]ferrocenophane.

1.1.1 [*n*]Metallocenophanes

Shortly after the discovery of ferrocene in 1952,[13] preparation of the first [*n*]ferrocenophanes were reported, metallocene-based species in which an *ansa* bridge of *n* atoms links the two Cp rings. These *ansa* metallocenes make up the broadest and most extensively studied class

of strained metal-containing rings,[14-18] but have been dominated by [*n*]ferrocenophanes due to the stability originating from the 18 valence electron (VE) ferrocene unit, and the ease by which their synthesis can be performed. The seminal synthesis of tetramethyldicarba[2]ferrocenophane (**1.1**) was reported by Rinehart Jr in 1960,[19] and followed fifteen years later with the first sila[1]ferrocenophane (**1.2**) by Osborne and co-workers.[20] Since then a multitude of [*n*]ferrocenophanes have been reported, including those with boron,[21] aluminium,[22] gallium,[23] germanium,[24] tin,[25] phosphorus,[26] arsenic,[27] sulfur,[28] selenium,[29] and various transition metal[30-32] bridges, a range of which are detailed in Figure 1.1. Sila[1]ferrocenophanes in particular, have been exploited as strained precursors for ring-opening polymerisation to afford materials that incorporate ferrocene units within the polymer main-chain.[15]

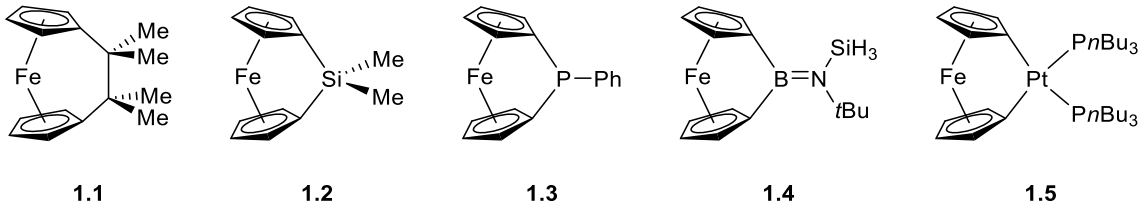

1.1 **1.2** **1.3** **1.4** **1.5**

Figure 1.1. Examples of [*n*]ferrocenophanes.

In [*n*]metallocenophanes, distortion of cyclopentadienyl (Cp) rings from the lowest energy parallel arrangement occurs when the *ansa* bridge is sufficiently short. This ring tilt can be expressed quantitatively by the angle, α, measured between the two tilted Cp rings relative to when they are parallel. Other angles used to describe the structure of [*n*]metallocenophanes include: β, the angle between the Cp plane and the C_{ipso}–E bond; δ, the Cp_{cent}–M–Cp'_{cent} angle; and θ, the C_{ipso}–E–C'_{ipso} angle (Figure 1.2). An additional angle, τ, applies to [2]metallocenophanes, and is used to describe the angle between the Cp_{cent}–M–Cp'_{cent} axis and the E–E bond vector. For [*n*]metallocenophanes with at least five *d* electrons, large α angles are associated with high energy structures, for which the inherent ring strain can function as a thermodynamic driving force for ring-opening reactions.

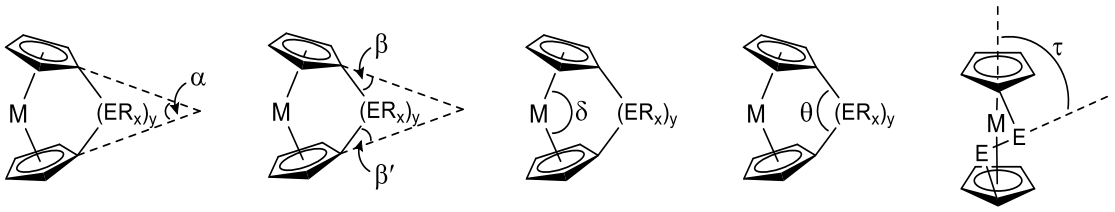

Figure 1.2. Geometric parameters characterising the structural distortions in the molecular structures of [*n*]metallocenophanes.

1.1.2 Structure and Bonding

Ferrocene, with 18 VE, is one of the few metallocenes with a diamagnetic ground state. Whilst much of the chemistry of ferrocene is reflected in the heavier group eight metallocenes, ruthenocene and osmocene, studies on these heavier analogues are hindered by cost and non-trivial syntheses.[33, 34] Variation of the metal atom in $[M(\eta^5\text{-}C_5H_5)_2]$ across the *3d* series leads to significant structural and electronic changes as the neutral metallocenes vary from 18 VE (Figure 1.3).[35] In the doublet ground-state cobaltocene (19 VE) and triplet ground-state nickelocene (20 VE) occupation of e''_1 antibonding orbitals by the additional unpaired electron(s) renders the metallocenes paramagnetic, in addition to lengthening and altering the bond order of the M–Cp bond (Fe–Cp_{cent} = 1.660 Å,[36] Co–Cp_{cent} = 1.722 Å,[37] Ni–Cp_{cent} = 1.817 Å).[38] The contribution of the metal atomic orbitals to the approximately non-bonding a'_1 and e'_2 orbitals in ferrocene is >60%, and is ~55% for antibonding e''_1 orbitals, although the contribution to the latter decreases from ferrocene through to nickelocene as the electrons become more extensively delocalised in the ligand π-system.[39]

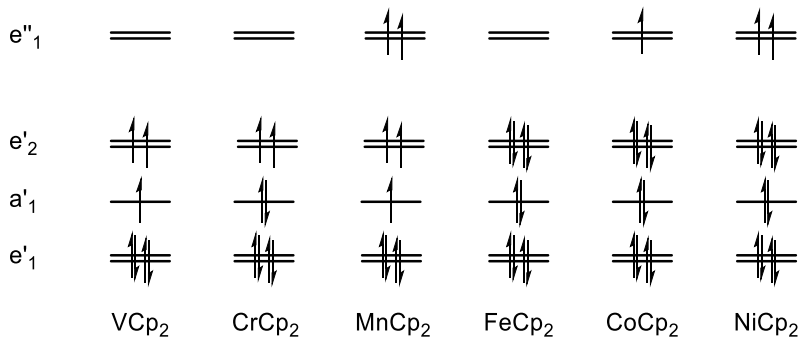

Figure 1.3. Qualitative ordering and occupation of frontier molecular orbitals for various *3d* metallocenes.

The late transition metal metallocenes adopt a parallel ring structure with D_{5h} symmetry to minimise the overlap between the metal d_z^2 orbital and ring π orbitals. Introduction of an *ansa* bridge to the metallocene unit can alter the normal geometry by tilting the two Cp rings away from their preferred parallel structure. The metal atom tends to lie in closer proximity to the Cp_{ipso} atoms than to the other four Cp carbon atoms, which causes a shortening of the C–C bond that lies opposite it within the ring. The angle θ at the bridging element is also generally smaller than is optimum. The molecular symmetry is thus altered from D_{5h} to C_{2v}, and an increase in antibonding interactions and electron-electron repulsion within the metallocene is observed. For metals with greater than four *d* electrons, this results in a considerable increase in total energy of the molecule (strain), and lengthening of the Cp_{ipso}–E and M–Cp bonds.[40] Density functional theory (DFT) calculations summarised in Figure 1.4 confirm that the overall energy increase upon tilting the Cp rings differs according to the *d* electron configuration of the metal, due to increasing occupation of the $4a_1$ and $2b_1$ molecular orbitals (which increase significantly in energy upon tilting).[40] Additionally, this increase in energy of the $4a_1$ orbital on tilting produces a decrease in the HOMO–LUMO gap for late transition metal metallocenes, and a consequential bathochromic shift of the lowest energy absorbance can be observed by UV/Vis spectroscopy.[41]

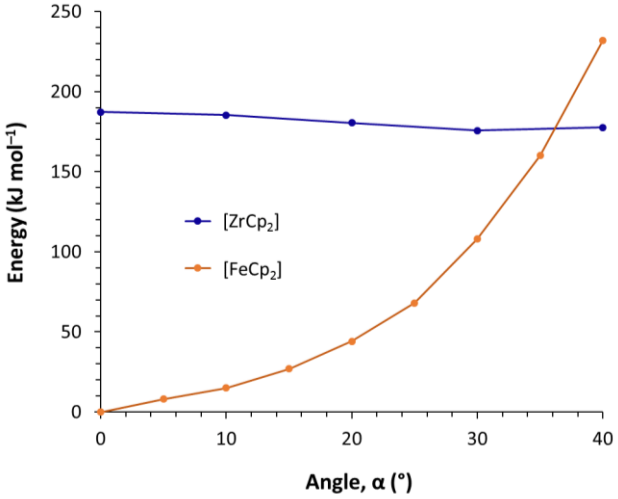

Figure 1.4. Calculated variation of the relative energy of $FeCp_2$ and $ZrCp_2$ as a function of tilt angle α. Adapted with permission from ref. 40.

In [*n*]ferrocenophanes, the decrease in HOMO–LUMO gap manifests itself as a colour gradient, from the characteristic amber colour of ferrocene (α = 0°), to red for sila[1]ferrocenophanes (α = 16–21°),[42, 43] then purple for the sulfur-bridged [1]ferrocenophane (α = 31°).[29] This is accompanied by an increase in colour intensity, as a loss in the centrosymmetric nature of metallocenes occurs upon increased tilting, and *d*–*d* transitions become more allowed as the Laporte selection rule is relaxed. An increase in α angle is also observed moving along analogous 3*d* metallocenophanes, due to an increase in M–Cp bond length. As discussed earlier, the increase in M–Cp bond length in the 19 and 20 VE species is ascribed to population of orbitals with antibonding character, for example: $[M(\eta^5\text{-}C_5H_4)_2(SiMe_2)_2]$ Fe–Cp_{cent} = 1.644(2) Å,[44] Co–Cp_{cent} = 1.711(1) Å,[45] Ni–Cp_{cent} = 1.808(1) Å,[46] with corresponding α angles of: 4.19(2)°,[44] 5.09(1)°,[45] and 9.37(8)°,[46] respectively. The decreasing M–Cp bond strength across the series from iron to nickel accounts for the ready accessibility of dicarba[2]ferrocenophane and dicarba[2]cobaltocene,[47] while attempted syntheses of dicarba[2]nickelocenophane have resulted in the formation of oligo- and polymeric species (the parent species is not isolable as it too highly strained, with highly labile bonds).[48]

1.1.3 Synthesis of [*n*]Metallocenophanes

[*n*]Metallocenophanes are commonly prepared by one of two salt metathesis routes (Scheme 1.3): either the reaction between a dilithiated metallocene and an element dihalide, or the 'fly-trap' method involving the reaction of an appropriately bridged $(C_5H_4)_2$ dianionic ligand with a metal(II) salt. The former method has been used to great effect to prepare [1]ferrocenophanes featuring alkyl, aryl, amino, and halo substituents, in addition to those bridged by boron, phosphorus, aluminium, germanium, tin, arsenic, sulphur, selenium, and several transition metals.[49] It has also been applied to the synthesis of selected rutheno- and osmocenophanes.[50-52] The alternative 'fly-trap' approach is more generally applicable, and has been used to synthesise [*n*]ferrocenophanes ($n \geq 2$), in addition to [*n*]metallocenophanes where a suitable dimetallated metallocene precursor is not accessible, such as for nickel and cobalt derivatives. As a result, fewer [*n*]cobaltocenophanes, and [*n*]nickelocenophanes have been synthesised relative to the iron analogues. Reported [*n*]cobaltocenophanes are limited to species with carbon-based *ansa* bridges[53] or those with disila-linkers.[45] Similarly, [*n*]nickelocenophanes are particularly few in number, perhaps partially due to the very weak Ni–Cp bond, and are currently limited to species bridged by disila linkers,[25] unsubstituted alkyl chains where *n* is greater than 2,[27] and 1,8-disubstituted naphthalene.[28]

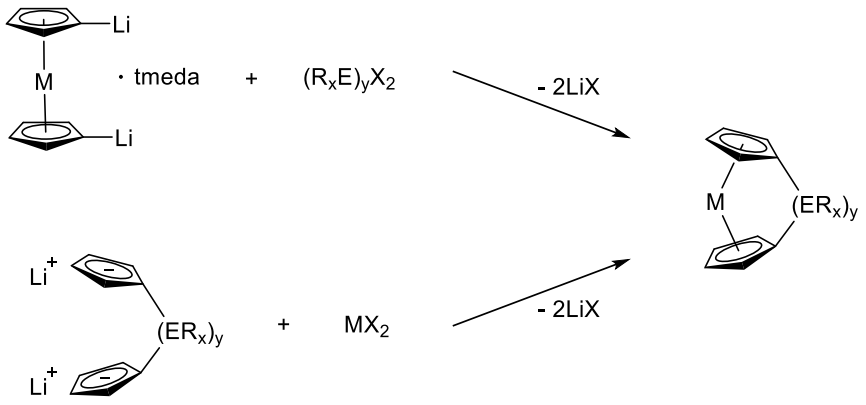

Scheme 1.3. Common synthetic routes to late transition metal [*n*]metallocenophanes.

In addition, some [*n*]metallocenophanes have been reported via less common routes, either utilising the formation of bonds between Cp ring substituents in acyclic 1,1′-disubstituted

metallocene precursors,[54-56] or via reductive coupling of fulvenes followed by transmetallation.[53, 57]

1.1.4 Ring-Opening Polymerisation of [*n*]Metallocenophanes

It is well established that [*n*]metallocenophanes undergo ROP to yield high molecular-weight polymetallocenes, driven by a thermodynamic release of the ring strain present in the monomer.[58] Polymerisation can proceed via a variety of methods including cationic,[59] thermal,[60] living anionic,[61] photolytic,[62] solvent mediated,[63] or transition-metal catalysed routes.[64] These are classified into three broad categories based on bond-cleavage pathways: cleavage of the Cp_{ipso}–E bond; cleavage of the M–Cp bond; and, for a variety of [2]metallocenophanes, cleavage of the E–E linkage. The nature and location of bond-cleavage is generally dictated by the relative strength of the individual bonds within the metallocycle, and thus the choice of both metal centre and bridging moiety. While E–E bond cleavage occurs in ring-opening reactions, it has yet to be utilised for polymerisation purposes, so will not be discussed in any further detail.

1.1.4.1 E–Cp_{ipso} Bond Cleavage

A thermal method of synthesising high-molecular weight PFSs from silicon-bridged [1]ferrocenophanes was first reported in 1992 (Scheme 1.4),[60] and has since been used to access alkyl, alkoxy, aryl, aryloxy, amino, and chloro functionalised PFSs.[65-69] It was shown to proceed via cleavage of the Cp_{ipso}–Si bond, and in the case of Cp rings with a different degree of methylation, nonselective cleavage of the Si–Cp bonds occured.[70] It was also proposed that the bond cleavage could be initiated by nucleophilic impurities in the [1]ferrocenophane monomers such as water or tetramethylethylenediamine (tmeda),[70] similar to the ROP of stanna[1]ferrocenophanes (a process catalysed by neutral nucleophilic impurities).[71]

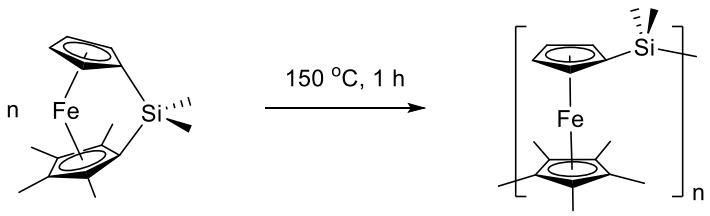

1.6 **1.7**

Scheme 1.4. Thermal polymerisation of a silicon-bridged [1]ferrocenophane.

A variety of late transition metal complexes, featuring platinum (Pt^0, Pt^{II}),[72, 73] palladium (Pd^0, Pd^{II}), and rhodium (Rh^I),[74] can also catalyse the ROP of sila[1]ferrocenophanes to yield high molecular weight PFSs.[75, 76] For silicon-bridged ferrocenophanes in which one Cp ring is methylated, Pt^{II}-catalysed ROP proceeds solely by selective cleavage of the Si–Cp^H (Cp^H = C_5H_4) bond to yield a regioregular, crystalline PFS, unlike thermal ROP which affords a regioirregular amorphous material.[77]

Living anionic ROP of sila[1]ferrocenophanes was developed in the mid-1990s,[78, 79] and allows access to PFSs with molecular weight control and predetermined chain-end function, provided that low levels of impurity are present.[79, 80] Induced by nucleophilic attack of an anionic initiator at the bridging silicon atom, ROP proceeds via Si–Cp bond cleavage, generating a basic iron-coordinated cyclopentadienyl anion. Fast initiation is followed by rapid chain propagation, which occurs with minimal chain transfer or termination, and therefore yields polymers of controlled molecular weight and narrow molecular weight distributions (poly dispersity index (PDI) < 1.2).[79, 81-84] Subsequent end functionalisation can occur at the lithiated site on the polymer using a variety of reagents to modify the polymer properties or yield block and graft copolymers.[85-87] For instance, if 4-[(trimethylsilyl)ethynyl]-benzaldehyde is added to quench the living chain, a terminal alkyne is generated, which can then undergo a Cu(I)-catalysed alkyne/azide cycloaddition with azide end-capped polymers.[88]

1.1.4.2 M–Cp Bond Cleavage

Dicarba[2]ferrocenophane derivatives containing either zero or one non-hydrogen substituent on the bridge are known to undergo thermal ROP,[47, 89, 90] and NMR analysis has indicated that ROP does not occur via homolytic C–C bridge cleavage. Indeed, comparative NMR of copolymers formed between [Fe(η^5-C_5H_4)$_2$(CH(Ph)CH_2)] and [Fe(η^5-C_5H_4)$_2$(CH_2)$_2$] or [Fe(η^5-C_5H_4)$_2$(CD_2)$_2$] suggested that polymerisation had proceeded via an Fe–Cp bond cleavage mechanism. Moreover, ring-opened species isolated from thermolysis experiments conducted with excess $MgCp_2$ indicated that Fe–Cp bonds can undergo heterolytic cleavage under thermal ROP conditions.[47]

In addition to that discussed in Section 1.1.4.1, another living anionic polymerisation method was reported in the mid 2000s involving the photoactivation of sila[1]ferrocenophanes.[62, 91] In this case, ROP proceeds with irradiation of the monomer ($\lambda > 310$ nm) in a donor solvent such as THF (Scheme 1.5). The subsequent, presumably solvated, ring-slipped structure can react with an anionic initiator, e.g. sodium cyclopentadienide (Na[C_5H_5]).[91] Cleavage of the Fe–η^1-Cp bond in the photoexcited monomer affords a ring-opened species possessing a free silyl-substituted Cp anion that can propagate via attack on another ring-slipped photoexcited monomer. The living polymer chain can then be capped with, for example, a proton to give neutral PFS.[92] Crucially for 'photo-controlled' anionic ROP, the delocalised free cyclopentadienyl initiating and propagating sites are far less basic than the charge localised iron-coordinated alternative that occurs in the classical anionic ROP.[93] This reaction is therefore more tolerant of sensitive functional monomers; for example, it has allowed the preparation of PFSs with pendant alkynyl,[94] amino,[95] fluoroalkyl groups,[93] and ruthenocenyl groups.[96] Recent advances also include photolytic ROP of a range of dicarba[2]ferrocenophanes and phosphorus-bridged [1]ferrocenophanes.[97, 98] Due to the ease by which the polymerisation can be controlled (switching the UV light on/off), sequential addition of monomers to produce block copolymers is facile.[15, 99, 100]

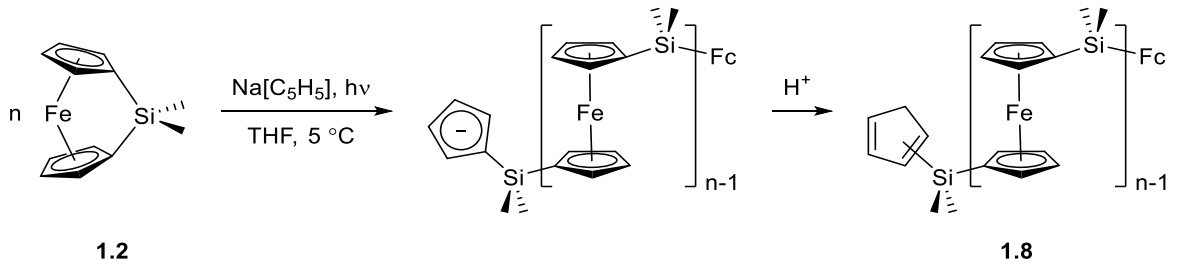

1.2 **1.8**

Scheme 1.5. Photolytic ROP of dimethylsila[1]ferrocenophane, **1.2**.

Although the mechanism of photocontrolled anionic ROP of [*n*]ferrocenophanes has not been completely elucidated, the presence of an *ansa* bridge causes the cyclopentadienyl rings to tilt, and is known to weaken the Fe–Cp bond. Metal-ligand charge transfer may then occur under photoirradiation, and is suggested to further weaken this bond and increase the electrophilicity at iron and, probably, to induce Cp ring-slippage in the presence of a donor solvent (such as THF). These effects all combine to favour polymerisation when an anionic initiator is present. Kinetic studies of the photopolymerisation at various temperatures demonstrated that the reaction was a living process (PDI < 1.1).[62] While the photoactivation of the monomer is independent of temperature, deactivation of the photoexcited system or the subsequently formed ring-slipped product to the ground state monomer is favoured at higher temperatures. As a consequence, at elevated temperatures the rates of initiation and propagation are decreased, and ROP is slower. Moreover, the polymers obtained have a broader molecular weight distribution (PDI = 1.2–1.3).[62]

Whilst photolytic ring-opening polymerisation of iron-based metallocenophanes is well documented, the method has also been extended to non-iron analogues. Thermal polymerisation of dicarba[2]cobaltocenophane **1.9** with subsequent oxidation of the $CoCp_2$ moieties by atmospheric oxygen, in the presence of excess $[NH_4][NO_3]$, yielded oligo(cobaltoceniumethylene) presumably via cleavage of the Co–Cp bond. It was later discovered, however, that the polymerisation could proceed in the absence of UV light with the weakly nucleophilic initiator Li[*t*BuC_5H_4] in THF. This difference was attributed to the weak M–Cp bond in the [2]cobaltocenophane compared to the stronger bond in analogous

iron-containing species. The synthesis of high molar mass poly(cobaltoceniumethylene) (PCE) nitrate **[1.10][NO$_3$]**, a yellow/green, water-soluble and air-stable polyelectrolyte, was achieved by thermal ROP of **1.9** at 140 °C followed by oxidation (Scheme 1.6).[101]

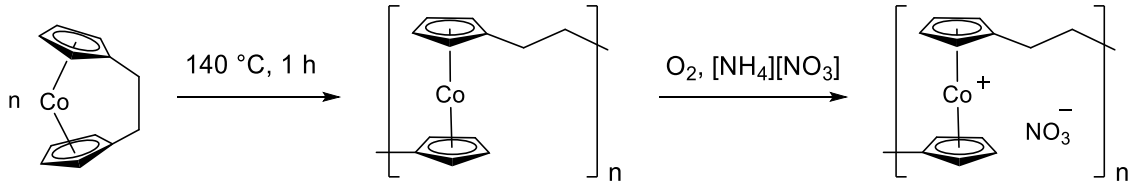

1.9 **1.10** **[1.10][NO$_3$]**

Scheme 1.6. Thermal ROP of dicarba[2]cobaltocenophane, and subsequent oxidation in atmospheric oxygen.

Dynamic light scattering (DLS) experiments estimated a value of ~55,000 g mol^{-1} for the molecular weight of **[1.10][NO$_3$]** (degree of polymerisation (DP_n): ~200). Unlike the thermal ROP of sila[1]ferrocenophanes, where cleavage of the Cp_{ipso}–Si bond is initiated by trace impurities, the polymerisation of dicarba[2]cobaltocenophane **1.9** proceeds by cleavage of the Co–Cp bond (presumably due to the increased lability of the latter relative to [*n*]ferrocenophanes). Sequential addition of dimethylsila[1]ferrocenophane and dicarba[2]cobaltocenophane via photocontrolled ROP has also been demonstrated.[102] Monomer **1.9** was added to a living PFS macro-initiator, then subjected to UV irradiation and subsequent oxidation of the resultant poly(cobaltocenylethylene) block, to yield PFS-*b*-PCE copolymers.

In depth studies have shown that poly(nickelocenylpropylene) results from the ROP of tricarba[3]nickelocenophane **1.11** [α = 16.6(1)°], which proceeds spontaneously when stirred in polar solvents such as pyridine at ambient temperature (Scheme 1.7).[48, 63] A colour change from blue to green was observed during the reaction, consistent with the release of ring-strain. The polymerisation is thought to proceed via initial coordination of pyridine to the nickel centre, with subsequent cleavage of the Ni–Cp bond, similar to that for the photolytic ROP of [*n*]ferrocenophanes.[91] However, both the presence of a weakly

nucleophilic initiator and photoexcitation of the monomer are unnecessary in this case due to the particular lability of the Ni–Cp bond (M–Cp dissociation energy is 250 kJ mol^{-1} for nickelocene vs 305 kJ mol^{-1} for ferrocene).[103] In addition, it was demonstrated that as a consequence of the weak Ni–Cp bonds polynickelocene **1.12$_x$**/**1.13** can exist in either a kinetically static or labile state depending on the solvent conditions, and, in the case of the latter, form a dynamic equilibrium between monomer **1.11** and oligomers **1.12$_x$**/**1.13**.[63]

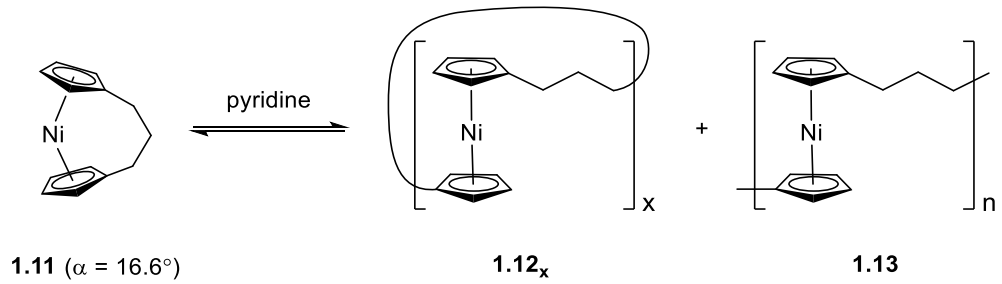

Scheme 1.7. Reversible ROP of tricarba[3]nickelocenophane **1.11**.

Analysis of **1.12$_x$**/**1.13** by dynamic light scattering estimated a molecular weight of ~40,000 g mol^{-1} (DP$_n$ of ~175).[48] Matrix-assisted laser desorption/ionisation time-of-flight (MALDI-TOF) mass spectrometry revealed the presence of both cyclic and linear polymeric species, the former suggesting that the initiating pyridine is substitutionally labile when coordinated at a nickel centre, and may be easily displaced by the propagating Cp end groups.[63]

1.2 Polycondensation

After the condensation between phenol and formaldehyde to produce Bakelite resins was discovered in 1907, pioneering work by Carothers and coworkers afforded two of the most widely used synthetic polymers: nylon and polyester.[104] Polycondensations, including the formation of polyesters and polyamides, are step growth reactions in which the addition of difunctional and sometimes polyfunctional compounds is accompanied by elimination of a small molecule by-product (for example, water, alcohols, and hydrogen halides). The main principle of step growth polymerisations is that the functional groups of all species present during the reaction (monomers, dimers, trimers, etc.) display the same reactivity independent

of molecular size.[105] To yield a high molar mass polymer, a near-perfect stoichiometric ratio of the two difunctional monomers is required alongside a high degree of monomer purity.[106] In addition, absence of side-reactions and effective removal of small molecule byproducts are essential criteria to ensure a high reaction rate and conversion, and thus high molar mass products. Whilst numerous materials synthesised by polycondensations have notable industrial applications, the majority are organic polymers. Nevertheless, some notable examples of metal-containing polymers have been reported via polycondensation routes, including the following examples.[107]

Seminal work by Sonogashira and coworkers reported a cross-coupling condensation protocol that enabled the formation of carbon-carbon bonds efficiently and under mild conditions.[108] This method has been applied to synthesise a series of rhenium containing polymers (e.g. **1.14**) by coupling the rhenium complex of 5,5-diethynyl-2,2-bipyridine, 4,4-diethynylbiphenyl, and dialkoxydiiodobenzene.[109] By increasing the rhenium content of the polymers, the quantum yield and lifetime of fluorescence (caused by the main chain π^*–π emission) decreased due to quenching by the rhenium complex. The Sonogashira condensation has also been applied to produce further rhenium containing oligomers with defined molecular weights,[110] and a variety of platinum-based metallopolyynes with different organic congeners.[111]

Other C–C bond formation condensations, such as the Heck and Yamamoto coupling reactions, have been used to great effect to produce polymers containing coordination complexes of cadmium, zinc, ruthenium, nickel, and cobalt.[111, 112] For example, a π-conjugated poly(aryleneethynylene) polymer consisting of *N*,*N*′-bis(salicylidene)-1,2-phenylenediamine-nickel complex units (**1.15**, Figure 1.5) was prepared in high yield by the palladium-catalysed polycondensation between H–≡–Ar–≡–H (Ar = fluorene or 2,5-dialkoxy-*p*-phenylene) and a dibromosalophen nickel complex.[113] Low polymer solubility precluded molecular weight determination by GPC, but the DP_n was estimated to be ~10 by NMR spectroscopic end group analysis. Molecular weights of a polyplatinyne, (–*trans*-

$(Pt(PBu_3)_2C{\equiv}C(p\text{-}C_6H_4)C{\equiv}C{-})_n$ (**1.16**, Figure 1.5), were found to be dependent on the method of polycondensation: employing Hagihara's copper(I)-catalysed coupling produced longer-chain platinum(II) polymers, whereas a second method based on the Stille reaction using stannyl-protected dialkynes resulted in oligomeric species.[114]

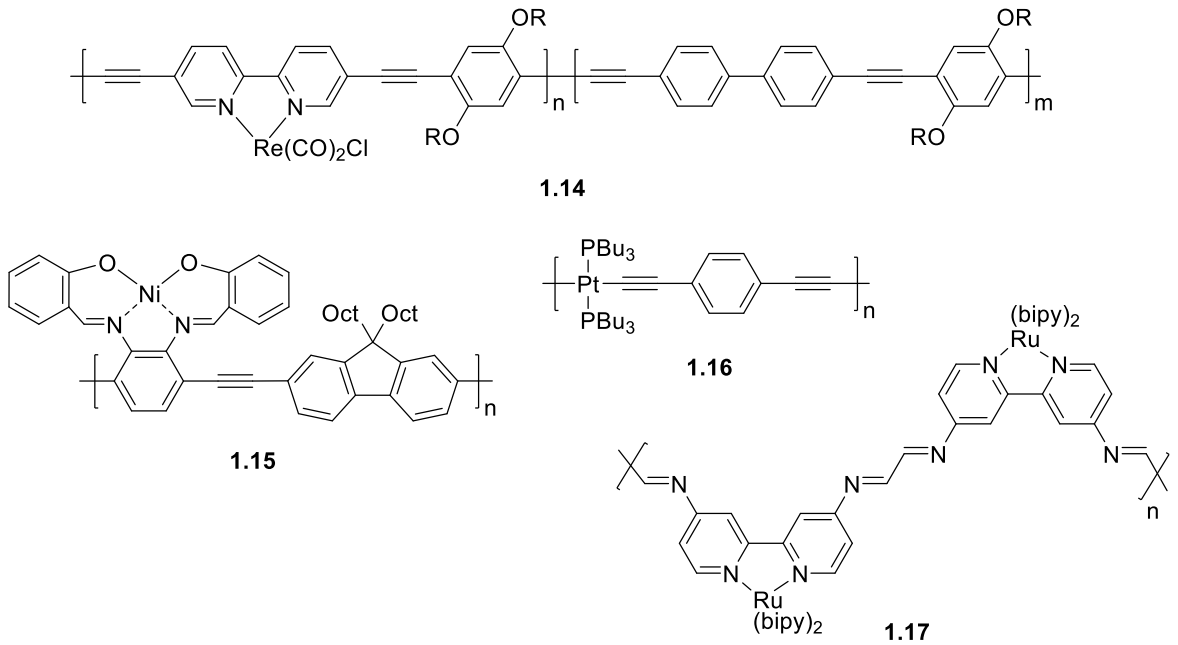

Figure 1.5. Metallopolymers formed by polycondensation routes.

More traditional polycondensation reactions to produce polyesters, polyamides, and polyimides have also been reported.[115] For example, a 2,2-bipyridine (bipy) containing conjugated polymer was constructed with imine linkages by a condensation reaction between $Ru(bipy)_2(dabpy)_2$ (dabpy = 4,4-diamino-2,2-bipyridine) and glyoxal (**1.17**, Figure 1.5).[116]

In addition to the routes discussed in Section 1.1, main-chain ferrocene containing polymers have also been reported by polycondensation methods,[117-119] beginning with two routes patented in the 1960s.[120, 121] Although all isolated polymeric material was of low molar mass, the studies initiated research into condensation routes to polymetallocenes. For instance, the reaction of $[(Fe(C_5H_4)_2)(BBr_2)_2]$ and $HSiEt_3$ yielded the borylene-bridged polyferrocene $[(Fe(C_5H_4)_2)B(Br)]_n$. Additional treatment with $[CuMes]_n$ gave a soluble polymer $[(Fe(C_5H_4)_2)B(Mes)]_n$ with three-coordinate boron centres, and subsequent π-overlap

between the empty *p* orbital on boron and the ferrocene units promoted electron delocalisation along the polymer chain. A wide variety of amide- and ester-based ferrocene polymers have also been synthesised from polycondensation reactions involving 1,1′-bis(chlorocarbonyl)ferrocene with bisamines or diols, respectively.[122]

Whilst similar polycondensation reactions have been attempted with dicarboxy- and dicarbonylchloride-substituted cobaltocenium molecules, very few attempts resulted in well-defined polymers.[123, 124] Cuadrado and coworkers prepared a siloxane-based polymer with main-chain amide linked cobaltocenium moieties by condensation of 1,3-bis(3-aminopropyl)-1,1,3,3-tetramethyldisiloxane with 1,1′-bis(chlorocarbonyl)cobaltocenium hexafluorophosphate (Scheme 1.8).[125] The product was isolated as a green solid, but was found to be essentially insoluble in most common organic solvents, which precluded complete characterisation including a determination of molecular weight.

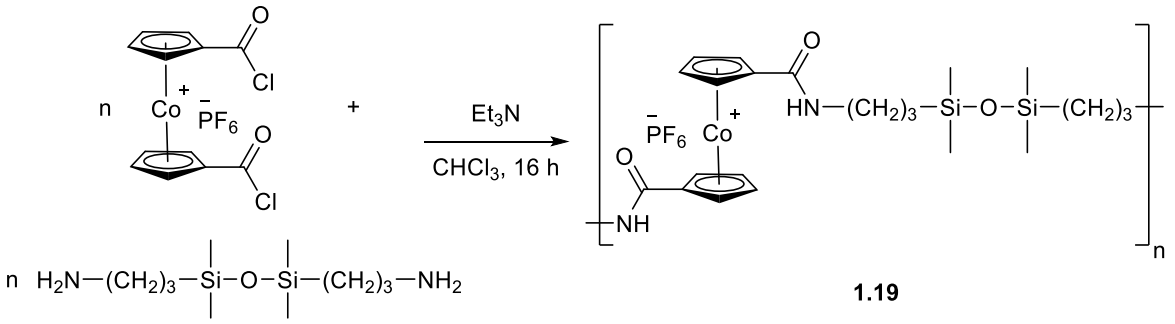

Scheme 1.8. Polycondensation of 1,3-bis(3-aminopropyl)-1,1,3,3-tetramethyldisiloxane with 1,1′-bis(chlorocarbonyl)cobaltocenium hexafluorophosphate to give **1.19**.

1.3 Addition Polymerisation

Alongside polycondensation routes, addition polymerisation is another step growth method, the principles of which were described in Section 1.2, although in this case, no small molecule by-products are produced. Use of an initiator species to induce addition between multiply-bonded species can transform the mechanism into a chain-growth route and provide access to high molar mass polymeric products.

Whilst such addition routes to polymers containing 3*d* metals do exist, their scope is not particularly broad compared to the other methods reviewed here. However, one monomer for which there has been significant study is vinylferrocene, which has been polymerised to give poly(vinylferrocene) using the radical initiator azobisisobutyronitrile (AIBN), in solution and in bulk (Scheme 1.9).[126] Choice of initiator is particularly important, as in the presence of strongly oxidising initiators ferrocene-containing monomers can undergo reversible oxidation instead of polymerisation (vinylferrocene: $E_{1/2}$ = 0.56 V vs an aqueous saturated calomel electrode, SCE).[127] The AIBN-catalysed, free-radical method was also applied to access poly(ferrocenylmethyl acrylate) and poly(ferrocenylmethyl methacrylate).[128] Treatment of these polymers with compounds such as dichlorodicyanoquinone, *o*-chloranil, and tetracyanoethylene gave poly(ferrocenium) salts or polymeric charge-transfer derivatives, which were characterised using Mössbauer spectroscopy. Copolymerisations of vinyl ferrocene and a variety of organic comonomers such as styrene, methacrylate, maleic anhydride, acrylonitrile, methyl methacrylate, *N*-vinylpyrolidine, and vinyl acetate were also performed.[129]

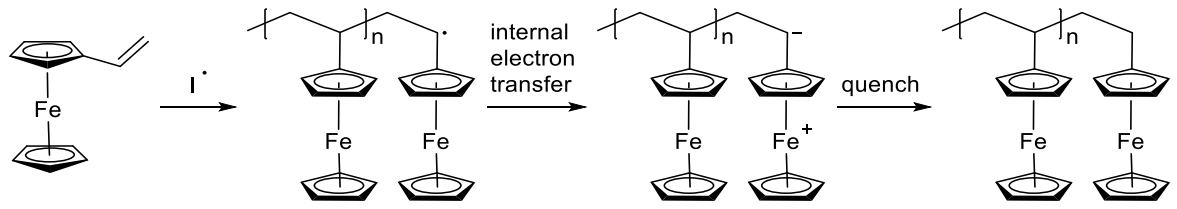

1.20 **1.21**

Scheme 1.9. Synthesis of poly(vinylferrocene) **1.21** from vinylferrocene **1.20**, where I represents initiator.

AIBN has also been utilised in the addition polymerisation of (vinylcyclopentadienyl)tricarbonylmanganese to give a product with pendant half-sandwich complexes.[130] This reaction was readily extended to include a large series of copolymers with styrene, methyl acrylate, acrylonitrile, vinyl acetate, and vinylferrocene.[131, 132] In a similar manner, homo- and copolymerisations involving

(vinylcyclopentadienyl)dicarbonylnitrosylchromium were performed yielding only moderate molecular weight products (~11,000–19,000 g mol^{-1}) in all cases.[133]

1.4 Ring-Opening Metathesis Polymerisation

Olefin metathesis has found a widespread number of applications in small molecule and polymer synthesis after the discovery by Schrock and Grubbs of well-defined molybdenum, tungsten, and ruthenium carbene metathesis catalysts.[134] Ring-opening metathesis polymerisation (ROMP, Scheme 1.10) has proved an ideal method for the conversion of ring-strained cyclic monomers, as the catalysts employed are highly active, chemoselective, and tolerant to a variety of functionalities and reaction conditions. Furthermore, the polymerisation can be 'living' in nature, leading to narrow molecular weight distributions and low polydispersities. It is worth noting that the number of double bonds in the monomeric species are preserved in the polymer, thus allowing for synthesis of conjugated macromolecules. A wide range of main-chain, side-chain, hyperbranched, dendritic, and star polymers have also been prepared by this method.[135]

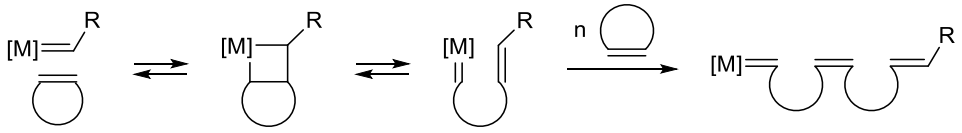

Scheme 1.10. Ring-opening metathesis polymerisation, which utilises a transition metal carbene catalyst.

Polyferrocenes have been synthesised via ROMP of ferrocenophanes bridged by unsaturated groups such as 1,3-butadienyl and 1-butenyl (Figure 1.6).[136] The resultant polymers, poly(ferrocenylenedivinylene) and poly(ferrocenylenebutenylene), were insoluble in typical organic solvents, though the solubility of this type of polymer was later tuned by incorporation of alkyl groups in the unsaturated *ansa* bridge.[137] Recent work by Craig and Tang explored the ROMP of a significant number of cyclic ferrocenyl-substituted olefins, leading to main-chain ferrocene-containing homopolymers, random copolymers, and block

copolymers.[138] In addition, they explored the crystallisation-driven self-assembly (CDSA) of one of the semi-crystalline polymers to generate platelet nanostructures.

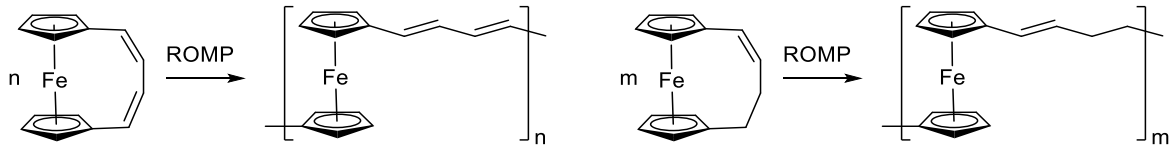

Figure 1.6. ROMP of [*n*]ferrocenophanes bridged by 1,3-butadiene and 1-butene.

Side-chain metallocene-containing polymers have been realised by the ROMP of norbornene dicarboximide derivatives (norbornene is one of the principal cyclic olefins utilised in metathesis reactions due to its facile functionalisation and high reactivity).[139, 140] For instance, this method has allowed the synthesis of polymers with side-chains containing either a ferrocene or cobaltocenium moiety, and diblock copolymers containing both a ferrocene-containing block and a cobaltocenium-containing block. Such polymers have found use in a variety of applications such as sensors,[141] catalysts,[142] biomedical agents,[143] and in room temperature ferromagnetic materials.[144]

1.5 σ-Bound Metal-Containing Polymers

Metal-based systems are ubiquitous throughout nature, participating in a variety of highly complex functions such as oxygen transport, catalysis in peptidases, molecular transport, and gene activation.[145] The field of metal-containing synthetic polymers has evolved relatively recently compared to macromolecular science in general, but includes a broad range of processable materials with functions that complement those of state-of-the-art organic macromolecules. Within this, a multitude of metal centres have been exploited to modify macromolecular properties, ranging from main-group metals, to transition metals, to lanthanides.[146] Such metallopolymers have potential applications in nanomaterials, information storage, smart materials, sensors, catalyst systems, artificial metalloenzymes, energy storage devices, and photovoltaics.[1, 147]

1.5.1 Nickel-Containing Magnetic Polymers

Polymers containing nickel remain relatively scarce throughout the literature when compared to those based on other transition metals such as iron. The macromolecules can be either diamagnetic or paramagnetic, with examples of the former including bis(phosphine)nickel(II)-1,4-tetrafluorophenylene polymers,[148-150] metallophthalocyanine covalent organic frameworks,[151] π-conjugated nickel-polyyne copolymers,[152] methacrylate-based side-chain nickel containing polymers,[153] and polymers containing nickel(II) complexes of Goedken's macrocycle (4,11-dihydro-5,7,12,14-tetramethyldibenzo[b,i]-[1,4,8,11]tetraazacyclotetra-decine).[154, 155] A (salophen)Ni(II) ladder polymer containing planar (salophen)Ni(II) units was reported to generate a diamagenetic conjugated helical structure. However, when polymeric/oligomeric and macrocyclic (salophen)Ni(II) complexes were synthesised from biphenol dialdehydes (**1.22**, Figure 1.7), it was found that they contained paramagnetic non-planar Ni(II) coordination.[156] The steric strain in the macrocycle was found to distort the repeat unit structure such that it contained both a planar (salophen)Ni(II) unit and a tetrahedral Ni(II) centre, and paramagnetism was attributed to the latter of these species.

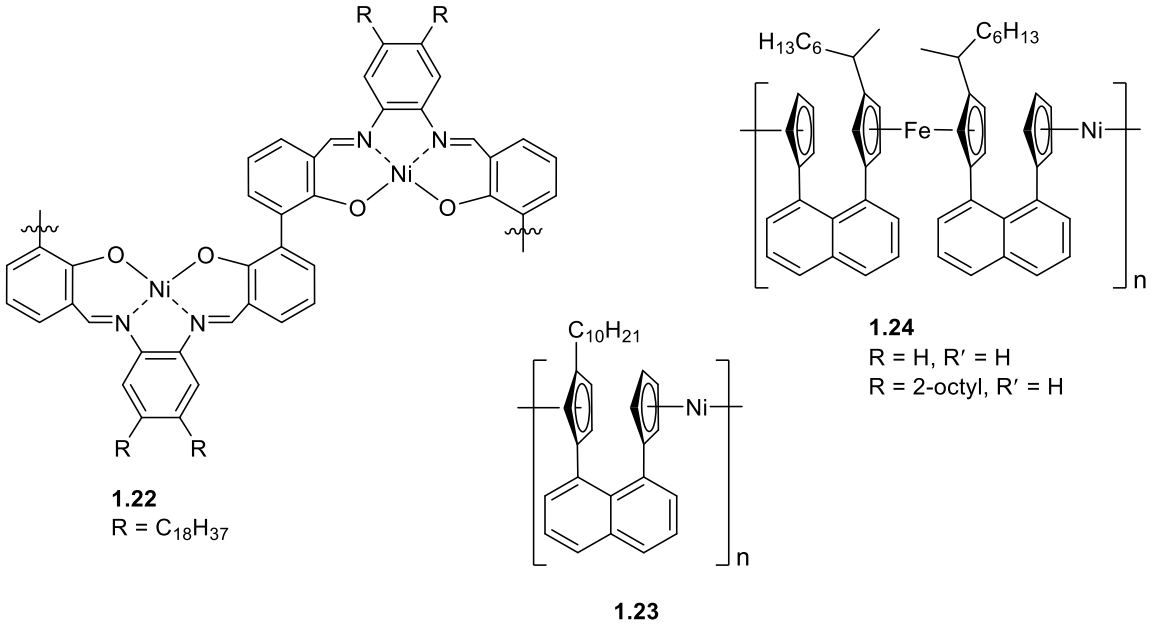

Figure 1.7. Examples of nickel-containing magnetic polymers.

A nickelocene-based polymer with naphthalene linkers synthesised via a polycondensation route was also found to be unsurprisingly paramagnetic (**1.23**, Figure 1.7).[157] Bulk susceptibility measurements of **1.23** determined a room temperature magnetic moment (μ_{eff}) of 5.30 μ_B. Similar copolymers featuring both ferrocene and nickelocene units bridged by naphthalene moieties were also prepared, but in the case of **1.24** (Figure 1.7), the effective magnetic moment reported at room temperature was lower (μ_{eff} = 3.51 μ_B).[157] Regardless, magnetic moments for both **1.23** and **1.24** are significantly larger than the moment of nickelocene itself (μ_{eff} = 2.86 μ_B), which is consistent with a cooperative effect.[158]

Polynickelocene **1.12$_x$**/**1.13** is an example of a soluble high molecular weight material containing *S* = 1 centres, for which superconducting quantum interference device (SQUID) magnetometry was used to determine its magnetic properties.[48] Above 28 K, **1.12$_x$**/**1.13** was found to behave as a simple paramagnet, and the magnetic susceptibility per monomer unit could be fitted to the Curie-Weiss law (with a small additional term for temperature-independent paramagnetism). In addition, a large, negative Weiss constant suggested significant antiferromagnetic spin-spin interactions. The magnetic susceptibility for **1.12$_x$**/**1.13** deviated from that expected for a simple paramagnet below 28 K; however, the exact nature of the spin-spin interactions was not determined.[48]

1.5.2 Cobalt-Containing Polyelectrolytes

The low ionisation potential of 19 VE cobaltocene (5.56 V)[159] allows the facile loss of an electron to form cobaltocenium (18 VE), isoelectronic to ferrocene. Cobaltocenium salts are an attractive target due to their resistance to strong oxidising agents, as they can thus form kinetically stable, water soluble molecules, something not possible for the neutral ferrocene analogues. Methylcyclopentadiene is commonly utilised to yield methyl- and dimethylcobaltocenium salts, which are general precursors to carboxylic acids, esters, amides, amines, and nitro derivatives.[125, 160-164]

The use of polycondensation routes to covalent main-chain polycobaltoceniums were pioneered by Carraher, Pittman, and Sheats in reactions employing 1,1′-bis(chlorocarbonyl)cobaltocene with diols in harsh conditions, but the resultant polymers were also hampered by insolubility and poor characterisation. As discussed in Section 1.2, in the late 1990s Cuadrado and coworkers achieved a polycobaltocenium by condensation of 1,3-bis(3-aminopropyl)-1,1,3,3-tetramethyldisiloxane with 1,1′-bis(chlorocarbonyl)cobaltocenium hexafluorophosphate in the presence of chloroform and triethylamine.[125] Again, however, complete characterisation was not attained, including an estimate for molecular weight. Significant advances were made recently when 1,l′-dicarboxycobaltocenium hexafluorophosphate and 3,3′,4,4′-biphenyltetramine were heated to 200 °C in the presence of polyphosphoric acid. The resulting imidazole-based polycobaltocenium (**1.25**, Figure 1.8), determined to have a molecular weight of ~83,000 g mol^{-1}, was then employed in alkaline anion exchange membrane applications.[165] A variety of other main-chain cobaltocenium-containing polymers have been reported,[166] including coordination polymers based on supramolecular interactions between 1,1′-cobaltoceniumdicarboxylate linkers,[167] and these have a wide range of potentially interesting applications.

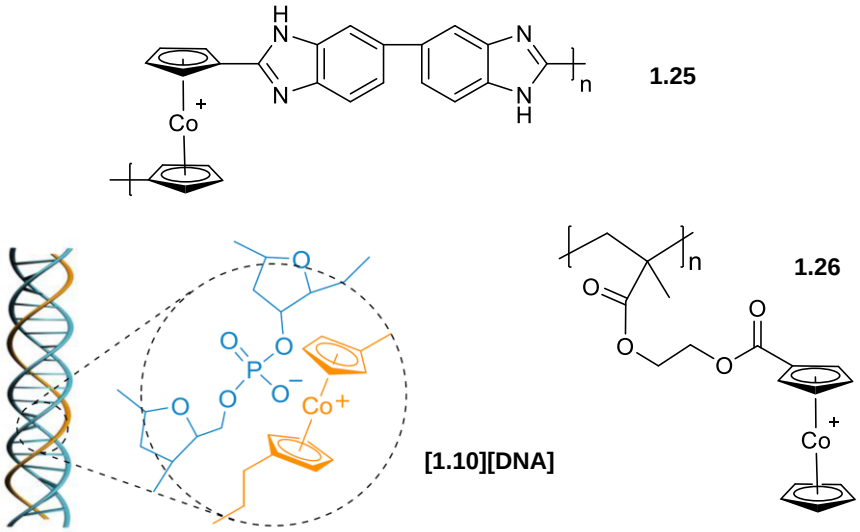

Figure 1.8. Cobaltocenium-containing polymers. Representation of **[1.10][DNA]** adapted with permission from ref. 168.

Achiral main-chain cobaltocenium polyelectrolyte, **[1.10]$^{n+}$** (see Section 1.1.4.2),[101, 169] has been shown to undergo electrostatic complexation with anionic polyelectrolytes. For instance, DNA was employed as an anionic template to induce chirality of **[1.10]$^{n+}$**, facilitated by the main-chain positive charges and the polymer structural flexibility (compared to polyelectrolytes with pendant charges).[168] This was proven by circular dichroism (CD), as the CD spectrum of **[1.10][DNA]** displayed a negative band at 280 nm (the adsorption band of PCE), which indicated a transfer of chirality to **[1.10]$^{n+}$**. Thus, it was suggested that PCE adopts a helical conformation, embedded in either the major or minor groove along the DNA helix (Figure 1.8).

Side-chain cobaltocenium-containing polymers have also been the focus of significant recent attention with applications in areas of polyelectrolyte multilayers, gene delivery, anticancer agents, antimicrobials, and ion exchange for transport.[143] For example, poly(2-(methacrylolyoxy)ethyl cobaltoceniumcarboxylate hexafluorophosphate (**1.26**, Figure 1.8), which contains a pendant cobaltocenium moiety, can conjugate with β-lactam antibiotics to protect them from hydrolysis by β-lactamase enzymes (produced by some bacteria in antibiotic resistance mechanisms).[170] At the same time, cobaltocenium polyelectrolytes have

also displayed synergistic effects to lyse drug-resistant bacterial cells whilst exhibiting non-toxic behaviour towards mammalian cells.

1.6 Supramolecular Polymerisation

As well as covalently-bound species, the field of metallopolymers also encompasses metal-containing supramolecular polymers, formed by non-covalent interactions in the main chain. Conventional polymerisations, like those discussed so far, generally occur under kinetic control as the barrier to depolymerisation is high since it involves breakage of covalent bonds. On the other hand, for supramolecular systems the degree of polymerisation tends to be severely influenced by thermodynamic factors such as solution concentration, temperature, and pressure due to low energy barriers to depolymerisation. Despite the relative novelty of supramolecular polymerisations compared to covalent examples, a variety of systems have been reported including extensive work on hexa-*peri*-hexabenzocoronenes, perylene bisimide derivatives, and porphyrin complexes.[171] To create such systems, it is important to examine the mechanisms and energy pathways by which supramolecular polymers form.

1.6.1 Supramolecular Polymerisation Mechanisms

The simplest class of supramolecular polymerisations is described by an isodesmic model, in which the reversible formation of non-covalent interactions is identical throughout the polymerisation process (Figure 1.9). The polymerisation is defined by a single association constant (K) for each reversible addition of monomer, and as the reactivity of each small molecule is independent of the degree of polymerisation, each successive addition causes the same decrease in free energy.[172] Due to the equivalence of each supramolecular polymerisation step, isodesmic models are distinguished by a lack of critical concentration and temperature, alongside an inability to form cyclic intermediates. Nevertheless, the polymerisation pathway can still be complicated by kinetic barriers. As with the analogous

covalent polymerisation, a reversible step-growth polycondensation, only moderate degrees of polymerisation with large polydispersities are achieved unless the percentage conversion or binding affinity is particularly high.

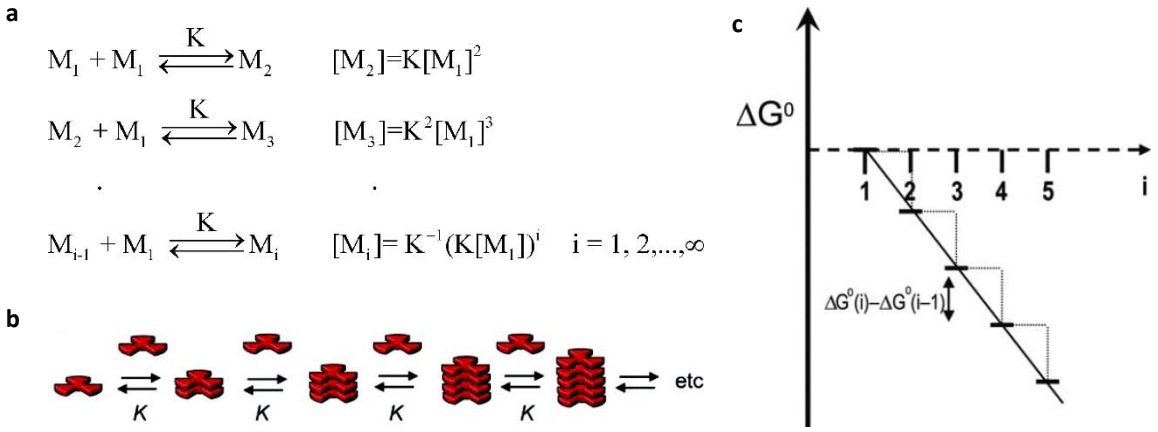

Figure 1.9. An isodesmic supramolecular polymerisation: a) general scheme in which M_1 represents monomer and K the molar equilibrium constant; b) schematic representation; c) energy diagram which depicts free energy (ΔG^0) in terms of oligomer size (i). Reproduced with permission from ref. 171.

In the second class of supramolecular polymerisations explored in this section, the growth of the polymer occurs in two distinct states, resulting in either a cooperative or anti-cooperative process. The first (unfavourable) step in a cooperative supramolecular polymerisation follows a linear isodesmic model, governed by equilibrium constant K_n (Figure 1.10).[172] The initial stage continues until a free energy maximum is reached and a nucleus of degree of polymerisation *s* is formed. Then, as the polymerisation becomes energetically favourable, a linear isodesmic elongation of the polymer chain proceeds with an association constant K_e that is higher than K_n. In a cooperative system (i.e. when elongation is far more favoured than nucleation), below a critical concentration or above a critical temperature almost no polymerisation occurs. The presence of a critical concentration/temperature along with two further features serves to distinguish the supramolecular nucleation-elongation model from an isodesmic mechanism: firstly, the

presence of a 'lag time' between molecular dissolution and supramolecular polymerisation, which, secondly, can be circumvented by the addition of a nucleating agent.[173]

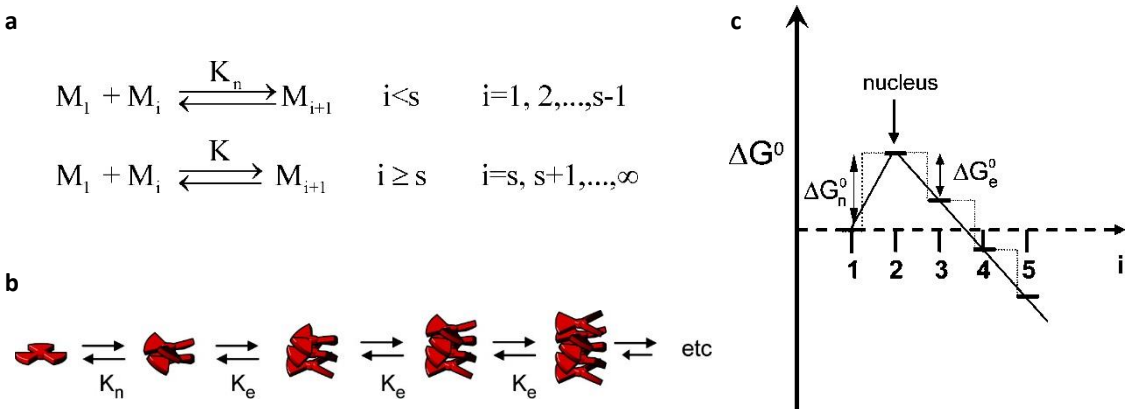

Figure 1.10. A cooperative supramolecular polymerisation: a) general scheme in which M_1 represents monomer, M_i represents a polymer chain of length i, K_n the nucleation equilibrium constant, and K_e the elongation equilibrium constant; b) schematic representation; c) free energy (ΔG^0) diagram. Reproduced with permission from ref. 171.

1.6.2 Thermodynamic versus Kinetic Control

The mechanisms of supramolecular polymerisation have been subjected to considerable research, but systems of a living nature, i.e. that demonstrate control over the degree of polymerisation in the absence of chain termination or transfer, have only been established very recently and remain in their infancy. The majority of supramolecular polymers reported are of a dynamic nature and formed under thermodynamic control; whilst this gives rise to many desirable characteristics such as stimuli-responsive behaviour and low-viscosity for ease of processing, control over the dimensions, size distributions, and morphologies of the resulting structures is challenging.[171, 172] However, living supramolecular polymerisations have been realised by applying kinetic control to the initiation and propagation steps, in a manner analogous to the initiation and propagation stages of conventional, living chain growth polymerisations. Lack of transfer and termination processes have allowed the possibility of accessing supramolecular polymers of controlled lengths and architectures

with narrow polydispersities, although these systems require carefully designed energy landscapes (Figure 1.11a–c).

The complexity of the supramolecular self-assembly pathway was demonstrated by De Greef, Meijer, and coworkers in seminal work that revealed two distinct pathways for the aggregation of an (*S*)-chiral oligo(*p*-phenylenevinylene).[174] An on-pathway mechanism yielded thermodynamically favoured left-handed aggregates, whilst an off-pathway process gave the right-handed species that later transformed into the more stable form. However, addition and removal of an (*S*)-chiral directing agent was able to force the aggregation of solely the kinetically favoured, metastable helix. Only with a careful understanding of this pathway complexity can supramolecular systems be designed to yield useful structures that exist far from equilibrium.

Formative living supramolecular polymerisation was demonstrated by Sugiyasu and Takeuchi for a zinc porphyrin-based system, via a nucleation-elongation mechanism coupled with a kinetically controlled pre-equilibrium to inhibit spontaneous nucleation.[175] Initial metastable 'J-aggregate' nanoparticles were formed by an isodesmic mechanism, but these were found to slowly transform into stable 'H-aggregates', with nanofibre morphologies, by means of a cooperative process. Under kinetic control fibres of controlled lengths were formed via addition of H-aggregate initiators to a solution of the nanoparticles.[175] Later work by the same authors extended living zinc porphyrin self-assembly into two dimensions.[176] The careful design of an energy landscape was revealed by the use of an azobenzene-based molecule which remained dormant in the ground state, but upon photo-activation, underwent isomerisation and was thus able to polymerise (Figure 1.11d–e).[177] If activation occurred in the presence of a seed micelle, the free monomer was able to polymerise in a living manner.

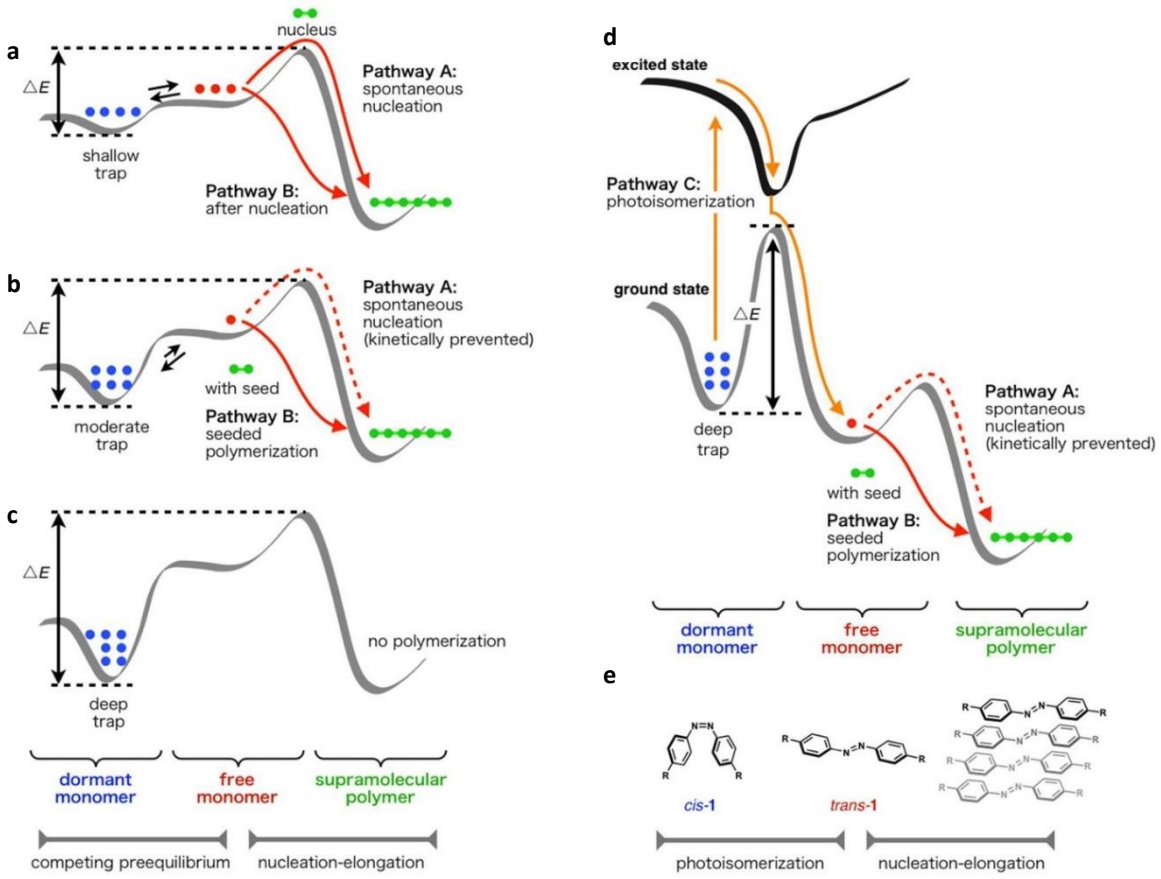

Figure 1.11. Energy landscapes of a supramolecular polymerisation coupled with a competing kinetic trap: a) the kinetic trap is too shallow to prevent spontaneous nucleation; b) the ideal landscape for living polymerisation, in which spontaneous nucleation is kinetically prevented, but polymerisation can be initiated by the addition of a seed; c) the kinetic trap is too deep to induce polymerisation; d) the deep kinetic trap can be circumvented through photoisomerisation, supplying free monomer for subsequent seeded polymerisation. e) photoisomerisation and supramolecular polymerisation of an azobenzene-based molecule, upon which the energy landscape (d) was based. Reproduced with permission from ref. 177.

1.6.3 An Interaction Toolbox

While hydrogen bonds between neutral species are far from the strongest non-covalent interaction, they are the most commonly employed approach to construct supramolecular polymers due to their directionality and versatility.[178] Their use in nature is ubiquitous, with examples present in DNA and proteins. Without employing other non-covalent interactions, stable supramolecular systems can be obtained by inclusion of four hydrogen-bonding units

into the small molecule structure.[179-181] Another valuable interaction employed in the design of supramolecular arrays is π–π stacking; however, the strength and cause of these interactions is incredibly solvent dependent. The interaction between aromatic molecules in water is stronger and driven by the hydrophobic effect, whilst in non-polar solvents, solvophobic forces have only a minor effect. A practical model describing various geometries of π–π interactions was developed by Hunter and Sanders,[182] but it is important to note that the majority of supramolecular systems display face-to-face stacking.

Some metal complexes have the ability to form supramolecular architectures, supported by metal–metal interactions alongside π–π stacking and hydrogen bonding. These metal-based interactions were first identified by close Au···Au contacts (smaller than the sum of their van der Waal radii) in several Au(I) complexes and termed aurophilicity, although metallophilicity is now used as a general term. The contacts have a strength comparable to that of a hydrogen bond, and are understood to occur due to a dispersion interaction between the electron densities on large, relatively reduced metal centres. Metallophilic interactions are most commonly displayed by d^{10} metals (Hg(II) Au(I), Pt(0), etc.) as well as those with d^8 and s^2 configurations, but are particularly strong for Au(I) due to the increased relativistic effects experienced by its electrons. Figure 1.12 demonstrates a general molecular orbital diagram for the homodinuclear metallophilic interaction between pairs of d^8 and d^{10} metals.

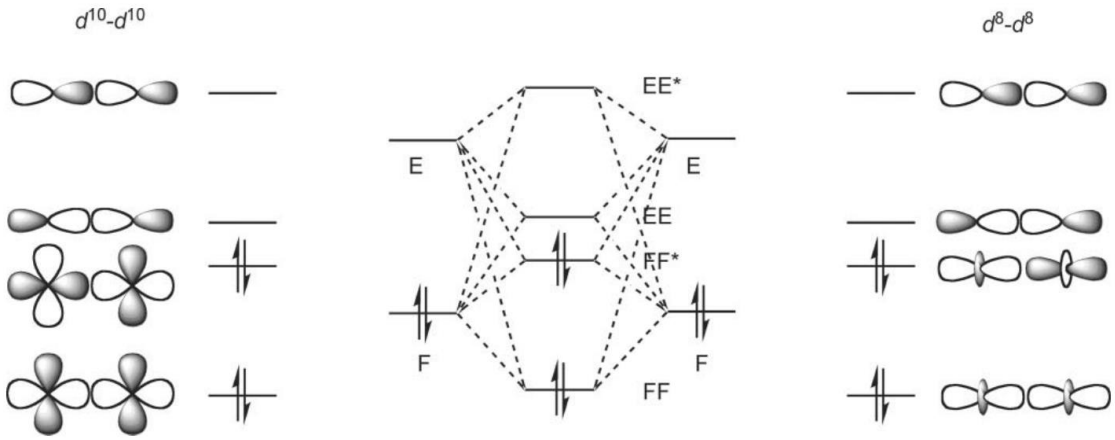

Figure 1.12. General molecular orbital diagram for the homodinuclear metallophilic interactions between pairs of d^{10} ions (left) and d^8 ions (right). Identical filled orbitals (F) on two metal centres overlap to form filled bonding (FF) and antibonding (FF*) orbitals. Low energy empty valence orbitals (E) of the same local symmetry mix with the filled orbitals and create unfilled, bonding (EE) and antibonding combinations (EE*), which stabilises the FF and FF* orbitals, and results in a net lowering of energy in the metallophilic pair relative to the individual precursors. Reproduced with permission from ref. 183.

1.7 Supramolecular Metal-Containing Polymers

Extensive research has been conducted on the supramolecular chemistry of organic molecules, encouraged by the award of the Nobel Prize to Lehn, Cram, and Pedersen in 1987. The majority of these self-assembly processes appear to be driven by non-covalent interactions such as hydrogen bonding, π–π stacking, and electrostatic interactions. Conversely, the related aggregation behaviour of metal complexes under the unique set of forces that these molecules possess has been vastly less explored, although it is expanding into an important topic of research. Complexes involving iron, copper, zinc, lanthanum, palladium, platinum, and gold, to name just a few, have been assembled into various supramolecular structures and architectures.[184, 185] In particular, assemblies based on d^8 and d^{10} transition metal systems represent important classes of supramolecular polymers that offer promising emissive properties, anticancer activity, and potential bioimaging applications.[186-188] However, the ability to control the aggregation behaviour to give

assemblies of a defined morphology and size is still in its infancy; such control is highly desirable as it may allow for enhanced optoelectronic properties and long-term colloidal stability.

1.7.1 Gold(I) Complexes

Within the field of supramolecular metallopolymers, an impressive array of gold-containing complexes have been reported with potential applications as optical materials, liquid crystals, inorganic pharmaceuticals, and precursors to gold coatings.[189] Gold(I) and gold(III), which have $5d^{10}$ and $5d^{8}$ electron configurations, respectively, are the preferred common oxidation states. The latter strongly favours a square-planar arrangement, whereas gold(I) tends to prefer a linear two-coordinate geometry (but can also form trigonal planar and tetrahedral complexes).[190]

As discussed in Section 1.6.3, gold(I) centres are able to form aurophilic interactions, which can direct the formation of supramolecular polymers, and/or the secondary structure of such polymers. Most commonly, gold(I) complexes associate by face-to-face stacking (Figure 1.13a), although slipped structures are also known (Figure 1.13b).[190] Additionally, if the ligands are not sterically demanding, then further association can occur between polymer chains to give ribbon- or sheet-like networks.

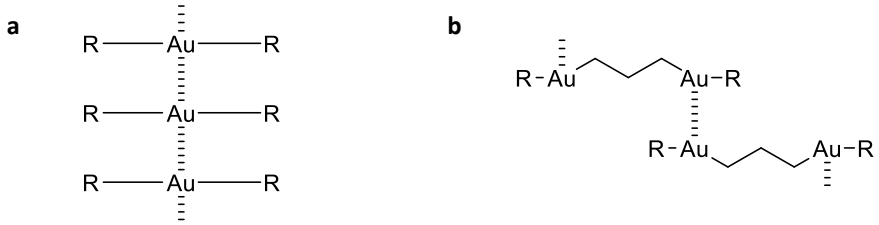

Figure 1.13. Modes (a and b) of Au···Au bonding in gold(I) supramolecular polymers.

In addition to directing self-assembly, aurophilic bonding has a marked effect on the emission properties of the aggregated complexes. Ito and Sawamura reported the reversible mechanochromic luminescence of $[(C_6F_5Au)_2(\mu\text{-}1,4\text{-diisocyanobenzene})]$, synthesised by the reaction of $[C_6F_5Au(tht)]$ (tht = tetrahydrothiophene) with 1,4-diisocyanobenzene in

dichloromethane.[191] Upon gentle grinding of the complex, the initial blue luminescence changed into an intense yellow luminescence, which could be reversed by addition of various solvents (such as ethyl acetate, diethyl ether, and chloroform, Figure 1.14). It was thought that grinding transforms the microcrystalline powder into a metastable amorphous phase, with aurophilic interactions responsible for the lower energy emission. Upon addition of solvent though, the amorphous phase rearranges into the more stable crystalline phase which lacks aurophilic and π–π interactions.

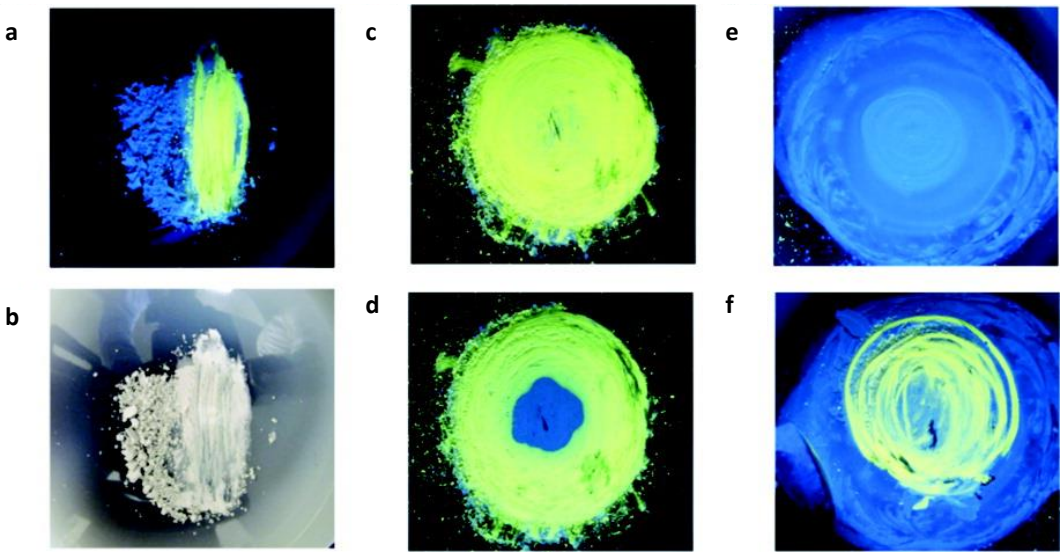

Figure 1.14. Photographs of [$(C_6F_5Au)_2$(μ-1,4-diisocyanobenzene)] on an agate mortar under UV irradiation with black light (365 nm): a) powder after grinding the right-half with a pestle; b) a same sample under ambient light; c) entirely ground powder; d) partial reversion to the blue luminescence by dropwise treatment using dichloromethane onto the centre of the ground powder; e) powder after treatment with dichloromethane; f) repetition of the yellow emission by scratching the powder with a pestle. Reproduced with permission from ref. 191.

Alkynylgold(I) complexes are also often strongly emissive, and in a multitude of examples the emission energies were shown to bathochromically-shift with increasing degrees of aggregation, presumably due to increased aurophilic interactions.[192, 193] This is not unexpected for systems in which a degree of electron delocalisation is possible along the chain direction is possible (despite the fairly large band gap).

Although the aggregation properties of gold(I) complexes are well-established, the majority of studies focus on the interesting photophysical behaviour described above,[194] or on crystal packing in the solid state.[195] For instance, a Au(I) complex of 4-mercaptobenzoic acid, [Au(SC_6H_4-4-COOH)(PMe_2Ph)], displayed interesting photoluminescence properties such as a large photoluminescent quantum yield and lifetime, and multicomponent emission.[196] Moreover, X-ray diffraction allowed the elucidation of the coordination polymer structure: the planar molecules form dimers via hydrogen bonding between carboxyl groups, and these stack to form an extended structure, Figure 1.15. The distance between two gold atoms was determined to be 3.534 Å, thus the photoluminescence was suggested to arise from aurophilic interactions. Indeed, in solution, the monomeric complexes displayed different electronic spectra.

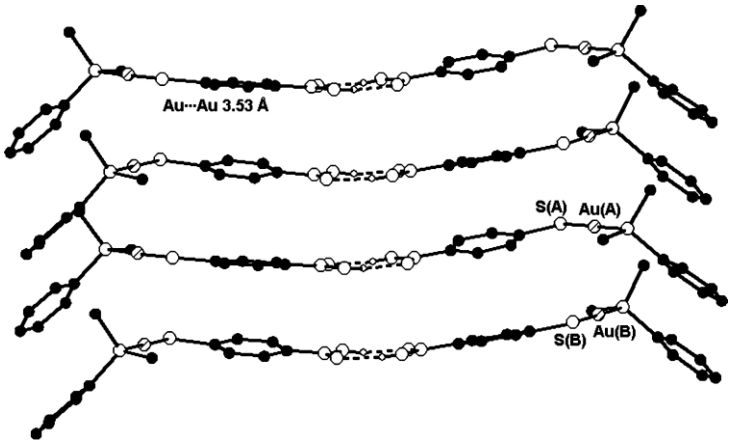

Figure 1.15. Side view of a stack of hydrogen-bonded dimers of [Au(SC_6H_4-4-COOH)(PMe_2Ph)], directed by Au···Au interactions. Reproduced with permission from ref. 196.

In contrast, solid state structures of (isocyanide)gold(I) thiosalicylates revealed extended chains of the type in Figure 1.13b.[197] These formed by initial association of two molecules (parallel and head to tail) yielding centrosymmetric dimers via Au···Au contacts (3.3186(5) Å), which then further aggregated via hydrogen bonding between the carboxylic acid groups to give a one-dimensional polymer, Figure 1.16.

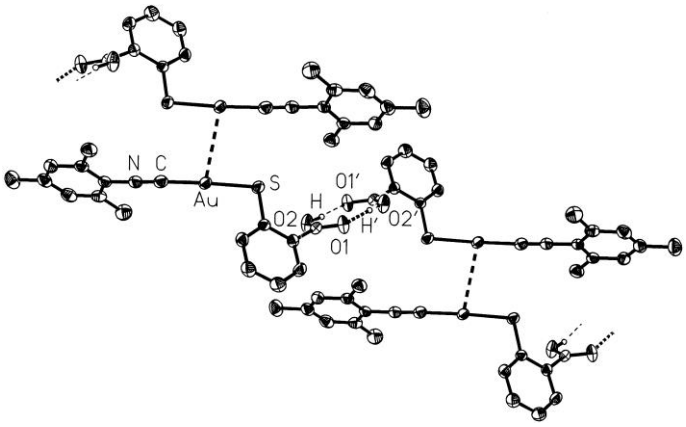

Figure 1.16. Four (isocyanide)gold(I) thiosalicylate molecules aggregated via Au···Au interactions and hydrogen bonding as part of an extended chain. Reproduced with permission from ref. 197.

Compared to solid-state coordination polymers, the solution-based self-assembly of gold(I) complexes is relatively limited. Recently, alkynyl gold(I) complexes were synthesised and demonstrated to undergo self-assembly in THF–water mixtures via a cooperative growth mechanism.[198] Modification of the length of the coronal alkyl chains was found to have a significant effect on the thermodynamic parameters of self-assembly and on the aggregate morphologies: complexes with C_6 and C_{16} alkyl chains displayed spherical morphologies, but when this was increased to twenty carbon atoms, two-dimensional nano sheets were observed. The difference in morphology was ascribed to increased hydrophobicity and directing effects driven by the longer chains.[198]

1.7.2 Platinum(II) Complexes

Alongside gold(I) complexes, platinum(II) compounds are well known to undergo self-assembly and demonstrate metallophilic interactions.[183, 186, 199] There are a wide variety of platinum(II) complexes, including mononuclear, dinuclear, and metallacyclic structures, and these normally exist with square-planar coordination at the metal centre(s). Among metallo-supramolecular polymers, those containing Pt(II) have been well-studied, such that fairly good control over size and morphology of the resulting self-assembled nanostructures has been achieved.

In 2015 Manners and coworkers reported the living supramolecular polymerisation of planar Pt(II) complexes via a seeded growth method, analogous to the crystallisation-driven self-assembly of covalent block copolymers. For conventional living CDSA, long, polydisperse cylindrical micelles are subject to sonication to yield small crystallites (seeds), then addition of further unimer results in bidirectional epitaxial growth at the seed to yield monodisperse micelles. With the Pt(II) complexes, nanofibre structures were achieved with a small width (<15 nm), tuneable length, and narrow length distributions up to ~400 nm by employing conditions for kinetic control, and using small seed fibres as initiators (Figure 1.17).[200] By reducing the length of the solubilising ancillary ligand from poly(ethylene glycol)$_{16}$ to poly(ethylene glycol)$_7$, they were later able to exclusively form two-dimensional platelet structures.[201]

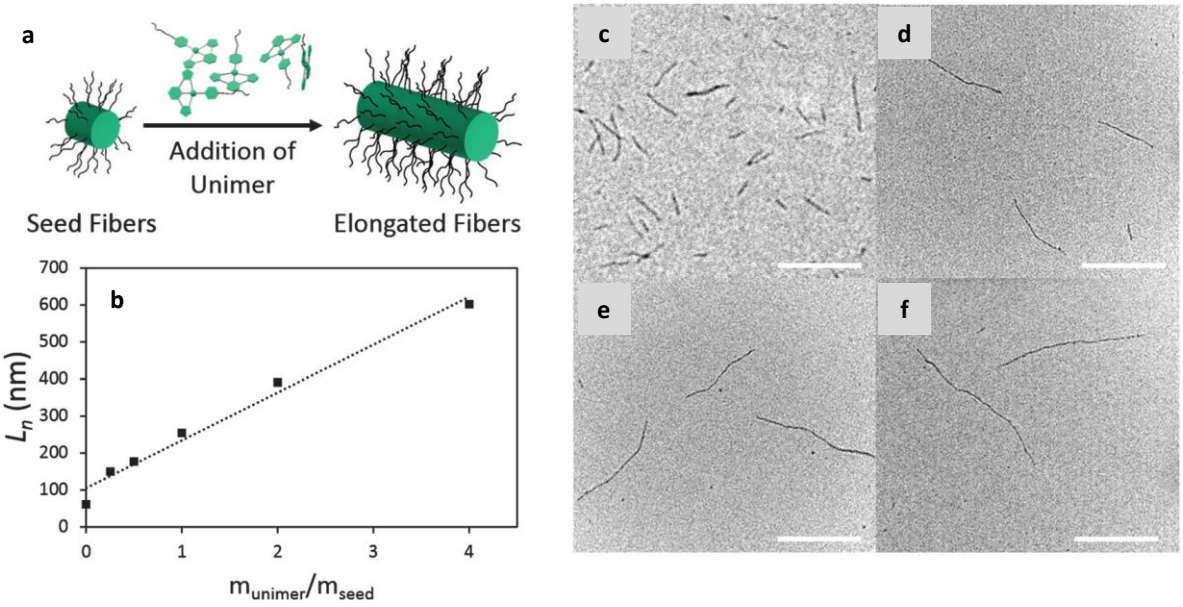

Figure 1.17. a) Schematic representation of the formation of Pt(II) elongated fibres. b) Linear dependence of average contour length (L_n) on the unimer to seed mass ratio. c) Seed fibres formed through gentle sonication of polydisperse fibres, to which (d) 1 eq., (e) 2 eq., and (f) 4 eq. of unimer was added to give elongated fibres. Scale bars: 250 nm. Reproduced with permission from ref. 200.

1.8 Thesis Summary and Acknowledgements

This introductory chapter has outlined the major developments in the polymerisation of metallocene-containing species to form main-chain polymers, noting that cobaltocene-, cobaltocenium-, and nickelocene-based metallopolymers are highly limited in number compared to those containing ferrocene. In addition, there are few reported examples of supramolecular polymers containing gold(I) centres which persist in solution. Thus, the following chapters in this thesis aim to describe the synthesis, characterisation, and properties of novel σ-bound and supramolecular metallopolymers, and to offer an understanding of the driving forces behind these polymerisation processes. Chapter 2 describes the ROP of [*n*]nickelocenophanes and the characterisation of the magnetic properties of the monomers and polymers by SQUID magnetometry. Chapter 3 evaluates the synthesis and ROP of further [*n*]nickelocenophanes, and the thermodynamic parameters which characterise the polymerisations. Chapter 4 encompasses the application of poly(cobaltoceniumethylene) materials in the protection of β-lactam antibiotics, in addition to the syntheses of cobaltocenium-containing polymers via polycondensation routes. Chapter 5 describes the synthesis and supramolecular self-assembly of three gold(I)-containing complexes, and their energy landscapes of polymerisation. Contributions made to the research are noted below by Chapter:

Chapter 1: Introduction. Some inspiration was taken from the review R. L. N. Hailes†, A. M. Oliver†, J. Gwyther‡, G. R. Whittell‡, I. Manners, *Chem. Soc. Rev.* **2016**, *45*, 5358–5407 and R. L. N. Hailes, R. A. Musgrave, A. F. R. Kilpatrick, A. D. Russell, G. R. Whittell, D. O'Hare, I. Manners, *Chem. Eur. J.* **2019**, *25*, 1044–1054.

Chapter 2: Ring-Opening Polymerisation of Low-Strain Nickelocenophanes: Synthesis and Magnetic Properties of Polynickelocenes with Carbon and Silicon Main Chain Spacers. This chapter is reproduced from R. L. N. Hailes, R. A. Musgrave, A. F. R. Kilpatrick, A. D. Russell, G. R. Whittell, D. O'Hare, I. Manners, *Chem. Eur. J.* **2019**, *25*,

1044–1054. The work in this chapter benefited greatly from scientific input from Dr Rebecca Musgrave, who also carried out initial syntheses and ROP of **2.6** and **2.10**, and the copolymerisation to produce **2.15**. Dr Andrew Russell carried out the initial copolymerisation to produce **2.16**. WAXS measurements were conducted by Dr George Whittell, SQUID magnetometry by Dr Alexander Kilpatrick at The University of Oxford, ESI-MS by Dr Paul Gates, and X-ray crystallography by Dr Rebecca Musgrave.

Chapter 3: Influence of Monomer Structure on the Ring-Opening Polymerisation Behaviour of Low Strain [*n*]Nickelocenophanes. DFT calculations were conducted by the author and Dr Rebecca Musgrave (who also synthesised **3.13**) with assistance from Dr Natalie Fey and scientific input from Prof. Jeremy Harvey. ESI-MS was performed by Dr Paul Gates, and X-ray crystallographic analysis was conducted by Dr Rebecca Musgrave and Dr Vincent Annibale.

Chapter 4: Evaluation of Poly(cobaltoceniumethylene) as an Antimicrobial and the Synthesis of New Main Chain Cobaltocenium Polyelectrolytes. Experiments to determine antimicrobial activity of polymers were performed by Dr Jim Spencer. X-ray crystallography was conducted by Dr Theresa Dellerman, who also provided useful scientific input.

Chapter 5: Impact of a Subtle Structural Difference on the Self-Assembling Behaviour of Gold(I) Complexes. Dr Xiaoming He synthesised compounds **5.2**–**5.4**, and Dr Robert Harniman performed AFM analyses.

Chapter 6: Outlook. The photograph in Figure 6.2 was provided by Dr Xiaoming He.

Additional publications: R. A. Musgrave, R. L. N. Hailes, A. Schäfer, A. D. Russell, P. J. Gates, I. Manners, *Dalton Trans.*, **2018**, *47*, 2759–2768

1.9 References

1. G. R. Whittell, M. D. Hager, U. S. Schubert and I. Manners, *Nat. Mater.*, 2011, **10**, 176-188.

2. C. Fouquey, J. M. Lehn and A. M. Levelut, *Adv. Mater.*, 1990, **2**, 254-257.

3. A. Duda and A. Kowalski, in *Handbook of Ring-Opening Polymerization*, eds. P. Dubois, O. Coulembier and J.-M. Raquez, Wiley-VCH Verlag GmbH & Co., Weinheim, 2009, ch. 1.

4. W.-F. Su, in *Principles of Polymer Design and Synthesis*, Springer Berlin Heidelberg, Berlin, Heidelberg, 2013, pp. 267-299.

5. M. P. Dreyfuss and P. Dreyfuss, *J. Polym. Sci. A: Polym. Chem.*, 1966, **4**, 2179-2200.

6. A. V. Tobolsky and A. Eisenberg, *J. Am. Chem. Soc.*, 1959, **81**, 780-782.

7. A. Eisenberg and A. V. Tobolsky, *J. Polym. Sci.*, 1960, **46**, 19-28.

8. B. V. Lebedev, N. N. Mukhina and T. G. Kulagina, *Vysokomol. Soedin. A*, 1978, **20**, 1297-1303.

9. A. V. Tobolsky and A. Eisenberg, *J. Am. Chem. Soc.*, 1960, **82**, 289-293.

10. R. Resendes, J. M. Nelson, A. Fischer, F. Jäkle, A. Bartole, A. J. Lough and I. Manners, *J. Am. Chem. Soc.*, 2001, **123**, 2116-2126.

11. R. Rulkens, D. P. Gates, D. Balaishis, J. K. Pudelski, D. F. McIntosh, A. J. Lough and I. Manners, *J. Am. Chem. Soc.*, 1997, **119**, 10976-10986.

12. W. Finckh, B. Z. Tang, D. A. Foucher, D. B. Zamble, R. Ziembinski, A. Lough and I. Manners, *Organometallics*, 1993, **12**, 823-829.

13. S. A. Miller, J. A. Tebboth and J. F. Tremaine, *J. Chem. Soc.*, 1952, **0**, 632-635.

14. I. Manners, *Adv. Mater.*, 1994, **6**, 68-71.

15. R. L. N. Hailes, A. M. Oliver, J. Gwyther, G. R. Whittell and I. Manners, *Chem. Soc. Rev.*, 2016, **45**, 5358-5407.

16. D. E. Herbert, U. F. J. Mayer and I. Manners, *Angew. Chem. Int. Ed.*, 2007, **46**, 5060-5081.

17. M. Tamm, *Chem. Commun.*, 2008, **0**, 3089-3100.

18. A. D. Russell, R. A. Musgrave, L. K. Stoll, P. Choi, H. Qiu and I. Manners, *J. Organomet. Chem.*, 2015, **784**, 24-30.

19. K. L. Rinehart, Jr., A. K. Frerichs, P. A. Kittle, L. F. Westman, D. H. Gustafson, R. L. Pruett and J. E. McMahon, *J. Am. Chem. Soc.*, 1960, **82**, 4111-4112.

20. A. G. Osborne and R. H. Whiteley, *J. Organomet. Chem.*, 1975, **101**, C27-C28.

21. H. Braunschweig, R. Dirk, M. Müller, P. Nguyen, R. Resendes, D. P. Gates and I. Manners, *Angew. Chem. Int. Ed.*, 1997, **36**, 2338-2340.

22. J. A. Schachner, C. L. Lund, J. W. Quail and J. Müller, *Organometallics*, 2005, **24**, 785-787.

23. J. A. Schachner, C. L. Lund, J. W. Quail and J. Müller, *Organometallics*, 2005, **24**, 4483-4488.

24. D. A. Foucher, M. Edwards, R. A. Burrow, A. J. Lough and I. Manners, *Organometallics*, 1994, **13**, 4959-4966.

25. R. Rulkens, A. J. Lough and I. Manners, *Angew. Chem. Int. Ed.*, 1996, **35**, 1805-1807.

26. D. Seyferth and H. P. Withers, Jr., *J. Organomet. Chem.*, 1980, **185**, C1-C5.

27. D. Seyferth and H. P. Withers Jr., *Organometallics*, 1982, **1**, 1275-1282.

28. J. K. Pudelski, D. P. Gates, R. Rulkens, A. J. Lough and I. Manners, *Angew. Chem. Int. Ed.*, 1995, **34**, 1506-1508.

29. R. Rulkens, D. P. Gates, D. Balaishis, J. K. Pudelski, D. F. McIntosh, A. J. Lough and I. Manners, *J. Am. Chem. Soc.*, 1997, **119**, 10976-10986.

30. G. R. Whittell, B. M. Partridge, O. C. Presly, C. J. Adams and I. Manners, *Angew. Chem. Int. Ed.*, 2008, **47**, 4354-4357.

31. R. Broussier, A. Da Rold, B. Gautheron, Y. Dromzee and Y. Jeannin, *Inorg. Chem.*, 1990, **29**, 1817-1822.

32. I. Matas Ruiz, G. R. Whittell, B. M. Partridge, J. P. Holland, M. F. Haddow, J. C. Green and I. Manners, *J. Am. Chem. Soc.*, 2010, **132**, 13279-13289.

33. G. Wilkinson, *J. Am. Chem. Soc.*, 1952, **74**, 6146-6147.

34. E. O. Fischer and H. Grubert, *Chem. Ber.*, 1959, **92**, 2302-2309.

35. N. J. Long, *In Metallocenes: An Introduction to Sandwich Complexes*, Wiley-Blackwell, 1st edn., 1998.

36. J. D. Dunitz, L. E. Orgel and A. Rich, *Acta Crystallogr.*, 1956, **9**, 373-375.

37. M. Y. Antipin, R. Boese, N. Augart and G. Schmid, *Struct. Chem.*, 1993, **4**, 91-101.

38. P. Seiler and J. D. Dunitz, *Acta Crystallogr. Sect. B*, 1980, **36**, 2255-2260.

39. S. Lu, V. V. Strelets, M. F. Ryan, W. J. Pietro and A. B. P. Lever, *Inorg. Chem.*, 1996, **35**, 1013-1023.

40. J. C. Green, *Chem. Soc. Rev.*, 1998, **27**, 263-271.

41. J. A. Schachner, S. Tockner, C. L. Lund, J. W. Quail, M. Rehahn and J. Müller, *Organometallics*, 2007, **26**, 4658-4662.

42. A. Berenbaum, F. Jäkle, A. J. Lough and I. Manners, *Organometallics*, 2001, **20**, 834-843.

43. R. A. Musgrave, A. D. Russell and I. Manners, *Organometallics*, 2013, **32**, 5654-5667.

44. W. Finckh, B. Z. Tang, D. A. Foucher, D. B. Zamble, R. Ziembinski, A. Lough and I. Manners, *Organometallics*, 1993, **12**, 823-829.

45. H. Braunschweig, F. Breher, M. Kaupp, M. Gross, T. Kupfer, D. Nied, K. Radacki and S. Schinzel, *Organometallics*, 2008, **27**, 6427-6433.

46. H. Braunschweig, M. Gross and K. Radacki, *Organometallics*, 2007, **26**, 6688-6690.

47. J. B. Gilroy, A. D. Russell, A. J. Stonor, L. Chabanne, S. Baljak, M. F. Haddow and I. Manners, *Chem. Sci.*, 2012, **3**, 830-841.

48. S. Baljak, A. D. Russell, S. C. Binding, M. F. Haddow, D. O'Hare and I. Manners, *J. Am. Chem. Soc.*, 2014, **136**, 5864-5867.

49. J. J. Bishop, A. Davison, M. L. Katcher, D. W. Lichtenberg, R. E. Merrill and J. C. Smart, *J. Organomet. Chem.*, 1971, **27**, 241-249.

50. U. Vogel, A. J. Lough and I. Manners, *Angew. Chem. Int. Ed.*, 2004, **43**, 3321-3325.

51. H. Braunschweig, A. Damme, K. Hammond and J. Mager, *Organometallics*, 2012, **31**, 6317-6321.

52. H. Braunschweig, F. Hupp, T. Kramer and J. Mager, *Inorg. Chem.*, 2013, **52**, 9060-9065.

53. M. J. Drewitt, S. Barlow, D. O'Hare, J. M. Nelson, P. Nguyen and I. Manners, *Chem. Commun.*, 1996, **0**, 2153-2154.

54. W. Buchowicz, L. B. Jerzykiewicz, A. Krasińska, S. Losi, A. Pietrzykowski and P. Zanello, *Organometallics*, 2006, **25**, 5076-5082.

55. C. Moser, F. Belaj and R. Pietschnig, *Chem. Eur. J.*, 2009, **15**, 12589-12591.

56. Y. Tanimoto, Y. Ishizu, K. Kubo, K. Miyoshi and T. Mizuta, *J. Organomet. Chem.*, 2012, **713**, 80-88.

57. S. Fox, J. P. Dunne, M. Tacke, D. Schmitz and R. Dronskowski, *Eur. J. Inorg. Chem.*, 2002, 3039-3046.

58. D. E. Herbert, U. F. J. Mayer and I. Manners, *Angew. Chem. Int. Ed.*, 2007, **46**, 5060-5081.

59. R. Resendes, P. Nguyen, A. J. Lough and I. Manners, *Chem. Commun.*, 1998, **9**, 1001-1002.

60. D. A. Foucher, B. Z. Tang and I. Manners, *J. Am. Chem. Soc.*, 1992, **114**, 6246-6248.

61. I. Manners, *Chem. Commun.*, 1999, **10**, 857-865.

62. M. Tanabe, G. W. M. Vandermeulen, W. Y. Chan, P. W. Cyr, L. Vanderark, D. A. Rider and I. Manners, *Nat. Mater.*, 2006, **5**, 467-470.

63. R. A. Musgrave, A. D. Russell, D. W. Hayward, G. R. Whittell, P. G. Lawrence, P. J. Gates, J. C. Green and I. Manners, *Nat. Chem.*, 2017, **9**, 743-750.

64. K. Temple, F. Jäkle, J. B. Sheridan and I. Manners, *J. Am. Chem. Soc.*, 2001, **123**, 1355-1364.

65. I. Manners, *Chem. Commun.*, 1999, **0**, 857-865.

66. J.-J. Wang, L. Wang, T. Chen, X.-J. Wang, C.-L. Wang, X.-C. Dong and J.-H. Yang, *Eur. Polym. J.*, 2006, **42**, 843-848.

67. K. Kulbaba and I. Manners, *Macromol. Rapid Commun.*, 2001, **22**, 711-724.

68. J.-J. Wang, L. Wang, X.-J. Wang, T. Chen, H.-J. Yu, W. Wang and C.-L. Wang, *Mater. Lett.*, 2006, **60**, 1416-1419.

69. R. A. Musgrave, A. D. Russell, G. R. Whittell, M. F. Haddow and I. Manners, *Organometallics*, 2015, **34**, 897-907.

70. J. K. Pudelski and I. Manners, *J. Am. Chem. Soc.*, 1995, **117**, 7265-7266.

71. F. Jäkle, R. Rulkens, G. Zech, J. A. Massey and I. Manners, *J. Am. Chem. Soc.*, 2000, **122**, 4231-4232.

72. P. W. Cyr, D. A. Rider, K. Kulbaba and I. Manners, *Macromolecules*, 2004, **37**, 3959-3961.

73. K. N. Power-Billard and I. Manners, *Macromolecules*, 2000, **33**, 26-31.

74. K. Temple, S. Dziadek and I. Manners, *Organometallics*, 2002, **21**, 4377-4384.

75. Y. Ni, R. Rulkens, J. K. Pudelski and I. Manners, *Macromol. Rapid Commun.*, 1995, **16**, 637-641.

76. N. P. Reddy, H. Yamashita and M. Tanaka, *J. Chem. Soc., Chem. Commun.*, 1995, 2263-2264.

77. P. Gómez-Elipe, R. Resendes, P. M. Macdonald and I. Manners, *J. Am. Chem. Soc.*, 1998, **120**, 8348-8356.

78. R. Rulkens, Y. Ni and I. Manners, *J. Am. Chem. Soc.*, 1994, **116**, 12121-12122.

79. Y. Ni, R. Rulkens and I. Manners, *J. Am. Chem. Soc.*, 1996, **118**, 4102-4114.

80. R. G. H. Lammertink, M. A. Hempenius, I. Manners and G. J. Vancso, *Macromolecules*, 1998, **31**, 795-800.

81. J. A. Massey, K. Temple, L. Cao, Y. Rharbi, J. Raez, M. A. Winnik and I. Manners, *J. Am. Chem. Soc.*, 2000, **122**, 11577-11584.

82. D. A. Rider, K. A. Cavicchi, K. N. Power-Billard, T. P. Russell and I. Manners, *Macromolecules*, 2005, **38**, 6931-6938.

83. A. Canet, A. H. Mark, G. J. Vancso and H. Jurriaan, *Nanotechnology*, 2009, **20**, 135304.

84. J. Gwyther and I. Manners, *Polymer*, 2009, **50**, 5384-5389.

85. C. Kloninger and M. Rehahn, *Macromolecules*, 2004, **37**, 1720-1727.

86. J. A. Massey, M. A. Winnik, I. Manners, V. Z. H. Chan, J. M. Ostermann, R. Enchelmaier, J. P. Spatz and M. Möller, *J. Am. Chem. Soc.*, 2001, **123**, 3147-3148.

87. K. N. Power-Billard, P. Wieland, M. Schäfer, O. Nuyken and I. Manners, *Macromolecules*, 2004, **37**, 2090-2095.

88. M. Zhang, P. A. Rupar, C. Feng, K. Lin, D. J. Lunn, A. Oliver, A. Nunns, G. R. Whittell, I. Manners and M. A. Winnik, *Macromolecules*, 2013, **46**, 1296-1304.

89. J. M. Nelson, P. Nguyen, R. Petersen, H. Rengel, P. M. Macdonald, A. J. Lough, I. Manners, N. P. Raju, J. E. Greedan, S. Barlow and D. O'Hare, *Chem. Eur. J.*, 1997, **3**, 573-584.

90. J. M. Nelson, H. Rengel and I. Manners, *J. Am. Chem. Soc.*, 1993, **115**, 7035-7036.

91. M. Tanabe and I. Manners, *J. Am. Chem. Soc.*, 2004, **126**, 11434-11435.

92. W. Y. Chan, A. J. Lough and I. Manners, *Chem. Eur. J.*, 2007, **13**, 8867-8876.

93. G. S. Smith, S. K. Patra, L. Vanderark, S. Saithong, J. P. H. Charmant and I. Manners, *Macromol. Chem. Phys.*, 2010, **211**, 303-312.

94. W. Y. Chan, A. J. Lough and I. Manners, *Organometallics*, 2007, **26**, 1217-1225.

95. Z. Wang, G. Masson, F. C. Peiris, G. A. Ozin and I. Manners, *Chem. Eur. J.*, 2007, **13**, 9372-9383.

96. M. Erhard, K. Lam, M. Haddow, G. R. Whittell, W. E. Geiger and I. Manners, *Polym. Chem.*, 2014, **5**, 1264-1274.

97. D. E. Herbert, U. F. J. Mayer, J. B. Gilroy, M. J. López-Gómez, A. J. Lough, J. P. H. Charmant and I. Manners, *Chem. Eur. J.*, 2009, **15**, 12234-12246.

98. T. Mizuta, M. Onishi and K. Miyoshi, *Organometallics*, 2000, **19**, 5005-5009.

99. L. Chabanne, I. Matas, S. K. Patra and I. Manners, *Polym. Chem.*, 2011, **2**, 2651-2660.

100. S. K. Patra, G. R. Whittell, S. Nagiah, C. L. Ho, W. Y. Wong and I. Manners, *Chem. Eur. J.*, 2010, **16**, 3240-3250.

101. U. F. J. Mayer, J. B. Gilroy, D. O'Hare and I. Manners, *J. Am. Chem. Soc.*, 2009, **131**, 10382-10383.

102. J. B. Gilroy, S. K. Patra, J. M. Mitchels, M. A. Winnik and I. Manners, *Angew. Chem. Int. Ed.*, 2011, **50**, 5851-5855.

103. V. I. Tel'noi and I. B. Rabinovich, *Usp. Khim.*, 1977, **46**, 1337-1367.

104. A. Viswanathan, *World Pat. Inf.*, 2010, **32**, 300-305.

105. P. J. Flory, *Chem. Rev.*, 1946, **39**, 137-197.

106. J. K. Stille, *J. Chem. Educ.*, 1981, **58**, 862.

107. A. S. Abd-El-Aziz, P. O. Shipman, B. N. Boden and W. S. McNeil, *Prog. Polym. Sci.*, 2010, **35**, 714-836.

108. K. Sonogashira, *J. Organomet. Chem.*, 2002, **653**, 46-49.

109. K. D. Ley, C. E. Whittle, M. D. Bartberger and K. S. Schanze, *J. Am. Chem. Soc.*, 1997, **119**, 3423-3424.

110. K. D. Ley, Y. Li, J. V. Johnson, D. H. Powell and K. S. Schanze, *Chem. Commun.*, 1999, **0**, 1749-1750.

111. J. Xiang, C. L. Ho and W.-Y. Wong, *Polym. Chem.*, 2015, **6**, 6905-6930.

112. P. K. Ng, X. Gong, S. H. Chan, L. S. M. Lam and W. K. Chan, *Chem. Eur. J.*, 2001, **7**, 4358-4367.

113. H. Fukumoto, K. Yamane, Y. Kase and T. Yamamoto, *Macromolecules*, 2010, **43**, 10366-10375.

114. W.-Y. Wong and P. D. Harvey, *Macromol. Rapid Commun.*, 2010, **31**, 671-713.

115. W. K. Chan, *Coord. Chem. Rev.*, 2007, **251**, 2104-2118.

116. S. C. Rasmussen, D. W. Thompson, V. Singh and J. D. Petersen, *Inorg. Chem.*, 1996, **35**, 3449-3450.

117. J. B. Heilmann, M. Scheibitz, Y. Qin, A. Sundararaman, F. Jäkle, T. Kretz, M. Bolte, H.-W. Lerner, M. C. Holthausen and M. Wagner, *Angew. Chem.*, 2006, **118**, 934-939.

118. S. Mehdipour-Ataei and S. Babanzadeh, *Appl. Organomet. Chem.*, 2007, **21**, 360-367.

119. A. Nigar, M. A. Bashir and Z. Akhter, *Synth. Commun.*, 2007, **37**, 473-482.

120. H. Rosenberg and M. Rausch, *US Patent*, 1962, **3060215**.

121. H. Rosenberg, *Journal*, 1969.

122. A. S. Abd-El-Aziz and E. K. Todd, *Coord. Chem. Rev.*, 2003, **246**, 3-52.

123. C. E. Carraher and J. E. Sheats, *Makromol. Chem.*, 1973, **166**, 23-29.

124. C. U. Pittman, O. E. Ayers, B. Suryanarayanan, S. P. McManus and J. E. Sheats, *Makromol. Chem.*, 1974, **175**, 1427-1437.

125. I. Cuadrado, C. M. Casado, F. Lobete, B. Alonso, B. González, J. Losada and U. Amador, *Organometallics*, 1999, **18**, 4960-4969.

126. Y. Sasaki, L. L. Walker, E. L. Hurst and C. U. Pittman Jr., *J. Polym. Sci. A: Polym. Chem.*, 1973, **11**, 1213-1224.

127. J. B. Flanagan, S. Margel, A. J. Bard and F. C. Anson, *J. Am. Chem. Soc.*, 1978, **100**, 4248-4253.

128. C. U. Pittman, J. C. Lai, D. P. Vanderpool, M. Good and R. Prados, Boston, MA, 1971.

129. A. S. Abd-El-Aziz and I. Manners, *Frontiers In Transition Metal-Containing Polymers*, John Wiley & Sons, 2007.

130. C. U. Pittman Jr, C.-C. Lin and T. D. Rounsefell, *Macromolecules*, 1978, **11**, 1022-1027.

131. C. U. Pittman Jr. and P. L. Grube, *J. Polym. Sci. A: Polym. Chem.*, 1971, **9**, 3175-3186.
132. C. U. Pittman Jr, G. V. Marlin and T. D. Rounsefell, *Macromolecules*, 1973, **6**, 1-8.
133. C. U. Pittman, T. D. Rounsefell, E. A. Lewis, J. E. Sheats, B. H. Edwards, M. D. Rausch and E. A. Mintz, *Macromolecules*, 1978, **11**, 560-565.
134. C. W. Bielawski and R. H. Grubbs, *Prog. Polym. Sci.*, 2007, **32**, 1-29.
135. I. Dragutan, V. Dragutan and H. Fischer, *J. Inorg. Organomet. Polym. Mater.*, 2008, **18**, 311.
136. C. E. Stanton, T. Randall Lee, R. H. Grubbs, N. S. Lewis, J. K. Pudelski, M. R. Callstrom, M. S. Erickson and M. L. McLaughlin, *Macromolecules*, 1995, **28**, 8713-8721.
137. R. W. Heo, J. S. Park, J. T. Goodson, G. C. Claudio, M. Takenaga, T. A. Albright and T. Randall Lee, *Tetrahedron*, 2004, **60**, 7225-7235.
138. Y. Sha, Y. Zhang, T. Zhu, S. Tan, Y. Cha, S. L. Craig and C. Tang, *Macromolecules*, 2018, **51**, 9131-9139.
139. I. Dragutan, V. Dragutan, B. C. Simionescu, A. Demonceau and H. Fischer, *Beilstein J. Org. Chem.*, 2015, **11**, 2747-2762.
140. H. Gu, R. Ciganda, S. Gatard, F. Lu, P. Zhao, J. Ruiz and D. Astruc, *J. Organomet. Chem.*, 2016, **813**, 95-102.
141. H. Gu, R. Ciganda, R. Hernandez, P. Castel, P. Zhao, J. Ruiz and D. Astruc, *Macromolecules*, 2015, **48**, 6071-6076.
142. Y. Yan, J. Zhang, P. Wilbon, Y. Qiao and C. Tang, *Macromol. Rapid Commun.*, 2014, **35**, 1840-1845.
143. T. Zhu, Y. Sha, J. Yan, P. Pageni, M. A. Rahman, Y. Yan and C. Tang, *Nat. Commun.*, 2018, **9**, 4329.
144. Y. Zha, R. R. Maddikeri, S. P. Gido and G. N. Tew, *J. Inorg. Organomet. Polym. Mater.*, 2013, **23**, 89-94.
145. F. P. Guengerich, *J. Biol. Chem.*, 2009, **284**, 709-709.
146. J. E. Sheats, C. E. Carraher Jr and C. U. Pittman, *Metal-Containing Polymeric Systems*, Springer Science & Business Media, 2012.
147. X. S. Wang and R. McHale, *Macromol. Rapid Commun.*, 2010, **31**, 331-350.
148. R. McDonald, K. C. Sturge, A. D. Hunter and L. Shilliday, *Organometallics*, 1992, **11**, 893-900.
149. K. C. Sturge, A. D. Hunter, R. Mcdonald and B. D. Santarsiero, *Organometallics*, 1992, **11**, 3056-3062.

150. P. M. Macdonald, A. D. Hunter, G. Lesley and J. Li, *Solid State Nucl. Magn. Reson.*, 1993, **2**, 47-55.

151. X. S. Ding, J. Guo, X. A. Feng, Y. Honsho, J. D. Guo, S. Seki, P. Maitarad, A. Saeki, S. Nagase and D. L. Jiang, *Angew. Chem. Int. Ed.*, 2011, **50**, 1289-1293.

152. M. Yang, L. Zhang, Z. Lei, P. Ye, J. Si, Q. Yang and Y. Wang, *J. Appl. Polym. Sci.*, 1998, **70**, 1165-1172.

153. Y. Wang, D. Liu and W. Sun, *Des. Monomers Polym.*, 2017, **20**, 300-307.

154. J. A. Paquette, E. R. Sauvé and J. B. Gilroy, *Macromol. Rapid Commun.*, 2015, **36**, 621-626.

155. J. A. Paquette, A. Rabiee Kenaree and J. B. Gilroy, *Polym. Chem.*, 2017, **8**, 2164-2172.

156. H.-C. Zhang, W.-S. Huang and L. Pu, *J. Org. Chem.*, 2001, **66**, 481-487.

157. M. Rosenblum, H. M. Nugent, K. S. Jang, M. M. Labes, W. Cahalane, P. Klemarczyk and W. M. Reiff, *Macromolecules*, 1995, **28**, 6330-6342.

158. P. Baltzer, A. Furrer, J. Hulliger and A. Stebler, *Inorg. Chem.*, 1988, **27**, 1543-1548.

159. S. Evans, M. L. H. Green, B. Jewitt, G. H. King and A. F. Orchard, *J. Chem. Soc. Faraday Trans. 2*, 1974, **70**, 356-376.

160. N. El Murr, R. Dabard and E. Laviron, *J. Organomet. Chem.*, 1973, **47**, C13-C16.

161. J. E. Sheats, W. Miller and T. Kirsch, *J. Organomet. Chem.*, 1975, **91**, 97-104.

162. D. Braga, L. Maini, M. Polito, M. Rossini and F. Grepioni, *Chem. Eur. J.*, 2000, **6**, 4227-4235.

163. S. Inyushin, A. Shafir, J. E. Sheats, M. Minihane, C. E. Whitten and J. Arnold, *Polyhedron*, 2004, **23**, 2937-2942.

164. D. Braga, M. Polito and F. Grepioni, *Cryst. Growth Des.*, 2004, **4**, 769-774.

165. N. Chen, H. Zhu, Y. Chu, R. Li, Y. Liu and F. Wang, *Polym. Chem.*, 2017, **8**, 1381-1392.

166. L. Zhao, X. Liu, L. Zhang, G. Qiu, D. Astruc and H. Gu, *Coord. Chem. Rev.*, 2017, **337**, 34-79.

167. F. Kettner, M. Kischel and H. Krautscheid, *CrystEngComm*, 2013, **15**, 8437-8443.

168. H. Qiu, J. B. Gilroy and I. Manners, *Chem. Commun.*, 2013, **49**, 42-44.

169. U. F. J. Mayer, J. P. H. Charmant, J. Rae and I. Manners, *Organometallics*, 2008, **27**, 1524-1533.

170. J. Zhang, Y. P. Chen, K. P. Miller, M. S. Ganewatta, M. Bam, Y. Yan, M. Nagarkatti, A. W. Decho and C. Tang, *J. Am. Chem. Soc.*, 2014, **136**, 4873-4876.

171. T. F. A. De Greef, M. M. J. Smulders, M. Wolffs, A. P. H. J. Schenning, R. P. Sijbesma and E. W. Meijer, *Chem. Rev.*, 2009, **109**, 5687-5754.
172. D. Zhao and J. S. Moore, *Org. Biomol. Chem.*, 2003, **1**, 3471-3491.
173. M. M. J. Smulders, M. M. L. Nieuwenhuizen, T. F. A. de Greef, P. van der Schoot, A. P. H. J. Schenning and E. W. Meijer, *Chem. Eur. J.*, 2010, **16**, 362-367.
174. P. A. Korevaar, S. J. George, A. J. Markvoort, M. M. J. Smulders, P. A. J. Hilbers, A. P. H. J. Schenning, T. F. A. De Greef and E. W. Meijer, *Nature*, 2012, **481**, 492.
175. S. Ogi, K. Sugiyasu, S. Manna, S. Samitsu and M. Takeuchi, *Nat. Chem.*, 2014, **6**, 188.
176. T. Fukui, S. Kawai, S. Fujinuma, Y. Matsushita, T. Yasuda, T. Sakurai, S. Seki, M. Takeuchi and K. Sugiyasu, *Nat. Chem.*, 2016, **9**, 493.
177. M. Endo, T. Fukui, S. H. Jung, S. Yagai, M. Takeuchi and K. Sugiyasu, *J. Am. Chem. Soc.*, 2016, **138**, 14347-14353.
178. L. Brunsveld, B. J. B. Folmer, E. W. Meijer and R. P. Sijbesma, *Chem. Rev.*, 2001, **101**, 4071-4098.
179. S. V. Kolotuchin and S. C. Zimmerman, *J. Am. Chem. Soc.*, 1998, **120**, 9092-9093.
180. R. P. Sijbesma, F. H. Beijer, L. Brunsveld, B. J. B. Folmer, J. H. K. K. Hirschberg, R. F. Lange, J. K. Lowe and E. W. Meijer, *Science*, 1997, **278**, 1601-1604.
181. F. H. Beijer, H. Kooijman, A. L. Spek, R. P. Sijbesma and E. W. Meijer, *Angew. Chem. Int. Ed.*, 1998, **37**, 75-78.
182. C. A. Hunter and J. K. M. Sanders, *J. Am. Chem. Soc.*, 1990, **112**, 5525-5534.
183. L. H. Doerrer, *Dalton Trans.*, 2010, **39**, 3543-3553.
184. F. Herbst, D. Döhler, P. Michael and W. H. Binder, *Macromol. Rapid Commun.*, 2013, **34**, 203-220.
185. K. C. Bentz and S. M. Cohen, *Angew. Chem. Int. Ed.*, 2018, **57**, 14992-15001.
186. V. W.-W. Yam, V. K.-M. Au and S. Y.-L. Leung, *Chem. Rev.*, 2015, **115**, 7589-7728.
187. J.-J. Zhang, W. Lu , R. W.-Y. Sun and C.-M. Che, *Angew. Chem. Int. Ed.*, 2012, **51**, 4882-4886.
188. X.-S. Xiao, W.-L. Kwong, X. Guan, C. Yang, W. Lu and C.-M. Che, *Chem. Eur. J.*, 2013, **19**, 9457-9462.
189. J. Carlos Lima and L. Rodríguez, *Chem. Soc. Rev.*, 2011, **40**, 5442-5456.
190. R. J. Puddephatt, *Chem. Soc. Rev.*, 2008, **37**, 2012-2027.
191. H. Ito, T. Saito, N. Oshima, N. Kitamura, S. Ishizaka, Y. Hinatsu, M. Wakeshima, M. Kato, K. Tsuge and M. Sawamura, *J. Am. Chem. Soc.*, 2008, **130**, 10044-10045.
192. M. J. Irwin, J. J. Vittal and R. J. Puddephatt, *Organometallics*, 1997, **16**, 3541-3547.

193. G. Jia, R. J. Puddephatt, J. D. Scott and J. J. Vittal, *Organometallics*, 1993, **12**, 3565-3574.

194. R. J. Puddephatt, *Coord. Chem. Rev.*, 2001, **216-217**, 313-332.

195. M. J. Katz, K. Sakai and D. B. Leznoff, *Chem. Soc. Rev.*, 2008, **37**, 1884-1895.

196. U. Helmstedt, S. Lebedkin, T. Höcher, S. Blaurock and E. Hey-Hawkins, *Inorg. Chem.*, 2008, **47**, 5815-5820.

197. W. Schneider, A. Bauer and H. Schmidbaur, *Organometallics*, 1996, **15**, 5445-5446.

198. E. Y. H. Hong, H. L. Wong and V. W. W. Yam, *Chem. Eur. J.*, 2015, **21**, 5732-5735.

199. V. W.-W. Yam, K. M.-C. Wong and N. Zhu, *J. Am. Chem. Soc.*, 2002, **124**, 6506-6507.

200. M. E. Robinson, D. J. Lunn, A. Nazemi, G. R. Whittell, L. De Cola and I. Manners, *Chem. Commun.*, 2015, **51**, 15921-15924.

201. M. E. Robinson, A. Nazemi, D. J. Lunn, D. W. Hayward, C. E. Boott, M.-S. Hsiao, R. L. Harniman, S. A. Davis, G. R. Whittell, R. M. Richardson, L. De Cola and I. Manners, *ACS Nano*, 2017, **11**, 9162-9175.

2 Ring-Opening Polymerisation of Low-Strain Nickelocenophanes: Synthesis and Magnetic Properties of Polynickelocenes with Carbon and Silicon Main Chain Spacers

2.1 Abstract

Polymetallocenes based on ferrocene, and to a lesser extent cobaltocene, have been well-studied, whereas analogous systems based on nickelocene are virtually unexplored. We have previously shown that poly(nickelocenylpropylene) $[Ni(\eta^5\text{-}C_5H_4)_2(CH_2)_3]_n$ is formed as a mixture of cyclic (**2.11$_x$**) and linear (**2.12**) components by the reversible ring-opening polymerisation (ROP) of tricarba[3]nickelocenophane $[Ni(\eta^5\text{-}C_5H_4)_2(CH_2)_3]$ (**2.5**). Herein we demonstrate the generality of this approach to main-chain polynickelocenes and describe the ROP of tetracarba[4]nickelocenophane $[Ni(\eta^5\text{-}C_5H_4)_2(CH_2)_4]$ (**2.6**), and disila[2]nickelocenophane $[Ni(\eta^5\text{-}C_5H_4)_2(SiMe_2)_2]$ (**2.10**) to yield predominantly insoluble homopolymers poly(nickelocenylbutylene) $[Ni(\eta^5\text{-}C_5H_4)_2(CH_2)_4]_n$ (**2.13**) and poly(tetramethyldisilylnickelocene) $[Ni(\eta^5\text{-}C_5H_4)_2(SiMe_2)_2]_n$ (**2.14**)**,** respectively. The ROP of **2.6** and **2.10** were also found to be reversible at elevated temperature. To access soluble high molar mass materials, copolymerisations of **2.5**, **2.6**, and **2.10** were performed. Superconducting quantum interference device (SQUID) magnetometry measurements of **2.13** and **2.14** indicated that these homopolymers behave as simple paramagnets at temperatures greater than 50 K, with significant antiferromagnetic coupling that is notably larger in carbon-bridged **2.11$_x$**/**2.12** and **2.13** compared to the disilyl-bridged **2.14**. However, the behaviour of these polynickelocenes deviates substantially from the Curie-Weiss law at low temperatures due to considerable zero-field splitting.

2.2 Introduction

Metal-containing polymers (metallopolymers), in which the inherent functionality of metal centres is combined with the facile processing typical of organic polymers, have long been regarded as a desirable target.[1-4] The diverse structure and properties which result as a function of metal incorporation have proved crucial in a variety of applications including catalysis,[5] antibacterial activity,[6] photovoltaics,[7, 8] information storage,[9] light emission,[10, 11] self-healing,[12, 13] stimuli-responsive behaviour,[4, 14] ceramic formation,[15-18] and nanopatterning.[19-21] Although the metallopolymer field has been subject to considerable recent progress, there have been few reports of well-characterised nickel-based polymers. Examples include π-conjugated nickel-polyyne copolymers,[22] metallophthalocyanine covalent organic frameworks,[23] bis(phosphine)nickel(II)-1,4-tetrafluorophenylene polymers,[24-26] polymers featuring nickel(II) complexes of Goedken's macrocycle (4,11-dihydro-5,7,12,14-tetramethyldibenzo[b,i][1,4,8,11]tetraazacyclotetradecine),[27] and those included in Figure 2.1.[28-33]

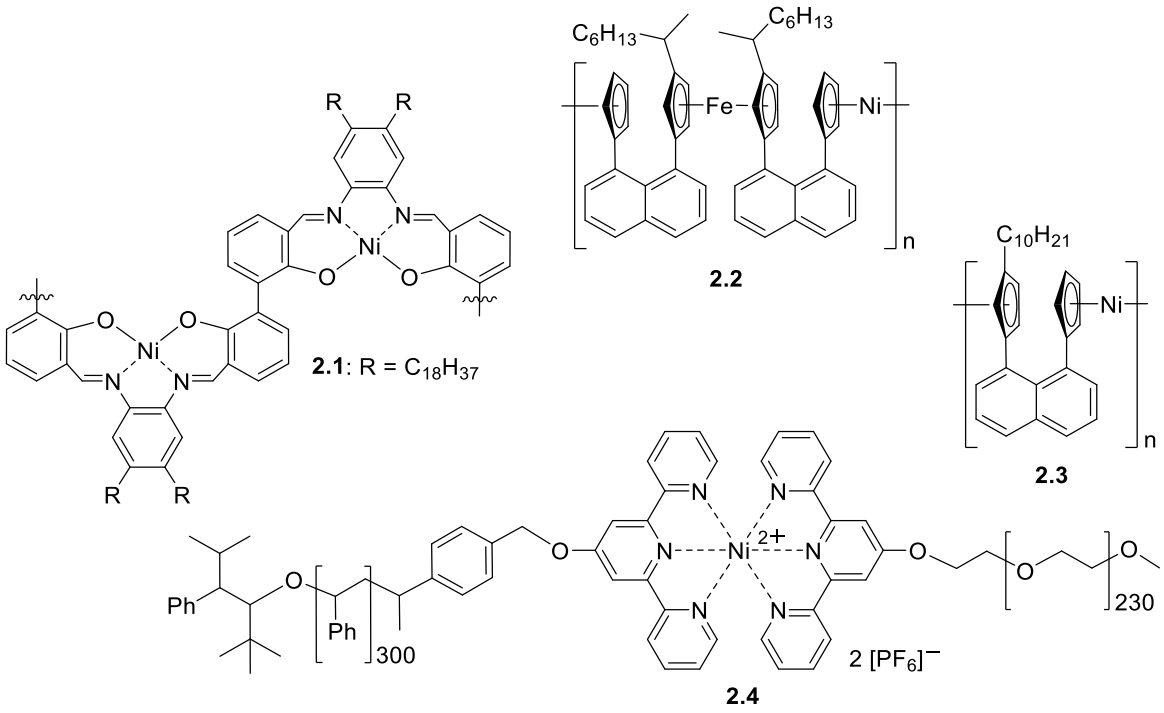

Figure 2.1. Examples of nickel-containing polymers.

ROP of strained [*n*]metallocenophanes has attracted extensive attention as a pathway to well defined metal-containing polymers and block copolymers.[34-37] In particular, polyferrocenylsilanes, prepared by the ROP of 18 valence electron (VE) silicon-bridged [1]ferrocenophanes, have been studied in depth[34, 38] and have thus attracted interest as redox active films, capsules, and gels,[39-41] precursors to catalytically active and magnetic ceramics,[42, 43] plasma and electron beam etch resists,[20, 44] and self-assembled materials with controlled lengths and architectures.[34, 45, 46] As a result of the 20 VE configuration of nickelocene, two electrons are accommodated in antibonding e''_1 orbitals, resulting in the elongation and weakening of the nickel–cyclopentadienyl (Ni–Cp) bond[47] and a subsequent increase in the Cp ligand tilt-angle, α, comparative to iron and cobalt metallocene analogues.[48-50] This weaker M–Cp bond is reflected in the low number of reported [*n*]nickelocenophane structures compared to well-studied [*n*]ferrocenophanes; currently reported species are limited to those bridged with unsubstituted alkylene chains where *n* is greater than 2, namely **2.5**–**2.8**,[51] naphthalene, **2.9**,[52] and disila linkers, **2.10**,[50] (Figure 2.2).

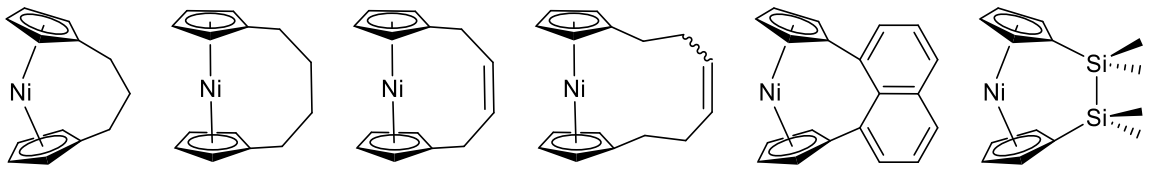

Figure 2.2. Currently structurally characterised [*n*]nickelocenophanes.

Currently, the only reported high molar mass polynickelocene, poly(nickelocenylpropylene) **2.12**, results from the ROP of tricarba[3]nickelocenophane **2.5** [α = 16.6(1)°] in pyridine (and a number of other polar organic solvents), Scheme 2.1.[51, 53] It was also demonstrated that, as a consequence of the weak Ni–Cp bonds (M–Cp dissociation energy is 250 kJ mol^{-1} for nickelocene vs. 305 kJ mol^{-1} for ferrocene),[54] the polynickelocene **2.12** can exist in either a static or labile state depending on the solvent conditions and, in the latter case, forms a dynamic equilibrium with monomer **2.5** and oligomers $\mathbf{2.11_x}$ (Scheme 2.1).[53] Studies of the

equilibrium between monomer **2.5** and polymer **2.11$_x$**/**2.12** allowed for the determination of enthalpic and entropic parameters that characterise this ROP process, revealing a small, favourable value of ΔH (−10 kJ mol^{-1}), and a very small and unfavourable value of ΔS (−21 J K^{-1} mol^{-1}).[53]

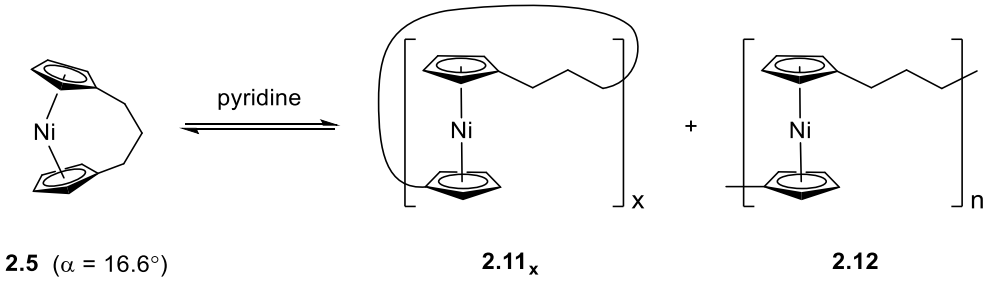

Scheme 2.1. Reversible ROP of tricarba[3]nickelocenophane **2.5**.

The polymerisation of **2.5** is believed to proceed via initial coordination of pyridine to the nickel centre and subsequent cleavage of the Ni–Cp bond,[53] a similar mechanism to that of the photolytic ROP of sila[1]ferrocenophanes,[55] although photoexcitation of the nickel-based monomer is unnecessary in this case presumably due to the inherent lability of the Ni–Cp bond. Analysis of the resulting poly(nickelocenylpropylene) by MALDI-TOF mass spectrometry revealed the presence of both cyclic and linear polymeric species, the former of which suggests that the pyridine initiator is substitutionally labile when coordinated at a [C_5H_4R]Ni centre, which may therefore allow for easy displacement by the propagating anionic Cp end group.[51]

SQUID magnetometry was used to determine the solid-state magnetic properties of poly(nickelocenylpropylene) **2.12**.[51] Above 28 K, polynickelocene **2.12** was found to behave as a simple paramagnet, and the magnetic susceptibility per monomer unit could be fitted to the Curie-Weiss law (with a small additional term for temperature-independent paramagnetism). In addition, a large, negative Weiss constant suggested significant antiferromagnetic spin-spin interactions. The magnetic susceptibility for **2.12** deviated from

that expected of a simple paramagnet below 28 K; however, the exact nature of the spin-spin interactions was not determined.[51]

Herein we report the synthesis of two novel polynickelocenes via ROP of low-strain nickelocenophanes, and a subsequent investigation of the ability of the parent [*n*]nickelocenophanes to copolymerise. Due to the presence of two unpaired electrons on every main-chain metal centre in polynickelocenes, the magnetic properties of the homopolymers were explored in detail using SQUID magnetometry.

2.3 Results and Discussion

2.3.1 Synthesis and ROP of Tetracarba[4]nickelocenophane (**2.6**)

In the case of the ROP of **2.5**, ΔH_{ROP} is small and negative, because the polymerisation is driven by the (albeit small) release of ring strain.[53] To provide an interesting comparison we explored the polymerisation of tetracarba[4]nickelocenophane **2.6**. This species has previously been prepared via the ring-closing metathesis of a divinyl substituted nickelocene followed by a subsequent hydrogenation.[56] In our work the synthesis of **2.6** was conducted via an analogous fly trap synthesis to that employed for the tricarba analogue **2.5**, involving the reaction of the dilithiated ligand $Li_2[(C_5H_4)_2(CH_2)_4]$ and $NiCl_2$. This gave **2.6** as a crystalline green solid in very low yield. Paramagnetic ^{1}H NMR spectroscopy revealed α and β cyclopentadienyl resonances at −251.2 and −256.6 ppm respectively, an α-CH_2 resonance at 138.2 ppm, and a β-CH_2 resonance at −1.1 ppm (Figure A2.1). These signals in the ^{1}H NMR spectrum are consistent with those previously reported.[56] Although the crystallographic data in the original report[56] were not provided in full due to poor refinement, in this case crystallisation from *n*-hexanes yielded dark green crystals which allowed for full characterisation by single crystal X-ray diffraction (Figure 2.3).[57]

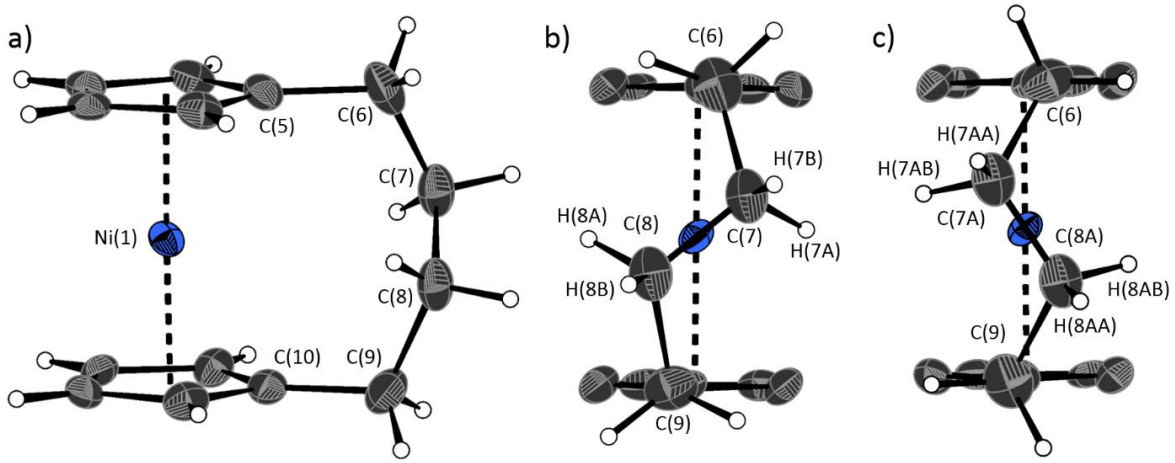

Figure 2.3. a) Molecular structure of **2.6**. Thermal ellipsoids displayed at the 50% probability level. Hydrogen atoms are pictured as spheres of arbitrary radii (and some have been omitted for clarity). The *ansa* bridge is disordered over two positions: C7/7A and C8/8A (for clarity, positions with highest relative occupancy (62%) are displayed). Alternate view of **2.6** displaying b) major (62%) and c) minor (38%) component of disordered bridge. Selected distances (Å) and angles (°): Ni(1)–Cp_{cent} 1.813(3)/1.817(3), α = 1.0(3), δ = 178.63(11) (the angle δ is defined as the Cp^C–Ni–Cp^C (Cp^C = Cp centroid) angle).

As expected, species **2.6** does not exhibit significant Cp ring tilt (α = 1.0(3)°; δ = 178.63(11)°). This lack of ring strain in **2.6** relative to the case of **2.5** led to the expectation that **2.6** would be resistant to ROP as, in general, the thermodynamic driving force for the ROP of [*n*]metallocenophanes is attributed to the strain imposed by *ansa*-bridging moieties in the cyclic monomers.[58-61] In order to probe the ROP propensity of **2.6** this species was exposed to similar ROP conditions to those successfully used for monomer **2.5** (pyridine, 0.74 M, 5 days, 20 °C, Scheme 2.2).[62] Although the green solution that was obtained upon dissolution of monomer **2.6** did not noticeably change colour, a light green solid (**2.13$_a$**) precipitated from solution, which was found to be insoluble in common organic solvents such as THF, dichloromethane, and benzene.

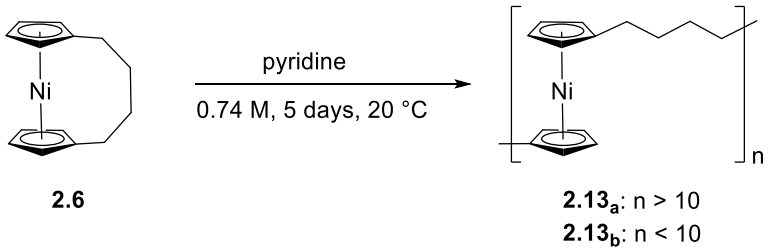

Scheme 2.2. ROP of **2.6** in pyridine (0.74 M).

The remaining solution was found to contain a small amount of oligomeric material (**2.13b**), which failed to precipitate upon addition of this solution to *n*-hexanes. Analysis by MALDI-TOF mass spectrometry led to the detection of oligomeric species up to n = 10 repeat units, with the presence of both linear and cyclic species (Figure 2.4). In addition, ^{1}H NMR spectroscopic analysis of the solution showed the presence of both the starting monomer **2.6** and new resonances at 225.9, between 176.3 and 194.9, and at −252.6 ppm, assigned to oligo(nickelocenylbutylene) **2.13b** (Figure A2.2).

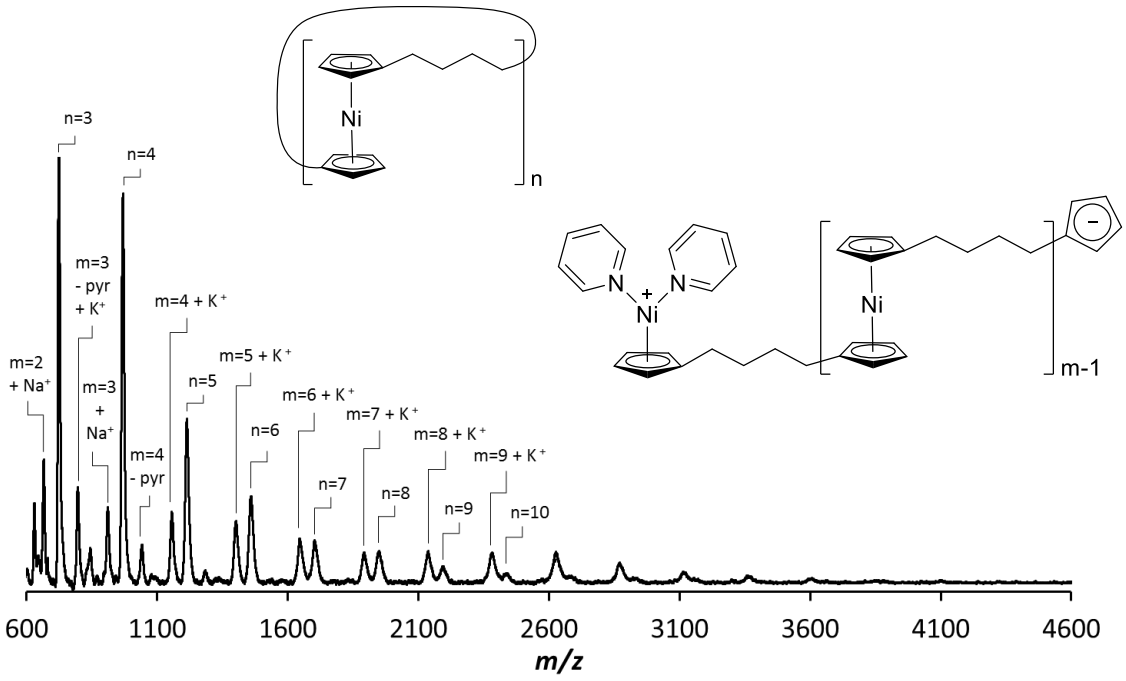

Figure 2.4. MALDI-TOF mass spectrum of the soluble, oligomeric product **2.13b**. Pyridine is represented by pyr, and sodium and potassium by their atomic symbols.

Wide-angle X-ray scattering (WAXS) analysis of the insoluble component (**2.13a**) led to the detection of crystalline reflections at 8.85, 5.93, 5.35, 5.05, 4.24, 3.63, and 2.95 Å (Figure

A2.3). We have tentatively assigned the structure of this insoluble component **2.13$_a$** to higher molecular weight poly(nickelocenylbutylene) (DP_n > 10). It appears that the polynickelocene becomes increasingly insoluble as the molecular weight of the polymer increases, which may at least partly be a consequence of the crystallinity. We previously reported that THF-soluble poly(nickelocenylpropylene) oligomers/polymer **2.11$_x$/2.12** displayed crystalline reflections in the WAXS analysis. As a result of the linear –$(CH_2)_4$– linkers, **2.13$_a$** appears to mirror linear polyethylene which lacks solubility in common organic solvents due to crystallinity and the lack of solubilising flexible side groups.

Low concentrations and increased temperatures were found to favour depolymerisation of **2.11$_x$/2.12** and [*n*]nickelocenophane formation.[53] To study whether an analogous depolymerisation of **2.13$_a$** would occur, this species was stirred in d_5-pyridine at low concentration (0.11 M, 20 °C) for 1 week; however, no paramagnetic resonances were observed by ^{1}H NMR spectroscopy suggesting that there was no retroconversion to monomer. This is a possible consequence of the insolubility of **2.13$_a$** at room temperature. The suspension of **2.13$_a$** was then heated for 24 h at a range of different temperatures, from 30 to 80 °C, and analysed by in situ ^{1}H NMR spectroscopy (Figure 2.5). The results indicated that below 50 °C **2.13$_a$** is essentially insoluble in pyridine. However, at 50 °C the emergence of resonances attributed to both **2.6** and **2.13** were detected, which suggests that a similar dynamic equilibrium exists to the case of **2.5** and **2.11$_x$/2.12**. This is only apparent at higher temperatures, presumably as heating is necessary to solubilise **2.13$_a$**. Temperature also affects the position of equilibrium, with monomer increasingly favoured at higher temperatures as in the case of **2.5** and **2.11$_x$/2.12**.[53]

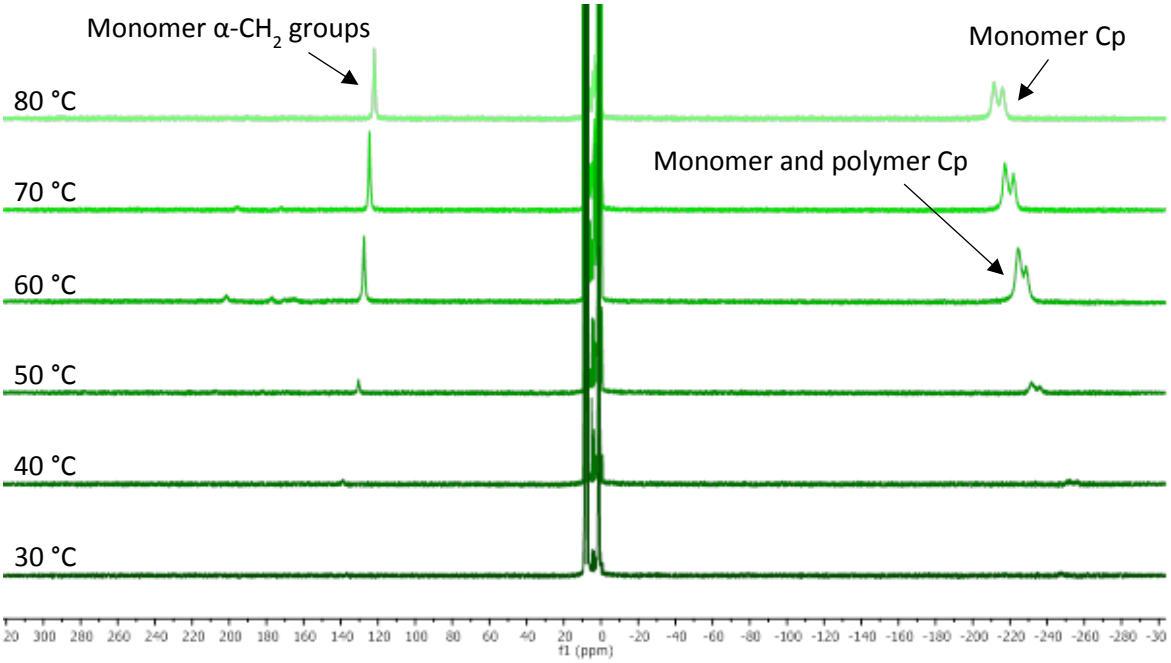

Figure 2.5. Stacked ^{1}H NMR spectra (500 MHz, d_5-pyridine) that show the effect of temperature on the retroconversion of polymer **2.13$_a$** into monomer **2.6**.

2.3.2 ROP of Tetramethyldisila[2]nickelocenophane (**2.10**)

Disila[2]nickelocenophane **2.10**, which has been previously reported by Braunschweig and co-workers,[50] was synthesised as previously described via lithiation of the 'fly trap' ligand and subsequent reaction with $NiCl_2$ to give a green crystalline solid. Species **2.10** possesses a tilt-angle of 9.4(8)°, an intermediate value between the tilt-angles of **2.5** and **2.6** (α = 16.6° and 1.0°, respectively). Monomer **2.10** was also subjected to similar ROP conditions found for **2.6** to probe its propensity to polymerise (pyridine, 0.35 M, 32 h, 20 °C). In a similar manner to the ROP of **2.6**, a light green solid (**2.14$_a$**) precipitated from solution, which was found to be insoluble in common organic solvents such as THF, dichloromethane, and benzene (Scheme 2.3).

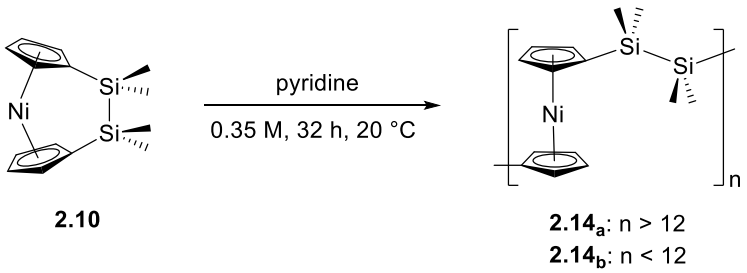

Scheme 2.3. ROP of disila[2]nickelocenophane **2.10** in pyridine.

A small portion of the product (5%) was found to be soluble in THF, and upon transfer into *n*-hexanes, precipitation of light green material (**2.14$_b$**) was observed. ^{1}H NMR spectroscopy of **2.14$_b$** revealed Cp resonances at −243 and −229 ppm (Figure A2.4), and $SiMe_2$ resonances at 15.3 ppm. MALDI-TOF analysis revealed the presence of oligomers (DP_n < 12) assigned to two linear modes (Figure 2.6).

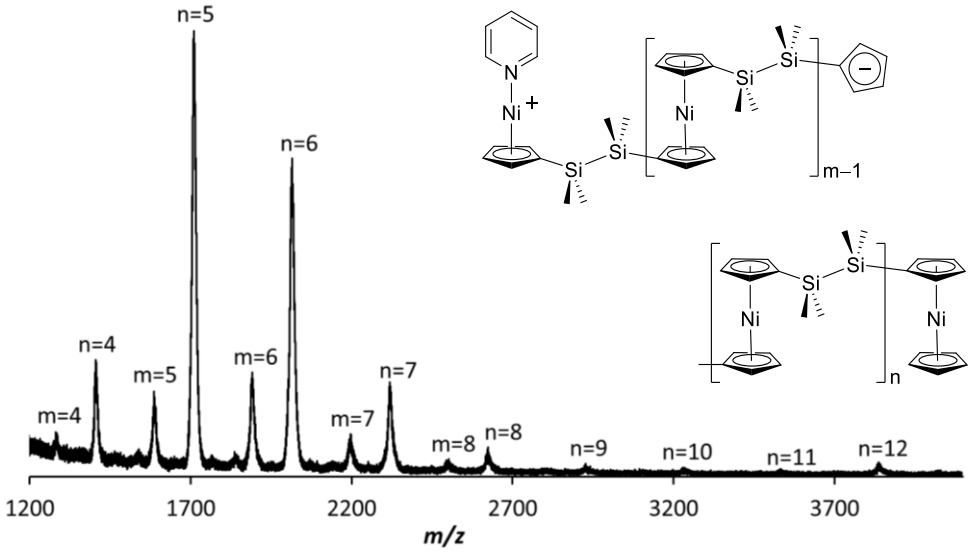

Figure 2.6. MALDI-TOF mass spectrum of oligo(tetramethyldisilylnickelocene) **2.14$_b$**.

The insoluble polymeric material **2.14$_a$** is likely to be a high molecular weight (DP_n > 12) fraction of poly(tetramethyldisilylnickelocene), which is analogous to the case of **2.13$_a$** formed during the ROP of **2.6**. Crystallinity may again contribute to the insolubility as WAXS analysis of **2.14$_a$** showed reflections at 9.09, 6.24, 5.81, 4.57, and 3.70 Å (Figure A2.5).

In a similar manner to poly(nickelocenylbutylene) **2.13**, when reintroduced to (deuterated)

pyridine at room temperature and low concentration (0.11 M), no depolymerisation of **2.14$_a$** occurred, as evidenced by a lack of monomer resonances in the ^{1}H NMR spectrum. The insoluble polymer **2.14$_a$** was then equilibrated in d_5-pyridine at low concentration (0.11 M) for 24 h at a range of different temperatures, from 30 to 80 °C, and analysed by in situ ^{1}H NMR spectroscopy (Figure A2.6). At temperatures up to 50 °C an increase in the intensity of resonances attributed to **2.10** could be observed. At 50 °C a small shoulder resonance attributed to polymer can also be observed in the paramagnetic region. This clearly demonstrates the retroconversion of **2.14** to give **2.10**. Above 50 °C however, Cp resonances decrease in intensity alongside the emergence of new unassigned resonances in the diamagnetic region, suggesting the onset of decomposition of the nickelocene-based species.

2.3.3 Copolymerisation Experiments

In general, although there are some reported examples of copolymers containing nickelocene units in the main chain,[30, 31, 63] they are far less common than their iron and cobalt analogues. In order to circumvent the insolubility of homopolymers **2.13$_a$** and **2.14$_a$** with tetracarba and disilyl linkers, respectively, we explored random copolymerisation of the respective monomers **2.6** and **2.10**. This was expected to reduce the crystallinity of the resulting materials by incorporating repeat units derived from a different [*n*]nickelocenophane, and to thereby promote solubility.

2.3.3.1 Random Copolymerisation of **2.5** and **2.10**

A copolymerisation of equimolar amounts of tricarba-bridged **2.5** and disilyl-bridged **2.10** was conducted (pyridine, 0.08 M, 32 h, 20 °C, Scheme 2.4). Unlike the ROP of **2.10**, the solution remained clear during the reaction. The pyridine was removed, and precipitation of the resulting material from THF into a vortex of *n*-hexanes allowed the isolation of copolymer **2.15** as a light green powder in 39% yield.

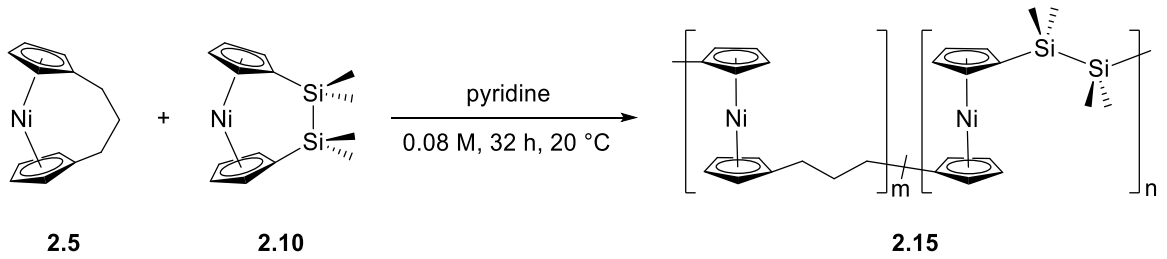

2.5 **2.10** **2.15**

Scheme 2.4. Co-ROP of [*n*]nickelocenophanes **2.5** and **2.10**.

^{1}H NMR spectroscopy in d_6-benzene revealed eight broad resonances which were assigned to the Cp environments (ranging from −272 to −228 ppm: see Figure A2.9). Resonances at 15.3, 10.2 and between 173–176 ppm were assigned to $SiMe_2$ groups, and the β-CH_2 and α-CH_2 protons of the propyl linker respectively, indicating that the polymer **2.15** contained repeat units derived from both monomers **2.5** and **2.10**. These assignments were made based on the resonances of homopolymers **2.11$_x$**/**2.12** and **2.14$_b$** in their respective spectra.

Further evidence for copolymerisation was provided by MALDI-TOF mass spectrometry (Figure 2.7), which revealed the presence of low molecular weight linear and cyclic polymer material (< 3,000 g mol^{-1}), assigned to combinations of repeat units derived from both **2.5** and **2.10** (in addition to cyclic homopolymer derived solely from **2.5**). The proposed mechanism for polymerisation of **2.5** in donor solvents involves cleavage of the Ni–Cp bond to give a 14 VE nickel cation, and subsequent coordination of solvent, with polymer formation by either a chain-growth or step-growth mechanism (or a combination of both).[53] The formation of copolymer **2.15** suggests that both [*n*]nickelocenophanes **2.5** and **2.10** polymerise via a similar Ni–Cp bond cleavage pathway. DLS measurements on copolymer **2.15** (R_h = 3.9 nm, Figure A2.10) indicated a molecular weight, M_w, of ~25,000 g mol^{-1} and DP_n of ~95 (relative to calibration with poly(ferrocenyldimethylsilane) in THF)[64, 65] which, alongside evidence from MALDI-TOF mass spectrometry, demonstrates the inclusion of monomer units derived from **2.10** into a high molecular weight soluble polymer. The DLS measurements also suggest that MALDI-TOF detects only the low-molecular-weight fraction, as has been observed previously with poly(nickelocenylpropylene).[51]

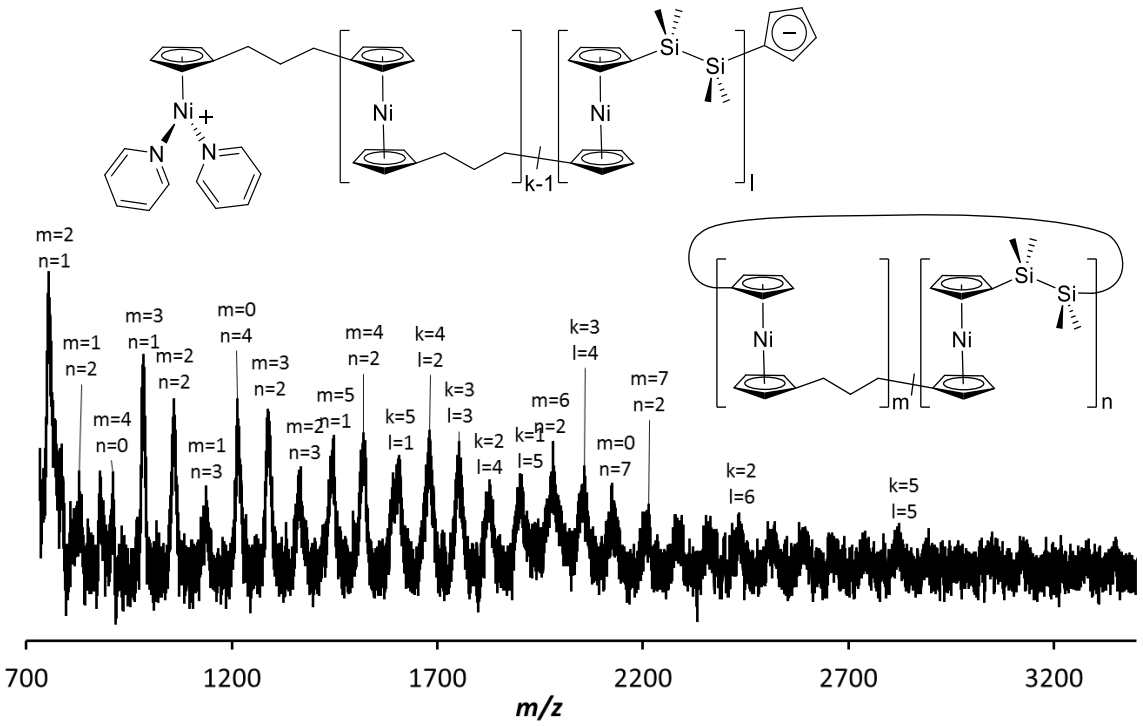

Figure 2.7. MALDI-TOF mass spectrum of copolymer **2.15**.

2.3.3.2 Random Copolymerisation of **2.6** and **2.10**

The potential copolymerisation of tetracarba-derived **2.6** with disilyl-bridged **2.10**, which both polymerise spontaneously in pyridine to give largely insoluble products **2.13**$_{\mathbf{a}}$ and **2.14**$_{\mathbf{a}}$, was also studied (Scheme 2.5). Precipitation of light green material (**2.16**$_{\mathbf{a}}$) was observed during the course of the reaction, and this solid was found to be insoluble in organic solvents. However, a soluble polymeric fraction **2.16**$_{\mathbf{b}}$ was also isolated in 15% yield after precipitation into *n*-hexanes. It is interesting to note that the yield of isolable soluble copolymeric material is only slightly increased relative to the two independent homopolymerisations of monomers **2.6** and **2.10** (~5% in each case).

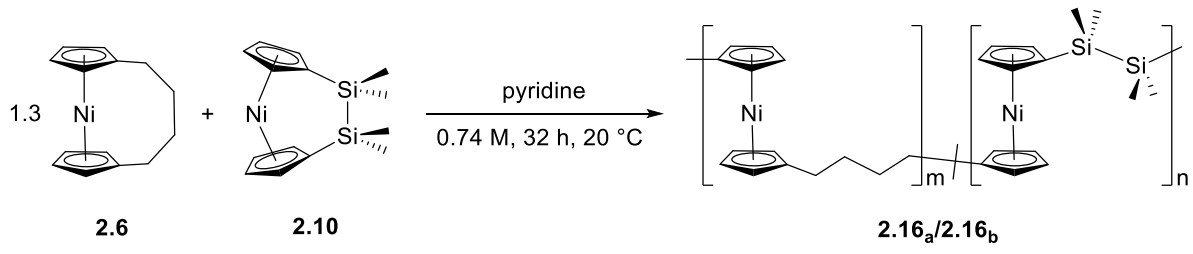

Scheme 2.5. Co-ROP of [*n*]nickelocenophanes **2.6** and **2.10**.

^{1}H NMR spectroscopy of **2.16$_b$** indicated formation of a new polymeric product, with resonances ranging from −258 to −236 ppm (see Figure A2.11) corresponding to Cp environments. The resonance at 15.2 ppm was assigned to $SiMe_2$ groups, and that at 176 ppm to the protons within the C_4 linker. MALDI-TOF MS (Figure 2.8) of the polymeric product detected cyclic oligomeric copolymeric species of up to 22 repeat units (incorporating monomer units derived from both **2.6** and **2.10**). DLS indicated the presence of an oligomeric species (R_h = 1.4 nm, Figure A2.12) of M_w = ~3,800 g mol^{-1} and DP_n = ~14 (relative to calibration with poly(ferrocenyldimethylsilane) in THF).[65, 66] WAXS analysis of the insoluble component **2.16$_a$** was very similar to that of disilyl-bridged homopolymer **2.14$_a$**, with reflections detected at 6.12, 5.74, and 3.63 Å (Figure A2.13).

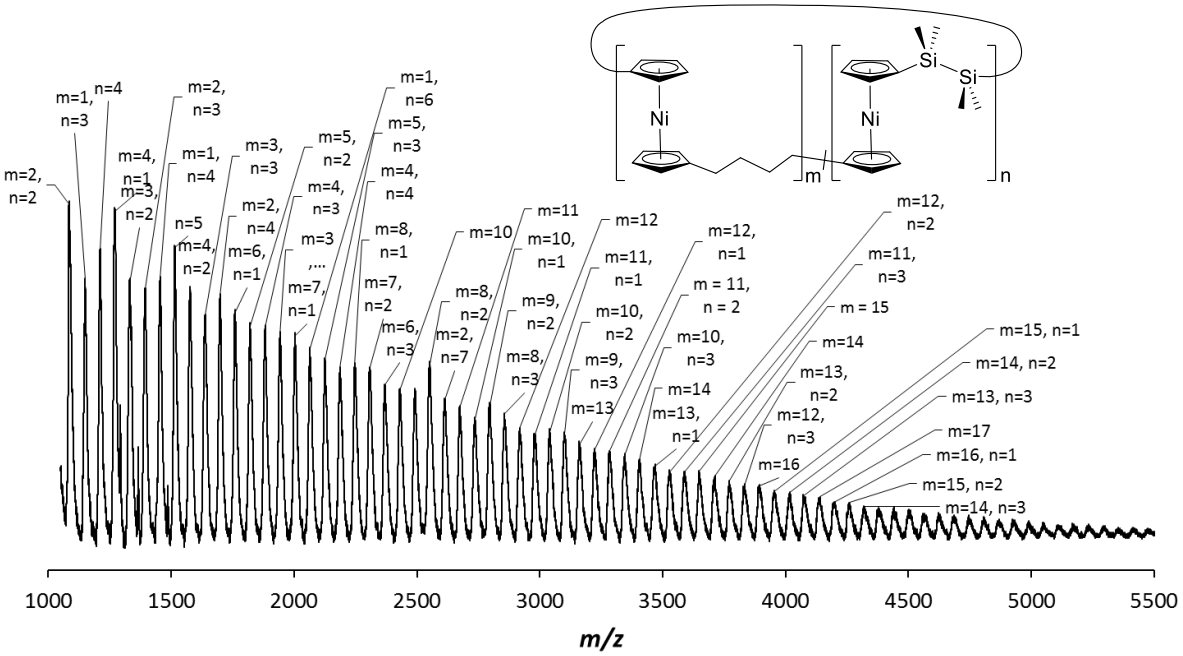

Figure 2.8. MALDI-TOF mass spectrum of copolymer **2.16$_b$**.

2.3.3.3 Random Copolymerisation of **2.5** and **2.6**

Finally, the copolymerisation of the C_3- and C_4-bridged monomers, **2.5** and **2.6**, was attempted (Scheme 2.6). A colour change was observed from dark blue to dark green and a small amount of a light-green precipitate **2.17$_a$** formed. A THF-soluble light-green polymeric product (**2.17$_b$**) was isolated via precipitation into *n*-hexanes, in 28% yield. ^{1}H NMR

spectroscopy of **2.17b** showed a broad singlet resonance assigned to be overlapping Cp environments (−252 ppm, Figure A2.14); the parent tricarba- and tetracarba-bridged homopolymers display single Cp resonances at −254 and −253 ppm respectively. Two resonances at 174 and 176 ppm were assigned to environments similar to those in **2.12** and **2.13**, respectively, with reference to the homopolymer ^{1}H NMR spectra. ^{1}H NMR analysis of **2.13** also displayed a peak at 226 ppm assigned to the tetracarba-spacer, but this did not appear in the spectrum for **2.17b**.

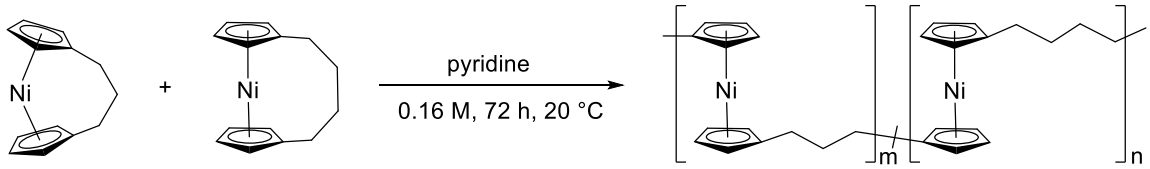

2.5 **2.6** **2.17a/2.17b**

Scheme 2.6. Co-ROP of [*n*]nickelocenophanes **2.5** and **2.6**.

MALDI-TOF of **2.17b** indicated the presence of some co-oligomeric species, with peaks identifiable up to a molecular weight of ~3600 g mol^{-1} (Figure A2.15). In addition, DLS analysis indicated the formation of a polymeric product with a molecular weight of ~24,000 g mol^{-1} and a DP_n of ~103 (relative to calibration with poly(ferrocenyldimethylsilane) in toluene, see Figure A2.16).[65, 67]

The WAXS data of the insoluble component **2.17a** was similar to that of both the tricarba- and tetracarba-bridged homopolymers with reflections detected at 8.70, 6.05, 5.34, 5.10, and 3.65 Å (Figure A2.17).

2.3.3.4 Attempted Random Copolymerisation of **2.5** and [2]Cobaltocenophane **2.18**

To expand the scope of copolymerisations further, we also explored whether the method of synthesising soluble random copolymers could be extended to include cobaltocene repeat units. The copolymerisation of equimolar amounts of **2.5** and [2]cobaltocenophane **2.18**[35, 68, 69] was therefore attempted (Scheme 2.7). No obvious colour change was observed during

the reaction from the original red/brown, but a dark grey solid (**2.19$_a$**) precipitated from the reaction solution which proved insoluble in common organic solvents such as THF, dichloromethane, and benzene. Upon precipitation of the THF-soluble portion of the residue into *n*-hexanes, a grey solid (**2.19$_b$**) with poor solubility in organic solvents was isolated in very low yield. For comparison, homopolymerisation of the parent [*n*]nickelocenophane gave green poly(nickelocenylpropylene), whereas the parent [*n*]cobaltocene yielded a dark purple polymer.[35]

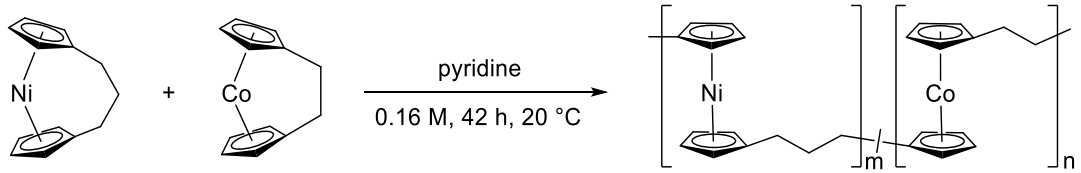

2.5 **2.18** **2.19$_a$/2.19$_b$**

Scheme 2.7. Co-ROP of [*n*]nickelocenophane **2.5** and [*n*]cobaltocenophane **2.18**.

^{1}H NMR spectroscopy of **2.19$_b$** revealed a peak at −250.5 ppm assigned to the cyclopentadienyl resonances of nickelocene environments, and resonances at −46.1 and −64.9 ppm attributed to cobaltocene environments (Figure A2.18). The nickelocene-based cyclopentadienyl resonance appears at the same chemical shift as that observed for homopolymer **2.11$_x$/2.12**. As a ^{1}H NMR spectrum was not available for the homopolymer formed by the ROP of **2.18** due to its insolubility,[35] the assignments made for the cobalt Cp resonances are given credibility as they did not match the resonances of **2.18**, and by the MALDI spectrum of the product, which clearly demonstrated the presence of oligomeric species. A peak at 173.7 ppm was attributed to the CH_2 groups in the carbon linker of the copolymer. ^{1}H NMR spectroscopic analysis (Figure A2.19) of the hexanes soluble supernatant revealed the presence of unreacted **2.5** and **2.18**, alongside a new resonance at −29 ppm which we assign to the cyclopentadienyl environment of oligomeric cobaltocene (higher molecular weight poly(cobaltocenylethylene) is insoluble).

MALDI-TOF mass spectrometry also provided evidence for the formation of copolymer

2.19 (Figure A2.20). Peaks up to ~1100 g mol^{-1} were recorded for **2.19$_b$**, as well as those for oligomeric species derived from both monomers. Analysis by DLS indicated the presence of an oligomeric product (R_h = 1.2 nm) with a molecular weight of ~2900 g mol^{-1} and a DP of ~13 (relative to calibration with poly(ferrocenyldimethylsilane) in toluene, see Figure A2.21).[65, 70]

It is perhaps not unexpected that co-oligomer **2.19$_b$** displays poor solubility in organic solvents. The homopolymerisation of **2.18** yields a highly insoluble product which was characterised following oxidation to the polyelectrolyte.[35] It is likely that the difference in the rates of ROP of **2.5** and **2.18** leads to a "block-like" co-oligomeric product which possesses segments derived from the Ni and Co monomers, where the latter are insoluble in organic solvents.

2.3.4 Magnetic Properties of Polynickelocenes **2.11$_x$/2.12**, **2.13$_a$**, and **2.14$_a$**

Polynickelocenes are unusual materials with two unpaired electrons on every main chain metal centre. With the preparation of two new polynickelocenes, **2.13$_a$** and **2.14$_a$**, we expanded the original study of **2.11$_x$/2.12** by SQUID magnetometry to include these materials and the parent [*n*]nickelocenophanes. We focussed primarily on the materials that were more compositionally homogeneous in nature, and so the copolymers were excluded from this study.

The magnetic susceptibilities of polynickelocenes **2.13$_a$** and **2.14$_a$**, as well as [*n*]nickelocenophanes **2.6** and **2.10**, were studied in the solid state using SQUID magnetometry at an applied magnetic field of 0.1 Tesla in the temperature range 6–300 K. The insoluble fractions of the tetracarba- and disila-bridged polynickelocenes were studied due to their high yields compared to the soluble fractions. For each material the observed magnetic susceptibility per mole of nickel (χ_m) at each temperature was almost identical for zero-field cooled (ZFC) and field cooled (FC) measurements (Figures A2.22 and A2.23),

hence only ZFC data are shown. Furthermore, no evidence was found for magnetic hysteresis at 5 and 300 K (Figures A2.24 and A2.25).

The plot of χ_m^{-1} vs T (Figures A2.26b – A2.30b) is linear in the region 50–300 K for all complexes studied. Hence, the observed susceptibility data were fitted to the Curie-Weiss law, where C is the Curie constant and Θ is the Weiss temperature, with the addition of a small term for a temperature-independent paramagnetic contribution, χ_{TIP} (Equation 1).

$$\chi_m = \frac{C}{T-\Theta} + \chi_{TIP} \qquad \textbf{Equation 1}$$

The parameters obtained from the least-squares Curie-Weiss fits for **2.13a**, **2.14a**, **2.6**, and **2.10**, are collected in Table 2.1, together with data for the tricarba[3]nickelocenophane **2.5**, and those previously reported for poly(nickelocenylpropylene), **2.11x/2.12**.[51]

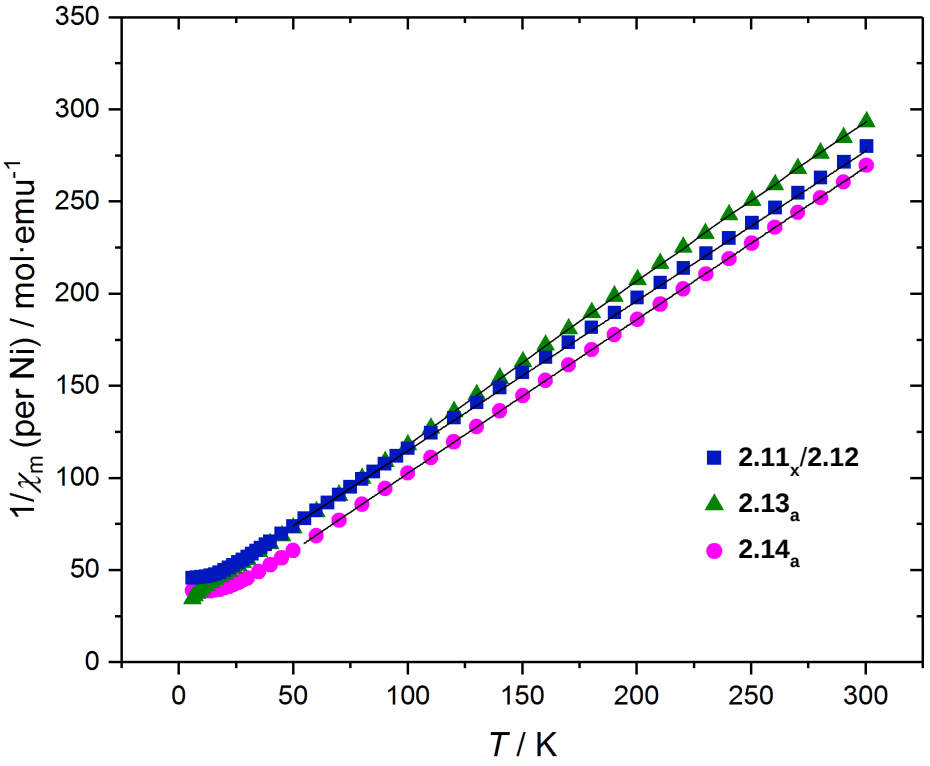

Figure 2.9. Temperature dependence of inverse magnetic susceptibility per nickel ($1/\chi_m$) for poly(nickelocenylpropylene), **2.11x/2.12**, poly(nickelocenylbutylene), **2.13a**, and poly(nickelocenyltetramethyldisilane), **2.14a**. The black lines represent the best fits of the data to Equation 1 in the Curie-Weiss regime (50–300 K).

The μ_{eff} values for **2.13a** and **2.14a** (2.94 and 3.01 μ_B, respectively) agree well with the value

previously reported for **2.11$_x$/2.12** (2.94 μ_B) in the Curie-Weiss regime.[51] These are slightly greater than μ_{eff} values reported for monomeric nickelocenes (2.88–2.92 μ_B).[52, 71-73]

In a Curie-Weiss model, interactions between magnetic centres are considered in a mean field approach, parameterised by the Weiss temperature (Θ). All complexes studied showed negative values of Θ, characteristic of antiferromagnetic spin-spin interactions. The magnitude of Θ is significantly larger for polynickelocenes **2.11$_x$/2.12**, **2.13$_a$**, and **2.14$_a$** (range −37.1 to −21.3 K), as compared with nickelocenophanes **2.5**, **2.6**, and **2.10** (range −5.0 to −3.4 K), which suggests greater antiferromagnetic coupling in the polymeric species. The antiferromagnetic spin-spin interactions found in **2.5**, **2.6**, and **2.10** can be attributed to intermolecular interactions, and, assuming these are same order of magnitude for mononuclear and polynuclear nickelocenes, we postulate that the greater antiferromagnetic coupling in the **2.11$_x$/2.12**, **2.13$_a$**, and **2.14$_a$** is caused by a through-bond coupling via the main chain spacers. This is in contrast to magnetic behaviour for the heteroleptic polyvanadocene $[V(\eta^5\text{-}C_5H_4)(\eta^7\text{-}C_7H_6)Sn^tBu_2]_n$ ($n \approx 99/204$) reported by Braunschweig et al., which shows a smaller negative Θ value than the corresponding mononuclear vanadocenophane, $[V(\eta^5\text{-}C_5H_4)(\eta^7\text{-}C_7H_6)Sn^tBu_2]$.[74]

Comparing the Curie-Weiss Θ values within the series of polynickelocenes reveals that the strength of antiferromagnetic interaction decreases in the order of **2.11$_x$/2.12** > **2.13$_a$** > **2.14$_a$**, suggesting that the all-carbon bridges in **2.11$_x$/2.12** and **2.13$_a$** better mediate spin-spin interactions compared to the disilyl-bridge in **2.14$_a$**. However, we can only draw tentative conclusions based on Curie-Weiss Θ values alone. Differential Scanning Calorimetry (DSC) allowed the cautious assignation of the small melt transitions of **2.13$_a$** and **2.14$_a$** close to 373 K (Figures A2.7 and A2.8). This is consistent with the WAXS data acquired at 295 K, which shows several peaks characteristic of the presence of a significant degree of crystallinity. Below 300 K polynickelocene Cp rings would likely display little molecular motion;[75] thus,

any difference between the polymers could be attributed to the bridging moieties. Reports have described greater motion in silicon-based materials at low temperature due to the inherent flexibility and lower chain torsion manifested in the longer C–Si and Si–Si bonds compared to C–C bonds.[76-78] This may contribute to the lower antiferromagnetic spin-spin interactions in the disilyl-bridged polynickelocene **2.14$_a$** compared to those in the carbon-bridged **2.11$_x$**/**2.12** and **2.13$_a$**.

The magnetic susceptibility of the mononuclear and polynuclear nickelocenes in this study deviate significantly from simple paramagnetic behaviour below 50 K. Similar low temperature magnetic behaviour has been observed in nickelocene by Prins et al., who attributed it to the large zero-field spitting (*D*) in the triplet ground state.[73] Therefore, the SQUID data for **2.5**, **2.6**, **2.10**, **2.11$_x$**/**2.12**, **2.13$_a$**, and **2.14$_a$** were simulated using a fitting procedure to the spin Hamiltonian for the Zeeman splitting (Equation 2).[79]

$$\hat{H} = \hat{H}_{Zee} + \hat{H}_{ZFS} \qquad \textbf{Equation 2}$$

where

$$\hat{H}_{Zee} = g\mu_B \vec{B} \cdot \vec{S} \qquad \textbf{Equation 3}$$

$$\hat{H}_{ZFS} = D[S^2 - {}^1/_3\, S(S+1)] \qquad \textbf{Equation 4}$$

All complexes were treated as individual $S = 1$ units, using the variables g, Θ, χ_{TIP}, and D across the entire temperature range, 6–300 K. The best fit to the $\chi_m T$ data are shown in Figure 2.10, and the simulated parameters are listed in Table 2.1. The magnitude of the zero-field splitting simulated for [*n*]nickelocenophanes **2.5**, **2.6**, and **2.10** (range 32.0–32.3 cm^{-1}), is of a similar order to those previously reported for nickelocene.[73, 80-82] The *D* values for **2.11$_x$**/**2.12**, **2.13$_a$**, and **2.14$_a$** (range 42.0–57.6 cm^{-1}) are significantly larger than those of the parent [*n*]nickelocenophanes, suggesting a larger zero-field splitting in the polymeric species. The Weiss temperatures (Θ) obtained from these simulations have significantly larger negative values for carbon-bridged polynickelocenes **2.11$_x$**/**2.12** and **2.13$_a$** (−23.5 and

−25.0 K respectively) compared with disilyl-bridged polynickelocene **2.14a** (−7.0 K), and are almost negligible for nickelocenophanes **2.5**, **2.6**, and **2.10**.

Solid state samples of **2.13a** and **2.14a** did not show an X-band electron paramagnetic resonance (EPR) spectrum at 85 K. Nussbaum *et al.* also failed in measuring an EPR signal of nickelocene, which was attributed to a strong zero-field splitting in the triplet ground state.[83]

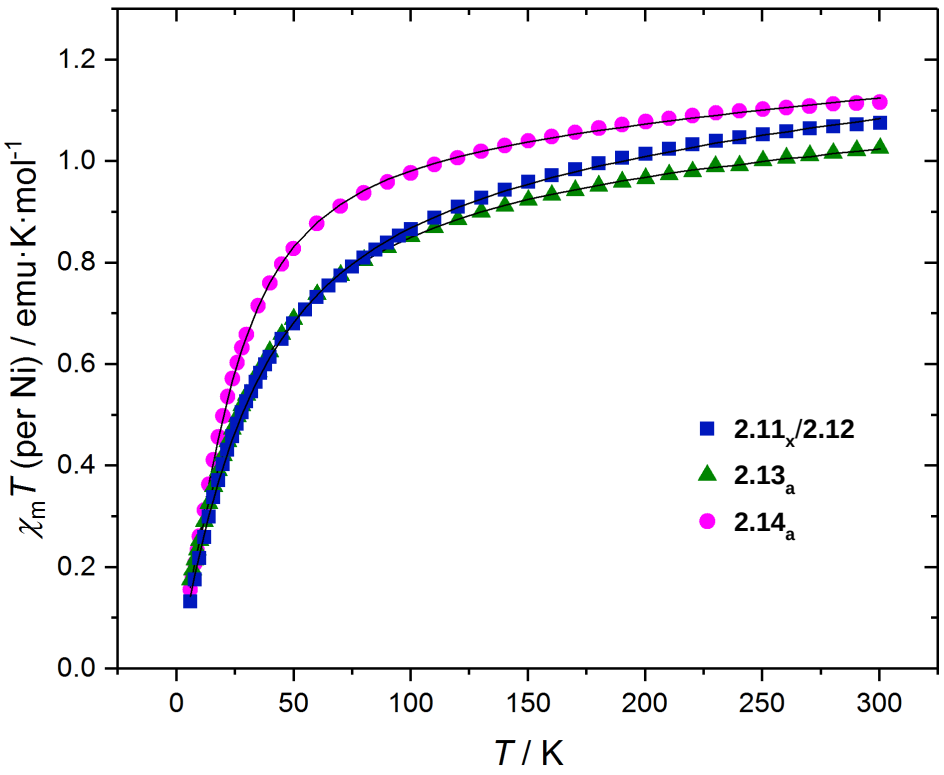

Figure 2.10. Temperature dependence of the observed $\chi_m T$ product (per Ni) for poly(nickelocenylpropylene), **2.11x/2.12**, poly(nickelocenylbutylene), **2.13a**, and poly(nickelocenyltetramethyldisilane), **2.14a**. The black lines represent the simulated data in the range 6–300 K.

Table 2.1. Parameters derived from fitting of the variable temperature magnetic susceptibility data to the Curie-Weiss law (Equation 1) or the spin Hamiltonian (Equation 2).

	Curie-Weiss fit (50–300 K)			***JulX simulation (6–300 K)***			
	μ_{eff} (μ_B)	Θ (K)	χ_{TIP} /10^6 (emu mol^{-1})	μ_{eff} (μ_B)	Θ (K)	χ_{TIP} /10^6 (emu mol^{-1})	D (cm^{-1})
2.11$_x$/2.12[51]	2.94	−37.1	168	2.90	−23.5	366	57.6
2.13$_a$	2.94	−29.2	109	2.91	−25.0	167	42.0
2.14$_a$	3.01	−21.3	53.1	2.89	−7.0	353	55.4
2.5	2.83	−4.2	0	2.82	−0.8	0	32.2
2.6	2.90	−5.0	0	2.88	−0.7	49.0	32.3
2.10	2.97	−3.4	0	2.92	0.6	66.4	32.0

2.4 Summary

Due to the recent discovery of the reversible nature of the polymerisation of moderately strained [3]nickelocenophane **2.5** to give polynickelocene **2.11$_x$/2.12**,[53] we aimed to expand the field and synthesise further polynickelocenes. The ROP of untilted [Ni(η^5-C_5H_4)$_2$(CH_2)$_4$] (**2.6**) was performed in pyridine to yield predominantly insoluble poly(nickelocenylbutylene) (**2.13$_a$**), an unusual example of the ROP of an [*n*]metallocenophane in the absence of Cp ring tilt. ROP of moderately strained [Ni(η^5-C_5H_4)$_2$($SiMe_2$)$_2$] (**2.10**) also yielded predominantly insoluble polymeric products, although polymeric material with increased solubility was synthesised by copolymerisation of [*n*]metallocenophane monomers. Additionally, the ROPs of **2.6** and **2.10** were found to be reversible at elevated temperatures. As polynickelocenes **2.11$_x$/2.12**, **2.13$_a$**, and **2.14$_a$** contain two unpaired electrons per nickelocene unit, we performed SQUID magnetometry

measurements that indicated that they act as simple paramagnets at higher temperatures and display significant antiferromagnetic coupling that occurs primarily in a through-bond manner. However, at low temperatures these polynickelocenes deviate from the Curie-Weiss behaviour due to substantial zero-field splitting. Further work will focus on determining why **2.6** undergoes ROP to give **2.13**, despite its apparent lack of ring strain. Additionally, the redox properties of the nickelocenophanes and polynickelocenes explored here are also of interest and are under exploration.

2.5 Experimental

2.5.1 Materials and Equipment

All reactions and product manipulations of molecular species were carried out under an inert atmosphere of dinitrogen or argon using standard Schlenk line or glovebox techniques (MBraun glovebox MB150G-B maintained at < 0.1 ppm H_2O and < 0.1 ppm O_2), unless otherwise stated. Dry hexanes, dichloromethane, and toluene were obtained from a Grubbs-type solvent system employing alumina and supported copper columns.[84] THF was distilled under dinitrogen from Na/benzophenone. Pyridine and d_5-pyridine were purchased from Fluka and Sigma-Aldrich respectively and distilled from CaH_2 prior to use, and d_6-benzene was purchased from Sigma-Aldrich and stored over molecular sieves.[85] Silica gel (for flash chromatography was purchased from VWR and used as received. Celite 521 was obtained from Sigma-Aldrich and heated to 200 °C for 16 h prior to use. Sodium metal, dicyclopentadiene, anhydrous nickel(II) chloride and 1,2-dichloro-1,1,2,2-tetramethyldisilane were used as supplied by Sigma-Aldrich. 1,3-dibromopropane and 1,4-dibromobutane were purchased from Sigma-Aldrich and distilled from CaH_2 prior to use. Anhydrous 1,3-dimethyl-3,4,5,6-tetrahydro-2(1H)-pyrimidinone (DMPU) was purchased from Sigma-Aldrich and degassed via three freeze-pump-thaw cycles. $Na[C_5H_5]$[86] and the fly trap ligands $Li_2[(C_5H_4)_2(CH_2)_3]$ and $Li_2[(C_5H_4)_2(CH_2)_4]$ and were prepared as described

in the literature.[87, 88]

Electrospray ionisation (ESI) mass spectra were recorded using a cone potential of +150 V in a THF/acetonitrile mixture on a Bruker Daltonics Apex IV Fourier transform ion cyclotron mass spectrometer.

^{1}H NMR spectra were recorded at ambient temperature on a VARIAN NMR 500MHz spectrometer. All spectra are reported relative to external TMS and are referenced to the most downfield residual solvent resonance (d_5-pyridine: 8.74 ppm, C_6D_6: δ_H 7.16 ppm). In all ^{1}H NMR spectra of paramagnetic [*n*]nickelocenophane and polynickelocene species, backward linear prediction from 0 to 15 data points was employed to remove baseline distortion, phase correction was addressed manually, and a Bernstein Polynomial Fit was applied (polynomial order = 10). ^{1}H NMR spectra were collected between +310 and −310 ppm to observe signals at both low and high field (number of scans = 2048, receiver gain = 50, relaxation delay = 0.1 s and acquisition time = 0.8389 s).

Dynamic Light Scattering (DLS) experiments were performed to determine hydrodynamic radii of polymer solutions. Samples (2 mL) of different polymer concentrations (1 and 2 mg mL^{-1}) in toluene or THF were filtered through a 0.45 μm membrane filter into an optical glass cuvette (10.0 mm path length). The measurements were performed on a Malvern Instruments Zetasizer Nano S using a 5 mW He-Ne laser (633 nm) at 20 °C. The correlation function was acquired in real time and analysed with a function capable of modelling multiple exponentials. This process enabled the diffusion coefficients for the component particles to be extracted, and these were subsequently expressed as effective hydrodynamic radius, by volume, using the Stokes-Einstein relationship. DP_n for copolymers was determined using an average molecular weight value (calculated from the two monomer molecular weights) relative to poly(ferrocenylsilane).[65]

Visible absorption data were obtained on an Agilent Cary 300 spectrometer employing standard quartz cells (1 cm) from 800 to 400 nm with a scan rate of 1 nm s^{-1}.

Photoirradiation experiments were carried out using Pyrex-glass-filtered emission ($\lambda > 310$ nm) from a 125 W high pressure Hg vapour lamp (Photochemical Reactors Ltd.).

Elemental analyses were carried out by the Laboratory for Microanalysis at the University of Bristol (Model 3000 Euro EA Elemental Analyzer) using V_2O_5 to promote combustion. Combustion analyses were often outside the normal range for carbon; we attribute this to air and moisture sensitivity, and ceramic formation.

Single crystal X-ray diffraction experiments for compound **2.6** was carried out at 100 K on a Bruker APEX II diffractometer using Mo Kα radiation ($\lambda = 0.71073$ Å). Data collections were performed using a CCD area detector from a single crystal mounted on a glass fibre. Intensities were integrated,[89] from several series of exposures measuring 0.5° in ω or φ. Absorption corrections were based on equivalent reflections using SADABS.[90] The structure was solved using SHELXS and refined against all F_o^2 data with hydrogen atoms located geometrically and refined using a riding model in SHELXL.[91] Crystallographic details are provided in Appendix II.

Wide angle X-ray scattering (WAXS) experiments were carried out on a D8 Advance diffractometer fitted with an 0.6 mm fixed divergence slit, knife-edge collimator and a LynxEye area detector using Cu Kα radiation ($\lambda = 1.5418$ Å). Data was collected between 5 and 50 degrees 2θ in θ/2θ mode with a step width of 0.5°. Samples were prepared by the loading of solid polymer samples (~30 mg) onto a silicon wafer prior to analysis.

Magnetic measurements of powdered samples of polynickelocenes **2.11$_x$**/**2.12**, **2.13$_a$** and **2.14$_a$**, and the parent nickelocenophanes **2.5**, **2.6** and **2.10** were carried out using a Quantum Design MPMS-5 Superconducting quantum interference device (SQUID) magnetometer at a field of 0.1 Tesla and different temperatures (6–300 K). Accurately weighed samples (~30 mg) were placed into gelatine capsules and then loaded into nonmagnetic plastic straws before being lowered into the cryostat. Values of the magnetic susceptibility were corrected for the underlying diamagnetic increment by using tabulated Pascal constants,[92] per

nickelocenylpropyl unit for **2.11$_x$/2.12** (χ_{dia} = −1.4742 × 10^{-4} emu mol^{-1}), per nickelocenylbutyl unit for **2.13$_a$** (χ_{dia} = −1.5928 × 10^{-4} emu mol^{-1}), and per nickelocenyltetramethyldisilyl unit for **2.14$_a$** (χ_{dia} = −1.970 × 10^{-4} emu mol^{-1}). The mass magnetic susceptibility, χ_g, was multiplied by the molar mass of a nickelocenylpropyl unit for **2.11$_x$/2.12** (228.94 g mol^{-1}), a nickelocenylbutyl unit for **2.13$_a$** (242.97 g mol^{-1}), and a nickelocenyltetramethyldisilyl unit for **2.14$_a$** (303.17 g mol^{-1}) to obtain the magnetic susceptibility per mole of nickel atoms, χ_m. Samples used for magnetisation measurements were checked for chemical composition and purity by elemental analysis, and where possible, MALDI-TOF mass spectrometry and ^{1}H NMR spectroscopy. Data reproducibility was carefully checked on two independently synthesised and measured samples. Average data of three measurements are provided for **2.14$_a$**. For each sample, Curie-Weiss behaviour was determined from the linear region in the χ_m^{-1} vs. T plot. Least-squares fitting to Equation 5 in the Curie-Weiss regime provided values for the Curie constant, C (in emu K mol^{-1}), Weiss temperature, Θ (in K), and a temperature independent paramagnetism contribution to the magnetic susceptibility, χ_{TIP} (in emu mol^{-1}).[93]

$$\chi_m = \frac{C}{T - \Theta} + \chi_{TIP} \qquad \textbf{Equation 5}$$

The effective magnetic moment (in Bohr Magneton, μ_B) was then calculated using Equation 6.

$$\mu_{eff} = 2.828\sqrt{C}\,\mu_B \qquad \textbf{Equation 6}$$

Experimental data across the entire temperature range (6–300 K) were simulated using a fitting procedure to the spin Hamiltonian for the Zeeman interaction and the axial zero-field splitting (Equation 7).[79]

$$\hat{H} = \hat{H}_{Zee} + \hat{H}_{ZFS} \qquad \textbf{Equation 7}$$

where

$$\hat{H}_{Zee} = g\mu_B \vec{B} \cdot \vec{S} \qquad \textbf{Equation 8}$$

$$\widehat{H}_{ZFS} = D[S^2 - {}^1/_3\, S(S+1)] \qquad \textbf{Equation 9}$$

A temperature independent paramagnetism contribution to the magnetic susceptibility, χ_{TIP}, was included in the fits. Intermolecular interactions were considered in a mean field approach by using a Weiss temperature, Θ.[94] The Weiss temperature (defined as $\Theta = zJS(S+1)/3k_B$) relates to intermolecular interactions zJ, where J is the interaction parameter between two nearest-neighbour magnetic centres, k_B is the Boltzmann constant (0.695 cm^{-1}), and z is the number of nearest neighbours.

The simulated g value for an S=1 system leads to a new effective magnetic moment (in μ_B) calculated using Equation 10.

$$\mu_{eff} = g\sqrt{S(S+1)}\,\mu_B \qquad \textbf{Equation 10}$$

2.5.2 Synthesis of Tricarba[3]nickelocenophane (**2.5**)

The synthesis of **2.5** involved a modified literature procedure.[51] The reaction was carried out as described, but heated at 40 °C (vs. −78 °C in the original report), which resulted in the yield increasing from 17% to 44% (the higher temperature favours **2.5** in the monomer/polymer equilibrium).

2.5.3 Synthesis of Tetracarba[4]nickelocenophane (**2.6**)

$Na[C_5H_5]$ (12.5 g, 0.14 mol) was dissolved in THF (125 mL) and cooled to −78 °C before 1,3-dimethyl-3,4,5,6-tetrahydro-2-pyrimidinone (60 mL) was added. 1,4-Dibromobutane (6.10 mL, 0.051 mol) was also dissolved in THF (50 mL) and added to the $Na[C_5H_5]$ solution dropwise over 30 min. The mixture was stirred at −78 °C for 1 h, then at 0 °C for a further 2 h. H_2O (100 mL) was added to the pale pink suspension, and the organic phase was extracted with Et_2O. The aqueous phase was washed with Et_2O (3 × 200 mL) and the organic phase was washed with H_2O (10 × 100 mL) to remove all remaining cyclopentadiene. The organic solution was dried with $MgSO_4$, and flushed through a silica column (1” × 6”) with a DCM eluent. All solvent was removed to yield 8.07 g (0.044 mol) of a yellow oil. This

product was dissolved in dry hexanes (200 mL) and cooled to −78 °C. *n*BuLi (1.6 M hexane solution; 60 mL, 0.095 mol) was added dropwise over 10 min, and the resulting solution was stirred and allowed to warm to room temperature over 16 h. The suspension was filtered to collect the solid, which was washed with hexanes (5 × 50 mL) to remove excess *n*BuLi and dried under vacuum to yield $Li_2[(C_5H_4)_2(CH_2)_4]$ as a colourless, free-flowing solid (8.10 g, 0.041 mol) in 80% yield.

The fly trap ligand $Li_2[(C_5H_4)_2(CH_2)_4]$ (2.00 g, 10 mmol) and $NiCl_2$ (1.44 g, 11.1 mmol) were thoroughly mixed in the absence of solvent and cooled to −78 °C. Dry and degassed THF (250 mL) pre-cooled to −78 °C was then added rapidly via cannula. The reaction mixture was stirred and allowed to warm up to room temperature over a period of 16 h. After evaporation of the solvent under reduced pressure, the green residue was extracted with *n*-hexanes to give a dark green solution which was filtered through Celite (1" × 4"). Again, all volatiles were removed in vacuo and the resulting green solid was purified by sublimation (40 °C/−78 °C, 1.0×10^{-2} mbar) and subsequent recrystallisation from *n*-hexanes at −40 °C to afford dark green crystals of **2.6** suitable for X-ray crystallographic analysis. Yield: 0.24 g (0.99 mmol, 10%). ^{1}H NMR (500 MHz, C_6D_6): δ [peak width at half height] (ppm) 138.2 [514 Hz] (br s, C_5H_4–C*H*$_2$), −1.1 [62 Hz] (br s, C_5H_4–CH_2–C*H*$_2$), −251.2 [705 Hz] (br s, α-C_5H_4), −256.6 [721 Hz] (br s, β-C_5H_4). The signals in the ^{1}H NMR spectrum are consistent with those reported when this species was previously isolated through a ring-closing metathesis reaction of a divinyl substituted nickelocene, followed by a subsequent hydrogenation.[56] ESI-MS (positive ion mode, 1,2-difluorobenzene): *m*/*z* 242.0602 $[Ni(\eta^5\text{-}C_5H_4)_2(CH_2)_4]^+$.

2.5.4 ROP of **2.6** in Pyridine

Tetracarba[4]nickelocenophane **2.6** (0.050 g, 0.210 mmol) was charged into a Young's flask and pyridine (0.28 mL) was added via syringe to afford a dark blue solution. The solution

was stirred at 25 °C for 5 days at which point the solution appeared to have completely solidified into a light green solid. Pyridine was removed from the product in vacuo to afford a light green powder. The product was stirred in THF (3 mL) for 1 h and then left to settle out. The supernatant, THF soluble component was separated from the solid component (**2.13$_a$**) and transferred into hexanes (20 mL) but did not precipitate. The hexane solvent was removed in vacuo to afford 0.002 g of a pale green solid **2.13$_b$** (4% yield). ^{1}H NMR (500 MHz, C_6D_6): δ [peak width at half height] (ppm) 226.0 [567 Hz] (**2.13$_b$**: br s, alkyl bridge), 195.0 [528 Hz] (**2.13$_b$**: br s, alkyl bridge), 186.1 [377 Hz] (**2.13$_b$**: br s, alkyl bridge), 176.3 [444 Hz] (**2.13$_b$**: br s, alkyl bridge), 138.0 [502 Hz] (**2.6**: br s, C_5H_4–C*H*$_2$), −1.1 [65 Hz] (**2.6**: br s, C_5H_4–CH_2–C*H*$_2$), −249.3 to −258.7 [1723 Hz] (**2.6** and **2.13$_b$**: br m, C_5H_4). MALDI-TOF MS (linear, + mode): 969 (n = 4), 1047 (m = 4, −pyr), 1165 (m = 4, K^+), 1214 (n = 5), 1408 (m = 5, K^+), 1459 (n = 6), 1650 (m = 6, K^+), 1703 (n = 7), 1892 (m = 7, K^+), 1946 (n = 8), 2134 (m = 8, K^+), 2195 (n = 9), 2376 (m = 9, K^+).

The residual solvent was removed in vacuo from the insoluble product **2.13$_a$** to afford 0.030 g of light green powder (60% yield). Elemental analysis: calcd. for $C_{14}H_{16}Ni$: C 69.21%, H 6.64% Found: C 70.56%, H, 6.62%.

2.5.5 Temperature Dependency Studies of the Depolymerisation of **2.13$_a$**

In a typical experiment **2.13$_a$** (13 mg, 0.055 mmol) was added to deuterated pyridine (0.5 mL) to afford a mixture of maximum concentration 0.11 M, and added to an NMR tube. The sample was held at the desired temperature for 24 h and then a ^{1}H NMR spectrum was recorded at that temperature.

2.5.6 ROP of **2.10** in Pyridine

Tetramethyldisila[2]nickelocenophane (**2.10**) (105 mg, 0.35 mmol) was dissolved in pyridine (1 mL) to afford a green solution of concentration 0.35 M, and stirred for 32 h. No obvious colour change was observed during the course of the reaction, however a light green

solid was precipitated from solution. The pyridine was removed in vacuo and THF added to the products (5 mL). The resulting suspension was filtered and the THF soluble component of the products precipitated into rapidly stirring hexanes (15 mL) to afford a light green precipitate. The supernatant solution was separated, and the product dissolved in THF (1 mL) and precipitated again into hexanes (15 mL). The resulting light green solid was isolated and dried in vacuo to afford polymer **2.14$_b$** (0.005 g, 0.016 mmol). Yield = 5%. ^{1}H NMR (500 MHz, C_6D_6): δ [peak width at half height] (ppm) 15.3 (br s, $SiMe_2$), −229 (br m, C_5H_4), −243 (br m, C_5H_4). MALDI-TOF MS (linear, + mode): 1404 (n = 4), 1588 (m = 5), 1710 (n = 5), 1892 (m = 6), 2015 (n = 6), 2196 (m = 7), 2318 (n = 7), 2622 (n = 8), 2925 (n = 9), 3228 (n = 10), 3536 (n = 11), 3838 (n = 12).

The residual solvent was removed from the insoluble product to afford 86 mg of light green powder, **2.14$_a$**. Yield = 82%. Elemental analysis: calcd. for $C_{14}H_{20}NiSi_2$: C 55.46%, H 6.65% Found: C 54.42%, H 6.55%.

2.5.7 Temperature Dependency Studies of the Depolymerisation of **2.14$_a$**

In a typical experiment **2.14$_a$** (17 mg, 0.055 mmol) was added to deuterated pyridine (0.5 mL) to afford a mixture of maximum concentration 0.11 M and added to an NMR tube. The sample was held at the desired temperature for 24 h and then a ^{1}H NMR spectrum was recorded at that temperature.

2.5.8 Synthesis of Copolymer **2.15**

Tricarba[3]nickelocenophane **2.5** (0.038 g, 0.165 mmol) and tetramethyldisila[2]nickelocenophane **2.10** (0.050 g, 0.165 mmol) were combined in pyridine (4 mL) and the resulting dark green solution (0.08 M) stirred at 20 °C for 32 h, at which point no obvious change in colour was observed. The pyridine was removed in vacuo and the resulting dark green solid dissolved in THF (2 mL) and precipitated into hexanes (15 mL) to afford a light green precipitate. The precipitate was isolated, dissolved in THF (2

mL), filtered and re-precipitated into hexanes (15 mL). The precipitate was centrifuged and dried (0.039 g) to afford copolymer **2.15**. Yield = 44%. ^{1}H NMR (500 MHz, C_6D_6): δ [peak width at half height] (ppm) 173.8 to 174.8 (overlapping br m, C_5H_4–C*H*$_2$–CH_2), 15.3 [15 Hz] (br s, $SiMe_2$), 10.2 [176 Hz] (br s, C_5H_4–CH_2–C*H*$_2$), −29.4 [191 Hz] (br s, C_5H_4–CH_2–C*H*$_2$: see text below), −228.5 [667 Hz] (br m, C_5H_4), −235.6 [615 Hz] (br m, C_5H_4), −238.4 [632 Hz] (br m, C_5H_4), −242.6 [680 Hz] (br m, C_5H_4), −246.5 [537 Hz] (br m, C_5H_4), −251.0 [998 Hz] (br m, C_5H_4), −255.4 [598 Hz] (br m, C_5H_4), −257.3 [656 Hz] (br m, C_5H_4), −272.3 [698 Hz] (br m, C_5H_4). The resonance at 29.4 ppm is at a similar shift to that observed for the β-CH_2 protons within the propyl linker of monomer **2.5**. However, it is concluded that the presence of **2.5** is highly unlikely as **2.15** is purified through multiple precipitations into hexanes (the supernatant solution was colourless after the last precipitation). However, exact assignment of this resonance is not possible at this point. MALDI-TOF MS (linear, + mode): 990 (m = 3, n = 1), 1064 (m = 2, n = 2), 1138 (m = 1, n = 3), 1213 (m = 0, n = 4), 1293 (m = 3, n = 2), 1367 (m = 2, n = 3), 1448 (m = 5, n = 1), 1606 (k = 5, l = 1), 1680 (k = 4, l = 2), 1755 (k = 3, l = 3), 1829 (k = 2, l = 4), 1906 (m = 7, n = 1), 1983 (k = 4 , l = 3), 2058 (k = 3, l = 4), 2128 (m = 4, n = 4), 2212 (k = 5, l = 3). DLS (THF, 20 °C, 1 mg mL^{-1} and 0.5 mg mL^{-1}): R_h = 3.9 nm (corresponding to a M_w of ~25,000 g mol^{-1} and a DP_n of 95).

2.5.9 Synthesis of Copolymer **2.16**

Disila[2]nickelocenophane **2.10** (0.050 g, 0.165 mmol, 1 equiv.) and tetracarba[4]nickelocenophane **2.6** (0.050 g, 0.206 mmol, 1.3 equiv.) were combined in pyridine (0.5 mL) and the green solution (0.74 M) was stirred at 20 °C for 48 h. No obvious colour was observed, and some light green precipitate (**2.16$_a$**) was formed. The solvent was removed in vacuo and dry THF (2 mL) added to the green residue. The THF soluble component of the product was precipitated into a vortex of dry hexanes (20 mL), and solvent removed and the product dried to afford the soluble component, **2.16$_b$** (0.015 g) in low yield (15%). ^{1}H NMR (C_6D_6, 500 MHz): δ [peak width at half height] (ppm) 176 (br m, alkyl

bridge) [770 Hz], 15.3 (br s, $SiMe_2$) [37 Hz], −236 (br m, C_5H_4) [482 Hz], −239 (br m, C_5H_4) [527 Hz], −243 (br m, C_5H_4) [692 Hz], −252 (br m, C_5H_4) [1034 Hz], −256 to −259 (br m, C_5H_4) [1211 Hz]. MALDI-TOF MS (linear, + mode): 1084 (m = 2, n = 2), 1150 (m = 1, n = 3), 1211 (m = 0, n = 4), 1272 (m = 4, n = 1), 1331 (m = 3, n = 2), 1394 (m = 2, n = 3), 1456 (m = 6, n = 0), 1515 (m = 0, n = 5), 1577 (m = 4, n = 2), 1639 (m = 3, n = 3), 1699 (m = 2, n = 4), 1762 (m = 6, n = 1), 1824 (m = 5 , n = 2), 1883 (m = 4, n = 3), 1943 (m = 8, n = 0), 2004 (m = 7, n = 1), 2064 (m = 6, n = 2), 2125 (m = 5, n = 3), 2189 (m = 9, n = 0), 2252 (m = 8, n =1), 2308 (m = 7, n = 2), 2370 (m = 6, n = 3), 2431 (m = 10, n = 0), 2491 (m = 9, n = 1), 2553 (m = 8, n = 2), 2612 (m = 7, n = 3), 2674 (m = 11, n = 0), 2739(m = 10, n = 1), 2797 (m = 9, n = 2), 2857 (m = 8, n = 3), 2918 (m = 12, n = 0), 2979 (m = 11, n = 1), 3040 (m = 10, n = 2), 3100 (m = 9, n = 3), 3159 (m = 13, n = 0), 3221 (m = 12, n = 1), 3287 (m = 11, n = 2), 3345 (m = 10, n = 3), 3404 (m = 14, n = 0), 3469 (m = 13, n = 1), 3528 (m = 12, n = 2), 3589 (m = 11, n = 3), 3649 (m = 15, n = 0), 3712 (m = 14, n = 1), 3769 (m = 13, n = 2), 3828 (m = 12, n = 3), 3894 (m = 16, n = 0), 3953 (m = 15, n = 1), 4013 (m = 14, n = 2), 4071 (m = 13, n = 3), 4134 (m = 17, n = 0), 4200 (m =16 , n = 1), 4256 (m = 15, n = 2), 4320 (m = 14, n = 3), 4378 (m = 18, n = 0), 4441 (m = 17, n = 1), 4501 (m = 16, n = 2), 4364 (m = 15, n = 3), 4624 (m = 19, n = 0), 4680 (m = 18, n = 1), 4746 (m = 17, n = 2), 4808 (m = 16, n = 3), 4870 (m = 20, n = 0), 4933 (m = 19, n = 1), 4990 (m = 18, n = 2), 5050 (m = 17, n = 3), 5105 (m = 21, n = 0), 5172 (m = 20, n = 1), 5233 (m = 19, n = 2), 5300 (m = 18, n = 3), 5352 (m = 22, n = 0), 5413 (m = 21, n = 1), 5470 (m = 20, n = 2), 5536 (m = 19, n = 3). DLS (THF, 20 °C, 5 mg mL^{-1}): R_h = 1.4 nm (corresponding to a M_w of 3,800 g mol^{-1} and a DP_n of 14). UV/Vis (THF, 20 °C): λ_{max} (ε) = 685 nm (138 M^{-1} cm^{-1}).

The residual solvent was removed from the insoluble product to afford 0.020 g of light green powder (**2.16$_a$**). Elemental analysis: calcd. for $C_{28}H_{36}Ni_2Si_2$ (assuming 1:1 ratio of **2.10**:**2.6**): C 61.58%, H 6.64%; Found: C 62.35%, H 6.92%.

2.5.10 Synthesis of Copolymer **2.17**

Tricarba[3]nickelocenophane **2.5** (0.034 g, 0.150 mmol) and tetracarba[4]nickelocenophane **2.6** (0.036 g, 0.150 mmol) were combined in pyridine (0.91 mL) and the resulting dark green solution stirred at 20 °C for 3 days. A colour change from dark blue to dark green was observed, and some light green precipitate formed **2.17ₐ**. The pyridine was removed in vacuo and dry THF (2 mL) added to the green solid. The THF soluble component of the product was precipitated into a vortex of dry hexanes (20 mL) to afford a light green precipitate. The precipitate was isolated, dissolved in THF (2 mL), filtered and re-precipitated into hexanes (20 mL). The precipitate was centrifuged and dried (0.020 g) to afford polymer **2.17ᵦ**. Yield = 28%. The yield provided was calculated assuming 100% incorporation of the tricarba[3]nickelocenophane unit into polymer **2.17ᵦ**. ^{1}H NMR (500 MHz, C_6D_6): δ [peak width at half height] (ppm) 176 (br s, alkyl bridge), 174 (br s, alkyl bridge), −252 (br s, C_5H_4) [482 Hz]. MALDI-TOF MS (linear, + mode): 929 (m = 3, n = 1), 942 (m = 2, n = 2), 955 (m = 1, n = 3), 1087 (k = 3, l = 1), 1171 (m = 3, n = 2), 1113 (k = 1, l = 3), 1184 (m = 2, n = 3), 1197 (m = 1, n = 4), 1316 (k = 4, l = 1), 1329 (k = 3, l = 2), 1342 (k = 2, l = 3), 1400 (m = 4, n = 2), 1413 (m = 3, n = 3), 1426 (m = 2, n = 4), 1439 (m = 1, n = 5), 1545 (k = 5, l = 1), 1558 (k = 4, l = 2), 1616 (m = 6, n = 1), 1629 (m = 5, n = 2), 1642 (m = 4, n = 3), 1655 (m = 3, n = 4), 1668 (m = 2, n = 5), 1681 (m = 1, n = 6), 1787 (k = 5, l = 2), 1800 (k = 4, l = 3), 1871 (m = 5, n = 3), 1884 (m = 4, n = 4), 1897 (m = 3, n = 5), 1910 (m = 2, n = 6), 1923 (m = 1, n = 7), 2087 (m = 7, n = 2), 2100 (m = 6, n = 3), 2113 (m = 5, n = 4), 2126 (m = 4, n = 5), 2139 (m = 3, n = 6), 2152 (m = 2, n = 7), 2165 (m = 1, n = 8), 2355 (m = 5, n = 5), 2368 (m = 4, n = 6), 2381 (m = 3, n = 7), 2394 (m = 2, n = 8), 2407 (m = 1, n = 9), 2597 (m = 5, n = 6), 2610 (m = 4, n = 7), 2623 (m = 3, n = 8), 2636 (m = 2, n = 9), 2650 (m = 1, n = 10), 2826 (m = 6, n = 6), 2839 (m = 5, n = 7), 2852 (m = 4, n = 8), 2865 (m = 3, n = 9), 2878 (m = 2, n = 10), 2892 (m = 1, n = 11), 3068 (m = 6, n = 7), 3081 (m = 5, n = 8), 3094 (m = 4, n = 9), 3107 (m = 3, n = 10), 3120 (m = 2, n = 11), 3134 (m = 1, n = 12), 3310 (m = 6, n = 8),

3336 (m = 4, n = 10), 3350 (m = 3, n = 11), 3363 (m = 2, n = 12). Peaks were detected within a few *m/z* of the calculated values in all cases. DLS (toluene, 20 °C, 1 mg mL^{-1}): R_h = 3.8 nm (corresponding to a M_w of 24,000 g mol^{-1} and a DP_n of 103).

2.5.11 Synthesis of Copolymer **2.19**

Dicarba[2]cobaltocenophane **2.18** (0.036 g, 0.165 mmol, 1 equiv.) and tricarba[4]nickelocenophane **2.5** (0.038 g, 0.165 mmol, 1 equiv.) were combined in pyridine (0.5 mL) and the brown solution (0.66 M) was stirred at 20 °C for 42 h. No obvious colour change was observed and a dark grey precipitate **2.19$_a$** formed. The solvent was removed in vacuo and dry THF (2 mL) added to the residue. The THF soluble component of the product was precipitated into a vortex of dry hexanes (20 mL), and solvent removed and the product dried to afford the grey component, **2.19$_b$** (0.015 g) in low yield (20%). The polymeric species **2.19$_b$** proved to have poor solubility in organic solvents and thus it should be noted that only one precipitation was performed in this case rather than the two employed in the previous ROPs. ^{1}H NMR (500 MHz, C_6D_6): δ [peak width at half height] (ppm) 174 (br s, alkyl bridge) [1609 Hz], −46.1 (br s, Co-C_5H_4) [1078], −64.9 (br s, Co-C_5H_4) [669 Hz], −250 (br s, Ni-C_5H_4) [2782 Hz]. MALDI-TOF MS (linear, + mode): 624 (k=1, l=1, 2×pyr, Na^+), 640 (k=1, l=1, 2×pyr, K^+), 653 (k=2, 2×pyr, K^+), 684 (m=3), 717 (l=3, THF), 731 (k=1, l=2, THF), 743 (k=2, l=1, THF), 756 (l=3, THF, K^+), 812 (l=3, 2×THF, Na^+), 825 (k=1, l=2, 2×THF, Na^+), 886 (m=2, n=2), 1004 (l=4, 2×THF), 1023 (k=4, THF, K^+), 1044 (k = 2, l = 2, 2×pyr), 1067 (k = 2, l = 2, 2×pyr, Na^+), 1103 (m = 2, n = 3), 1117 (m = 3, n = 2), 1130 (m = 4, n = 1). DLS (toluene, 20 °C, 1 mg mL^{-1}): R_h = 1.2 nm (corresponding to a M_w of 2,900 g mol^{-1} and a DP_n of 11).

2.6 References

1. J. Xiang, C. L. Ho and W.-Y. Wong, *Polym. Chem.*, 2015, **6**, 6905-6930.

2. G. R. Whittell, M. D. Hager, U. S. Schubert and I. Manners, *Nat. Mater.*, 2011, **10**, 176-188.

3. Y. Yan, J. Zhang, L. Ren and C. Tang, *Chem. Soc. Rev.*, 2016, **45**, 5232-5263.

4. H. Gu, S. Mu, G. Qiu, X. Liu, L. Zhang, Y. Yuan and D. Astruc, *Coord. Chem. Rev.*, 2018, **364**, 51-85.

5. J. Collot, J. Gradinaru, N. Humbert, M. Skander, A. Zocchi and T. R. Ward, *J. Am. Chem. Soc.*, 2003, **125**, 9030-9031.

6. J. Zhang, Y. P. Chen, K. P. Miller, M. S. Ganewatta, M. Bam, Y. Yan, M. Nagarkatti, A. W. Decho and C. Tang, *J. Am. Chem. Soc.*, 2014, **136**, 4873-4876.

7. C. W. Tse, K. Y. K. Man, K. W. Cheng, C. S. K. Mak, W. K. Chan, C. T. Yip, Z. T. Liu and A. B. Djurisic, *Chem. Eur. J.*, 2007, **13**, 328-335.

8. W.-Y. Wong and C.-L. Ho, *Acc. Chem. Res.*, 2010, **43**, 1246-1256.

9. T. L. Choi, K. H. Lee, W. J. Joo, S. Lee, T. W. Lee and M. Y. Chae, *J. Am. Chem. Soc.*, 2007, **129**, 9842-9843.

10. F.-I. Wu, X.-H. Yang, D. Neher, R. Dodda, Y.-H. Tseng and C.-F. Shu, *Adv. Funct. Mater.*, 2007, **17**, 1085-1092.

11. J. M. Stanley and B. J. Holliday, *Coord. Chem. Rev.*, 2012, **256**, 1520-1530.

12. M. Burnworth, L. Tang, J. R. Kumpfer, A. J. Duncan, F. L. Beyer, G. L. Fiore, S. J. Rowan and C. Weder, *Nature*, 2011, **472**, 334-337.

13. S. Bode, L. Zedler, F. H. Schacher, B. Dietzek, M. Schmitt, J. Popp, M. D. Hager and U. S. Schubert, *Adv. Mater.*, 2013, **25**, 1634-1638.

14. H. J. Kim, J. H. Lee and M. Lee, *Angew. Chem. Int. Ed.*, 2005, **44**, 5810-5814.

15. M. J. MacLachlan, M. Ginzburg, N. Coombs, N. P. Raju, J. E. Greedan, G. A. Ozin and I. Manners, *J. Am. Chem. Soc.*, 2000, **122**, 3878-3891.

16. M. Ginzburg, M. J. MacLachlan, S. M. Yang, N. Coombs, T. W. Coyle, N. P. Raju, J. E. Greedan, R. H. Herber, G. A. Ozin and I. Manners, *J. Am. Chem. Soc.*, 2002, **124**, 2625-2639.

17. C. Ruttiger, V. Pfeifer, V. Rittscher, D. Stock, D. Scheid, S. Vowinkel, F. Roth, H. Didzoleit, B. Stühn, J. Elbert, E. Ionescu and M. Gallei, *Polym. Chem.*, 2016, **7**, 1129-1137.

18. J. Zhang, Y. Yan, M. W. Chance, J. Chen, J. Hayat, S. Ma and C. Tang, *Angew. Chem. Int. Ed.*, 2013, **52**, 13387-13391.

19. D. A. Rider, K. Liu, J. C. Eloi, L. Vanderark, L. Yang, J. Y. Wang, D. Grozea, Z. H. Lu, T. P. Russell and I. Manners, *ACS Nano*, 2008, **2**, 263-270.

20. I. Korczagin, R. G. H. Lammertink, M. A. Hempenius, S. Golze and G. J. Vancso, *Adv. Polym. Sci.*, 2006, **200**, 91-117.

21. Y. Wang, L. Salmon, J. Ruiz and D. Astruc, *Nat. Commun.*, 2014, **5**, 3489-3489.

22. M. Yang, L. Zhang, Z. Lei, P. Ye, J. Si, Q. Yang and Y. Wang, *J. Appl. Polym. Sci.*, 1998, **70**, 1165-1172.

23. X. S. Ding, J. Guo, X. A. Feng, Y. Honsho, J. D. Guo, S. Seki, P. Maitarad, A. Saeki, S. Nagase and D. L. Jiang, *Angew. Chem. Int. Ed.*, 2011, **50**, 1289-1293.

24. R. McDonald, K. C. Sturge, A. D. Hunter and L. Shilliday, *Organometallics*, 1992, **11**, 893-900.

25. K. C. Sturge, A. D. Hunter, R. Mcdonald and B. D. Santarsiero, *Organometallics*, 1992, **11**, 3056-3062.

26. P. M. Macdonald, A. D. Hunter, G. Lesley and J. Li, *Solid State Nucl. Magn. Reson.*, 1993, **2**, 47-55.

27. J. A. Paquette, E. R. Sauvé and J. B. Gilroy, *Macromol. Rapid Commun.*, 2015, **36**, 621-626.

28. Y. J. Dai and T. J. Katz, *J. Org. Chem.*, 1997, **62**, 1274-1285.

29. Y. J. Dai, T. J. Katz and D. A. Nichols, *Angew. Chem. Int. Ed.*, 1996, **35**, 2109-2111.

30. M. Rosenblum, H. M. Nugent, K. S. Jang, M. M. Labes, W. Cahalane, P. Klemarczyk and W. M. Reiff, *Macromolecules*, 1995, **28**, 6330-6342.

31. H. M. Nugent, M. Rosenblum and P. Klemarczyk, *J. Am. Chem. Soc.*, 1993, **115**, 3848-3849.

32. C. Mugemana, J. F. Gohy and C. A. Fustin, *Langmuir*, 2012, **28**, 3018-3023.

33. J. A. Paquette, A. Rabiee Kenaree and J. B. Gilroy, *Polym. Chem.*, 2017, **8**, 2164-2172.

34. R. L. N. Hailes, A. M. Oliver, J. Gwyther, G. R. Whittell and I. Manners, *Chem. Soc. Rev.*, 2016, **45**, 5358-5407.

35. U. F. J. Mayer, J. B. Gilroy, D. O'Hare and I. Manners, *J. Am. Chem. Soc.*, 2009, **131**, 10382-10383.

36. B. Bagh, J. B. Gilroy, A. Staubitz and J. Müller, *J. Am. Chem. Soc.*, 2010, **132**, 1794-1795.

37. H. Braunschweig, C. J. Adams, T. Kupfer, I. Manners, R. M. Richardson and G. R. Whittell, *Angew. Chem. Int. Ed.*, 2008, **47**, 3826-3829.

38. E. Khozeimeh Sarbisheh, H. Bhattacharjee, M. P. T. Cao, J. Zhu and J. Müller, *Organometallics*, 2017, **36**, 614-621.

39. L. Espada, K. H. Pannell, V. Papkov, L. Leites, S. Bukalov, I. Suzdalev, M. Tanaka and T. Hayashi, *Organometallics*, 2002, **21**, 3758-3761.

40. Y. Ma, W.-F. Dong, M. A. Hempenius, H. Möhwald and G. J. Vancso, *Nat. Mater.*, 2006, **5**, 724-729.

41. M. A. Hempenius, C. Cirmi, J. Song and G. J. Vancso, *Macromolecules*, 2009, **42**, 2324-2326.

42. M. J. MacLachlan, M. Ginzburg, N. Coombs, T. W. Coyle, N. P. Raju, J. E. Greedan, G. A. Ozin and I. Manners, *Science*, 2000, **287**, 1460-1463.

43. S. Lastella, G. Mallick, R. Woo, S. P. Karna, D. A. Rider, I. Manners, Y. J. Jung, C. Y. Ryu and P. M. Ajayan, *J. Appl. Phys.*, 2006, **99**, 024302.

44. J. Lu, D. Chamberlin, D. A. Rider, M. Liu, I. Manners and T. P. Russell, *Nanotechnology*, 2006, **17**, 5792-5797.

45. T. Gädt, N. S. Ieong, G. Cambridge, M. A. Winnik and I. Manners, *Nat. Mater.*, 2009, **8**, 144-150.

46. X. Wang, G. Guerin, H. Wang, Y. Wang, I. Manners and M. A. Winnik, *Science*, 2007, **317**, 644-647.

47. N. J. Long, in *Metallocenes: An Introduction to Sandwich Complexes*, Wiley-Blackwell, 1st edn., 1998.

48. W. Finckh, B. Z. Tang, D. A. Foucher, D. B. Zamble, R. Ziembinski, A. Lough and I. Manners, *Organometallics*, 1993, **12**, 823-829.

49. H. Braunschweig, F. Breher, M. Kaupp, M. Gross, T. Kupfer, D. Nied, K. Radacki and S. Schinzel, *Organometallics*, 2008, **27**, 6427-6433.

50. H. Braunschweig, M. Gross and K. Radacki, *Organometallics*, 2007, **26**, 6688-6690.

51. S. Baljak, A. D. Russell, S. C. Binding, M. F. Haddow, D. O'Hare and I. Manners, *J. Am. Chem. Soc.*, 2014, **136**, 5864-5867.

52. S. Trtica, E. Meyer, M. H. Prosenc, J. Heck, T. Böhnert and D. Görlitz, *Eur. J. Inorg. Chem.*, 2012, 4486-4493.

53. R. A. Musgrave, A. D. Russell, D. W. Hayward, G. R. Whittell, P. G. Lawrence, P. J. Gates, J. C. Green and I. Manners, *Nat. Chem.*, 2017, **9**, 743-750.

54. V. I. Tel'noi and I. B. Rabinovich, *Usp. Khim.*, 1977, **46**, 1337-1367.

55. M. Tanabe, G. W. M. Vandermeulen, W. Y. Chan, P. W. Cyr, L. Vanderark, D. A. Rider and I. Manners, *Nat. Mater.*, 2006, **5**, 467-470.

56. W. Buchowicz, L. B. Jerzykiewicz, A. Krasińska, S. Losi, A. Pietrzykowski and P. Zanello, *Organometallics*, 2006, **25**, 5076-5082.

57. The crystallographic data for compound **2.6** was deposited into the Cambridge Crystallographic Database CCDC 1863827.

58. D. E. Herbert, U. F. J. Mayer and I. Manners, *Angew. Chem. Int. Ed.*, 2007, **46**, 5060-5081.

59. R. A. Musgrave, A. D. Russell and I. Manners, *Organometallics*, 2013, **32**, 5654-5667.
60. R. A. Musgrave, A. D. Russell, G. R. Whittell, M. F. Haddow and I. Manners, *Organometallics*, 2015, **34**, 897-907.
61. D. A. Foucher, B. Z. Tang and I. Manners, *J. Am. Chem. Soc.*, 1992, **114**, 6246-6248.
62. It should be noted that the reaction time allowed for the ROP of **2.6** (5 days) was increased relative to that of **2.5** (32 h) to allow for the production of a small proportion of soluble oligomers, whilst also giving a significant amount of insoluble higher molecular weight poly(nickelocenylbutylene).
63. R. D. A. Hudson, B. M. Foxman and M. Rosenblum, *Organometallics*, 1999, **18**, 4098-4106.
64. The DP_n in this case was calculated using an average molecular weight for the monomer units derived from **2.5** (228.9 g mol^{-1}) and **2.10** (303.2 g mol^{-1}), and assuming a 1:1 ratio of incorportion of these units into copolymer **2.15**.
65. J. A. Massey, K. Kulbaba, M. A. Winnik and I. Manners, *J. Polym. Sci. B: Polym. Phys.*, 2000, **38**, 3032-3041.
66. The DP_n in this case was calculated using an average molecular weight for the monomer units derived from **2.6** (243.0 g mol^{-1}) and **2.10** (303.2 g mol^{-1}), and assuming a 1:1 ratio of encorportion of these units into polymer **2.16**.
67. The DP_n in this case was calculated using an average molecular weight for the monomer units derived from **2.5** (228.9 g mol^{-1}) and **2.6** (243.0 g mol^{-1}), and assuming a 1:1 ratio of encorportion of these units into polymer **2.17**.
68. U. F. J. Mayer, J. P. H. Charmant, J. Rae and I. Manners, *Organometallics*, 2008, **27**, 1524-1533.
69. J. B. Gilroy, S. K. Patra, J. M. Mitchels, M. A. Winnik and I. Manners, *Angew. Chem. Int. Ed.*, 2011, **50**, 5851-5855.
70. The DP_n in this case was calculated using an average molecular weight for the monomer units derived from **2.5** (228.9 g mol^{-1}) and **2.18** (215.1 g mol^{-1}), and assuming a 1:1 ratio of encorportion of these units into polymer **2.19**.
71. Von E. O. Fischer and R. Jira, *Z. Naturforsch.*, 1953, **8 b**, 217-219.
72. G. Wilkinson, P. L. Pauson and F. A. Cotton, *J. Am. Chem. Soc.*, 1954, **76**, 1970-1974.
73. R. Prins, J. D. W. Van Voorst and C. J. Schinkel, *Chem. Phys. Lett.*, 1967, **1**, 54-55.
74. H. Braunschweig, A. Damme, S. Demeshko, K. Dück, T. Kramer, I. Krummenacher, F. Meyer, K. Radacki, S. Stellwag-Konertz and G. R. Whittell, *J. Am. Chem. Soc.*, 2015, **137**, 1492-1500.

75. K. Kulbaba, I. Manners and P. M. Macdonald, *Macromolecules*, 2002, **35**, 10014-10025.
76. H. W. Spiess, *Colloid Polym. Sci.*, 1983, **261**, 193-209.
77. D. Hentschel, H. Sillescu and H. W. Spiess, *Makromol. Chem.*, 1979, **180**, 241-249.
78. L. V. Interrante, Q. Liu, I. Rushkin and Q. Shen, *J. Organomet. Chem.*, 1996, **521**, 1-10.
79. Simulations of the experimental magnetic data were carried out using the JulX program (version 1.5), written by Dr. Eckhard Bill (Max-Planck-Institut für Bioanorganische Chemie, Mühlheim an der Ruhr, Germany).
80. A. V. Zvarykina, E. V. Karimov, S. Yu, E. V. Leonova and R. B. Lyubovskii, *Sov. Phys.-Solid State*, 1970, **12**, 385.
81. N. Oswald, ETH Zürich, 1977.
82. P. Baltzer, A. Furrer, J. Hulliger and A. Stebler, *Inorg. Chem.*, 1988, **27**, 1543-1548.
83. M. Nussbaum and J. Z. Voitlander, *Z. Naturforsch. A*, 1965, **20 A**, 1417.
84. A. B. Pangborn, M. A. Giardello, R. H. Grubbs, R. K. Rosen and F. J. Timmers, *Organometallics*, 1996, **15**, 1518-1520.
85. D. Bradley, G. Williams and M. Lawton, *Journal of Organic Chemistry*, 2010, **75**, 8351-8354.
86. T. K. Panda, M. T. Gamer and P. W. Roesky, *Organometallics*, 2003, **22**, 877-878.
87. S. C. You, M. Gubler and M. Neuenschwander, *Helv Chim Acta*, 1994, **77**, 1346-1362.
88. S. Collins, Y. Hong and N. J. Taylor, *Organometallics*, 1990, **9**, 2695-2703.
89. Bruker-AXS SAINT V7.68A, Madison, Wisconsin.
90. G. M. Sheldrick, SADABS V2008/1 or TWINABS V2008/4, University of Göttingen, Germany.
91. G. M. Sheldrick, *Acta Crystallogr.*, 2008, **A64**, 112-122.
92. G. A. Bain and J. F. Berry, *J. Chem. Educ.*, 2008, **85**, 532.
93. Least-squares Curie-Weiss fitting of the experimental magnetic data was carried out using OriginPro program (2017 version).
94. O. Kahn, *Molecular Magnetism*, VCH, Weinheim, Germany, 1993.

3 Influence of Monomer Structure on the Ring-Opening Polymerisation Behaviour of Low Strain [*n*]Nickelocenophanes

3.1 Abstract

Ring-opening polymerisation (ROP) of strained [1]- and [2]metallocenophanes and related species is well-established, and the accompanying ring-strain is manifest in a substantial tilting of the cyclopentadienyl ligands to give α angles of ~14–33°. Highly unexpectedly, tetracarba[4]nickelocenophane [Ni(η^5-C_5H_4)$_2$(CH_2)$_4$] (**3.2**) undergoes ring-opening polymerisation (ROP) (pyridine, 20 °C, 5 days) to give primarily insoluble poly(nickelocenylbutylene) [Ni(η^5-C_5H_4)$_2$(CH_2)$_4$]$_n$ (**3.12**) despite the lack of significant ring-tilt. The exoenthalpic nature of the ROP was confirmed by DFT calculations involving the cyclic precursor and model oligomers (ΔH^0_{ROP} = −14±2 kJ mol^{-1}), and is proposed to be a consequence of torsional strain present in the *ansa* bridge of **3.2**. The similarly untilted 1,1,3,3-tetramethyldisila-2-oxa[3]nickelocenophane [Ni(η^5-C_5H_4)$_2$($SiMe_2$)$_2$O] (**3.13**) and 1,3-dimethyl-1,3-diphenyldisila-2oxa[3]nickelocenophane [Ni(η^5-C_5H_4)$_2$($SiMePh$)$_2$O] (**3.14**) were found to be resistant to ROP under the same conditions. In contrast, 1-methyltricarba[3]nickelocenophane [Ni(η^5-C_5H_4)$_2$(CH_2)$_2$(CH(CH_3))] **3.15** was found to undergo ROP to give soluble polymer [Ni(η^5-C_5H_4)$_2$(CH_2)$_2$(CH(CH_3))]$_n$ **3.18**. The reversibility of the process allowed for the effects of temperature and reaction concentration on the equilibrium of this polymerisation to be explored and thereby thermodynamic data to be elucidated (ΔH^0_{ROP} = −8.9 kJ mol^{-1}, ΔS^0_{ROP} = −20 J K^{-1} mol^{-1}, ΔG^0_{ROP} = −3.1 kJ mol^{-1}). Compared to the previously described ROP of the unsubstituted tricarba[3]nickelocenophane [Ni(η^5-C_5H_4)$_2$(CH_2)$_3$] **3.1** (ΔH^0_{ROP} = −10 kJ mol^{-1}, ΔG^0_{ROP} = −4.0 kJ mol^{-1}), the presence of the additional methyl substituent to the *ansa* bridge appears

to marginally disfavour ROP in the equilibrium between monomer and polymer. In addition, the small change in ΔG^0_{ROP} is sufficient to significantly decrease the yields of **3.18** compared to poly(nickelocenylpropylene) $[Ni(\eta^5\text{-}C_5H_4)_2(CH_2)_3]_n$ **3.7$_x$**/**3.8** under analogous conditions.

3.2 Introduction

Metal-containing polymers (metallopolymers) are of widespread interest due to the large variety of properties that can result from incorporation of a diverse range of metal centres. The metals can be located either in the main-chain of the polymer or in side groups, and the interactions between the metal ions and ligands can be covalent, leading to essentially static binding, or non-covalent/labile, which can allow for a reversible, dynamic nature.[1-3] Metallopolymers have proved crucial in a variety of applications, including data storage,[4] antibacterial activity,[5] artificial metalloenzymes,[6, 7] emissive materials,[8, 9] nanopatterning,[10-12] stimuli-responsive behaviour,[13] and sensors.[14, 15]

Since the first report of the ring-opening polymerisation (ROP) of dimethylsila[1]ferrocenophane in 1992,[16] this method has become a well-used pathway to main-chain iron-containing polymers with a variety of bridging elements. The resulting polyferrocenes have attracted interest as a result of their redox responses,[17, 18] self-assembly behaviour,[19-22] and preceramic properties[23, 24] amongst others.[25] In contrast, polynickelocenes, synthesised from the ROP of [*n*]nickelocenophanes, are limited in number. For the 20 valence electron (VE) [*n*]nickelocenophanes, the two extra VEs (compared to [*n*]ferrocenophanes which have 18 VEs) are accommodated in molecular orbitals with antibonding character, which results in a weaker and elongated Ni–Cp bond.[26] This bond elongation causes a concomitant increase in the angle between the Cp ring planes, α, compared to analogous iron and cobalt species,[27-29] and the low bond strength helps to explain the small number of reported [*n*]nickelocenophanes (all structurally characterised examples, **3.1**–**3.6**, are included in Figure 3.1).[29-32]

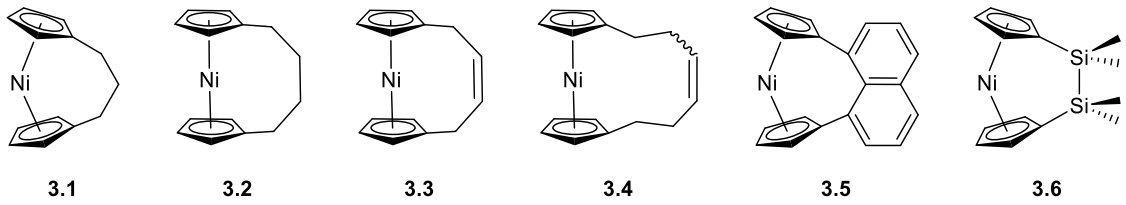

Figure 3.1. Currently structurally characterised [*n*]nickelocenophanes.

Recently the ROP of tricarba[3]nickelocenophane **3.1** to yield polynickelocene **3.7$_x$**/**3.8** was reported.[30, 33] It was demonstrated that **3.7$_x$**/**3.8** exists in a labile state and can form a dynamic equilibrium with **3.1** in polar organic solvents as a consequence of the weak Ni–Cp bonds (M–Cp dissociation energy is 250 kJ mol^{-1} for nickelocene vs. 305 kJ mol^{-1} for ferrocene), Scheme 3.1.[33, 34]

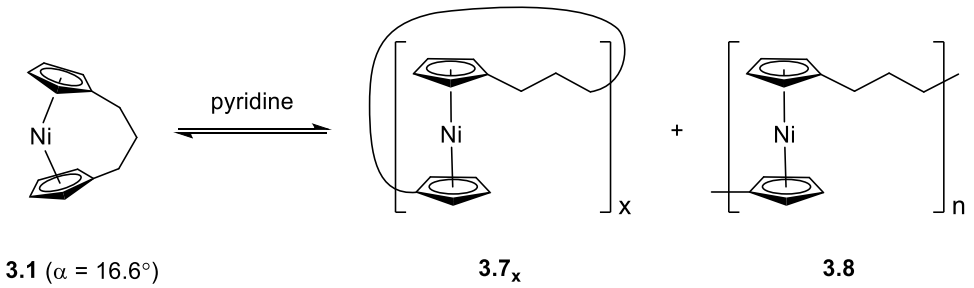

Scheme 3.1. Reversible ROP of tricarba[3]nickelocenophane, **3.1**.

Variable temperature ^{1}H NMR spectroscopy allowed for the elucidation of the entropic and enthalpic parameters characterising this ROP process: a small, favourable value of ΔH (−10 kJ mol^{-1}), and a very small, unfavourable value for ΔS (−20 J K^{-1} mol^{-1}).[33] The thermodynamic driving force for the ROP of [*n*]metallocenophanes is ascribed to the strain in these precursors,[35-37] which is generally quantified by the tilt-angle, α, the angle between the Cp plane and the Cp−(ER$_x$)$_y$ bond, β, and the angle δ, which is defined as the Cp^C–Ni–Cp^C (Cp^C = Cp centroid) angle, Figure 3.2. Estimations of the value for the ROP enthalpy, ΔH_{ROP}, for [*n*]ferrocenophanes were previously made on the basis of differential scanning calorimetry (DSC) analyses of ROP exotherms. These values range from ~12 kJ mol^{-1} for carbaphospha[2]ferrocenophane **3.11** (α = 15.0°)[38] to ~130 kJ mol^{-1} for thia[1]ferrocenophane **3.9** (α = 31.0°),[39] with the ΔH_{ROP} value for the well-known

dimethylsila[1]ferrocenophane **3.10** ~80 kJ mol^{-1} (α = 20.8°).[27] The value for the ROP of tricarba[3]nickelocenophane is comparable to that of **3.9**, with which it has a comparable tilt angle (**3.1**: α = 16.6°),[33, 38] and is consistent with the relatively low energy penalty for tilting nickelocene (presumably expressed in the elongated, weaker Ni–Cp bonds and the consequential ease of bending about the Cp–Ni–Cp axis).[33] It is also not dissimilar to ΔH^0_{ROP} values for moderately strained rings such as THF (ΔH^0_{ROP} = −19 kJ mol^{-1}) and hexamethylcyclotrisiloxane (ΔH^0_{ROP} = −23 kJ mol^{-1}).[40]

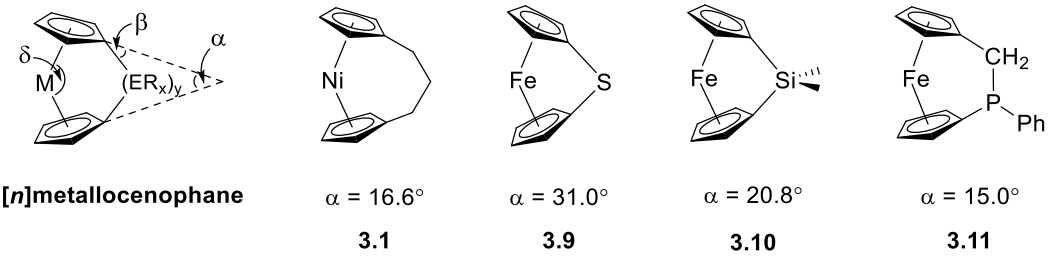

Figure 3.2. [*n*]Metallocenophanes **3.1**, **3.9**, **3.10**, **3.11** and their respective tilt-angles.

Whilst the ROP of **3.1** is a highly unusual example of [*n*]metallocenophane ROP due the presence of a dynamic equilibrium, these types of reversible ROP are more common for organic cyclic species, for example: THF in the presence of Lewis acids;[41] cyclopentene in the presence of various metal alkylidene complexes;[42, 43] and substituted cyclic six-membered carbonates in the presence of DBU.[44]

Based on the small value for the ΔH^0_{ROP} of **3.1**,[33] which has a tilt angle of 16.6°, we were recently surprised to find that tetracarba[4]nickelocenophane **3.2**, which possesses a negligible tilt-angle (α = 1.0(3)°; δ = 178.63(11)°), also undergoes ROP (pyridine, 0.74 M, 5 days, 20 °C).[45] The resulting polynickelocene **3.12** (Figure 3.3) was isolated as a predominantly insoluble material. Herein we examine the nature of the thermodynamic driving force for the ROP of **3.2** using DFT calculations. We also describe and attempt to explain the ROP behaviour of several new [3]nickelocenophanes **3.13**, **3.14**, and **3.15** (Figure 3.3).

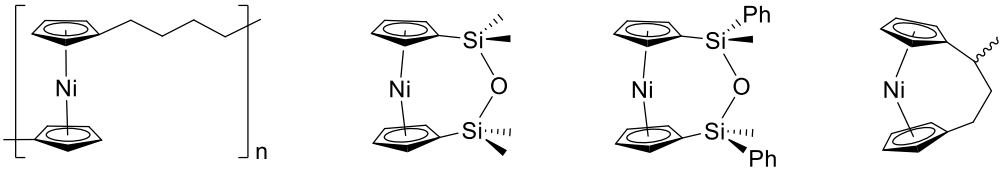

3.12$_a$: n > 9
3.12$_b$: n < 9

3.13 **3.14** **3.15**

Figure 3.3. Nickelocene-containing species discussed in Chapter 3.

3.3 Results and Discussion

3.3.1 Comparative Structural Data for Tricarba[3]nickelocenophane **3.1** and Tetracarba[4]nickelocenophane **3.2**

The lack of ring-strain exhibited by **3.2** demonstrates that the thermodynamic driving force for this polymerisation is clearly not manifested in the reduction of tilt upon ring-opening. Whilst the ROP of **3.2** may still be exoenthalpic, it not feasible to prove this experimentally as in the case of **3.1**, due to the insolubility of the oligomeric **3.12** at 20 °C and the resulting lack of dynamic equilibrium. It should be noted that the ROP of **3.2** is reversible at increased temperatures (above 50 °C), presumably as heating is necessary to solubilise **3.12**.

Ring-strain energy in cyclic monomers is manifested in the enthalpic component of the free energy of ring-opening, which can also comprise other contributions in addition to the strain resulting from ring tilt about the metal centre. These include: angle strain, caused by deviation of bond angles from the ideal; torsional strain due to repulsion occurring when ring substituents separated by three bonds appear in an eclipsed conformation instead of the more stable staggered conformation; and transannular strain, generated by non-bonding interactions between ring substituents on non-adjacent atoms. Thus, these aspects of strain must also be considered when analysing the ROP of **3.2**. The structures of **3.2** and **3.1**, shown in Figure 3.4 and Figure 3.5, respectively, possess different degrees of these types of strain.

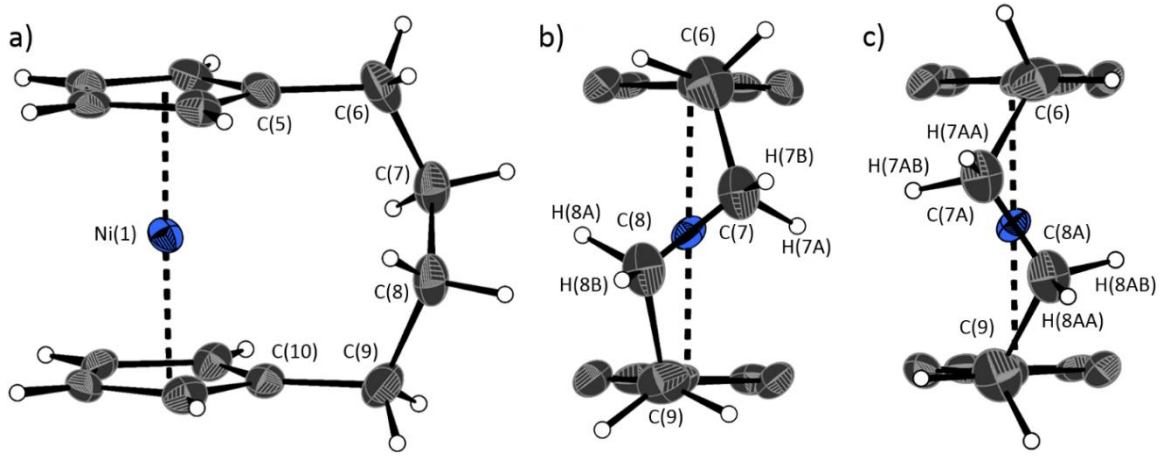

Figure 3.4. Three views of the molecular structure of **3.2**.[45] Thermal ellipsoids displayed at the 50% probability level. Hydrogen atoms are pictured as spheres of arbitrary radii (and some have been omitted for clarity). a) The *ansa* bridge is disordered over two positions: C7/7A and C8/8A (for clarity, positions with highest relative occupancy (62%) are displayed). Alternate view of **3.2** displaying b) major (62%) and c) minor (38%) component of disordered bridge. Selected distances (Å) and angles (°): Ni(1)–Cp_{cent} 1.813(3)/1.817(3), α = 1.0(3), δ = 178.63(11).

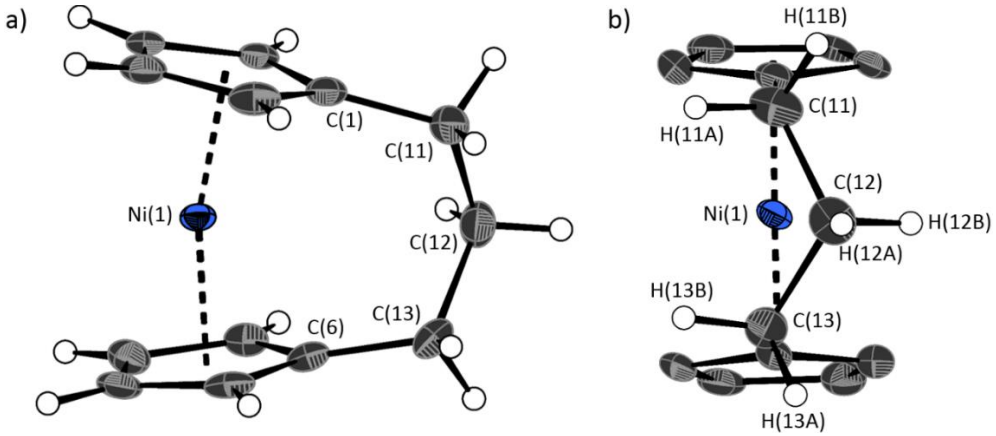

Figure 3.5. Two views a) and b) of the molecular structure of **3.1**.[30] Thermal ellipsoids displayed at the 50% probability level. Hydrogen atoms are pictured as spheres of arbitrary radii (and some have been omitted for clarity). Selected distances (Å) and angles (°): Ni(1)–Cp_{cent} = 1.8039(14)/1.8035(14), α = 16.64(13), β = 4.2(3), δ = 166.33(5).

Firstly, whilst both **3.1** and **3.2** appear to exhibit angle strain as the bond angles within the *ansa* bridge deviate from the ideal tetrahedral geometry, these deviations are smaller in **3.2** (C(5)–C(6)–C(7): 113.9(6)°, C(6)–C(7)–C(8): 112.4(7)°) than in **3.1** (C(1)–C(11)–C(12):

115.8(3)°, C(11)–C(12)–C(13): 115.0(2)°) (Table 3.1). While this does not rule it out as a driving force for ROP, there appears to be a far more significant factor: torsional strain appears to be considerably greater in **3.2** than in **3.1**. This is apparent when studying Figures 3.4 and 3.5. The protons on the bridging carbons of **3.1** adopt a fairly staggered conformation (H(11B)–C(11)–C(12)–H(12A): 47.6(3)°, H(12A)–C(12)–C(13)–H(13A): 41.3(4)°); whereas, the protons on the central C–C bond in the *ansa* bridge of **3.2** are almost eclipsed in conformation (H(7B)–C(7)–C(8)–H(8B): 10.2(8)°, H(7AA)–C(7A)–C(8A)–H(8AA): 5.6(12)°). The appearance of torsional strain in **3.2** may result in an exothermic ROP process, in line with the ROP of **3.1**. Whilst it is also possible that the ROP of **3.2** is entropically favoured, i.e. driven by greater conformational freedom allowed in the polymer versus the monomer, the ROP of **3.1** is known to be endoentropic[33] (as is typical of most ROP processes)[40] and it is unlikely to be significantly different in the case of **3.2**.

Table 3.1. Selected distances (Å) and angles (°) in the *ansa* bridges of both **3.1** and **3.2**. (α = angle between the plane of each Cp ring, β = [180° − (Cp_{cent}–Cp_{ipso}–C_{bridge})] angle, δ = Cp_{cent}–Ni–Cp'_{cent} angle).[30, 45]

	Distances (Å)		Angles (°)	
3.2	Ni(1)–Cp_{cent}	1.813(3), 1.817(3)	α	1.0(3)
			β (C(5), C(10))	0.5(6), 1.6(5)
			δ	178.63(11)
	C(6)–C(7)	1.531(11)	C(5)–C(6)–C(7)	113.9(6)
	C(7)–C(8)	1.515(13)	C(6)–C(7)–C(8)	112.4(7)
	C(8)–C(9)	1.548(11)	C(7)–C(8)–C(9)	115.3(7)
	H(7B)···H(8B)	2.15906(8)	C(8)–C(9)–C(10)	114.6(6)
	C(6)–C(7A)	1.556(12)	H(7B)–C(7)–C(8)–H(8B)	10.2(8)
	C(7A)–C(8A)	1.51(2)	C(5)–C(6)–C(7A)	112.3(8)
	C(8A)–C(9)	1.543(15)	C(6)–C(7A)–C(8A)	116.2(10)
	H(7AA)···H(8AA)	2.1464(1)	C(7A)–C(8A)–C(9)	113.3(11)
			C(8A)–C(9)–C(10)	112.3(7)
			H(7AA)–C(7A)–C(8A)–H(8AA)	5.6(12)
3.1	Ni(1)–Cp_{cent}	1.8039(14), 1.8035(14)	α	16.64(13)
			β (both are identical)	4.2(3)
			δ	166.33(5)
	H(12A)···H(13A)	2.26006(8)	C(1)–C(11)–C(12)	115.8(3)
	H(12A)···H(11B)	2.28442(8)	C(11)–C(12)–C(13)	115.0(2)
	C(11)–C(12)	1.529(5)	C(12)–C(13)–C(6)	115.28(19)
	C(12)–C(13)	1.533(3)	H(11B)–C(11)–C(12)–H(12A)	47.6(3)
			H(12A)–C(12)–C(13)–H(13A)	41.3(4)

3.3.2 DFT Calculations of the Enthalpy of Ring-Opening for **3.1** and **3.2**

Due to the lack of feasibility of investigating the enthalpic contribution to ΔG^0_{ROP} of monomer **3.2** experimentally, we explored the ROP of this [*n*]nickelocenophane and **3.1** using DFT. Calculations were performed by modelling the cyclic precursors and a series of linear oligomers (Schemes 3.2 and 3.3). Firstly, we studied the ring opening of **3.1** using the

molecule **3.1$_a$**, which is related by the addition of dihydrogen across the carbon backbone and serves as a model for polymer **3.8**. Addition of one monomer molecule to yield the linear dimer provided the enthalpic change upon ring-opening of the monomer. Further addition of two successive monomer units produced the linear trimer **3.1$_c$**, then the linear tetramer **3.1$_d$**. The enthalpy change upon ring-opening was estimated in each case and averaged over all linear oligomer models. As the calculated enthalpy of ring-opening, ΔH_{RO}, for **3.1** (-11 ± 3 kJ mol^{-1}) compares well to the experimental ΔH_{ROP} value (-10 kJ mol^{-1}),[33] the computational model was deemed appropriate. Thus, the model was applied in the same manner to ring-opened monomer **3.2$_a$** (Scheme 3.3). The calculated enthalpy of ring-opening for **3.2** (-14 ± 2 kJ mol^{-1}) is both negative and within error of that calculated for **3.1**. This suggests that the ROP of **3.2** is exoenthalpic, driven by the release of ring-strain that is manifested not in the usual ring-tilt but presumably in the torsional strain present in the *ansa* bridge instead. All computational details regarding these calculations are provided in Appendix III.

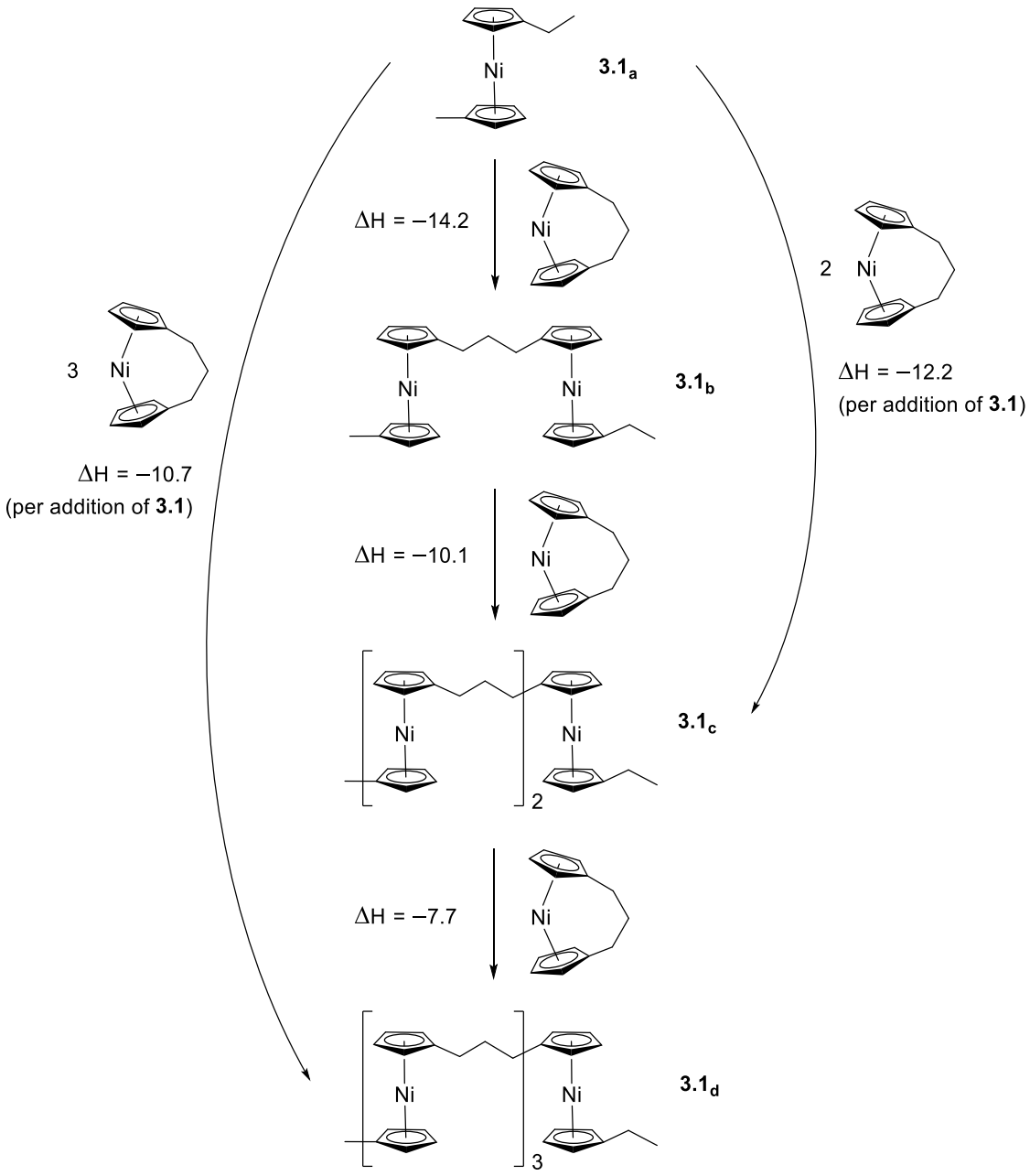

Scheme 3.2. Scheme describing DFT calculations of the ring-opening of monomer **3.1** to form linear oligomeric species and values of enthalpic ring-opening (kJ mol^{-1}).

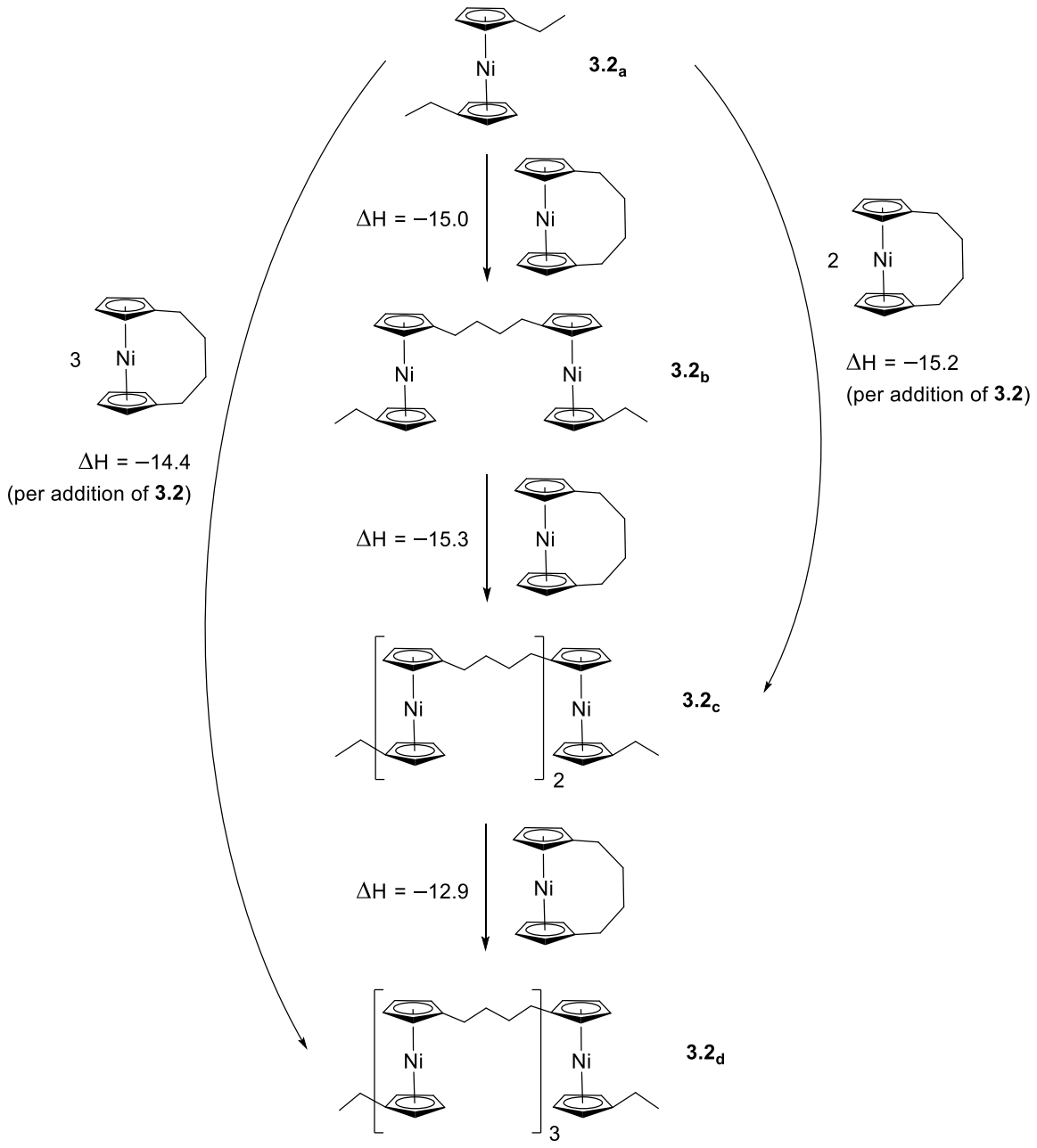

Scheme 3.3. Scheme describing DFT calculations of the ring-opening of monomer **3.2** to form linear oligomeric species and values of enthalpic ring-opening (kJ mol^{-1}).

In addition to the polynickelocenes mentioned above, we previously reported the formation of poly(tetramethyldisilylnickelocene) $[Ni(\eta^5\text{-}C_5H_4)_2(SiMe_2)_2]_n$ **3.16** from a tetramethyldisila-bridged [2]nickelocenophane **3.6** (Figure 3.1). Whilst ring strain is clearly present in the monomer **3.6** ($\alpha = 9.4(8)°$), this species possesses a lower degree of strain than **3.1** ($\alpha = 16.6(1)°$). Despite this, the polymerisation of **3.6** proceeds in pyridine to give predominantly insoluble polynickelocene, reminiscent of the case of **3.12**, with no dynamic

equilibrium at 20 °C. We therefore applied a similar DFT model to **3.6** and the corresponding linear oligomers to determine the enthalpy of ring opening (ΔH_{RO} = −12±3 kJ mol^{-1}), which compares well to those determined for ring-opening of **3.1** and **3.2** (Scheme A3.1).

3.3.3 Synthesis and ROP Behaviour of Disila-2-oxa[3]nickelocenophanes **3.13** and **3.14**, and Substituted Nickelocene **3.17**

As discussed earlier, the insolubility of poly(nickelocenylbutylene) did not allow for the experimental determination of values of the entropy and enthalpy for ROP. Thus, other untilted monomers were targeted, that might undergo polymerisation to afford a soluble polymeric product. We considered the inclusion of a siloxane-based bridging element as it would be expected to significantly increase the solubility of a polynickelocene (syntheses of iron[46] and titanium[47] [*n*]metallocenophanes and [*n*]metalloarenophanes featuring a siloxane-based bridge have been previously reported).

The synthesis of 1,1,3,3-tetramethyldisila-2-oxa[3]nickelocenophane **3.13** (Figure 3.6) was conducted via a fly-trap procedure analogous to that previously employed for [*n*]nickelocenophanes **3.1**, **3.2**, and **3.6**, involving the reaction of the lithiated fly-trap ligand $Li_2[(C_5H_4)_2(SiMe_2)_2O]$ and $NiCl_2$.

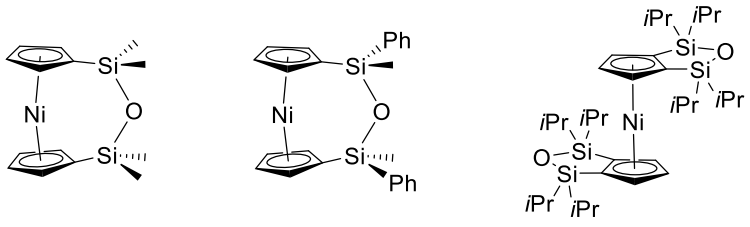

3.13 **3.14** **3.17**

Figure 3.6. [*n*]Nickelocenophanes **3.13** and **3.14**, and substituted nickelocene **3.17**.

The fly-trap reaction yielded **3.13** as a green crystalline solid in moderate yield (43%). ^{1}H NMR spectroscopy (C_6D_6) revealed resonances at −239 and −248 ppm which were assigned to the α- and β-Cp proton environments respectively, and at 8.6 ppm which was assigned to the $SiMe_2$ protons in the *ansa* bridge (Figure A3.1). Crystallisation from *n*-hexanes yielded

green crystals that allowed for full characterisation by X-ray diffraction. As expected, **3.13** exhibits a very small tilt-angle, α, of 3.76(10)° (Figure 3.7).

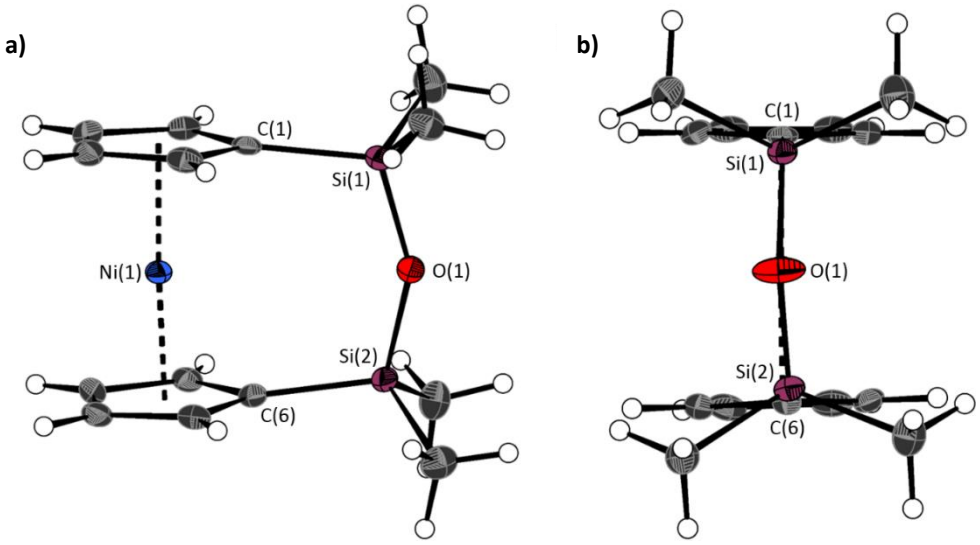

Figure 3.7. Two views a) and b) of the molecular structure of 1,1,3,3-tetramethyldisila-2-oxa[3]nickelocenophane **3.13**. Hydrogen atoms are pictured as spheres of arbitrary radii. Thermal ellipsoids displayed at the 50% probability level. Selected distances (Å) and angles (°): Ni(1)–Cp_{cent} = 1.8180(12)/1.8172(3), Si(1)–O(1) = 1.635(2), O(1)–Si(2) = 1.635(2), Ni(1)O(1) distance = 3.5217(18), α = 3.76(10), β = 4.3(2)/5.0(2), δ = 177.20(2).

A second siloxane-bridged [3]nickelocenophane with sterically demanding groups at silicon was also synthesised. 1,3-Dimethyl-1,3-diphenyldisila-2oxa[3]nickelocenophane **3.14** (Figure 3.6) was prepared by the reaction of the lithiated fly-trap ligand $Li_2[(C_5H_4)_2(SiMePh)_2O]$ with nickel dichloride in a similar procedure to **3.13**.[30, 45] Unlike other [*n*]nickelocenophanes, the green solid produced did not sublime, presumably due to its increased molar mass. Subsequent recrystallisations from *n*-hexanes and *n*-pentane allowed for the formation of green single crystals suitable for X-ray diffraction. Two diastereomers of **3.14** were possible given the diastereomeric nature of the fly trap ligand $Li_2[(C_5H_4)_2(SiMePh)_2O]$, but all isolated crystalline material proved to be the C_2-symmetric (*trans*) isomer (Figure 3.8). Compound **3.14** displays a very small tilt-angle of 4.18(8)°, marginally greater than that of **3.13**. ^{1}H NMR spectroscopy (C_6D_6) of the crystalline material revealed resonances at −237.2, −239.3, and −247.2 ppm assigned to the Cp proton

environments, at 0.40 ppm assigned to the methyl protons in the *ansa* bridge, and between 7.58–8.54 attributed to the phenyl proton environments (Figure A3.2).

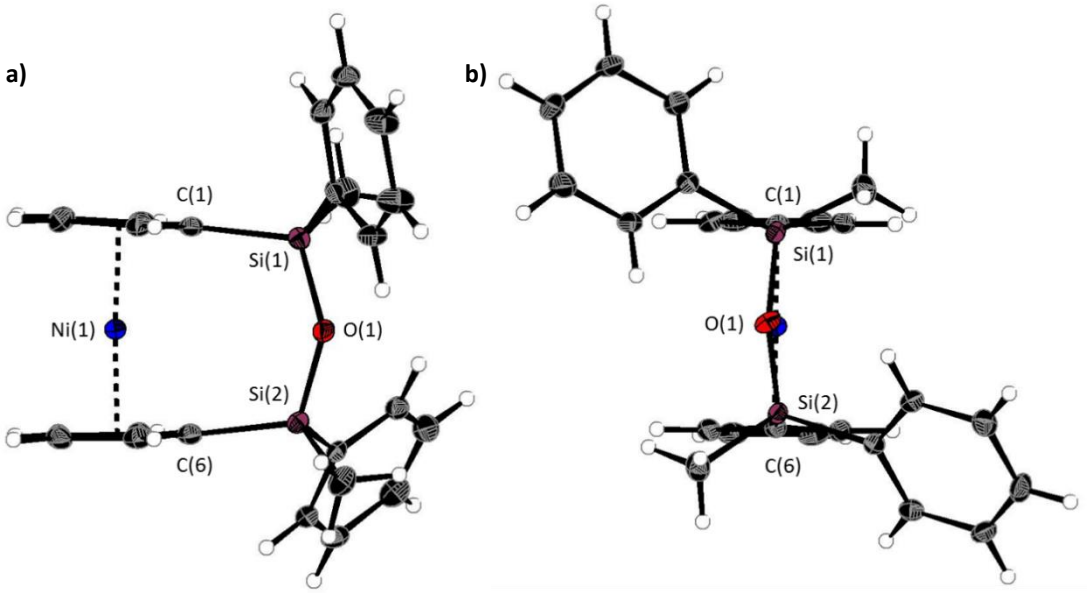

Figure 3.8. Two views a) and b) of the molecular structure of 1,3-dimethyl-1,3-diphenyldisila-2oxa[3]nickelocenophane **3.14**. Hydrogen atoms are pictured as spheres of arbitrary radii. Thermal ellipsoids displayed at the 50% probability level. Selected distances (Å) and angles (°): Ni(1)–Cp_{cent} = 1.8188(9)/1.8165(9), Si(1)–O(1) = 1.6366(14), O(1)–Si(2) = 1.656(14), Ni(1)O(1) distance = 3.5605(14), α =4.18(8)°, β = 3.11(10)/5.04(10), δ = 177.07(4).

Interestingly, attempts to produce 1,1,3,3-tetraisopropyldisila-2-oxa[3]nickelocenophane were foiled due to an unforeseen ring closure reaction in the ligand formation step, presumably due to the steric bulk of the isopropyl groups. The lithiated bulky Cp ligand was reacted with nickel dichloride to produce the unexpected species 1,1′,2,2′-bis(tetraisopropyldisiloxa)nickelocene, **3.17** (Figure 3.6), as a green crystalline solid in 54% yield. X-ray crystallography confirmed the presence of the substituted nickelocene, Figure 3.9. ^{1}H NMR resonances at −199.5 and −234.8 ppm were assigned to protons in Cp environments, and a series of resonances between 2.23 and 6.69 ppm to protons of the isopropyl groups (Figure A3.3). An attempt to produce a cross-linked polynickelocene from the substituted nickelocene, via addition of *s*BuLi and subsequent ring-opening of the Si_2OC_2

ring, were unsuccessful. A colour change from green to brown was observed but products were unidentifiable by ^{1}H NMR spectroscopy and ESI mass spectrometry. Although the synthesis of 1,1,3,3-tetraisopropyldisila-2-oxa[3]nickelocenophane was not successful, nor the ring-opening reaction of **3.17**, a facile route to lithiated, substituted Cp rings has been discovered, which may prove useful in other areas of metallocene chemistry.

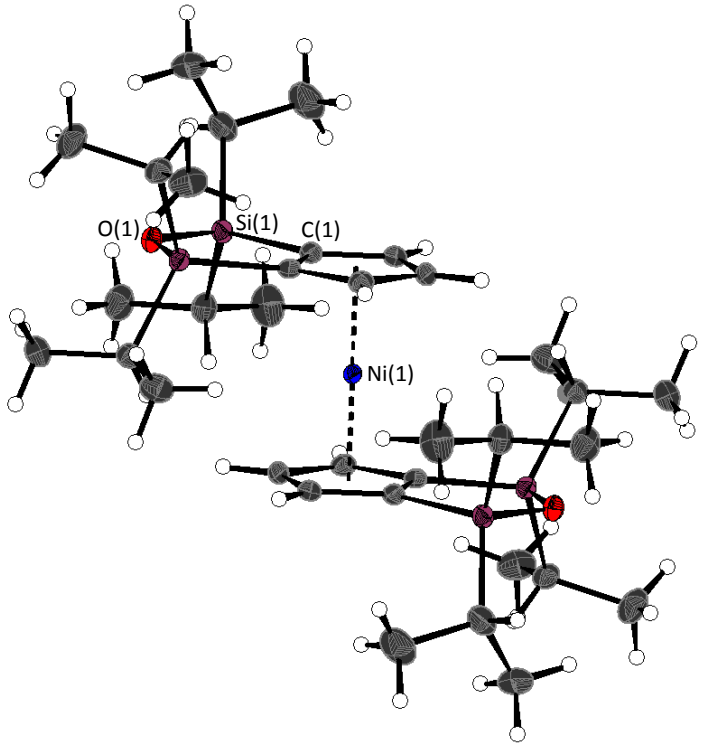

Figure 3.9. A view of the molecular structure of **3.17**. Hydrogen atoms are pictured as spheres of arbitrary radii. Thermal ellipsoids displayed at the 50% probability level. Selected distance (Å): Ni(1)–Cp_{cent} = 1.8239(11)/1.8239(11).

ROP conditions (d_5-pyridine, 0.79 M, 48 h, 20 °C) employed successfully for **3.1**, **3.2**, and **3.6** were then applied to **3.13**, but in contrast to the similarly unstrained tetracarba[4]nickelocenophane **3.2**, exposure to pyridine did not induce polymerisation. This was demonstrated by ^{1}H NMR spectroscopy, which showed only the presence of the unreacted monomer **3.13**. No evidence of reaction could be found even after repeating ROP at higher concentration (1.31 M) for an extended period of time (4 weeks). Several further attempts were made to induce polymerisation; firstly, by the reaction of Na[C_5H_5] (both as

an equimolar reagent and at substoichiometric quantities) with **3.13** under photolytic conditions (THF, 5 °C), but again no reaction occurred as evidenced by ^{1}H NMR spectroscopy. Additionally, **3.13** was treated with equimolar 1,2-bis(diphenylphosphino)ethane (dppe), but this resulted in complete expulsion of the ligand framework and formation of [Ni(dppe)$_2$] (observed by ^{31}P NMR spectroscopy at 44.8 ppm). Whilst similar reactivity has been observed for **3.1**[30] the driving force for this reaction was suggested to be the release of ring strain derived from ring tilt, which cannot be the case for **3.13**, because the ring-tilt value α is close to zero. To determine whether this [3]nickelocenophane would undergo thermal ROP, preliminary differential scanning calorimetry (DSC) experiments were performed. These indicated melt and crystallisation processes for **3.13**, in addition to a small exotherm feature at ~184 °C (Figure A3.4). No new transitions were observed even after repeated heating cycles, and thus we concluded that thermal ring-opening would also prove unsuccessful.

In a similar manner to **3.13**, exposure of **3.14** to ROP conditions (d_5-pyridine, 0.79 M, 48 h, 20 °C) did not induce polymerisation. The reaction was monitored by ^{1}H NMR spectroscopy, which displayed only the presence of the monomer after one week. Unreacted starting material was obtained quantitatively via removal of the solvent in vacuo.

The cause for the stability of **3.13** and **3.14** to ROP, where the similarly untilted **3.2** undergoes facile polymerisation, may be deduced from the structural parameters. The longer Si–O bonds in the *ansa* bridge of **3.13** and **3.14** (1.630(3)/1.640(3) and 1.6356(14)/1.6366(14) Å, respectively) compared to the C–C bonds in that of **3.2** (ranging from 1.51(2)–1.556(12) Å), and the lack of substituents at oxygen, ensure that the torsional strain present in **3.2** does not occur in the siloxane-bridged species. Without this strain, and the ring-tilt that occurs in [*n*]nickelocenophanes **3.1** and **3.6**, there is no thermodynamic propensity for polymerisation. In addition, in [3]nickelocenophane **3.14** there do not appear to be any interactions between the phenyl groups in the *ansa* bridge, which could have

introduced torsional strain.

We deemed it prudent to test our computational model for the ring-opening of [*n*]nickelocenophanes to form linear oligomers with the siloxane-bridged [3]nickelocenophane **3.13**, as this species was resistant to ROP, and thus the calculated ΔH_{RO} should prove unfavourable. As expected, the computational model predicted the enthalpy of ring-opening to be small and positive (ΔH_{RO} = 5±1 kJ mol^{-1}) (Scheme A3.2).

3.3.4 Synthesis and ROP Behaviour of Methyltricarba[3]nickelocenophane **3.15**

To accompany our study on the ROP behaviour of [*n*]nickelocenophanes, we investigated the ROP of a methylated derivative of **3.1**, namely methyltricarba[3]nickelocenophane **3.15**. The incorporation of a larger substituent on the bridge via the formal replacement of H by Me would be expected to make ROP less favourable.

[*n*]Nickelocenophane **3.15**, the first unsymmetrically substituted example, was synthesised as an enantiomeric mixture using the general method previously reported (reaction of lithiated ligand $Li_2[(C_5H_4)_2(CH_2)_2(CH(CH_3))]$ with nickel dichloride).[30, 45] Sublimation and subsequent recrystallisation in *n*-hexanes afforded dark green crystals of **3.15** in 30% yield. ^{1}H NMR spectroscopy of the crystalline material revealed resonances at −240, −243, and −247 ppm which were assigned to the α-Cp protons, and at −267 and −271 ppm which were assigned to the β-Cp protons respectively (see Figure A3.5). Resonances at −21 and −34 ppm were assigned to the β-H of the bridging carbons, and the resonance at 14 ppm was assigned to protons in the *ansa* bridge methyl group. X-ray crystallographic data confirmed the structure, but due to co-crystallisation of the two enantiomers (Figure 3.10), significant conformational restraints had to be applied and so the following data should be treated with prudence: α was determined as 16.3(2)°, very similar to that of **3.1 (**16.6(13)°).

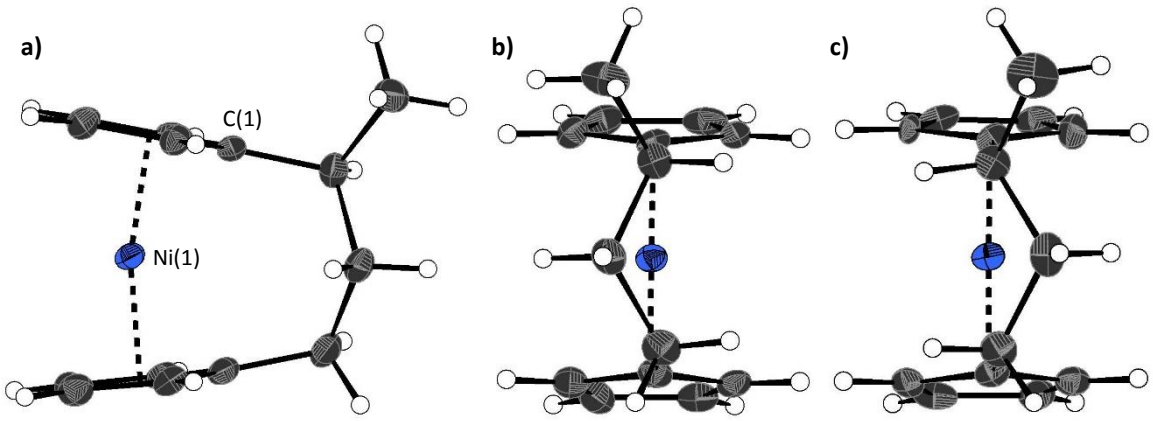

Figure 3.10. a) Molecular structure of **3.15**. Thermal ellipsoids displayed at the 50% probability level. Hydrogen atoms are pictured as spheres of arbitrary radii. Compound **3.15** is disordered over two positions b) major (62%) and c) minor (38%) component of disordered structure. Selected distances for major fragment (Å) and angles (°): Ni(1)–Cp_{cent} 1.795(6)/1.798(6), α = 16.3(2), δ = 166.0(3) (the angle δ is defined as the Cp^C–Ni–Cp^C (Cp^C = Cp centroid) angle).

As the ROP of **3.1** produces the soluble oligomeric product **3.7$_x$**/**3.8**, it was imagined that a polymeric product resulting from the ROP of **3.15** would also be soluble in common organic solvents. The ROP of this substituted [3]nickelocenophane was investigated in deuterated pyridine under the same conditions as used for tricarba[3]nickelocenophane (0.79 M, 20 °C), Scheme 3.4, and a gradual colour change from dark blue to green was observed.

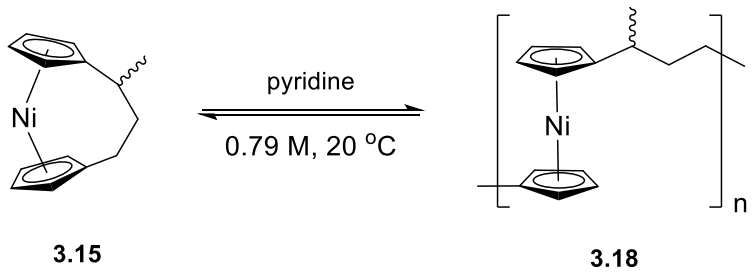

Scheme 3.4. ROP of **3.15** to give **3.18** in pyridine (0.79 M).

The reaction was followed by ^{1}H NMR spectroscopy: after 24 h, alongside shifts assigned to Cp-ring protons in **3.15**, a broad singlet was observed at −251 ppm that was assigned to polymer Cp-ring protons. Integration of the high field resonances corresponding to Cp protons indicated the presence of ~41% polynickelocene **3.18**. After a further 24 h, a

negligible increase in conversion to polymer was detected (~42%), and this remained constant after 7 days. This suggests the presence of an equilibrium that is reached after 24 h. Attempted isolation of the resulting polymer via precipitation of the reaction solution (0.79 M, 48 h, 20 °C) into rapidly stirring *n*-hexanes at 20 °C was unsuccessful. However, when a THF solution of the reaction mixture was precipitated into −78 °C *n*-hexanes, a green solid was isolated. ^{1}H NMR spectroscopy of the product (**3.18**) revealed resonances at 185.4, 179.6, and 146.7 ppm assigned to the α-protons of the carbon bridge and at 22.1 ppm which was assigned to the methyl protons (Figure A3.6). A broad resonance at −246.3 ppm was assigned to the Cp-proton environment. Analysis of the reaction mixture prior to precipitation by MALDI-TOF mass spectrometry revealed assignable peaks up to ~8000 g mol^{-1}, which corresponds to a DP_n of ~33 (Figure A3.7). MALDI-TOF mass spectrometry of the isolated polymer was unsuccessful, however, presumably due to difficulties in ionising the higher molar mass fraction. Polynickelocene **3.18** was then stirred in d_5-pyridine for 48 h at 20 °C. ^{1}H NMR spectroscopy displayed resonances assigned to protons in both monomer **3.15** and polymer **3.18**, consistent with the reversible nature of the polymerisation, and the presence of a dynamic equilibrium.

Percentage polymer concentration as a function of time was further investigated at a range of ROP concentrations (0.11–1.31 M, Table 3.2). ^{1}H NMR spectroscopic analysis revealed an increase in the proportion of **3.18** with increased reaction concentration. Additionally, the yield of isolated polymer increased with concentration (it was only possible to isolate polymer at 0.79 and 1.31 M). The discrepancy between the isolated polymer yield and that determined by integration of ^{1}H NMR shifts was presumably due to the presence of oligomeric species which did not precipitate upon workup of the reaction solution.

Table 3.2. A comparison of yields measured for **3.18** from ROP at different concentrations.

Sample	Conc. (M)	% of **3.18** (^{1}H NMR spectroscopy)			%Yield of **3.18** (20 °C)*	%Yield of **3.18** (−78 °C)*
		24 h	48 h	7 days		
3.18$_a$	1.31	59.8	60.8	59.5	23	65
3.18$_b$	0.79	41.1	41.8	42.2	#	29
3.18$_c$	0.44	16.9	25.0	24.3	#	#
3.18$_d$	0.22	13.7	14.3	14.3	#	#
3.18$_e$	0.11	10.7	11.6	11.5	#	#

*(T) indicates the temperature at which the reaction work-up was performed.

#No **3.18** was isolated in this case.

The effect of reaction concentration on polymer molecular weight was investigated by dynamic light scattering (DLS). DLS was performed in toluene, a marginal solvent for **3.18**, but one in which monomer/polymer equilibration is particularly slow.[33] Isolated polymer samples were prepared at a concentration of 1 mg mL^{-1} in toluene. In the preparation of the solution of **3.18$_b$** a small amount of insoluble material (presumably higher molar mass polymer) was observed, which was found in greater proportion for **3.18$_a$**, and was removed via filtration before analysis by DLS. Thus, the molecular weights measured (Table 3.3) may be slightly lower than the real values although all are estimated relative to poly(ferrocenyldimethylsilane) as a calibrant.

Table 3.3. DLS data for **3.18** isolated from ROP at various concentrations (relative to calibration with poly(ferrocenyldimethylsilane) in toluene).[48]

Sample	Conc. (M)	%Yield of **3.18**	T* / °C	R_h	Sigma	*M*w
3.18$_a$	1.31	23	20	7.42	1.69	82,700
		65	−78	9.35	3.04	126,000
3.18$_b$	0.79	#	20	#	#	#
		29	−78	6.90	1.65	72,300

*Temperature at which the reaction work-up was performed.

#No **3.18** was isolated in this case.

In comparison to the unsubstituted **3.7$_x$**/**3.8**, both isolated yields for **3.18** and polymer conversion determined by ^{1}H NMR spectroscopy are significantly lower (Table 3.4). As these polymerisations exist as dynamic equilibria with oligomers and monomer, this suggests that the introduction of the methyl substituent to the *ansa* bridge causes the reaction equilibrium to favour [*n*]nickelocenophane relative to the case of **3.1**. Generally, ROP processes are sensitive to the size of any side groups and become thermodynamically unfavourable with sterically demanding substituents.[49] However, when a series of unsymmetrically substituted sila[1]ferrocenophanes were subjected to thermal ROP, even those with bulky side groups produced high molar mass products in very good yield.[50] This is likely due to the high intrinsic strain present in the [1]ferrocenophanes (80 kJ mol^{-1} for dimethylsila[1]ferrocenophane).[16] Due to the lower strain present in [*n*]nickelocenophanes the introduction of a substituent may cause a lower propensity to ROP due to non-bonding interactions with hydrogens in the polymer bridge. Contrary to expectation, results collected using DLS appear to indicate that the isolated polynickelocene **3.18** is of higher molecular weight than the unsubstituted polynickelocene **3.7$_x$**/**3.8** isolated in analogous conditions. This result, however, should be treated with caution as the presence of a methyl substituent may lead to improved polymer-solvent interactions which would give a concomitant increase

in hydrodynamic radius.

Table 3.4. A comparison of yields measured for **3.7$_x$/3.8**[33] and **3.18**.

Conc. (M)	% of **3.18** (^{1}H NMR spectroscopy, 48 h)	%Yield of **3.18***	% of **3.7$_x$/3.8** (^{1}H NMR spectroscopy, 48 h)	%Yield of **3.7$_x$/3.8***
1.31	60.8	23	78.9	62
0.79	41.8	#	69.0	30
0.44	25.0	#	48.5	21
0.22	14.3	#	20.6	#
0.11	11.6	#	4.3	#

*Isolated yield of polymer when reaction work-up was performed at 20 °C.

#No polymer was isolated in this case.

Experimental determination of enthalpic values for ROP was performed in a similar manner to the case of **3.1** (though at increased concentration, **3.15**: 0.79 M, **3.1**: 0.44 M). Under ROP conditions (d_5-pyridine, 0.79 M) the polymerisation mixture was equilibrated for 48 h at a range of temperatures from −5 to 55 °C and then analysed by in situ ^{1}H NMR spectroscopy. As expected, temperature affects the position of the equilibrium, such that monomer is favoured at high temperature, and polymer at low temperature (Figure 3.11). Equilibrated monomer concentrations of **3.15** were fitted to Equation 1, an adaption of the Van't Hoff equation, to allow for determination of ΔH^0_{ROP} and ΔS^0_{ROP}.

$$\ln[M]_c = \frac{\Delta H^0_{ROP}}{RT} - \frac{\Delta S^0_{ROP}}{R} \qquad \textbf{Equation 1}$$

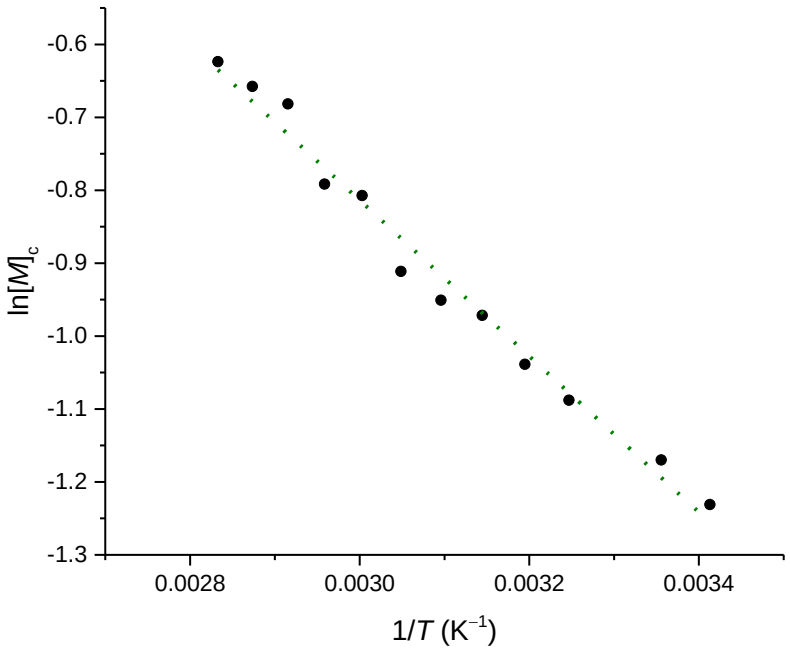

Figure 3.11. A Van't Hoff plot showing the relationship between $\log_e$ of the equilibrium monomer concentration and reciprocal temperature for the ROP of **3.15**.

The magnitudes of ΔH^0_{ROP} (−8.9 kJ mol^{-1}) and of ΔS^0_{ROP} (−20 J K^{-1} mol^{-1}) for **3.15** were comparable to those determined for the polymerisation of **3.1** (ΔH^0_{ROP} = −10 kJ mol^{-1} and ΔS^0_{ROP} = −20 J K^{-1} mol^{-1}).[33] The marginally smaller value for ΔH^0_{ROP} of **3.15** compared to that for **3.1** is likely due to the introduction of a methyl substituent to the *ansa* bridge. The entropy of ROP in both cases is relatively small and negative; this reflects the conformational flexibility of the polynickelocenes where the Cp rings exhibit free rotation about the Cp–Ni–Cp axis compared to the constrained structures of [*n*]nickelocenophanes, which partly compensates for the loss of translational entropy associated with polymerisation. At room temperature (20 °C) the values of ΔH^0_{ROP} and $T\Delta S^0_{ROP}$ for the ROP of **3.15** are similar in magnitude, resulting in a very small, favourable value for ΔG^0_{ROP} (−3.1 kJ mol^{-1}), marginally lower than that for the ROP of **3.1** (ΔG^0_{ROP} = −4.0 kJ mol^{-1}). The small value for the free energy explains the reversibility of the ROP of **3.15** to give **3.18**, and is consistent with the lower yields obtained for the ROP of **3.18** compared to **3.7$_x$**/**3.8** (Table 3.4). Employing

Equation 2 we were also able to determine a 'ceiling temperature' for the polymerisation of **3.15** at 0.79 M, T_c = 133 °C. The values of ΔH^0_{ROP} and ΔS^0_{ROP}, especially the latter, differ with depending on the state of monomer and polymer, which in turn affects T_c. Thus ΔS^0_{ROP} was recalculated using Equation 3, where x denotes a weight fraction corresponding to a monomer concentration of y mol L^{-1} (−6.8 J K^{-1} mol^{-1}). This was applied to an adapted form of Equation 2, with molar concentration replaced by wt fraction, to determine a bulk T_c, 1032 °C. This value is unsurprisingly similar to that reported for the ROP of **3.1** (1090 °C).[33]

$$T_c = \frac{\Delta H^0_{ROP}}{\Delta S^0_{ROP} + R \ln [M]_c} \qquad \textbf{Equation 2}$$

$$\Delta S^0_{ROP}(M) = \Delta S^0_{ROP}(wt \text{ fraction}) + R \ln \frac{x}{y} \qquad \textbf{Equation 3}$$

3.4 Summary

The highly unusual ring-opening polymerisation of untilted [Ni(η^5-C_5H_4)$_2$(CH_2)$_4$] (**3.2**) was studied via DFT calculations on the ring-opening of monomers to form model oligomers. The exoenthalpic nature of the ROP is proposed to manifest due to the torsional strain present in the *ansa* bridge of **3.2**. Disiloxa-bridged [3]nickelocenophanes (**3.13** and **3.14**), which also exhibit negligible ring-tilt, were synthesised and found to be stable with respect to polymerisation in pyridine. Unsymmetrically substituted methyltricarba[3]nickelocenophane **3.15** was synthesised and the reversible polymerisation of this species to give **3.18** was studied, along with the thermodynamic propensity of the monomer to ROP. The addition of a substituent to the *ansa* bridge appears to make only a marginal difference to enthalpy of polymerisation (**3.15**: ΔG^0_{ROP} = −3.1 kJ mol^{-1} vs **3.1**: ΔG^0_{ROP} = −4.0 kJ mol^{-1}), but this is sufficient to significantly decrease the yields of **3.18** compared to **3.7$_x$**/**3.8** under analogous conditions. Thus, we can conclude that the introduction of a methyl group on the *ansa* bridge disfavours ROP in the equilibrium

between monomer and polymer.

3.5 Experimental

3.5.1 Materials and Equipment

All reactions and product manipulations of molecular species were carried out under an inert atmosphere of dinitrogen or argon using standard Schlenk line or glovebox techniques (MBraun glovebox MB150G-B maintained at < 0.1 ppm H_2O and < 0.1 ppm O_2), unless otherwise stated. Dry hexanes, dichloromethane and toluene were obtained from a Grubbs-type solvent system employing alumina and supported copper columns.[51] THF was distilled under dinitrogen from Na/benzophenone. Pyridine and d_5-pyridine were purchased from Fluka and Sigma-Aldrich respectively and distilled from CaH_2 prior to use. d_6-Benzene was purchased from Sigma-Aldrich and stored over molecular sieves.[52] Silica gel (for flash chromatography was purchased from VWR and used as received. Celite 521 was obtained from Sigma-Aldrich and heated to 200 °C for 16 h prior to use. Sodium metal, dicyclopentadiene, anhydrous nickel(II) chloride, 1,3-dichloro-1,1,3,3-tetramethyldisiloxane, 1,3-dichloro-1,3-dimethyl-1,3-diphenyldisiloxane, dichloro-1,1,3,3-tetraisopropyldisiloxane, and 1,3-dibromobutane were used as supplied by Sigma-Aldrich. Anhydrous 1,3-dimethyl-3,4,5,6-tetrahydro-2(1H)-pyrimidinone (DMPU) was purchased from Sigma-Aldrich and degassed via three freeze-pump-thaw cycles. $Na[C_5H_5]$[53] and the fly trap ligands $Li_2[(C_5H_4)_2(SiMe_2)_2O]$ and $Li_2[(C_5H_4)_2(SiMePh)_2O]$, and $Li_2[(C_5H_4)_2(CH_2)_2(CH(CH_3))]$and were prepared as described in the literature.[54, 55]

Electrospray ionisation (ESI) mass spectra were recorded using a cone potential of +150 V in a THF/toluene mixture on a Bruker Daltonics Apex IV Fourier transform ion cyclotron mass spectrometer.

^1H NMR spectra were recorded at ambient temperature on a VARIAN NMR 500MHz spectrometer. All spectra are reported relative to external TMS and are referenced to the

most downfield residual solvent resonance (d_5-pyridine: 8.74 ppm, C_6D_6: δ_H 7.16 ppm). In all ^{1}H NMR spectra of paramagnetic [*n*]nickelocenophane and polynickelocene species, backward linear prediction from 0 to 15 data points was employed to remove baseline distortion, phase correction was addressed manually, and a Bernstein Polynomial Fit was applied (polynomial order = 10). ^{1}H NMR spectra were collected between +310 and −310 ppm to observe signals at both low and high field (number of scans = 2048, receiver gain = 50, relaxation delay = 0.1 s and acquisition time = 0.8389 s). Variable temperature ^{1}H NMR spectra were obtained on a Bruker Avance III HD 500 Cryo spectrometer and referenced to the solvent resonance (d_5-pyridine: 8.74 ppm).

Dynamic Light Scattering (DLS) experiments were performed to determine hydrodynamic radii of polymer solutions. Samples (2 mL) of different polymer concentrations (1 and 2 mg mL^{-1}) in toluene were filtered through a 0.45 μm membrane filter into an optical glass cuvette (10.0 mm path length). The measurements were performed on a Malvern Instruments Zetasizer Nano S using a 5 mW He-Ne laser (633 nm) at 20 °C. The correlation function was acquired in real time and analysed with a function capable of modelling multiple exponentials. This process enabled the diffusion coefficients for the component particles to be extracted, and these were subsequently expressed as effective hydrodynamic radius, by volume, using the Stokes-Einstein relationship.

Photoirradiation experiments were carried out using Pyrex-glass-filtered emission ($\lambda > 310$ nm) from a 125 W high pressure Hg vapour lamp (Photochemical Reactors Ltd.).

Elemental analyses were carried out by Elemental Microanalysis Ltd using the Dumas combustion method.

Single crystal X-ray diffraction experiments were carried out at 100 K on a Bruker APEX II diffractometer using Mo Kα radiation (λ = 0.71073 Å). Data collections were performed using a CCD area detector from a single crystal mounted on a glass fibre. Intensities were integrated,[56] from several series of exposures measuring 0.5° in ω or φ. Absorption

corrections were based on equivalent reflections using SADABS.[57] The structures were solved using SHELXS and refined against all F_o^2 data with hydrogen atoms located geometrically and refined using a riding model in SHELXL.[58] Crystallographic details are provided in the Appendix.

3.5.2 Synthesis of 1,1,3,3-Tetramethyldisila-2-oxa[3]nickelocenophane (**3.13**)

$Na[C_5H_5]$ (10 g, 0.11 mol) was dissolved in THF (100 mL) and cooled to −78 °C. 1,3-Dichloro-1,1,3,3-tetramethyldisiloxane (10.6 mL, 0.054 mol) was also dissolved in THF (25 mL) and added to the $Na[C_5H_5]$ solution dropwise over 30 min. The mixture was stirred and allowed to warm to room temperature over 16 h. H_2O (50 mL) was added to the pale pink suspension, resulting in a colour change to yellow/brown, and the organic phase was extracted with Et_2O. The aqueous phase was washed with Et_2O (3 × 20 mL) and the organic phase was washed with H_2O (10 × 20 mL) to remove all remaining cyclopentadiene. The organic solution was dried with $MgSO_4$ and all solvent removed to yield a yellow oil. This product was distilled (100 °C, 7.0 × 10^{-2} mbar) to yield 11.6 g (0.044 mol) of a colourless oil, $(C_5H_5)_2[(SiMe_2)O(SiMe_2)]$, which was dissolved in dry hexanes (250 mL) and cooled to −78 °C. *n*BuLi (1.6 M hexane solution, 70 mL, 0.114 mol) was added dropwise over 10 min, and the resulting solution was stirred and allowed to warm to room temperature over 16 h. The colourless suspension was filtered to collect the solid, which was washed with hexanes (8 × 20 mL) to remove excess *n*BuLi and dried under vacuum to yield $Li_2[(C_5H_4)_2(SiMe_2)_2O]$ as a colourless, free-flowing solid (10.8 g, 0.039 mol) in 73% yield.

The fly trap ligand $Li_2[(C_5H_4)_2(SiMe_2)_2O]$ (3.0 g, 10.9 mmol) and $NiCl_2$ (1.55 g, 12.0 mmol) were thoroughly mixed in the absence of solvent and cooled to −78 °C. Dry and degassed THF (200 mL) pre-cooled to −78 °C was then added rapidly via cannula. The reaction mixture was stirred and allowed to warm to room temperature over a period of 16 h. After

evaporation of the solvent under reduced pressure, the green residue was extracted with *n*-hexanes to give a dark green solution which was filtered through Celite (1" × 4"). Again, all volatiles were removed in vacuo and the resulting green solid was purified by sublimation (40 °C/−78 °C, 5.0×10^{-2} mbar) and subsequent recrystallisation from *n*-hexanes at −40 °C to afford dark green crystals of **3.13** suitable for X-ray crystallographic analysis. Yield: 1.5g (4.7 mmol, 43%). ^{1}H NMR (500 MHz, C_6D_6): δ [peak width at half height] (ppm) 8.58 [18 Hz] (br s, C_5H_4–Si(CH_3)$_2$), −239.4 [906 Hz] (br s, C_5H_4), −248.1 [969 Hz] (br s, C_5H_4). ESI-MS (positive ion mode, 1,2-difluorobenzene): *m*/*z* 318.0401 [Ni(η^5-C_5H_4)$_2$($SiMe_2$)$_2$O]$^+$. Elemental analysis: calcd. for $C_{14}H_{20}NiOSi_2$: C 52.68%, H 6.32% Found: C 53.35%, H 6.35%.

3.5.3 Attempted ROP of **3.13** in Pyridine

1,1,3,3-Tetramethyldisila-2-oxa[3]nickelocenophane **3.13** (126 mg, 0.39 mmol) was dissolved in d_5-pyridine (0.5 mL) to afford a 0.79 M solution, and stirred at room temperature for 32 h. No colour change was observed. ^{1}H NMR spectroscopy (500 MHz, d_5-pyridine) revealed no change. The procedure was repeated at higher concentration (1.31 M) and again, no change was observed after 32 h by ^{1}H NMR spectroscopy. After 1 month, no further change was observed by ^{1}H NMR spectroscopy.

3.5.4 Synthesis of 1,3-Dimethyl-1,3-diphenyldisila-2oxa[3]nickelocenophane (**3.14**)

Na[C_5H_5] (5.65 g, 0.064 mol) was dissolved in THF (70 mL) and cooled to −78 °C. 1,3-Dichloro-1,3-dimethyl-1,3-diphenyldisiloxane (8.67 mL, 0.031 mol) was also dissolved in THF (15 mL) and added to the Na[C_5H_5] solution dropwise over 30 min. The mixture was stirred and allowed to warm to room temperature over 16 h. H_2O (50 mL) was added to the pale pink suspension, resulting in a colour change to pale orange, and the organic phase was extracted with Et_2O. The aqueous phase was washed with Et_2O (3 × 20 mL) and the organic

phase was washed with H_2O (10 × 20 mL) to remove all remaining cyclopentadiene. The organic solution was dried with $MgSO_4$ and all solvent removed to yield an orange oil. This product was distilled (140 °C, 7.0×10^{-2} mbar) to yield 6.49 g (0.017 mol) of a colourless oil, $(C_5H_5)_2$[(SiMePh)O(SiMePh)], which was dissolved in dry hexanes (150 mL) and cooled to −78 °C. *n*BuLi (1.6 M hexane solution; 26 mL, 0.042 mol) was added dropwise over 10 min, and the resulting solution was stirred and allowed to warm to room temperature over 16 h. The colourless suspension was filtered to collect the solid, which was washed with hexanes (8 × 20 mL) to remove excess *n*BuLi and dried under vacuum to yield $Li_2[(C_5H_4)_2(SiMePh)_2O]$ as a colourless, free-flowing solid (5.24 g, 0.013 mol) in 42% yield. The fly trap ligand $Li_2[(C_5H_4)_2(SiMePh)_2O]$ (1.0 g, 2.51 mmol) and $NiCl_2$ (0.34 g, 2.63 mmol) were thoroughly mixed in the absence of solvent and cooled to −78 °C. Dry and degassed THF (100 mL) pre-cooled to −78 °C was then added rapidly via cannula. The reaction mixture was stirred and allowed to warm to room temperature over a period of 16 h. After evaporation of the solvent under reduced pressure, the green residue was extracted with *n*-hexanes to give a dark green solution which was filtered through Celite (1" × 4"). Again, all volatiles were removed in vacuo and the resulting green solid was recrystallised in *n*-hexanes at −40 °C to afford a green solid and a dark green solution. The solid was separated from the solution and then recrystallised in *n*-pentane at −40 °C to give green crystals of **3.14** suitable for X-ray crystallographic analysis. Yield: 0.18 g (0.41 mmol, 16%). ^{1}H NMR (500 MHz, C_6D_6): δ [peak width at half height] (ppm) 8.54-7.58 (m, C_5H_4–Si(C_6H_5)$_2$), 0.40 (s, C_5H_4–Si(CH_3)$_2$), −237.2 [887 Hz] (br s, C_5H_4), −239.3 [891 Hz] (br s, C_5H_4), and −247.2 [1008 Hz] (br s, C_5H_4). ESI-MS (positive ion mode, toluene): *m*/*z* 442.0718 [Ni(η^5-C_5H_4)$_2$(SiMePh)$_2$O]$^+$. Elemental analysis: calcd. for $C_{24}H_{24}NiOSi_2$: C 65.02%, H 5.46% Found: C 64.09 %, H 5.67%.

3.5.5 Attempted ROP of **3.14** in Pyridine

1,3-Dimethyl-1,3-diphenyldisila-2oxane[3]nickelocenophane **3.14** (126 mg, 0.39 mmol) was dissolved in d_5-pyridine (0.5 mL) to afford a 1.31 M solution, and stirred at room temperature for 1 week. ^{1}H NMR spectroscopy (500 MHz, d_5-pyridine) revealed no change.

3.5.6 Synthesis of 1,1',2,2'-Bis(tetraisopropyldisiloxa)nickelocene (**3.17**)

$Na[C_5H_5]$ (7.87 g, 0.089 mol) was dissolved in THF (100 mL) and cooled to −78 °C. 1,3-Dichloro-1,1,3,3-tetraisopropyldisiloxane (13.0 mL, 0.041 mol) was also dissolved in THF (20 mL) and added to the $Na[C_5H_5]$ solution dropwise over 30 min. The mixture was stirred and allowed to warm to room temperature over 16 h. H_2O (50 mL) was added to the pale pink suspension, resulting in a colour change to pale orange, and the organic phase was extracted with Et_2O. The aqueous phase was washed with Et_2O (3 × 20 mL) and the organic phase was washed with H_2O (10 × 20 mL) to remove all remaining cyclopentadiene. The organic solution was dried with $MgSO_4$ and all solvent removed to yield an orange oil. This product was distilled (150 °C, 7.0 × 10^{-2} mbar) to yield 7.07 g (0.022 mol) of a colourless oil, $(C_5H_4)[(SiiPr_2)O(SiiPr_2)]$, which was dissolved in dry hexanes (100 mL) and cooled to −78 °C. *n*BuLi (1.6 M hexane solution; 27 mL, 0.043 mol) was added dropwise over 10 min, and the resulting solution was stirred and allowed to warm to room temperature over 16 h. The colourless suspension was filtered to collect the solid, which was washed with hexanes (8 × 20 mL) to remove excess *n*BuLi and dried under vacuum to yield $Li[(C_5H_3)(SiiPr_2)_2O]$ as a colourless, free-flowing solid (5.78 g, 0.018 mol) in 45% yield.

The ligand $Li[(C_5H_3)(SiiPr_2)_2O]$ (1.0 g, 3.18 mmol) and $NiCl_2$ (0.21 g, 1.59 mmol) were thoroughly mixed in the absence of solvent and cooled to −78 °C. Dry and degassed THF (90 mL) pre-cooled to −78 °C was then added rapidly via cannula. The reaction mixture was stirred and allowed to warm to room temperature over a period of 16 h. After evaporation of the solvent under reduced pressure, the green/brown residue was extracted with *n*-hexanes

to give a dark green/brown solution which was filtered through Celite (1" × 4"). Again, all volatiles were removed in vacuo and the resulting green solid was recrystallised from *n*-hexanes at −40 °C to afford light green crystals of **3.17** suitable for X-ray crystallographic analysis. Yield: 0.44 g (0.65 mmol, 41%). ^{1}H NMR (500 MHz, C_6D_6): δ [peak width at half height] (ppm) 6.68 (s, C_5H_4–SiC*H*), 5.43 (s, C_5H_4–SiC(CH_3)$_2$), 5.09 (s, C_5H_4–SiC(CH_3)$_2$), 3.12 (s, C_5H_4–SiC*H*), 2.59 (s, C_5H_4–SiC(CH_3)$_2$), 2.23 (s, C_5H_4–SiC(CH_3)$_2$), −199.5 [1593 Hz] (br s, C_5H_4), −234.8 [2557 Hz] (br s, C_5H_4). ESI-MS (positive ion mode, THF): *m*/*z* 672.3175 [Ni(η^5-C_5H_4)$_2$(Si*i*Pr$_2$)$_2$O]$^+$. Elemental analysis: calcd. for $C_{34}H_{62}NiO_2Si_4$: C 60.60%, H 9.27% Found: C 61.25%, H 9.45%.

3.5.7 Synthesis of 1-Methyltricarba[3]nickelocenophane (**3.15**)

Na[C_5H_5] (11.4 g, 0.13 mol) was dissolved in THF (125 mL) and cooled to −78 °C before 1,3-dimethyl-3,4,5,6-tetrahydro-2-pyrimidinone (40 mL) was added. 1,3-Dibromobutane (5.56 mL, 0.046 mol) was also dissolved in THF (50 mL) and added to the Na[C_5H_5] solution dropwise over 30 min. The mixture was stirred at −78 °C for 1 h, then at 0 °C for a further 2 h. H_2O (100 mL) was added to the pale pink suspension, and the organic phase was extracted with Et_2O. The aqueous phase was washed with Et_2O (3 × 200 mL) and the organic phase was washed with H_2O (10 × 100 mL) to remove all remaining cyclopentadiene. The organic solution was dried with $MgSO_4$ and flushed through a silica column (1" x 6") with a DCM eluent. All solvent was removed to yield 6.768 g (0.036 mol) of (C_5H_4)$_2$[(CH_2)$_3$(CH_3)] as a pale yellow oil. This product was dissolved in dry hexanes (200 mL) and cooled to −78 °C. *n*BuLi (1.6 M hexane solution; 57 mL, 0.091 mol) was added dropwise over 10 min, and the resulting solution was stirred and allowed to warm to room temperature over 16 h. The suspension was filtered to collect the solid, which was washed with hexanes (5 × 50 mL) to remove excess *n*BuLi and dried under vacuum to yield Li_2[(C_5H_4)$_2$(CH_2)$_2$(CH(CH_3))] as a colourless, free-flowing solid (5.71 g, 0.029 mol) in 62% yield.

The fly trap ligand $Li_2[(C_5H_4)_2(CH_2)_2(CH(CH_3))]$ (2.00 g, 10 mmol) and $NiCl_2$ (1.37 g, 10.6 mmol) were thoroughly mixed in the absence of solvent and cooled to −78 °C. Dry and degassed THF (250 mL) pre-cooled to −78 °C was then added rapidly via cannula. The reaction mixture was stirred and allowed to warm up to room temperature over a period of 16 h. After evaporation of the solvent under reduced pressure, the green residue was extracted with *n*-hexanes to give a dark green solution which was filtered through Celite (1" × 4"). Again, all volatiles were removed in vacuo and the resulting green solid was purified by sublimation (40 °C/−78 °C, 1.0×10^{-2} mbar) and subsequent recrystallisation from *n*-hexanes at −40 °C to afford dark green crystals of **3.15**. Yield: 0.73 g (2.98 mmol, 30%). ^{1}H NMR (500 MHz, C_6D_6): δ [peak width at half height] (ppm) 14.14 (s, –C*H*$_3$), −20.8 (s, C_5H_4–CH_2–C*H*$_2$), −34.2 (s, C_5H_4–CH_2–C*H*$_2$), −240.4 (br s, α-C_5H_4), −242.9 (br s, α-C_5H_4), −246.5 (br s, α-C_5H_4), −266.9 (br s, β-C_5H_4), −270.8 (br s, β-C_5H_4). The lack of a signal corresponding to the C_5H_4–C*H*$_2$–CH_2 protons is consistent with similar *ansa* [*n*]nickelocenophanes. ESI-MS (positive ion mode, toluene): *m*/*z* 242.0605 $[Ni(\eta^5\text{-}C_5H_4)_2(CH_2)_2(CH(CH_3))]^+$. Elemental analysis calc. for $C_{14}H_{16}Ni$: C, 69.21; H, 6.64; found: C, 70.04; H, 6.56.

3.5.8 Concentration Dependency of the ROP of **3.15** to Give Poly(nickelocenyl-1-methyl-propylene) **3.18**

All the polymerisations were carried out in an analogous manner: **3.15** was dissolved in d_5-pyridine (0.5 mL) to afford a dark blue solution. The solution was stirred at room temperature for 24 h, where at low concentrations, no colour change was observed, and at higher concentrations a colour change from dark blue to green was evident. ^{1}H NMR spectra were recorded after 24 h, 48 h, and 7 days.

A green solid was isolated in the cases of $\mathbf{3.18_a}$ and $\mathbf{3.18_b}$ via precipitation of the polymerisation solution into rapidly stirred −78 °C *n*-hexanes (30 mL). The precipitate was

separated, dissolved in a minimum volume of THF (0.5 mL) and precipitated into −78 °C *n*-hexanes again (30 mL). The solid was isolated and dried in vacuo to yield green polymeric material, **3.18**. In the case of **3.18$_a$** (1.31 M), polymeric material was also isolated from precipitation into 20 °C *n*-hexanes. ^{1}H NMR (500 MHz, C_6D_6): δ [peak width at half height] (ppm) 185.4 (br s, C_5H_4–C*H*(CH_3)–CH_2), 179.6 (br s, C_5H_4–C*H*$_2$–CH_2), 146.7 (br s, C_5H_4–C*H*$_2$–CH_2), 22.1 (m, CH(C*H*$_3$)), −246.3 (br s, C_5H_4). Further characterisation can be found for specific concentrations in Tables 3.2 and 3.3.

3.5.9 Depolymerisation of **3.18**

Polynickelocene **3.18** (53 mg, 0.22 mmol) was stirred in d_5-pyridine (0.5 mL) for 48 h at 20 °C to yield a mixture of monomer and polymer. ^{1}H NMR spectroscopy displayed resonances in line with those reported above for **3.15** and **3.18**.

3.6 References

1. T. Aida, E. W. Meijer and S. I. Stupp, *Science*, 2012, **335**, 813-817.
2. R. P. Sijbesma, F. H. Beijer, L. Brunsveld, B. J. B. Folmer, J. H. K. K. Hirschberg, R. F. M. Lange, J. K. L. Lowe and E. W. Meijer, *Science*, 1997, **278**, 1601-1604.
3. X. G. Liu, Y. Zhang, D. K. Goswami, J. S. Okasinski, K. Salaita, P. Sun, M. J. Bedzyk and C. A. Mirkin, *Science*, 2005, **307**, 1763-1766.
4. T. L. Choi, K. H. Lee, W. J. Joo, S. Lee, T. W. Lee and M. Y. Chae, *J. Am. Chem. Soc.*, 2007, **129**, 9842-9843.
5. J. Zhang, Y. P. Chen, K. P. Miller, M. S. Ganewatta, M. Bam, Y. Yan, M. Nagarkatti, A. W. Decho and C. Tang, *J. Am. Chem. Soc.*, 2014, **136**, 4873-4876.
6. J. Collot, J. Gradinaru, N. Humbert, M. Skander, A. Zocchi and T. R. Ward, *J. Am. Chem. Soc.*, 2003, **125**, 9030-9031.
7. R. R. Davies, H. Kuang, D. F. Qi, A. Mazhary, E. Mayaan and M. D. Distefano, *Bioorg. Med. Chem. Lett.*, 1999, **9**, 79-84.
8. F.-I. Wu, X.-H. Yang, D. Neher, R. Dodda, Y.-H. Tseng and C.-F. Shu, *Adv. Funct. Mater.*, 2007, **17**, 1085-1092.
9. J. M. Stanley and B. J. Holliday, *Coord. Chem. Rev.*, 2012, **256**, 1520-1530.

10. D. A. Rider, K. Liu, J. C. Eloi, L. Vanderark, L. Yang, J. Y. Wang, D. Grozea, Z. H. Lu, T. P. Russell and I. Manners, *ACS Nano*, 2008, **2**, 263-270.

11. I. Korczagin, R. G. H. Lammertink, M. A. Hempenius, S. Golze and G. J. Vancso, *Adv. Polym. Sci.*, 2006, **200**, 91-117.

12. Y. L. Wang, L. Salmon, J. Ruiz and D. Astruc, *Nat Commun*, 2014, **5**, 1-12.

13. H. J. Kim, J. H. Lee and M. Lee, *Angew. Chem. Int. Ed.*, 2005, **44**, 5810-5814.

14. K. L. Robinson and N. S. Lawrence, *Anal. Chem.*, 2006, **78**, 2450-2455.

15. B. J. Holliday, T. B. Stanford and T. M. Swager, *Chem. Mater.*, 2006, **18**, 5649-5651.

16. D. A. Foucher, B. Z. Tang and I. Manners, *J. Am. Chem. Soc.*, 1992, **114**, 6246-6248.

17. L. Espada, K. H. Pannell, V. Papkov, L. Leites, S. Bukalov, I. Suzdalev, M. Tanaka and T. Hayashi, *Organometallics*, 2002, **21**, 3758-3761.

18. Y. Ma, W.-F. Dong, M. A. Hempenius, H. Mohwald and G. Julius Vancso, *Nat. Mater.*, 2006, **5**, 724-729.

19. J. Massey, K. N. Power, I. Manners and M. A. Winnik, *J. Am. Chem. Soc.*, 1998, **120**, 9533-9540.

20. J. A. Massey, K. N. Power, M. A. Winnik and I. Manners, *Adv. Mater.*, 1998, **10**, 1559-1562.

21. T. Gädt, N. S. Ieong, G. Cambridge, M. A. Winnik and I. Manners, *Nat. Mater.*, 2009, **8**, 144-150.

22. X. Wang, G. Guerin, H. Wang, Y. Wang, I. Manners and M. A. Winnik, *Science*, 2007, **317**, 644-647.

23. M. J. MacLachlan, M. Ginzburg, N. Coombs, T. W. Coyle, N. P. Raju, J. E. Greedan, G. A. Ozin and I. Manners, *Science*, 2000, **287**, 1460-1463.

24. S. Lastella, G. Mallick, R. Woo, S. P. Karna, D. A. Rider, I. Manners, Y. J. Jung, C. Y. Ryu and P. M. Ajayan, *J. Appl. Phys.*, 2006, **99**, 024302.

25. R. L. N. Hailes, A. M. Oliver, J. Gwyther, G. R. Whittell and I. Manners, *Chem. Soc. Rev.*, 2016, **45**, 5358-5407.

26. N. J. Long, in *Metallocenes: An Introduction to Sandwich Complexes*, Wiley-Blackwell, 1st edn., 1998.

27. W. Finckh, B. Z. Tang, D. A. Foucher, D. B. Zamble, R. Ziembinski, A. Lough and I. Manners, *Organometallics*, 1993, **12**, 823-829.

28. H. Braunschweig, F. Breher, M. Kaupp, M. Gross, T. Kupfer, D. Nied, K. Radacki and S. Schinzel, *Organometallics*, 2008, **27**, 6427-6433.

29. H. Braunschweig, M. Gross and K. Radacki, *Organometallics*, 2007, **26**, 6688-6690.

30. S. Baljak, A. D. Russell, S. C. Binding, M. F. Haddow, D. O'Hare and I. Manners, *J. Am. Chem. Soc.*, 2014, **136**, 5864-5867.

31. W. Buchowicz, L. B. Jerzykiewicz, A. Krasińska, S. Losi, A. Pietrzykowski and P. Zanello, *Organometallics*, 2006, **25**, 5076-5082.

32. S. Trtica, M. H. Prosenc, M. Schmidt, J. Heck, O. Albrecht, D. Görlitz, F. Reuter and E. Rentschler, *Inorg. Chem.*, 2010, **49**, 1667-1673.

33. R. A. Musgrave, A. D. Russell, D. W. Hayward, G. R. Whittell, P. G. Lawrence, P. J. Gates, J. C. Green and I. Manners, *Nat. Chem.*, 2017, **9**, 743-750.

34. V. I. Tel'noi and I. B. Rabinovich, *Usp. Khim.*, 1977, **46**, 1337-1367.

35. D. E. Herbert, U. F. J. Mayer and I. Manners, *Angew. Chem. Int. Ed.*, 2007, **46**, 5060-5081.

36. R. A. Musgrave, A. D. Russell and I. Manners, *Organometallics*, 2013, **32**, 5654-5667.

37. S. Barlow, M. J. Drewitt, T. Dijkstra, J. C. Green, D. O'Hare, C. Whittingham, H. H. Wynn, D. P. Gates, I. Manners, J. M. Nelson and J. K. Pudelski, *Organometallics*, 1998, **17**, 2113-2120.

38. R. Resendes, J. M. Nelson, A. Fischer, F. Jäkle, A. Bartole, A. J. Lough and I. Manners, *J. Am. Chem. Soc.*, 2001, **123**, 2116-2126.

39. R. Rulkens, D. P. Gates, D. Balaishis, J. K. Pudelski, D. F. McIntosh, A. J. Lough and I. Manners, *J. Am. Chem. Soc.*, 1997, **119**, 10976-10986.

40. A. Duda and A. Kowalski, in *Handbook of Ring-Opening Polymerization*, eds. P. Dubois, O. Coulembier and J.-M. Raquez, Wiley-VCH Verlag GmbH & Co., Weinheim, 2009, ch. 1.

41. P. Kubisa and S. Penczek, *Prog. Polym. Sci.*, 1999, **24**, 1409-1437.

42. R. Tuba and R. H. Grubbs, *Polym Chem-Uk*, 2013, **4**, 3959-3962.

43. G. Odian, *Principles of Polymerization*, John Wiley & Sons, New Jersey, 4th edn., 2004.

44. P. Olsén, J. Undin, K. Odelius, H. Keul and A.-C. Albertsson, *Biomacromolecules*, 2016, **17**, 3995-4002.

45. R. Hailes, R. A. Musgrave, A. F. R. Kilpatrick, A. D. Russell, G. R. Whittell, D. O'Hare and I. Manners, *Chem. Eur. J.*, 2019, **25**, 1044-1054.

46. C. Angelakos, D. B. Zamble, D. A. Foucher, A. J. Lough and I. Manners, *Inorg. Chem.*, 1994, **33**, 1709-1718.

47. A. C. T. Kuate, M. Alexandru, M. Freytag, C. Racles, M. Cazacu, P. G. Jones and M. Tamm, *J. Organomet. Chem.*, 2014, **751**, 628-637.

48. J. A. Massey, K. Kulbaba, M. A. Winnik and I. Manners, *J. Polym. Sci. B: Polym. Phys.*, 2000, **38**, 3032-3041.

49. M. Cypryk, Y. Gupta and K. Matyjaszewski, *J. Am. Chem. Soc.*, 1991, **113**, 1046-1047.

50. D. Foucher, R. Ziembinski, R. Petersen, J. Pudelski, M. Edwards, Y. Ni, J. Massey, C. R. Jaeger, G. J. Vancso and I. Manners, *Macromolecules*, 1994, **27**, 3992-3999.

51. A. B. Pangborn, M. A. Giardello, R. H. Grubbs, R. K. Rosen and F. J. Timmers, *Organometallics*, 1996, **15**, 1518-1520.

52. D. B. G. Williams and M. Lawton, *J. Org. Chem.*, 2010, **75**, 8351-8354.

53. T. K. Panda, M. T. Gamer and P. W. Roesky, *Organometallics*, 2003, **22**, 877-878.

54. S. C. You, M. Gubler and M. Neuenschwander, *Helv Chim Acta*, 1994, **77**, 1346-1362.

55. S. Collins, Y. Hong and N. J. Taylor, *Organometallics*, 1990, **9**, 2695-2703.

56. *Bruker-AXS SAINT V7.68A, Madison, Wisconsin*.

57. *G. M. Sheldrick, SADABS V2008/1 or TWINABS V2008/4, University of Göttingen, Germany*.

58. G. M. Sheldrick, *Acta Crystallogr.*, 2008, **A64**, 112-122.

4 Evaluation of Poly(cobaltoceniumethylene) as an Antimicrobial and the Synthesis of New Main Chain Cobaltocenium Polyelectrolytes

4.1 Abstract

This chapter is concerned with main chain cobaltocenium polyelectrolytes. It is divided into two sections: the first (4.2) explores the antimicrobial activity of poly(cobaltoceniumethylene), **[4.2]$^{n+}$**, including the potential inhibitory effect of the polyelectrolyte on *E. coli* at high concentrations. The lack of protection afforded to nitrocefin from β-lactam hydrolysis compared to analogous polymers with side chain cobaltocenium centres is also discussed, alongside the potential reasons for the differing results. In the second section (4.3), the development of polycondensation routes to main chain polycobaltocenium materials is presented, using 1,1′-dicarboxycobaltocenium hexafluorophosphate, **[4.3][PF$_6$]**, and a diamine reagent. Reactions in aqueous media led to the formation of oligomeric species, **[4.4][Cl]$_n$**, with low molar masses (maximum DP_n = 12). The isolation of crystalline, hydrogen-bonded supramolecular polymers involving **[4.3][PF$_6$]** and various diamine linkers was also demonstrated, and the subsequent thermally-induced, solid-state, covalent polymerisation of **4.5** was explored.

4.2 Antimicrobial Activity of Poly(cobaltoceniumethylene)

4.2.1 Background

Antibiotics are essential tools in medicine, but their overuse has accelerated a major global crisis in which their effectiveness is threatened by the evolution of resistance. β-Lactam antibiotics, containing a β-lactam ring in their molecular structure, comprise 50% of all antibiotic prescriptions worldwide due to their strong clinical effectiveness, low cost, ease

of delivery, and minimal toxicity.[1] Since the discovery of benzylpenicillin in the early twentieth century, the class has evolved to include cephalosporins, monobactams, carbapenems, and other penicillin derivatives, Figure 4.1. DD-Transpeptidases, penicillin-binding proteins which catalyse peptidoglycan cross-linking in bacterial cell walls, are specific for the peptide bonds between D-alanine residues. β-Lactam antibiotics are structurally similar to the D-alanyl-D-alanine residue of bacterial cell wall precursors, and thus can irreversibly acylate the catalytic serine residue of DD-transpeptidases. This prevents the final cross-linking step of cell wall assembly, disrupting the peptidoglycan layer, and leading to the lysis of bacterium.[2]

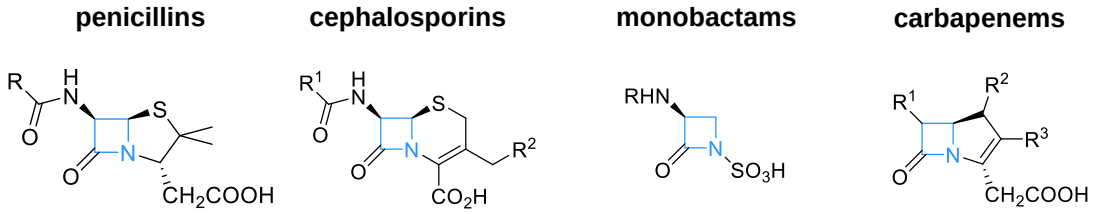

Figure 4.1. Common β-lactam antibiotics (β-lactam ring highlighted in blue).

Bacterial resistance to β-lactams occurs primarily by the production of β-lactamases, enzymes that hydrolyse the amide bond of the four-membered β-lactam ring, rendering the product biologically inactive, Scheme 4.1.[2] To avoid antibiotic resistance β-lactams were modified to include steric protection of the β-lactam ring, which allowed for stability to attack by β-lactamases.[3] However, within two years of clinical introduction of the modified β-lactam antibiotics, methicillin-resistant *S. aureus* (MRSA) isolates were observed.[4] Other methods of impeding β-lactamases have also been explored, for instance, β-lactamase inhibitors containing a four-membered β-lactam ring were developed for use in conjugation with antibiotics. The inhibitors mimic the antibiotic but bind the enzyme with high affinity in its place. Currently, there are five β-lactam-β-lactamase inhibitor formulations available upon prescription.[5] Non-β-lactam inhibitors, including boronic acids,[6-9] sulfones,[10, 11] and phosphonates,[12-14] were also widely reported but failed to pass clinical trials.

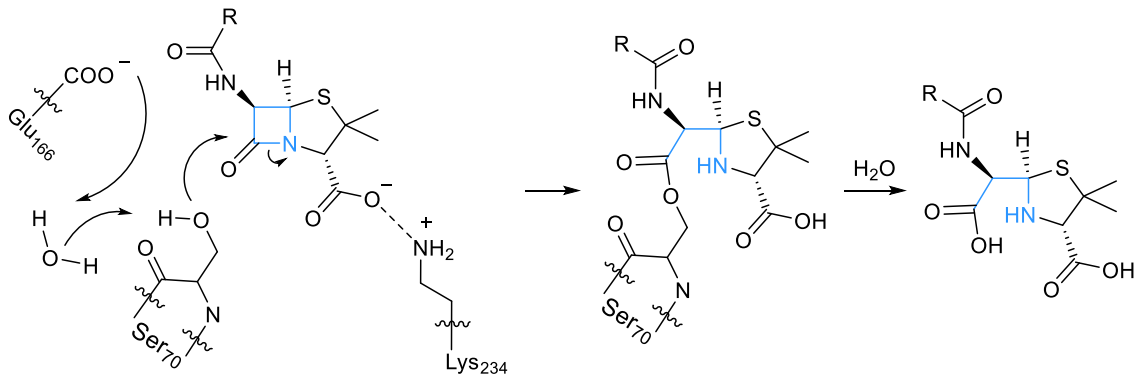

Scheme 4.1. Hydrolysis of penicillin by a class A β-lactamase enzyme.

Organometallic compounds and macromolecules have also been used as enzyme inhibitors.[15] It was demonstrated by Tang and coworkers that side-chain polycobaltocenium **4.1** (Figure 4.2) exhibits synergistic effects against MRSA by both inhibiting activity of β-lactamase and lysing bacterial cells.[16] When combined with various conventional β-lactam antibiotics, including the sodium salt of penicillin-G, it was demonstrated that the polymer acts as a macromolecular scaffold upon which electrostatic ion-pairs form between the anionic carboxylate groups of the antibiotic and the cationic cobaltocenium moieties. In experiments with MRSA, these antibiotic-metallopolymer bioconjugates displayed significant resistance toward hydrolysis by β-lactamases (thereby suggesting that the polymer had the ability to protect the antibiotic from recognition by the enzymes).[16] In addition, polymer **4.1** inhibits growth of various strains of MRSA via partial or complete membrane lysis, whilst maintaining low cytotoxicity. Its inhibitory concentration (IC_{90}) in MRSA cells was determined as 3–5 μM.

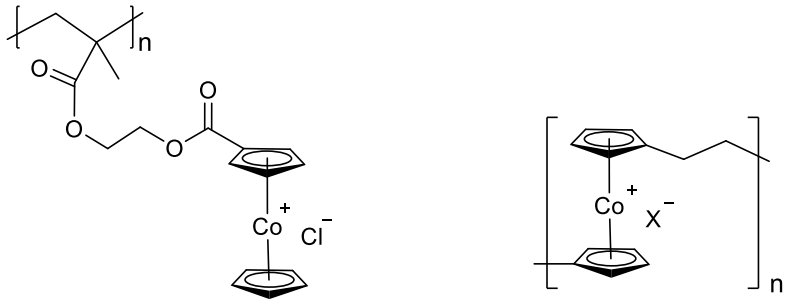

4.1 **[4.2][X]$_n$**

Figure 4.2. Polymers **4.1**[16] and **[4.2][X]$_n$**.

4.2.2 Antimicrobial Activity of **[4.2][NO$_3$]$_n$**

Poly(cobaltoceniumethylene), **[4.2]$^{n+}$**, was originally synthesised by Manners and coworkers via the thermal ROP of 19 valence electron (VE) dicarba[2]cobaltocenophane, followed by oxidation in the presence of an appropriate salt.[17, 18] The weight-average molecular weight was determined by dynamic light scattering (DLS) to be ~55,000 g mol^{-1} (degree of polymerisation (DP_n) = 198). Considering the results reported by Tang et al.,[16] the antimicrobial activity of **[4.2][NO$_3$]$_n$** was assessed against Gram-positive (MRSA) and Gram-negative (*E. coli*) bacterial cells. The results from broth microdilution assays indicated that **[4.2][NO$_3$]$_n$** does not inhibit growth of MRSA (5×10^5 colony-forming units (cfu) mL^{-1}) at concentrations up to 100 μM, but at far higher concentrations (500 μM) the polymer can inhibit growth of *E. coli*.

Then, it was determined whether **[4.2][NO$_3$]$_n$** could potentiate β-lactam activity against β-lactamase producing bacteria. As β-lactamase production is a major contributor to antibiotic resistance in Gram-negative bacteria, ATCC *E.coli* recombinants harbouring pSU18 vectors (empty vector, CTX-M, KPC-3, NDM-1) were employed.[19] Broth microdilution assays performed with meropenem, a β-lactam from the carbapenem class, afforded minimum inhibitory concentrations as expected (Table A4.4). However, addition of polymer/meropenem mixtures had no effect upon the minimal inhibitory concentration compared to meropenem controls (Table A4.5). An additional microdilution assay was performed with cephalothin, a first-generation cephalosporin antibiotic. In this case, ATCC *E.coli* cells producing β-lactamases survived all antibiotic controls performed. Whilst polymer/cephalothin mixtures lowered minimum inhibitory concentrations considerably, these displayed no difference to **[4.2][NO$_3$]$_n$** controls. Cefaclor, a second-generation cephalosporin, generated similar results to those of cephalothin. Thus, no clear effect of **[4.2][NO$_3$]$_n$** on β-lactam activity against β-lactamase producing bacteria could be established.

4.2.3 Binding Affinity of **[4.2][Cl]$_n$** to Penicillin-G

Prior to investigating the effect of **[4.2]$^{n+}$** upon β-lactamase-catalysed hydrolysis, the ability of the polymer to form bioconjugates with β-lactam antibiotics was confirmed. Polymer **[4.2][Cl]$_n$** and the sodium salt of benzylpenicillin (penicillin-G), were mixed thoroughly in a 1:1 ratio (Co^+:antibiotic) in deionised water, before the yellow solution was dialysed against deionised water to remove NaCl. The solution was then freeze-dried to give **[4.2][penicillin-G]$_n$** in 82% yield, and ^{1}H NMR spectroscopy (D_2O) confirmed the formation of a bioconjugate, Figure A4.1. Characterised by the single set of resonances, the exchange between bound and free penicillin-G appeared to be fast on the chemical shift timescale. Consequently, it was potentially possible to determine the dissociation constant, K_d, from the observed resonance i.e. the population-weighted average of free and bound antibiotic.[20] Polymer **[4.2][Cl]$_n$** was titrated with sodium penicillin-G in D_2O (Figure A4.2), and the proton chemical shift perturbation of a well-resolved penicillin-G resonance (~4.2 ppm, proton highlighted in Figure 4.3) measured relative to a sealed C_6D_6 standard (Figure 4.3).

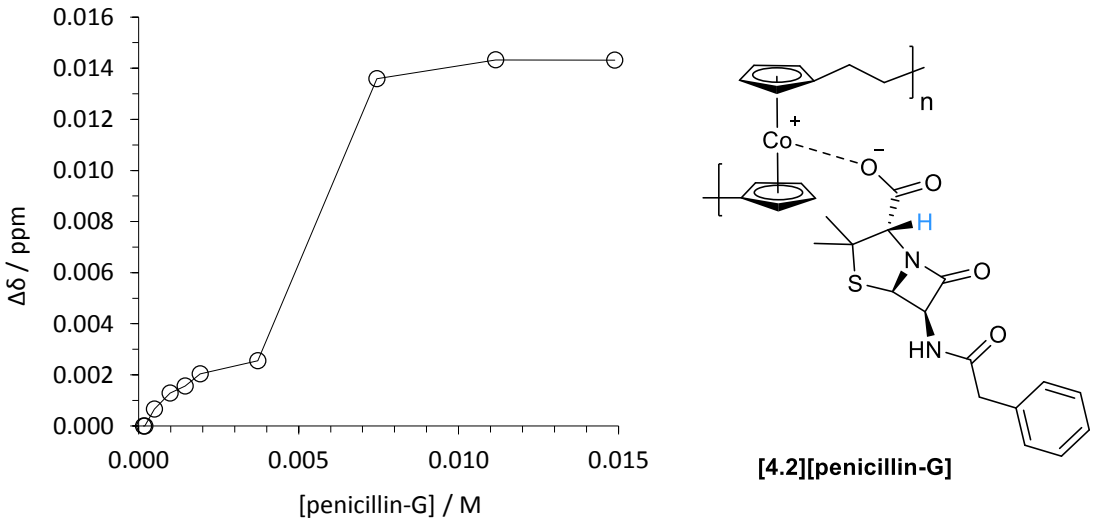

Figure 4.3. Titration curve measuring the chemical shift deviation of a proton environment in penicillin-G (~4.2 ppm, proton in blue), upon the addition of sodium penicillin-G to **[4.2][Cl]$_n$** in D_2O (1 mL, 2 mmol dm^{-3}).

Figure 4.3 does not display a simple saturation curve, but instead the data have a more complicated shape (seemingly two saturation curves). The complex shape suggests that the ratio of binding between cobaltocenium cation and antibiotic anion may not be constant throughout, differing between 1:1, 1:2, and/or 2:1 binding modes,[20] contrary to the 1:1 binding suggested by Tang et al. for polymer **4.1**.[16] Simple methods of elucidating dissociation constants rely on fitting a single saturation curve, thus it was not possible to elucidate a dissociation constant for **[4.2][penicillin-G]**.

4.2.4 Attempted Protection of β-Lactam Antibiotics

In a series of experiments, the effect of **[4.2][Cl]$_n$** and **[4.2][NO$_3$]$_n$** on β-lactamase-catalysed hydrolysis was investigated using nitrocefin, a chromogenic cephalosporin that does not have antimicrobial properties. Nitrocefin is commonly used to detect β-lactamase-catalysed hydrolysis due to a colour change from yellow (380 nm) to red (482 nm) that occurs upon β-lactam ring hydrolysis.[21] Polymer-antibiotic mixtures of various molar ratios (1:4, 1:2, 1:1, 2:1 and 4:1) were allowed to incubate at 5 °C for 16 h prior to introduction of KPC-3, a β-lactamase enzyme. Initial UV/Vis spectroscopy indicated a clear interaction between the polymer and antibiotic: the band at 380 nm was increasingly bathochromically shifted with greater concentrations of **[4.2][Cl]$_n$** and **[4.2][NO$_3$]$_n$** (Figures A4.3 and A4.6). However, after β-lactamase introduction, it became clear that **[4.2][Cl]$_n$** and **[4.2][NO$_3$]$_n$** had little effect on preventing the hydrolysis of nitrocefin, which was able to proceed to completion as indicated by the red/purple absorption after 45 min (Figure 4.4, A4.5, and A4.8). The purple colour observed at higher polymer concentrations indicates that although hydrolysis had occurred, it was not as expected. Hydrolysis occurs as a two-step process: cleavage of the C–N bond, followed by protonation of the nitrogen. The purple colour may arise due to the presence of a bioconjugate intermediate with anionic nitrogen centres, stabilised by the high concentration of cationic cobaltocenium moieties.[22-26]

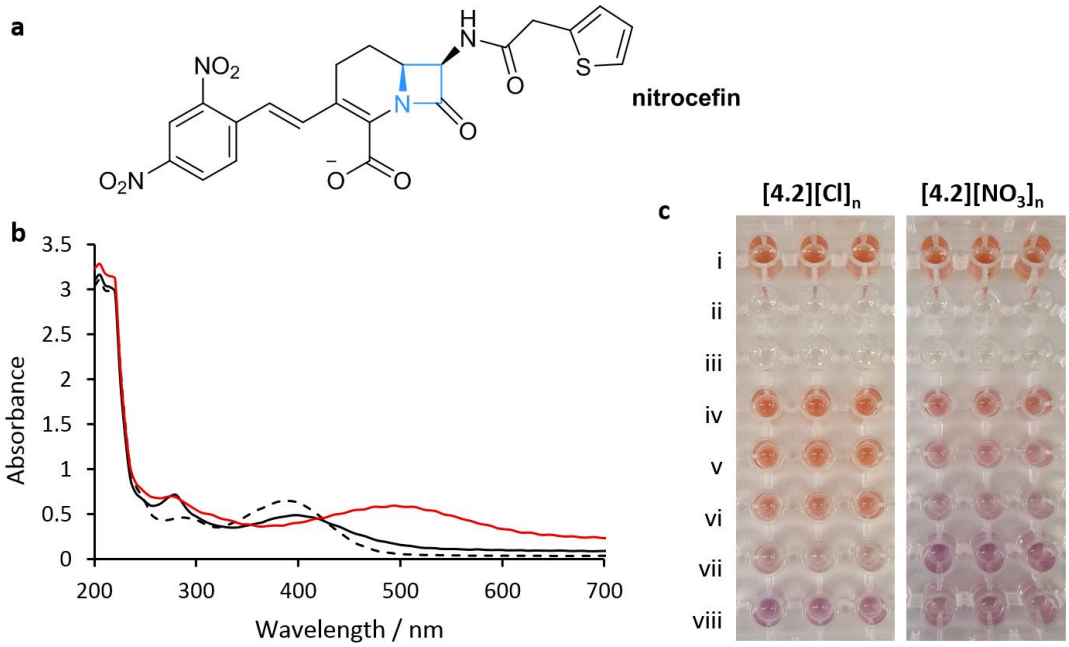

Figure 4.4. a) Structure of nitrocefin. b) Overlaid UV/Vis spectra of: nitrocefin (dashed line); **[4.2][Cl]$_n$**:nitrocefin 1:1 mixture prior to enzyme addition (black line); **[4.2][Cl]$_n$**:nitrocefin 1:1 mixture 45 min post enzyme addition (red line). c) Photos of well plate experiments 45 min post enzyme addition in triplicate. Key: i, nitrocefin control; ii and iii, **[4.2][X]$_n$** control; iv–viii, **[4.2][X]$_n$**:nitrocefin mixtures 1:0.25, 1:0.5, 1:1, 1:2, 1:4.

The low activity of **[4.2][Cl]$_n$** and **[4.2][NO$_3$]$_n$** in protecting β-lactam rings from hydrolysis compared to **4.1** presumably arises from the difference in structure. Polymer **4.1** contains cobaltocenium moieties in the polymer side chain, a feature which allows great conformational and spatial flexibility. In contrast, as the cationic cobaltocenium units are featured in the main-chain of **[4.2]$^{n+}$**, the spatial constraints of the two-atom bridging element may generate a barrier to effective nitrocefin complexation. In contrast, the bioconjugate **[4.2][penicillin-G]$_n$** may have been observed as penicillin-G exhibits significantly lower steric bulk than nitrocefin, and thus may be able to bind more effectively to the cobaltocenium centres. Polymer **[4.2]$^{n+}$** has a significantly higher molar mass than **4.1** (DP_n = 198 vs 41) but we do not believe that this has a significant effect compared to the structural differences. Main-chain cobaltocenium containing polymers represent an underdeveloped area of research, thus the work in Section 4.3 explores the synthesis of such polymers with

longer spacer groups, with the eventual aim of investigating their efficacy in preventing β-lactamase-catalysed hydrolysis of β-lactam containing antibiotics.

4.3 Towards a General Route to Cobaltocenium Polyelectrolytes

4.3.1 Background

Polycondensations are most commonly step growth reactions in which the combination of bifunctional molecules to form a polymer chain is accompanied by elimination of a small molecule by-product. The functional groups of all species present during a polycondensation (monomers, dimers, trimers etc.) display reactivity which is relatively independent of molecular size.[27] Due to the nature of the polymerisation mechanism, polymer molar mass increases only slowly with increased conversion of monomer until it accelerates exponentially in the latter stage of the reaction. Thus, it is difficult to control the molar mass of the resultant polymers, and in cases with two difunctional monomers, exact stoichiometry together with very high conversion is required to yield high molar mass polymer. In addition, polydispersities (PDI)s are, at best, 2. Regardless, polycondensation routes to polyesters, polyamides, and many other materials are well-known and widely utilised.[28, 29]

Some of the first examples of main-chain cobaltocenium polyelectrolytes were reported via polycondensation of a substituted cobaltocenium with an appropriate linker. In the 1970s Carraher and Sheats reported the reaction of the disodium salt of 1,l′-dicarboxycobaltocenium hexafluorophosphate and the claimed dicyclopentadienyltitanium bishexafluorophosphate, but the resulting species was poorly characterised.[30] Further attempts to produce polycobaltocenium polyesters and polyamides employed harsh conditions involving molten lead monoxide (175 °C, 5 h) or antimony trichloride (175 °C, 48 h), but were hindered by a combination of lack of reaction, low molar mass products, or unconvincing characterisation by present day standards.[31, 32] The first amide-based cobaltocenium main-chain polymer prepared under mild conditions was reported in 1999,

by use of a siloxane based diamine and di(chlorocarbonyl)cobaltocenium hexafluorophosphate in chloroform with triethylamine, but again, the polymer suffered from poor solubility in common organic solvents, which precluded assessment of the molecular weight.[33] Main-chain cobaltocenium-containing polybenzimidazole polymers have since been reported via polycondensation of 1,l′-dicarboxycobaltocenium hexafluorophosphate and 3,3′,4,4′-biphenyltetramine in the presence of polyphosphoric acid at 200 °C.[34] The resulting imidazole-based cobaltocenium polyelectrolyte was determined to have a molecular weight of ~83,000 g mol^{-1}, and subsequently employed in alkaline anion exchange membrane applications.

Modern condensation chemistry, especially amide bond formation, has advanced significantly in recent years with new methods allowing for the synthesis of amide linkages in a wide array of compounds, including many drug molecules. The reaction of carboxylic acids with amines does not occur spontaneously at ambient temperature, with the condensation only occurring at high temperatures (>160 °C).[35] Thus, activation of the carboxylic acid is generally required prior to the introduction of amine, a process in which the –OH moiety is transformed into a better leaving group. A wide variety of coupling reagents are available for this purpose, e.g. those in Figure 4.5, which generate compounds such as acyl halides, anhydrides, azides, or active esters.[35-37]

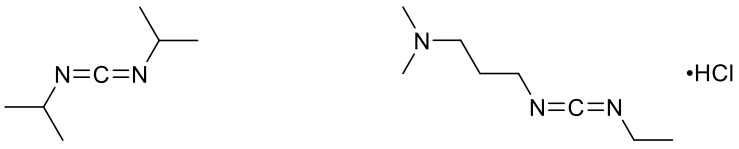

Figure 4.5. Examples of carbodiimide coupling reagents: *N*,*N*′-diisopropylcarbodiimide (left) and *N*-Ethyl-*N*′-(3-dimethylaminopropyl)carbodiimide hydrochloride (right).

4.3.2 Attempted Polycondensations in Organic Solvents

In this work, we initially chose to mimic and refine the early reaction conditions that employed organic solvents in the production of polycobaltocenium salts,[33] using 1,1′-

dicarboxycobaltocenium hexafluorophosphate, **[4.3][PF$_6$]**. Due to the polar nature of the cobaltocenium hexafluorophosphate salt, solubility was limited in non-aqueous media, although at increased temperatures some dissolution was detected in solvents such as acetonitrile and DMF.

Compound **[4.3][PF$_6$]** was stirred in the presence of the coupling agent *N*,*N*′-diisopropylcarbodiimide (DIC, Figure 4.5) and acetonitrile for 1 h at 60 °C to allow for production of the activated ester, before 2,2′-(ethylenedioxy)bis(ethylamine) was added, and the reaction continued for a further 48 h (Table A4.6, reaction 4.3.2a, Scheme 4.2). This led to the formation of a yellow, water-soluble material, which displayed ^{1}H NMR resonances at 6.02 and 5.75 ppm distinct from those of the starting material and assigned to the cyclopentadienyl (Cp) proton environments. However, signals originating from the protons in the diamine component were not apparent, suggesting a lack of formation of **[4.4][PF$_6$]$_n$**.

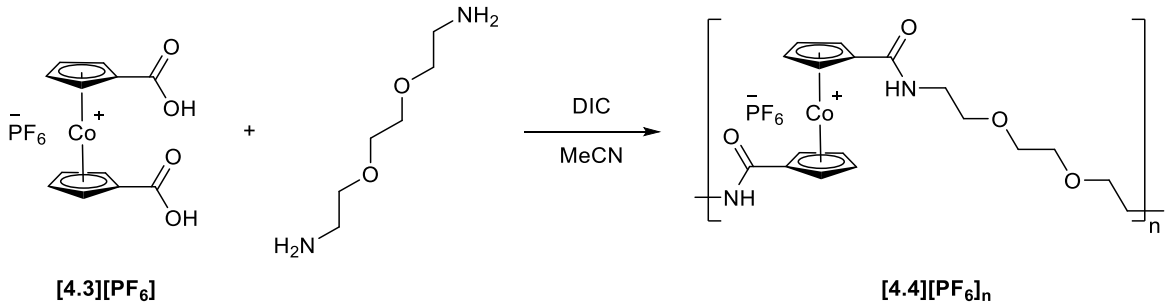

[4.3][PF$_6$] **[4.4][PF$_6$]$_n$**

Scheme 4.2. Attempted reaction between **[4.3][PF$_6$]** and 2,2′-(ethylenedioxy)bis(ethylamine) to give **[4.4][PF$_6$]$_n$**.

The use of base in peptide couplings is common to increase amine nucleophilicity (and is a requirement in reactions between carboxylic acids and alcohols), thus the reaction was repeated in the presence of hindered base *N*,*N*-diisopropylethylamine (DIPEA). Whilst the water-soluble product displayed the same ^{1}H NMR chemical shifts (D_2O) assigned to the Cp protons as described above, resonances at 3.80, 3.76, and 3.24 ppm were now ascribed to proton environments in the diamine linker. ^{31}P{^{1}H} NMR spectroscopy revealed a resonance at −144.4 ppm assigned to the hexafluorophosphate anion. IR spectroscopy displayed several

informative vibrations: 2471 cm^{-1} consistent with an RNH_3^+ group, and two bands centred around 3085 cm^{-1} assigned to a primary amine. Other broader X–H (X = N, O, C) and C=O bands were more ambiguous in terms of assignment and did not assist in structure determination. Limited solubility of the cobaltocenium-containing species in organic solvents prevented the use of traditional methods of polymer molar mass determination (such as GPC), and due to the presence of a positive charge on every cobaltocenium unit, mass spectrometry was also deemed inappropriate. Thus, calibration curves using samples of poly(ethylene glycol) (PEG) and poly(sodium 4-styrenesulfonate) (PSS) of various molar masses were produced with DOSY NMR spectroscopy in D_2O, and used henceforth for molar mass characterisation of any products (Figures A4.9 and A4.10, respectively).[38-40] As the molar mass determined suggested that little or no polymerisation had occurred (DP_n = 1.4, calibration to PSS), we concluded that reaction 4.3.2b had not yielded the desired species **[4.4][PF$_6$]$_n$**. Varying reaction time, equivalents of coupling reagent, coupling reagent, solvent, and temperature (Table A4.6, reactions 4.3.2c–4.3.2j) also appeared to make little difference to the reaction outcome based on spectroscopic analysis. In contrast, when **[4.3][PF$_6$]**, 2,2′-(ethylenedioxy)bis(ethylamine), DIC, and DIPEA were stirred in acetonitrile for one week at 60 °C, complete degradation of the cobaltocenium species appeared to occur, with the formation of a significant amount of an unidentified black, insoluble solid.

Spectroscopic analysis of the cobaltocenium containing species obtained from the reactions in organic solvents (Table A4.6, reactions 4.3.2b–4.3.2j) indicated that the polycondensation to produce **[4.4][PF$_6$]$_n$** was unsuccessful. To provide further characterisation, the isolated yellow solid products were dissolved in methanol, and recrystallised via slow diffusion of diethyl ether. Yellow crystals suitable for X-ray analysis were isolated in the case of reaction 4.3.2d. These revealed an unexpected result: a supramolecular polymer (**4.5**) consisting of infinite extended chains (Figure 4.6), that interact with one another via hydrogen bonds to

create a three-dimensional network. Further discussion of the crystallographic structure can be found in Section 4.3.4. Supramolecular cobaltocenium-containing polymers have been reported previously. For instance, Braga and coworkers revealed two-dimensional, step-ladder superstructure supramolecular polymers formed solely from **[4.3][PF$_6$]** via hydrogen-bonded dicarboxyl rings.[41] Krautscheid and coworkers also created supramolecular polymers by slow diffusion of **[4.3][PF$_6$]** with M(OAc)$_2$·2H$_2$O (M = Cd, Zn, Cu),[42] via coordination of the M^{2+} ions to the oxygen atoms of four carboxylate groups.

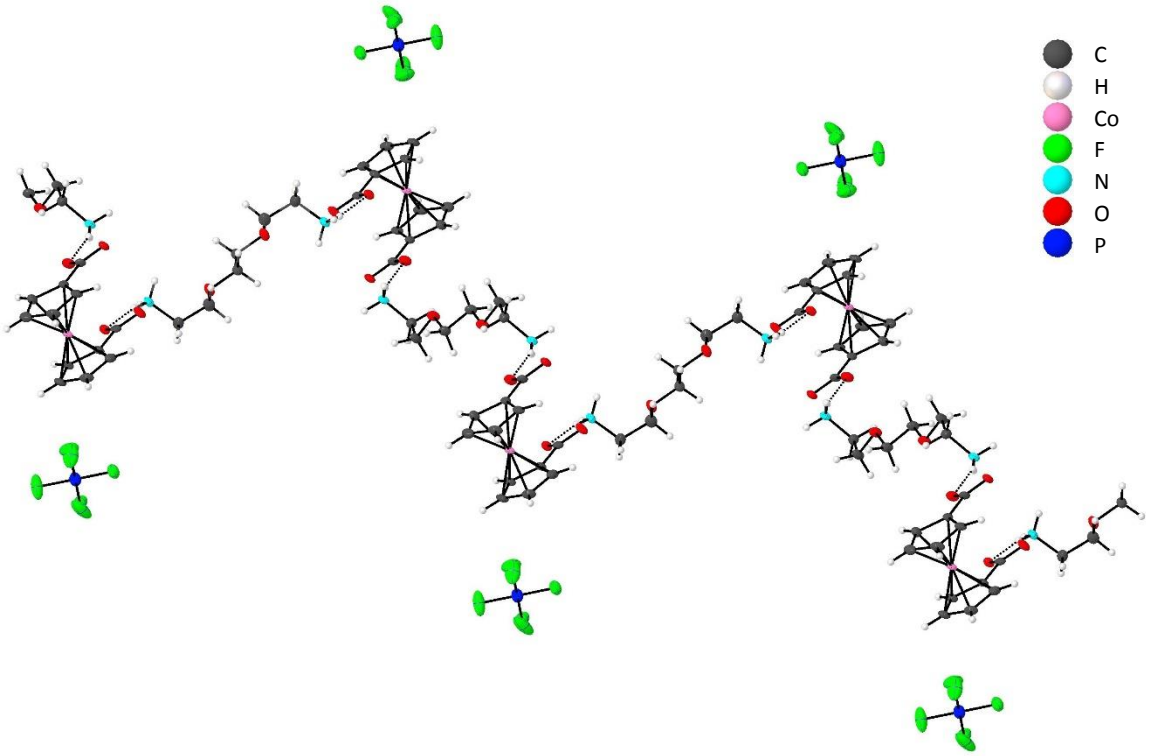

Figure 4.6. A section of the 3D supramolecular polymer **4.5** revealed by single-crystal X-ray diffraction. Thermal ellipsoids displayed at the 50% probability level. Hydrogen atoms are pictured as spheres of arbitrary radii.

In the supramolecular polymer **4.5** (Figure 4.6) it is worth noting that the hydrogen bonds occur between COO^- and NH_3^+ moieties, which is not unexpected, as often amide bond formation is hindered by this competing equilibrium.[43] The ion-pairs persist in D_2O, with ^1H NMR resonances at 6.02 and 5.74 ppm assigned to the Cp protons, and those at 3.78, 3.75, and 3.22 ppm arising from the bridging ether linker (Figure A4.11). These signals match,

within error, NMR spectral shifts observed from the products of reactions 4.3.2b–j and thus explain why it was not possible to produce **[4.4][PF$_6$]$_n$** in reactions employing organic solvents under the conditions studied.

The use of a 1,1′-di(chlorocarbonyl)cobaltocenium salt instead of the corresponding dicarboxy-species was considered to prevent the formation of a supramolecular polymer; however, the solubility of this species was also found to be low in organic solvents, and more importantly, purification of 1,1′-di(chlorocarbonyl)cobaltocenium hexafluorophosphate from the precursor (**[4.3][PF$_6$]**) was found to be difficult. As step-growth polymerisation reactions require exact stoichiometries of the two bifunctional monomeric species, high purity is essential. Instead, we returned to **[4.3][PF$_6$]** as a precursor and pursued a reaction medium that might prevent formation of a supramolecular polymer, and thus allow for polycondensation.

4.3.3 Polycondensations in Water

To prevent the formation of supramolecular polymer **4.5** that occurred in organic solvents (Section 4.3.2), water was employed for the polycondensation between **[4.3][PF$_6$]** and 2,2′-(ethylenedioxy)bis(ethylamine). Whilst peptide coupling reactions and reagents soluble in organic media have been well explored, those that operate in aqueous media are less developed, although recent research has targeted new examples.[44-48] *N*-Ethyl-*N*′-(3-dimethylaminopropyl)carbodiimide hydrochloride (EDC) is a commercially available coupling reagent that is soluble in aqueous media (Figure 4.5), and is usually used in conjunction with the nucleophile hydroxybenzotriazole (HOBt).[35, 36, 49]

Taking inspiration from reported peptide couplings,[50, 51] **[4.3][PF$_6$]** and 2,2′-(ethylenedioxy)bis(ethylamine) were stirred in deionised water in the presence of HOBt and DIPEA (2.05 and 3 eq. respectively) for 10 min at ambient temperature, before 2.05 eq. of EDC were added at 0 °C (Scheme 4.3). The yellow/orange solution was stirred for a further

3 days before two subsequent precipitations into acetone produced a yellow/brown, water-soluble material (reaction 4.3.3a, Table 4.1). Unfortunately, NMR spectroscopy (D_2O) revealed the presence of **[4.3][Cl]** instead of **[4.4][PF$_6$]$_n$**. Notwithstanding the lack of polycondensation, the counterion exchange is presumably due to the presence of the coupling reagent EDC, which is employed as the hydrochloride salt. However, when excess hydrochloric acid was added to **[4.3][PF$_6$]** no counterion exchange was observed, as was also the case when **[4.3][PF$_6$]** and EDC were stirred in deionised water. This suggested that HOBt, DIPEA, and/or the diamine were required to allow the anion exchange to occur. As the aim of this work was to eventually utilise cobaltocenium polyelectrolytes for antibiotic protection, chloride salts are beneficial, and remove the need for a later counterion exchange.[16] However, anion exchange aside, these initial conditions did not promote the desired reaction to yield **[4.4][PF$_6$]$_n$**.

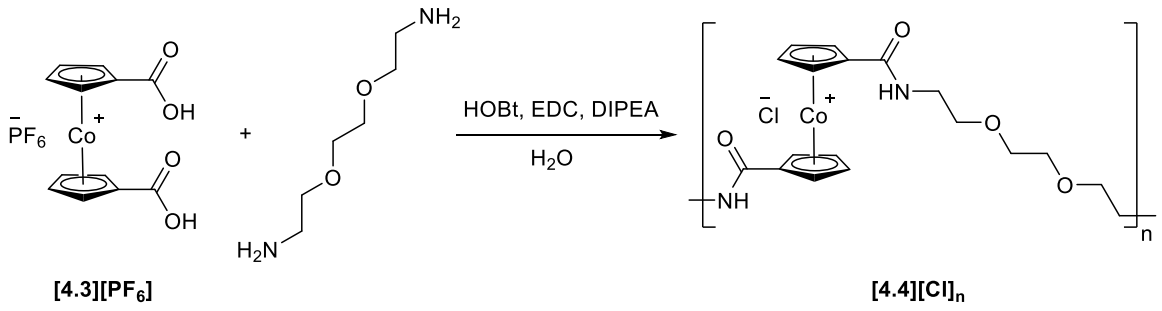

Scheme 4.3. General reaction between **[4.3][PF$_6$]** and 2,2′-(ethylenedioxy)bis(ethylamine) to give **[4.4][Cl]$_n$** in water. Counterion exchange from $[PF_6]^-$ to Cl^- occurs due to the presence of the coupling reagent, EDC, which is employed as the hydrochloride salt.

A large excess (10 eq.) of EDC and HOBt were employed in a second reaction at 20 °C for 72 h, reaction 4.3.3b. ^{1}H NMR spectroscopy (D_2O) of the yellow/brown water-soluble product **[4.4][Cl]$_n$** revealed a series of resonances between 5.48 and 6.20 ppm assigned to the Cp proton environments, and a series of signals between 2.93 and 3.79 ppm assigned to protons in the bridging ether linker. IR spectroscopy confirmed the presence of amide groups alongside end group amine moieties. Molar masses of **[4.4][Cl]$_n$** determined by DOSY

analysis were low: 2810–3490 Da and 1230–1720 Da (calibration to PEG and PSS, respectively), but clearly demonstrated the presence of oligomeric species and thus the potential of this polycondensation. Upon increasing the reaction time to 7 days (reaction 4.4.3c) a ~15% increase in molar mass of **[4.4][Cl]$_n$** was observed by DOSY spectroscopy (3310–3890 and 1590–2030 Da, calibration to PEG and PSS, respectively), suggesting that the majority of reaction progress occurs in the first three days. To determine the necessity of base, a reaction was performed with conditions analogous to reaction 4.3.3c, but without DIPEA (reaction 4.3.3d). ^{1}H NMR spectroscopy (D_2O) of the resulting brown solid revealed major resonances at 6.12 and 5.86 ppm accounting for 72% of the signals in the Cp region. DOSY analysis (D_2O) of **[4.4][Cl]$_n$** estimated molar masses corresponding to the major resonances of 2310 and 900 Da (calibration to PEG and PSS, respectively), lower than those reported in reactions including base. This suggested that although the amide coupling could occur without DIPEA, the addition of base does improve the nucleophilicity of the diamine, thus increasing the resulting mass of the cobaltocenium polyelectrolyte.

The reaction sequence used in the reactions detailed above was based on reported couplings involving EDC.[50, 51] The order of reagent addition was modified to investigate its effect on the polycondensation reaction. Deionised water was added to a mixture of **[4.3][PF$_6$]**, EDC, HOBt, and DIPEA, and the reaction stirred for 10 min before 2,2′-(ethylenedioxy)bis(ethylamine) was added. Then the reaction was allowed to continue for a further 7 days, reaction 4.3.3e. The molecular weights of **[4.4][Cl]$_n$** produced by this reaction (2290–3250 and 890–1540 Da by DOSY calibrated to PEG and PSS, respectively) were limited, and so this change in reaction sequence was not pursued.

Assuming that this polycondensation occurs in the same manner as an externally catalysed polyamidation, the rate of disappearance of a monomeric species is proportional to the concentration of each monomeric species (or the square of the concentration in the case of a single difunctional monomer).[52] Increasing reactant concentration should increase the rate

of reaction, thus it should be possible to access higher molar masses of polymer after a comparable time period. Therefore, two reactions were performed at higher concentrations (4.3.3f and 4.3.3g), in which **[4.3][PF$_6$]** and 2,2′-(ethylenedioxy)bis(ethylamine) were stirred in deionised water (0.25 or 0.1 mL vs 0.5 mL previously) in the presence of HOBt and DIPEA for 10 min, before EDC was added at 0 °C. The viscosity of both orange reaction solutions increased such that 0.1 mL of water was deemed the minimum amount of solvent required for mixing. After stirring for 7 days, and subsequent work up, DOSY spectroscopy (D_2O) estimated increased molar masses of **[4.4][Cl]$_n$**, especially for the reaction performed in 0.1 mL of water: 4.3.3g: 3150–5180 and 1470–3180 Da (max. DP_n = 12 and 7) by DOSY analysis calibrated to PEG and PSS, respectively, (Figure A4.14).

A final set of experiments were performed to determine the effect of varying the amounts of coupling reagent and base on oligocobaltocenium molar mass. Reactions 4.3.3h and 4.3.3i employed equal molar quantities of EDC, HOBt, and DIPEA, the former in a 3 eq. excess and the latter in a ten-fold molar quantity compared to **[4.3][PF$_6$]**. After work up, DOSY analysis displayed marginally higher molar masses of **[4.4][Cl]$_n$** when employing 10 eq. of coupling reagents and base compared to 3 eq. of both, which is perhaps not unsurprising: reaction 4.3.3h, 4340–4840 and 2410–2860 Da; reaction 4.3.3i, 4840–5180 and 2860–3180 Da (calibration to PEG and PSS, respectively, Figure A4.17). However, whilst increasing the amount of coupling reagents had an effect, with 10 eq. of each it was found to be unnecessary to also employ 10 eq. of base in the polycondensation. Reaction 4.3.3g employed just 3 eq. of base, and the molar masses calculated were the same as those estimated in the case of reaction 4.3.3i. In contrast, when utilising a three-fold molar excess of EDC and HOBt and a ten-fold excess of base compared to cobaltocenium and diamine monomers, the product ^{1}H NMR spectrum (D_2O) revealed resonances assigned to **[4.3][Cl]** instead of oligomeric **[4.4][Cl]$_n$**. This, alongside reaction 4.3.3a, suggests that the presence

of a molar excess of base compared to coupling reagents inhibits the polycondensation from occurring.

Table 4.1. Specific conditions for the syntheses of **[4.4][PF$_6$]$_n$** under aqueous conditions.*

Reaction	Solvent vol. / mL	Equivalents of EDC / HOBt / DIPEA	Reaction time / days	MW (PEG)$^{\#}$ / Da	MW (PSS)$^{\#}$ / Da
4.3.3a	0.5	2.05 / 2.05 / 3	3	‡	‡
4.3.3b	0.5	10 / 10 / 3	3	2810–3490	1230–1720
4.3.3c	0.5	10 / 10 / 3	7	3310–3890	1590–2030
4.3.3d	0.5	10 / 10 / 0	7	2310 (major)§	900 (major)§
4.3.3e†	0.5	10 / 10 / 3	7	2290–3250	890–1540
4.3.3f	0.25	10 / 10 / 3	7	3448–4840	1690–2860
4.3.3g	0.1	10 / 10 / 3	7	3150–5180	1470–3180
4.3.3h	0.1	3 / 3 / 3	7	4340–4840	2410–2860
4.3.3i	0.1	10 / 10 / 10	7	4840–5180	2860–3180
4.3.3j	0.1	3 / 3 / 10	7	‡	‡

*General conditions: **[4.3][PF$_6$]** (50 mg, 118 mmol) was dissolved in deionised water, to which 2,2′-(ethylenedioxy)bis(ethylamine) (17.3 μL, 118 mmol), DIPEA, and HOBt were added. The mixture was cooled to 0 °C and EDC was added to give a yellow/brown solution. The reaction was stirred for 3–7 days at 20 °C. $^{\#}$Molecular weights determined via DOSY analysis with PEG or PSS calibration. ‡No **[4.4][Cl]$_n$** was isolated in this case. †Reactant/reagent order of addition: **[4.3][PF$_6$]**, HOBt, EDC, and DIPEA were premixed, then deionised water added and the reaction stirred for 10 min, before 2,2′-(ethylenedioxy)bis(ethylamine) was added at 20 °C. §The molecular weights corresponded to resonances accounting for 72% of the signals in the Cp region. Other small signals corresponded to molecular weights between 2810–3680 Da and 1230–1870 Da (calibrated to PEG and PSS, respectively).

Although this work utilised mild conditions compared to those reported previously,[30, 31] the molar masses of the cobaltocenium polyelectrolytes produced by the series of reactions listed in Table 4.1 are low (max. DP_n = 12, calibrated to PEG). It was postulated that the counterion exchange from hexafluorophosphate to chloride may be limiting the reactivity of the

monomeric/oligomeric species, and thus preventing further reaction to give high molar mass polymer. To test this hypothesis, 1,1′-dicarboxycobaltocenium chloride, **[4.3][Cl]**, was reacted with 2,2′-(ethylenedioxy)bis(ethylamine) in deionised water in the presence of HOBt and DIPEA for 10 min, before EDC was added at 0 °C (analogous to reaction 4.3.3g). The yellow/orange solution was stirred for 7 days. After two subsequent precipitations into acetone, **[4.3][Cl]** was recovered in quantitative yield. The lack of reactivity of the chloride salt would explain the limited molar masses; the counterion exchange from hexafluorophosphate to chloride is clearly slower than the initial polycondensation, but as it begins to occur, it deactivates the carboxycobaltocenium carboxylate groups to further reaction.

It is also possible for the substituted cobaltocenium that upon amidation of one carboxyl group, the analogous reactivity of the other may be lowered. The acidic strength of carboxylic acids has been well-studied both experimentally and theoretically,[53-56] although dicarboxycobaltocenium salts should be regarded as non-classical acids, due to the cationic nature of the cobalt and the presence of a counterion. The pK_a values of **[4.3][PF$_6$]** and **[4.3][Cl]** were determined experimentally by titration with KOH and HCl (2.75 and 8.35, respectively). The two carboxylic acid moieties may lead to the expectation of two distinct pK_a values for each compound; however, the same pK_a was found for both carboxyl moieties in each case (Figure 4.7), suggesting that one carboxyl moiety within a molecule is not affected by the deprotonation of the other. Thus, we believe the reactivity of the two carboxylic acids within a molecule to be essentially independent.

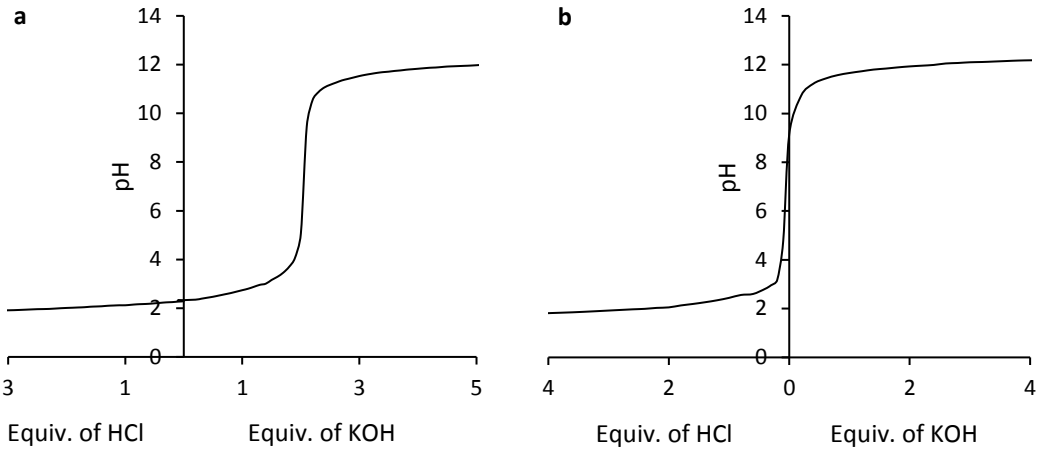

Figure 4.7. Titration curves of a) 1,1′-dicarboxycobaltocenium hexafluorophosphate, **[4.3][PF$_6$]**, and b) 1,1′-dicarboxycobaltocenium chloride, **[4.3][Cl]**.

The two cobaltocenium salts were found to have decidedly different pK_as: [Co(η^5-$C_5H_4COOH)_2$][PF_6], 2.75; [Co(η^5-$C_5H_4COOH)_2$]Cl, 8.35. A general mechanism for an amide coupling mediated by EDC and HOBt is described in Scheme 4.4. The initial proton transfer enables the reaction between the carboxylate and the protonated carbodiimide. The more facile this proton transfer, the greater the reactivity of the carboxylate. Thus, it follows that the more acidic dicarboxycobaltocenium hexafluorophosphate reacts with HOBt, whereas the basic chloride salt will not. In future, use of a stronger base than DIPEA may allow for reactivity of the dicarboxy moieties of the cobaltocenium chloride by facilitating this step.

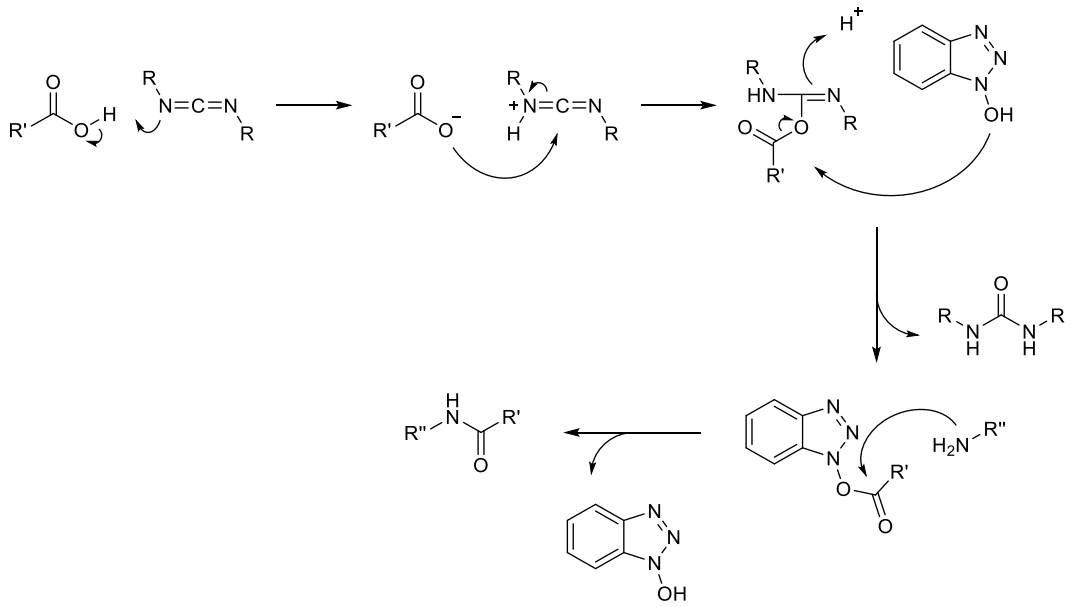

Scheme 4.4. General mechanism for the amide coupling reaction of a carboxylic acid and amine in the presence of EDC and HOBt.

Main-chain cobaltocenium containing polymers represent an underdeveloped area of research, thus future work will continue the research into producing cobaltocenium polyelectrolytes via polycondensation routes. Water will be retained as a reaction medium, but reaction conditions will focus on using either neutral coupling reagents or those with a hexafluorophosphate counterion to prevent anion exchange with the cobaltocenium moiety. This should allow for the formation of high molar mass polymers.

4.3.4 Isolation and Characterisation of Hydrogen-Bonded Supramolecular Polymers

In Section 4.3.2, 1,1′-dicarboxycobaltocenium hexafluorophosphate, **[4.3][PF$_6$]**, and 2,2′-(ethylenedioxy)bis(ethylamine) were reacted in the presence of DIC and acetonitrile at 60 °C (reaction 4.3.2d), and then the product (**4.5**) recrystallised via slow diffusion of diethyl ether into methanol. Yellow crystals of **4.5** suitable for X-ray analysis were isolated and revealed a supramolecular polymer. It was also possible to form **4.5** simply by mixing the dicarboxycobaltocenium and diamine monomers in methanol, followed by slow diffusion of diethyl ether. Figure 4.6 displays a section of an infinite extended chain, which interacts with

other chains via hydrogen bonds to create a three-dimensional network. As the C=O bonds of the cobaltocenium carboxylate groups are not completely delocalised, for one carboxylate group, one oxygen atom forms two hydrogen bonds: 1.909(6) Å as part of the infinite polymer chain, and 2.17(2) Å to a protonated diamine of another polymer chain, whilst the other oxygen forms a single hydrogen bond (1.955(10) Å) to the diamine of another polymer chain. The other carboxylate group is comparable: one oxygen atom forms a longer hydrogen bond (2.089(10) Å), whilst the other forms a short in-chain hydrogen bond (1.843(8) Å) and a longer one to another chain (1.15(17) Å).

In a similar manner to that described above, two other crystalline supramolecular polymers were formed by the addition of either *N*,*N*′-dimethylethylene diamine or ethylene diamine to **[4.3][PF$_6$]** in methanol, and slow diffusion of diethyl ether, **4.6** and **4.7**, respectively. In both cases, yellow crystals suitable for X-ray diffraction were isolated. A similar network structure to that of **4.5** was elucidated for **4.6**, Figure 4.8. Unlike the dicarboxycobaltocenium moieties in the supramolecular polymers formed with primary diamines, the carboxylate groups on the Cp rings appear to be staggered rather than eclipsed. This may be an influence of the secondary nature of the diamine, and the spatial packing thus possible. Each carboxylate group forms two hydrogen bonds of 1.705(2) and 1.802(3) Å. Cp–H···F distances range upwards from a minimum of 2.2623(19) Å. Taking the van der Waals radii to be 1.20 and 1.50 Å for hydrogen and fluorine, and thus the minimum distance indicative of an interaction as 2.70 Å,[57] these distances indicate interactions between the hexafluorophosphate fluorine atoms and the protons of the Cp rings, something not observed for the supramolecular polymers **4.5** and **4.7**.

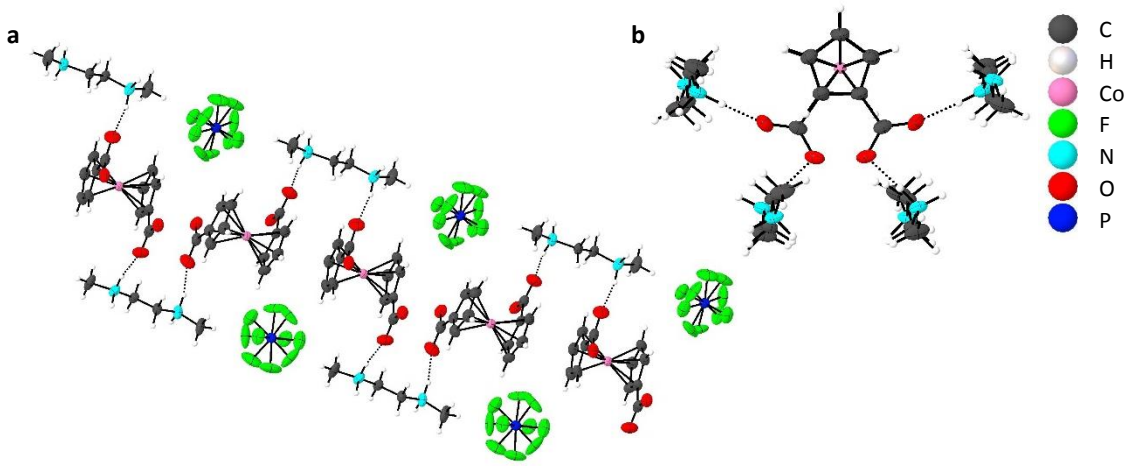

Figure 4.8. X-ray structures of **4.6**. a) A section of supramolecular network **4.6** displaying some of the hydrogen bonding that occurs, and the position of hexafluorophosphate anions. Hexafluorophosphate displays disorder over two positions. b) Top-down view of the cobaltocenium molecule displaying the staggered conformation of the hydrogen bonded carboxy groups on the Cp rings (hexafluorophosphate anion removed for clarity). Thermal ellipsoids displayed at the 50% probability level. Hydrogen atoms are pictured as spheres of arbitrary radii.

Whilst both **4.5** and **4.6** form extended networks, the X-ray structure of **4.7** revealed infinite chains in a two-dimensional, step-ladder superstructure, that do not display hydrogen bonding between chains (Figure 4.9). Hexafluorophosphate anions are encapsulated between polymer chains. Due to the short chain of ethylene diamine, both carboxy moieties in a cobaltocenium molecule are able to hydrogen bond to the same protonated diamine molecule (this is not a feature with the secondary diamine *N*,*N*′-dimethylethylene diamine). Each carboxylate group forms two hydrogen bonds, but for each di-protonated diamine, one amine forms three hydrogen bonds to three different cobaltocenium molecules (1.795(2), 1.883(3), and 1.883(3) Å), whilst the other forms one hydrogen bond to a fourth cobaltocenium molecule (1.946(3) Å). Cp–H···F distances are at minimum 3.412(4) Å, too long to indicate any interaction. The facile and tolerant nature of this crystallisation method suggests that a multitude of diamine linkers could be utilised to form crystalline supramolecular polymers with 1,1′-dicarboxycobaltocenium hexafluorophosphate.

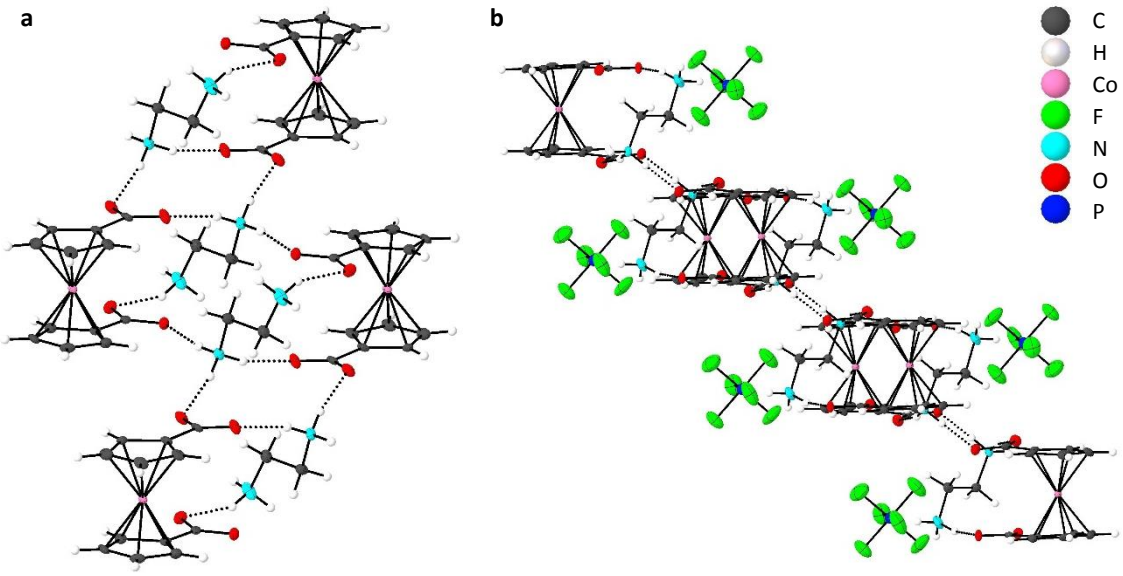

Figure 4.9. X-ray crystallographic structure of supramolecular polymer **4.7**. a) A section of polymer displaying hydrogen bonding along the chain (hexafluorophosphate anions removed for clarity). b) A section of polymer chain demonstrating the position of hexafluorophosphate anions between polymer chains. Thermal ellipsoids displayed at the 50% probability level. Hydrogen atoms are pictured as spheres of arbitrary radii.

4.3.5 Attempted, Thermally-Induced Covalent Polymerisation of **4.5**

Structural transformations of crystalline supramolecular polymers have been induced by temperature, light, and mechanical force.[58-60] The plausibility of thermally-induced covalent polymerisation to give **[4.4][PF$_6$]$_n$** occurring via the crystalline supramolecular polymer **4.5** was therefore investigated. Differential scanning calorimetric analysis of **4.5** between 35 and 210 °C revealed a weak transition at ~100 °C (Figure A4.21a). Thermogravimetric analysis (TGA) of a sample of **4.5** indicated several distinct, significant mass losses, (Figure A4.21b). An initial mass loss of 17% occurred between 210 and 240 °C, which is a far greater percentage than expected from the loss of two molecules of water per cobaltocenium (6%). Thermally-induced polymerisation of **4.5** was attempted at 200 °C (for 1 h under air), and an insoluble, black solid that could not be identified was produced (the solid was not magnetic thus presumed not to be metallic cobalt, 50%), alongside, via extraction with deionised water, a dark yellow solid, **[4.4][PF$_6$]$_n$** (50% yield). ^{1}H NMR spectroscopy (D_2O)

revealed a series of resonances between 5.54 and 6.07 ppm assigned to Cp proton environments, and resonances between 3.02–3.75 ppm which were assigned to protons in the ether bridge (Figure A4.22). ^{19}F NMR analysis revealed major resonances at −71.0 and −72.9 ppm with minor resonances at –126.0 and −150.1 ppm, Figure A4.23b. Alkali metal hexafluorophosphates and ionic liquids with hexafluorophosphate counterions have been reported to degrade thermally, especially in the presence of water, which would be produced here upon amide bond formation.[61-67] It is possible that hexafluorophosphate decomposition gave rise to the new ^{19}F NMR signals, although no additional ^{31}P{^{1}H} NMR signals aside from that at −144.6 ppm were observed. DOSY NMR analysis (in D_2O) estimated a low molar mass of only 2140–3690 Da (calibrated to PEG, Figure A4.24). Several other conditions were attempted but the results (Section 4.5.12) were less promising.

Thermal polymerisation of a crystalline supramolecular polymer with a chloride anion was considered to circumvent counterion degradation, but unfortunately it was not possible to produce such a polymer with **[4.3][Cl]** and 2,2′-(ethylenedioxy)bis(ethylamine) (details can be found in Section 4.5.13).

4.4 Summary

Antimicrobial investigations determined that whilst **[4.2][NO$_3$]$_n$** was found to have an inhibitory effect on the growth of *E. coli* at 500 μM, and **[4.2][Cl]$_n$** forms bioconjugates with penicillin-G, neither of the poly(cobaltoceniumethylene) salts effectively protect the antibiotic nitrocefin from hydrolysis by β-lactamase enzymes. This was thought to occur due to the short dicarba spacer which may generate a barrier to effective nitrocefin complexation. Thus, we attempted to prepare a main-chain cobaltocenium containing polymer from 1,1′-dicarboxycobaltocenium hexafluorophosphate and 2,2′-(ethylenedioxy)bis(ethylamine). In organic solvents no polycondensation was detected, and instead, a supramolecular polymer **4.5** was formed. In aqueous media, polycondensation reactions produced oligomeric species

as detected by DOSY analysis. However, reactions performed in water were hindered by counter-ion exchange between the cobaltocenium moiety and the coupling reagent, EDC (from hexafluorophosphate to chloride). Thus, future work will continue to probe polycondensation methods but employ a coupling reagent with a hexafluorophosphate counterion. Supramolecular polymer **4.5** was also isolated by slow diffusion crystallisation of **[4.3][PF$_6$]** and 2,2′-(ethylenedioxy)bis(ethylamine), and this method was applied to form various crystalline supramolecular polymers with different diamine linkers. The formation of a covalent analogue of **4.5** was attempted by heating to temperatures >180 °C (to yield **[4.4][PF$_6$]$_n$**). However, the process was accompanied by degradation and no high molar mass samples of the desired product were obtained.

4.5 Experimental

4.5.1 Materials and Equipment

MeCN and DMF were purchased from Acros. D_2O was purchased from Sigma-Aldrich. Dimethyldicyclopentadiene, anhydrous cobalt(II) chloride, *n*BuLi, potassium chloride, potassium hexafluorophosphate, potassium permanganate, 2,2′-(ethylenedioxy)bis(ethylamine), ethylene diamine, and *N*,*N*′-dimethylethylenediamine were used as supplied by Sigma-Aldrich. Poly(cobaltocenium ethylene) was synthesised as previously reported,[18] as were 1,1′-dicarboxycobaltocenium hexafluorophosphate **[4.3][PF$_6$]**, 1,1′-dicarboxycobaltocenium chloride **[4.3][Cl]**, 1,1′-di(chlorocarbonyl)cobaltocenium hexafluorophosphate, and 1,1′-di(chlorocarbonyl)cobaltocenium chloride.[68]

^{1}H NMR spectra were recorded at ambient temperature on a Jeol ECS 400 spectrometer and Varian VNMRS 500 MHz instrument. All spectra are reported relative to external TMS and are referenced to the most downfield residual solvent resonance (D_2O: δ_H 4.79 ppm). ^{1}H NMR titration spectra were recorded at ambient temperature on a VARIAN NMR 500MHz

spectrometer and referenced to a sealed standard solvent resonance (C_6D_6: δ_H 7.16 ppm). ^{13}C NMR spectra were obtained on a Bruker Avance III HD 500 Cryo spectrometer in D_2O and referenced to a sealed standard of 4,4-dimethyl-4-silapentane-1-sulfonic acid in D_2O (0 ppm).

Diffusion Ordered Spectroscopy (DOSY) experiments were carried out on a VARIAN NMR 500MHz spectrometer. Samples were analysed at 0.035 M in D_2O. To avoid distorted diffusion coefficients, the spectra were collected without sample spinning. Spectra were obtained over a 16 step gradient range from 10–90%, a diffusion delay of Δ = 500 ms. Spectra were processed using the MestReNova Peak Heights Fit transform function at 128 points in the diffusion dimension over a range of 1×10^{-9}–1×10^{-4} cm^2s^{-1}. Molar masses were estimated using a reported method,[38-40] using seven poly(ethyleneglycol) (550–20,000 Da) or six poly(sodium 4-styrenesulfonate) (4,300–150,000 Da) standards of known molar mass, purchased from Sigma-Aldrich. Plotting logD against logM_n produced a linear calibration curve, to which all polymers were compared.

IR spectra of solid samples were recorded on a Perkin Elmer Spectrum One FT-IR Spectrometer and analysed using Spectrum. Elemental analyses were carried out by Elemental Microanalysis Ltd using the Dumas combustion method. DSC was measured on a Thermal Advantage DSCQ100 at 10 °C min^{-1} and TGA was measured on a Thermal Advantage TGAQ500 at 10 °C min^{-1} under N_2. DSC and TGA results were analysed using WinUA V4.5A by Thermal Advantage.

Single crystal X-ray diffraction experiments for compounds **4.5**, **4.6**, and **4.7** were carried out at 100 K on a Bruker APEX II diffractometer using Mo Kα radiation (λ = 0.71073 Å). Data collections were performed using a CCD area detector from a single crystal mounted on a glass fibre. Intensities were integrated,[69] from several series of exposures measuring 0.5° in ω or φ. Absorption corrections were based on equivalent reflections using SADABS.[70] The structure was solved using SHELXS and refined against all F_o^2 data with

hydrogen atoms located geometrically and refined using a riding model in SHELXL.[71] Crystallographic details are provided in Appendix IV.

4.5.2 Synthesis of **[4.2][penicillin]$_n$** Bioconjugate

Poly(cobaltoceniumethylene) chloride **[4.2][Cl]$_n$** was synthesised as previously reported.[18] Polymer **[4.2][Cl]$_n$** (7.6 mg, 0.0239 mmol) was dissolved in deionised water (2 mL), then combined with penicillin-G sodium salt (12.0 mg, 0.0263 mmol), also in deionised water (2 mL). The yellow solution was stirred at room temperature for 24 h, then dialysed against 6 × 500 mL of deionised water for 24 h. The solution that remained in the dialysis bag was dried to yield a yellow powder (9 mg, 82%). ^{1}H NMR (D_2O, 400 MHz): δ (ppm) 7.39–7.30 (m, Ph, 5H), 5.51 (m, SCHCHNH, 1H), 5.50 (Cp, 4H), 5.43 (m, SCHCHNH, 1H) 5.42 (Cp, 4H) 4.21 (s, NC*H*COO, 1H), 3.66–3.64 (m, $PhCH_2$, 2H), 2.64 (br s, $CoCp_2(CH_2)_2$, 4H), 1.58–1.49 (m, $C(CH_3)_2$, 6H).

4.5.3 ^{1}H NMR Titration of Penicillin-G with **[4.2][Cl]$_n$**

To **[4.2][Cl]$_n$** in D_2O (1 mL, 2 mmol dm^{-3}) was added sodium penicillin-G incrementally. After each addition of penicillin-G a ^{1}H NMR spectrum (500 MHz) was obtained. Spectra were referenced to a sealed C_6D_6 standard, and the chemical shift perturbation of the proton resonance at ~4.2 ppm measured.

4.5.4 Experiments Involving **[4.2][X]$_n$** and Nitrocefin

Nitrocefin in DMSO:kinetic buffer (KB, Table A4.1) (1:9, v/v) was added to vials containing **[4.2][X]$_n$** (X: Cl, NO_3) in 5 mM Hepes 7 buffer; molar ratios of nitrocefin:**[4.2][X]$_n$**: 4:1, 2:1, 1:1, 1:2, 1:4. Two solutions of **[4.2][X]$_n$** (X: Cl, NO_3) in 5 mM Hepes 7 buffer, and one of nitrocefin in 5 mM Hepes 7 buffer were also prepared. These were all incubated at 5 °C for 16 h. 90 µL of each incubation sample was added to a 96 well plate, and a UV/Vis spectrum aquired. 10 µL of 10 µg mL^{-1} BSA with 1 nM KPC-3 was added to all of the wells such that the final well concentrations were: nitrocefin, 50 µM; **[4.2][X]$_n$**, 25 and 100 µM;

nitrocefin:**[4.2][X]$_n$**, 50 μM:12.5 μM, 50 μM :25 μM, 50 μM :50 μM, 50 μM :100 μM, and 50 μM :200 μM. The decrease in intensity of the UV/Vis peak at 395 nm and increase in intensity of the peak at 482 nm were measured across 45 min. A final UV/Vis spectrum was acquired after the kinetic measurements. All experiments were carried out in triplicate.

4.5.5 Attempted Polycondensations of **[4.3][PF$_6$]** and 2,2′-(Ethylenedioxy)bis(ethylamine) in Organic Solvents

Unless stated otherwise, 1,1′-dicarboxycobaltocenium hexafluorophosphate **[4.3][PF$_6$]** (50 mg, 118 mmol) was dissolved in acetonitrile (1 mL), to which DIPEA (41.3 μL, 237 mmol) and coupling reagent (2.05 equiv., 243 mmol) were added. The brown mixture was stirred at a specified temperature for 1 h, before 2,2′-(ethylenedioxy)bis(ethylamine) (17.3 μL, 118 mmol) was added. The reaction was then stirred at this temperature for 3–7 days. See Table A4.6 for individual reaction details. At the end of this period, all volatiles were removed in vacuo, and the solid triturated with chloroform. To the remaining solid, deionised water was added, and the solution was filtered and dried. Spectral analysis matched that determined for supramolecular polymer **4.5**.

4.5.6 Polycondensations of **[4.3][PF$_6$]** and 2,2′-(Ethylenedioxy)bis(ethylamine) in Water

Unless stated otherwise, **[4.3][PF$_6$]** (50 mg, 118 mmol) was dissolved in deionised water, to which 2,2′-(ethylenedioxy)bis(ethylamine) (17.3 μL, 118 mmol), DIPEA, and HOBt were added. The mixture was cooled to 0 °C and EDC was added to give a yellow/brown solution. The reaction was stirred for 3–7 days. See Table 4.1 for individual reaction details. At the end of this period, all volatiles were removed in vacuo. The solid was dissolved in the minimum volume of methanol and added to a vortex of rapidly stirring acetone (20 mL). The suspension was centrifuged, and then the supernatant liquor was removed to leave a dark yellow solid. This was repeated a second time. The solid, **[4.4][Cl]$_n$**, was dried in vacuo

at 40 °C for 24 h. Individual characterisation data is given below, but it is worth noting that, in all cases, no resonances were detected in the $^{31}P\{^{1}H\}$ and ^{19}F NMR spectra of the product. The appendix contains the spectra for reactions 4.3.3g and 4.3.3i as they produced the oligomeric species with the highest molar masses.

Reaction 4.3.3a: ^{1}H NMR chemical shifts match those of **[4.3][Cl]**.

Reaction 4.3.3b: Oligomer **[4.4][Cl]$_n$** (yield: 24 mg, 48%). ^{1}H NMR (400 MHz, D_2O): δ (ppm) 6.20 (m, Cp), 6.18 (m, Cp), 6.04 (m, Cp), 6.01 (m, Cp), 5.91 (m, Cp), 5.87 (m, Cp), 5.84 (m, Cp), 5.77 (m, Cp), 5.48 (m, Cp), 3.79 (m, CH_2), 3.77 (m, CH_2), 3.61 (m, CH_2), 3.25 (m, CH_2), 2.93 (m, CH_2). IR data (cm^{-1}) *ν*(N–H amine) 3363, *ν*(N–H amide) 3259, *ν*(C–H aromatic) 3089, *ν*(C–H) 2898, *ν*(O–H) 2515, *ν*(N–H) 1609, *ν*(N–H amide) 1560.

Reaction 4.3.3c: Oligomer **[4.4][Cl]$_n$** (yield: 19 mg, 38%). ^{1}H NMR (500 MHz, D_2O): δ (ppm) 6.26 (m, Cp), 6.24 (m, Cp), 6.22 (m, Cp), 6.20 (m, Cp), 6.17 (m, Cp), 6.04 (m, Cp), 6.00 (m, Cp), 5.98 (m, Cp), 5.95 (m, Cp), 5.91 (m, Cp), 5.88 (m, Cp), 5.87 (m, Cp), 5.83 (m, Cp), 5.77 (m, Cp), 3.76 (m, CH_2), 3.59 (m, CH_2), 3.22 (m, CH_2), 2.92 (m, CH_2). IR data (cm^{-1}) *ν*(N–H amide) 3212, *ν*(C–H aromatic) 3075, *ν*(C–H) 2928, *ν*(C–H) 2870, *ν*(O–H) 2382, *ν*(C=O) 1655, *ν*(N–H) 1614, *ν*(N–H amide) 1552.

Reaction 4.3.3d: Oligomer **[4.4][Cl]$_n$** (yield: 15 mg, 30%). ^{1}H NMR (500 MHz, D_2O): δ (ppm) 6.21 (m, Cp, minor), 6.19 (m, Cp, minor), 6.12 (m, Cp, major), 6.06 (m, Cp, minor), 5.92 (m, Cp, minor), 5.90 (m, Cp, minor), 5.86 (m, Cp, major), 3.76 (m, CH_2), 3.74 (m, CH_2), 3.58 (m, CH_2), 3.22 (m, CH_2), 2.91 (m, CH_2). IR data (cm^{-1}) *ν*(N–H amine) 3364, *ν*(N–H amide) 3251, *ν*(O–H) 3109, *ν*(C–H aromatic) 3085, *ν*(C–H) 2926, *ν*(C–H), 2874, *ν*(O–H) 2492, *ν*(C=O) 1713, *ν*(C=O) 1651, *ν*(N–H) 1605.

Reaction 4.3.3e: Oligomer **[4.4][Cl]$_n$** (yield: 28 mg, 56%). ^{1}H NMR (500 MHz, D_2O): δ (ppm) 6.20 (m, Cp), 6.18 (m, Cp), 6.07 (m, Cp), 6.05 (m, Cp), 6.03 (m, Cp), 5.91 (m, Cp), 5.88 (m, Cp), 5.87 (m, Cp), 5.84 (m, Cp), 5.82 (m, Cp), 3.76 (m, CH_2), 3.62 (m, CH_2), 3.36

(m, CH_2), 3.23 (m, CH_2), 2.92 (m, CH_2). IR data (cm^{-1}) *v*(N–H amine) 3374, *v*(N–H amide) 3195, *v*(C–H aromatic) 3083, *v*(C–H) 2923, *v*(C–H) 2873, *v*(O–H) 2515, *v*(C=O) 1711, *v*(N–H) 1603.

Reaction 4.3.3f: Oligomer **[4.4][Cl]$_n$** (yield: 17 mg, 34%). ^{1}H NMR (500 MHz, D_2O): δ (ppm) 6.26 (m, Cp), 6.24 (m, Cp), 6.21 (m, Cp), 6.17 (m, Cp), 6.03 (m, Cp), 6.00 (m, Cp), 5.95 (m, Cp), 5.87 (m, Cp), 5.86 (m, Cp), 5.82 (m, Cp), 3.74 (m, CH_2), 3.58 (m, CH_2), 3.36 (m, CH_2), 3.22 (m, CH_2), 2.92 (m, CH_2). IR data (cm^{-1}) *v*(N–H amide) 3229, *v*(C–H aromatic) 3082, *v*(C–H) 2922, *v*(C–H) 2870, *v*(O–H) 2483, *v*(C–H) 2366, *v*(C=O) 1651, *v*(N–H) 1610.

Reaction 4.3.3g: Oligomer **[4.4][Cl]$_n$** (yield: 21 mg, 42%). ^{1}H NMR (500 MHz, D_2O): δ (ppm) 6.27 (m, Cp), 6.24 (m, Cp), 6.22 (m, Cp), 6.20 (m, Cp), 6.17 (m, Cp), 6.03 (m, Cp), 6.00 (m, Cp), 5.95 (m, Cp), 5.90 (m, Cp), 5.86 (m, Cp), 5.82 (m, Cp), 5.75 (m, Cp), 3.76 (m, CH_2), 3.59 (m, CH_2), 3.45 (m, CH_2), 3.36 (s, CH_2), 3.22 (m, CH_2), 3.17 (s, CH_2), 2.92 (m, CH_2). IR data (cm^{-1}) *v*(N–H amine) 3357, *v*(N–H amide) 3237, *v*(C–H aromatic) 3082, *v*(C–H) 2927, *v*(C–H) 2872, *v*(C=O) 1650, *v*(N–H) 1617.

Reaction 4.3.3h: Oligomer **[4.4][Cl]$_n$** (yield: 19 mg, 38%). ^{1}H NMR (500 MHz, D_2O): δ (ppm) 6.21 (m, Cp), 6.18 (br s, Cp), 6.14 (m, Cp), 5.98 (m, Cp), 5.91 (m, Cp), 5.85 (m, Cp), 5.80 (br s, Cp), 5.73 (m, Cp), 3.73 (m, CH_2), 3.56 (m, CH_2), 3.42 (m, CH_2), 3.35 (s, CH_2), 3.31 (m, CH_2), 3.22 (m, CH_2), 2.90 (s, CH_2). IR data (cm^{-1}) *v*(N–H amide) 3366, *v*(N–H amide) 3229, *v*(C–H aromatic) 3084, *v*(C–H) 2932, *v*(C–H) 2870, *v*(C=O) 1646, *v*(N–H) 1614.

Reaction 4.3.3i: Oligomer **[4.4][Cl]$_n$** (yield: 24 mg, 48%). ^{1}H NMR (500 MHz, D_2O): δ (ppm) 6.26 (m, Cp), 6.23 (m, Cp), 6.21 (m, Cp), 6.16 (m, Cp), 5.99 (m, Cp), 5.95 (m, Cp), 5.93 (m, Cp), 5.87 (m, Cp), 5.82 (m, Cp), 3.74 (m, CH_2), 3.57 (m, CH_2), 3.44 (m, CH_2), 3.36 (s, CH_2), 3.33 (m, CH_2), 3.20 (m, CH_2), 2.90 (s, CH_2). IR data (cm^{-1}) *v*(N–H amine) 3361,

ν(N–H amide) 3230, *ν*(C–H aromatic) 3083, *ν*(C–H) 2935, *ν*(C–H) 2871, *ν*(C=O) 1646, *ν*(N–H) 1620.

Reaction 4.3.3j: ^{1}H NMR chemical shifts match those of **[4.3][Cl]**.

4.5.7 Attempted Polycondensation of **[4.3][Cl]** and 2,2'-(Ethylenedioxy)bis(ethylamine)

1,1′-Dicarboxycobaltocenium chloride, **[4.3][Cl]**, was stirred with 2,2′-(ethylenedioxy)bis(ethylamine), HOBt, and DIPEA for 10 min in water, before EDC was added at 0 °C. The yellow/orange solution was stirred for 7 days. After two subsequent precipitations into acetone, **[4.3][Cl]** was recovered in full yield.

4.5.8 pK_a Determination of **[4.3][PF$_6$]** and **[4.3][Cl]**

For pK_a determination of **[4.3][PF$_6$]** and **[4.3][Cl]**, a stock solution of the complex in deionised water (5 mL, 0.01 mol L^{-1}) was titrated with either aqueous KOH solution (0.10 mol L^{-1}) or aqueous HCl (0.1 mol L^{-1}). The pH of the solution was measured using a calibrated glass electrode on a Mettler Toledo SevenEasy pH meter at 295 K. The pK_a for each compound was then calculated using a reported procedure.[72]

4.5.9 Optimum Synthesis of Supramolecular Polymer **4.5**

To 1,1′-dicarboxycobaltocenium hexafluorophosphate **[4.3][PF$_6$]** (50 mg, 0.118 mmol) in methanol (2 mL) was added 2,2′-(ethylenedioxy)bis(ethylamine) (17.3 μL, 0.118 mmol). The solution was filtered into a 14 mL vial, which was placed into a capped bottle containing diethyl ether (2 mL). Slow vapour diffusion at 20 °C afforded yellow crystals of **4.5** within 24 h. Yield: 39 mg, 58%. ^{1}H NMR (500 MHz, D_2O): δ (ppm) 6.02 (t, $^{3}J_{HH}$ = 2.1 Hz, 4H, Cp), 5.74 (t, $^{3}J_{HH}$ = 2.1 Hz, 4H, Cp), 3.78 (t, $^{3}J_{HH}$ = 5.2 Hz, 4H, –O–CH_2−), 3.75 (s, 4H, −O−CH_2−CH_2−O–), 3.22 (t, $^{3}J_{HH}$ = 5.2 Hz, 4H, $^{+}H_3N$–CH_2−). ^{13}C NMR (500 MHz, D_2O): δ (ppm) 171.8, 97.8, 90.0, 88.3, 72.3, 69.3, 41.8. ^{31}P{^{1}H} NMR (400 MHz, D_2O): δ (ppm) −144.5 (sept, $^{1}J_{PF}$ = 708.7 Hz). ^{19}F NMR (400 MHz, D_2O): δ (ppm) −72.0 (d, $^{1}J_{FP}$ = 708.7

Hz). Elemental analysis: calcd. for $C_{18}H_{26}CoF_6N_2O_6P$: C 37.91%, H 4.6%, N 4.91% Found: C 38.42%, H 4.34%, N 5.33%.

4.5.10 Synthesis of Supramolecular Polymer **4.6**

To **[4.3][PF$_6$]** (10 mg, 0.024 mmol) in methanol (0.5 mL) was added *N*,*N*′-dimethylethylenediamine (2.6 μL, 0.024 mmol). The solution was filtered into a 4 mL vial, which was placed into a capped 14 mL vial containing diethyl ether (0.5 mL). Slow vapour diffusion at 20 °C afforded yellow crystals of **4.6** within 48 h. Yield: 4 mg, 33%. ^{1}H NMR (500 MHz, D_2O): δ (ppm) 6.02 (t, $^3J_{HH}$ = 2.1 Hz, 4H, Cp), 5.74 (t, $^3J_{HH}$ = 2.1 Hz, 4H, Cp), 3.42 (s, 4H, CH_2), 2.80 (s, 6H, CH_3). ^{13}C NMR (500 MHz, D_2O): δ (ppm) 171.8, 97.8, 90.0, 88.3, 47.1, 35.9. ^{31}P{^{1}H} NMR (400 MHz, D_2O): δ (ppm) −144.5 (sept, $^1J_{PF}$ = 708.7 Hz). ^{19}F NMR (400 MHz, D_2O): δ (ppm) −72.0 (d, $^1J_{FP}$ = 708.7 Hz). Elemental analysis: calcd. for $C_{16}H_{22}CoF_6N_2O_4P$: C 37.66%, H 4.35%, N 5.49% Found: C 37.99%, H 4.25%, N 5.65%.

4.5.11 Synthesis of Supramolecular Polymer **4.7**

To **[4.3][PF$_6$]** (10 mg, 0.024 mmol) in methanol (1 mL) was added ethylenediamine (1.6 μL, 0.024 mmol). The solution was filtered into a 4 mL vial, which was placed into a capped 14 mL vial containing diethyl ether (1 mL). Slow vapour diffusion at 20 °C afforded yellow crystals of **4.7** within 24 h. Yield: 5 mg, 43%. ^{1}H NMR (500 MHz, D_2O): δ (ppm) 6.02 (t, $^3J_{HH}$ = 2.1 Hz, 4H, Cp), 5.74 (t, $^3J_{HH}$ = 2.1 Hz, 4H, Cp), 3.34 (s, 4H, CH_2). ^{13}C NMR (500 MHz, D_2O): δ (ppm) 171.8, 97.8, 90.0, 88.3, 39.5. ^{31}P{^{1}H} NMR (400 MHz, D_2O): δ (ppm) −144.5 (sept, $^1J_{PF}$ = 708.7 Hz). ^{19}F NMR (400 MHz, D_2O): δ (ppm) −72.0 (d, $^1J_{FP}$ = 708.7 Hz).

4.5.12 Attempted Thermal Polymerisation of **4.5**

Supramolecular polymer **4.5** (20 mg, 0.033 mmol) in an uncapped 4 mL vial was clamped inside an oven (temperature specified in Table 4.2) for 1 h. The vial was allowed to cool to

room temperature before deionised water (2 mL) was added. The mixture was stirred for 1 h then filtered. The yellow solution was dried and subjected to spectroscopic analysis.

Table 4.2. Conditions and results for thermally induced polymerisations of **4.5** to yield **[4.4][PF$_6$]$_n$**.

Reaction	Temperature	Yield / %	MW (PEG)[#] / Da	MW (PSS)[#] / Da
4.3.5a	180	0	‡	‡
4.3.5b	190	37 (80)†	3014–3690	1370–1870
4.3.5c	200	50	2140–3690	800–1870

[#]Molecular weights determined via DOSY analysis with PEG or PSS calibration. †The first yield indicates the proportion of polymerised material, and that in brackets represents the recovered amount of material after thermal polymerisation (including starting material). ‡No **[4.4][PF$_6$]$_n$** was recovered in this case.

Reaction 4.3.5a: Spectral analysis matched that of supramolecular polymer **4.5**.

Reaction 4.3.5b: Spectroscopic data indicated a mixture of starting material (**4.5**) and oligomer **[4.4][PF$_6$]$_n$** (yield of **[4.4][PF$_6$]$_n$**: 37% by ^{1}H NMR resonance integration). Unless stated otherwise, resonances were assigned to **[4.4][PF$_6$]$_n$**: ^{1}H NMR (400 MHz, D_2O): δ (ppm) 6.21 (m, Cp), 6.18 (m, Cp), 6.15 (m, Cp), 6.02 (t, $^3J_{HH}$ = 2.1 Hz, Cp, **4.5**) 5.99 (m, Cp), 5.94 (m, Cp), 5.89 (m, Cp), 5.84 (m, Cp), 5.81 (m, Cp), 5.77 (t, $^3J_{HH}$ = 2.1 Hz, Cp, **4.5**), 3.78 (m, CH_2, **4.5**), 3.77 (m, CH_2), 3.75 (s, CH_2, **4.5**), 3.74 (m, CH_2), 3.59 (m, CH_2), 3.22 (m, CH_2, **4.5**), 3.21 (m, CH_2). ^{31}P{^{1}H} NMR (400 MHz, D_2O): δ (ppm) −144.5. ^{19}F NMR (377 MHz, D_2O): δ (ppm) −71.0, −72.9, −128.4, −150.2. IR data (cm^{-1}) *ν*(N–H amine) 3429, *ν*(N–H amide) 3281, *ν*(C–H aromatic) 3111, *ν*(C–H) 2923, *ν*(C–H) 2880, *ν*(C=O acid) 1638, *ν*(C=O amide) 1605.

Reaction 4.3.5c: Oligomer **[4.4][PF$_6$]$_n$** (yield: 9 mg, 50%). ^{1}H NMR (500 MHz, D_2O): δ (ppm) 6.07 (m, Cp), 6.02 (m, Cp), 5.97 (m, Cp), 5.94 (m, Cp), 5.80 (m, Cp), 5.74 (m, Cp), 5.67 (m, Cp), 5.65 (m, Cp), 5.62 (m, Cp), 5.54 (m, Cp), 3.75 (m, CH_2), 3.55 (m, CH_2), 3.38 (m, CH_2), 3.11 (m, CH_2), 3.02 (m, CH_2). ^{31}P{^{1}H} NMR (400 MHz, D_2O): δ (ppm) −144.6.

^{19}F NMR (400 MHz, D_2O): δ (ppm) −71.0, −72.9, −126.0, −150.1. IR data (cm^{-1}) *v*(N–H amide) 3266, *v*(C–H aromatic) 3114, *v*(C–H) 2950, *v*(C=O amide) 1599.

4.5.13 Attempted Synthesis of a Supramolecular Polymer from **[4.3][Cl]**

To **[4.3][PF_6]** (50 mg, 0.118 mmol) in methanol (2 mL) was added 2,2′-(ethylenedioxy)bis(ethylamine) (17.3 μL, 0.118 mmol). The solution was filtered into a 14 mL vial, which was placed into a capped bottle containing diethyl ether (2 mL). Slow vapour diffusion at 20 °C afforded a yellow/orange gum. ^{1}H NMR spectroscopy (D_2O) revealed as a 1:1 mixture of the two starting materials. The pK_a of **[4.3][Cl]** (8.35) accounts for the lack of deprotonation that occurs in the presence of the diamine, and the subsequent lack of formation of a supramolecular polymer.

4.6 References

1. K. Tahlan and S. E. Jensen, *J. Antibiot.*, 2013, **66**, 401.

2. M. S. Wilke, A. L. Lovering and N. C. J. Strynadka, *Curr. Opin. Microbiol.*, 2005, **8**, 525-533.

3. R. Sykes, *J. Antimicrob. Chemother.*, 2010, **65**, 1842-1852.

4. M. C. Enright, D. A. Robinson, G. Randle, E. J. Feil, H. Grundmann and B. G. Spratt, *Proc. Natl. Acad. Sci. USA*, 2002, **99**, 7687.

5. S. M. Drawz and R. A. Bonomo, *Clin. Microbiol. Rev.*, 2010, **23**, 160-201.

6. P. A. Kiener and S. G. Waley, *Biochem. J*, 1978, **169**, 197-204.

7. S. J. Hecker, K. R. Reddy, M. Totrov, G. C. Hirst, O. Lomovskaya, D. C. Griffith, P. King, R. Tsivkovski, D. Sun, M. Sabet, Z. Tarazi, M. C. Clifton, K. Atkins, A. Raymond, K. T. Potts, J. Abendroth, S. H. Boyer, J. S. Loutit, E. E. Morgan, S. Durso and M. N. Dudley, *J. Med. Chem.*, 2015, **58**, 3682-3692.

8. R. A. Powers, J. Blázquez, G. S. Weston, B. K. Shoichet, M.-I. Morosini and F. Baquero, *Protein Sci.*, 1999, **8**, 2330-2337.

9. O. Eidam, C. Romagnoli, E. Caselli, K. Babaoglu, D. T. Pohlhaus, J. Karpiak, R. Bonnet, B. K. Shoichet and F. Prati, *J. Med. Chem.*, 2010, **53**, 7852-7863.

10. J. L. Crandon and D. P. Nicolau, *Antimicrob. Agents Chemother.*, 2015, **59**, 2688-2694.

11. G. Bou, E. Santillana, A. Sheri, A. Beceiro, J. M. Sampson, M. Kalp, C. R. Bethel, A. M. Distler, S. M. Drawz, S. R. R. Pagadala, F. van den Akker, R. A. Bonomo, A. Romero and J. D. Buynak, *J. Am. Chem. Soc.*, 2010, **132**, 13320-13331.

12. S. Majumdar and R. F. Pratt, *Biochemistry*, 2009, **48**, 8285-8292.

13. P. Lassaux, M. Hamel, M. Gulea, H. Delbrück, P. S. Mercuri, L. Horsfall, D. Dehareng, M. Kupper, J.-M. Frère, K. Hoffmann, M. Galleni and C. Bebrone, *J. Med. Chem.*, 2010, **53**, 4862-4876.

14. S. A. Adediran, M. Nukaga, S. Baurin, J.-M. Frère and R. F. Pratt, *Antimicrob. Agents Chemother.*, 2005, **49**, 4410-4412.

15. K. J. Kilpin and P. J. Dyson, *Chem. Sci.*, 2013, **4**, 1410-1419.

16. J. Zhang, Y. P. Chen, K. P. Miller, M. S. Ganewatta, M. Bam, Y. Yan, M. Nagarkatti, A. W. Decho and C. Tang, *J. Am. Chem. Soc.*, 2014, **136**, 4873-4876.

17. U. F. J. Mayer, J. P. H. Charmant, J. Rae and I. Manners, *Organometallics*, 2008, **27**, 1524-1533.

18. U. F. J. Mayer, J. B. Gilroy, D. O'Hare and I. Manners, *J. Am. Chem. Soc.*, 2009, **131**, 10382-10383.

19. B. Bartolomé, Y. Jubete, E. Martínez and F. de la Cruz, *Gene*, 1991, **102**, 75-78.

20. M. P. Williamson, *Prog. Nucl. Magn. Reson. Spectrosc.*, 2013, **73**, 1-16.

21. C. H. O'Callaghan, A. Morris, S. M. Kirby and A. H. Shingler, *Antimicrob. Agents Chemother.*, 1972, **1**, 283-288.

22. Z. Wang, W. Fast and S. J. Benkovic, *J. Am. Chem. Soc.*, 1998, **120**, 10788-10789.

23. Z. Wang, W. Fast and S. J. Benkovic, *Biochemistry*, 1999, **38**, 10013-10023.

24. N. V. Kaminskaia, B. Spingler and S. J. Lippard, *J. Am. Chem. Soc.*, 2000, **122**, 6411-6422.

25. N. V. Kaminskaia, B. Spingler and S. J. Lippard, *J. Am. Chem. Soc.*, 2001, **123**, 6555-6563.

26. J. D. Garrity, B. Bennett and M. W. Crowder, *Biochemistry*, 2005, **44**, 1078-1087.

27. P. J. Flory, *Chem. Rev.*, 1946, **39**, 137-197.

28. H. Köpnick, M. Schmidt, W. Brügging, J. Rüter and W. Kaminsky, in *Ullmann's Encyclopedia of Industrial Chemistry*, Wiley-VCH, 7th edn., 2013, vol. 28, p. 623.

29. B. Herzog, M. I. Kohan, S. A. Mestemacher, R. U. Pagilagan and K. Redmond, in *Ullmann's Encyclopedia of Industrial Chemistry*, Wiley-VCH, 7th edn., 2013, vol. 28, pp. 537-572.

30. C. E. Carraher and J. E. Sheats, *Makromol. Chem.*, 1973, **166**, 23-29.

31. C. U. Pittman, O. E. Ayers, B. Suryanarayanan, S. P. McManus and J. E. Sheats, *Makromol. Chem.*, 1974, **175**, 1427-1437.

32. E. W. Neuse, in *Organometallic Polymers*, Academic Press, New York, 1978, p. 95.

33. I. Cuadrado, C. M. Casado, F. Lobete, B. Alonso, B. González, J. Losada and U. Amador, *Organometallics*, 1999, **18**, 4960-4969.

34. N. Chen, H. Zhu, Y. Chu, R. Li, Y. Liu and F. Wang, *Polym. Chem.*, 2017, **8**, 1381-1392.

35. C. A. G. N. Montalbetti and V. Falque, *Tetrahedron*, 2005, **61**, 10827–10852.

36. A. El-Faham and F. Albericio, *Chem. Rev.*, 2011, **111**, 6557-6602.

37. E. Valeur and M. Bradley, *Chem. Soc. Rev.*, 2009, **38**, 606-631.

38. K. Gu, J. Onorato, S. S. Xiao, C. K. Luscombe and Y.-L. Loo, *Chem. Mater.*, 2018, **30**, 570-576.

39. W. Li, H. Chung, C. Daeffler, J. A. Johnson and R. H. Grubbs, *Macromolecules*, 2012, **45**, 9595-9603.

40. S. Viel, D. Capitani, L. Mannina and A. Segre, *Biomacromolecules*, 2003, **4**, 1843-1847.

41. D. Braga, L. Maini, M. Polito, M. Rossini and F. Grepioni, *Chem. Eur. J.*, 2000, **6**, 4227-4235.

42. F. Kettner, M. Kischel and H. Krautscheid, *CrystEngComm*, 2013, **15**, 8437-8443.

43. R. V. Ulijn, B. D. Moore, A. E. M. Janssen and P. J. Halling, *J. Chem. Soc., Perkin Trans. 2*, 2002, **0**, 1024-1028.

44. C. M. Gabriel, M. Keener, F. Gallou and B. H. Lipshutz, *Org. Lett.*, 2015, **17**, 3968-3971.

45. A. S. Galanis, F. Albericio and M. Grøtli, *Org. Lett.*, 2009, **11**, 4488-4491.

46. K. Hojo, A. Hara, H. Kitai, M. Onishi, H. Ichikawa, Y. Fukumori and K. Kawasaki, *Chem. Cent. J.*, 2011, **5**, 49.

47. K. Hojo, H. Ichikawa, Y. Fukumori and K. Kawasaki, *Int. J. Pept. Res. Ther.*, 2008, **14**, 373-380.

48. Q. Wang, Y. Wang and M. Kurosu, *Org. Lett.*, 2012, **14**, 3372-3375.

49. W. Konig and R. Geiger, *Chem. Ber. Recl.*, 1970, **103**, 2024-2034.

50. Y. J. Pu, R. K. Vaid, S. K. Boini, R. W. Towsley, C. W. Doecke and D. Mitchell, *Org. Process Res. Dev.*, 2009, **13**, 310-314.

51. G.-J. Ho, K. M. Emerson, D. J. Mathre, R. F. Shuman and E. J. Grabowski, *J. Org. Chem.*, 1995, **60**, 3569-3570.

52. J. M. G. Cowie and V. Arrighi, *Polymers: Chemistry and Physics of Modern Materials*, Routledge, 3rd edn., 2007.

53. J. March, Wiley-Interscience, New York, 4th edn., 1992, ch. 8.

54. Z. Fei, D. Zhao, T. J. Geldbach, R. Scopelliti and P. J. Dyson, *Chem. Eur. J.*, 2004, **10**, 4886-4893.

55. C. O. Silva, E. C. da Silva and M. A. C. Nascimento, *J. Phys. Chem. A*, 2000, **104**, 2402-2409.

56. C. O. Silva, E. C. da Silva and M. A. C. Nascimento, *J. Phys. Chem. A*, 1999, **103**, 11194-11199.

57. J. E. Huheey, E. A. Keiter and R. L. Keiter, *Inorganic Chemistry: Principles of Structure and Reactivity*, New York: Harper and Row, 1983.

58. C.-P. Li, J. Chen, C.-S. Liu and M. Du, *Chem. Commun.*, 2015, **51**, 2768-2781.

59. J. Sun, F. Dai, W. Yuan, W. Bi, X. Zhao, W. Sun and D. Sun, *Angew. Chem. Int. Ed.*, 2011, **50**, 7061-7064.

60. I. J. Vitórica-Yrezábal, G. Mínguez Espallargas, J. Soleimannejad, A. J. Florence, A. J. Fletcher and L. Brammer, *Chem. Sci.*, 2013, **4**, 696-708.

61. T. C. Ehlert and M.-M. Hsia, *J. Chem. Eng. Data*, 1972, **17**, 18-21.

62. K. S. Gavritchev, G. A. Sharpataya, A. A. Smagin, E. N. Malyi and V. A. Matyukha, *J. Therm. Anal. Calorim.*, 2003, **73**, 71-83.

63. V. Kraft, M. Grützke, W. Weber, M. Winter and S. Nowak, *J. Chromatogr. A*, 2014, **1354**, 92-100.

64. M. Villanueva, A. Coronas, J. García and J. Salgado, *Ind. Eng. Chem. Res.*, 2013, **52**, 15718-15727.

65. D. H. Zaitsau, Y. U. Paulechka and G. J. Kabo, *J. Phys. Chem. A*, 2006, **110**, 11602-11604.

66. R. P. Swatloski, J. D. Holbrey and R. D. Rogers, *Green Chem.*, 2003, **5**, 361-363.

67. M. G. Freire, C. M. S. S. Neves, I. M. Marrucho, J. A. P. Coutinho and A. M. Fernandes, *J. Phys. Chem. A*, 2010, **114**, 3744-3749.

68. S. Inyushin, A. Shafir, J. E. Sheats, M. Minihane, C. E. Whitten and J. Arnold, *Polyhedron*, 2004, **23**, 2937-2942.

69. Bruker-AXS SAINT V7.68A, Madison, Wisconsin.

70. G. M. Sheldrick, SADABS V2008/1 or TWINABS V2008/4, University of Göttingen, Germany.

71. G. M. Sheldrick, *Acta Crystallogr.*, 2008, **A64**, 112-122.

72. A. Albert, *The Determination of Ionization Constants: A Laboratory Manual*, Springer Science & Business Media, 2012.

5 Impact of a Subtle Structural Difference on the Self-Assembling Behaviour of Gold(I) Complexes

5.1 Abstract

Living supramolecular polymerisation is in its infancy compared to conventional living covalent polymerisation of organic monomers, and an understanding of the effect molecular structure has on the self-assembly process remains limited. Herein, we report the capacity of three bimetallic gold(I) complexes (**5.2**–**5.4**) to differentiate into fibre-like micelles and nanoparticles upon self-assembly, and propose mechanisms and free energy landscapes underlying their formation. Increasing the conjugation length from a phenyl (in **5.2**) to biphenyl (in **5.3**) or 2,1,3-benzothiadiazole (in **5.4**) allowed for morphological transition from small particles (for which AFM data are consistent with spherical structures) to fibres. With **5.3** in a heptane solution the length distribution of the resulting fibres could be controlled by use of a seeded-growth methodology. Interestingly, fibre-like micelles of **5.4** showed unique time-dependent evolution to nanoparticles, which was understood to occur due to the relative thermodynamic stabilities of the species. It was hoped that the investigation into these three materials would provide an insight into the significant effects on self-assembly of core structural changes, and inform future work on the living supramolecular polymerisation of gold(I) compounds.

5.2 Introduction

In recent years the supramolecular chemistry of gold(I) complexes has attracted growing attention, provoked by the interesting and characteristic photochemistry that many derivatives display.[1-5] The luminescence in such compounds commonly derives from aurophilic interactions between the gold(I) centres (the relativistic effects in gold allow for closed-shell interactions), which are energetically comparable to hydrogen bonds (5–10 kcal

mol^{-1}).[6-8] Additionally, due to the similarity in the bond strength and directionality of aurophilic and hydrogen bonds, such interactions can provide significant impetus for aggregation in both solution and the solid state.[9] The toolbox used to build higher-ordered functional materials contains additional possible types of interactions, including enthalpically-driven hydrogen bonding (as mentioned) and π–π stacking, and entropically-driven hydrophobic-hydrophobic interactions. These interactions have been identified in the formation of gold(I)-containing fibre-like structures, spherical aggregates, vesicles, and gels with luminescent behaviour.[10-13]

Whilst there has been a steady development in general organogold chemistry since the discovery of gold(I)carbide in 1900,[14] research into gold alkynyl compounds has proved a particularly active area that includes both σ-[15-18] and π-bound complexes.[19, 20] The former are typically synthesised by reaction of Au(L)Cl (where L is a volatile ligand such as tetrahydrothiophene (tht)) with a terminal alkyne in the presence of a strong base.[15, 20] Although the aggregation properties of gold(I) acetylides are established, most studies are restricted to their structure and crystal packing in the solid state,[21] or to those focussing on photophysical behaviour.[22] The formation of one-dimensional nanostructures by supramolecular self-assembly is increasingly relevant to biological systems, for instance in understanding fibril formation in Alzheimer's disease,[23] and nanotechnology, e.g. molecular circuitry.[24] Herein, we describe the formation of fibre-like nanostructures and (potentially spherical) particles in solution via the self-assembly of bimetallic gold(I)acetylides, and the use of living supramolecular polymerisation to produce one dimensional structures of a defined length. In addition, we provide understanding of the pathways to these supramolecular assemblies.

5.3 Results and Discussion

5.3.1 Synthesis and Characterisation of **5.2**–**5.4**

To participate in cooperative supramolecular polymerisation, the monomeric units generally require the ability to form multiple non-covalent interactions with at least two neighbouring molecules.[25, 26] Following this principle, recent work by Zou and Wang featured the supramolecular polymerisation of platinum acetylides thorough use of a π-aromatic, bimetallic system, with an amide linker attached at each end of the platinum(II)acetylide rod.[27] Use of similar Au(I) systems was expected to also produce supramolecular polymers, but with aurophilic contacts throughout.

The ligand, **5.1**, was synthesised by the addition of 3,4,5-tris(dodecyloxy)benzoic acid, *N*-(3-dimethylaminopropyl)-*N′*-ethylcarbodiimide hydrochloride (EDC), and 4-dimethylaminopyridine (DMAP) to dry dichloromethane with stirring for 30 min, before 4-isocyanophenylamine was added and the reaction allowed to stir for a further 24 h. After work up and purification by column chromatography, a white solid was isolated in 90% yield. Derivatisation was then achieved by addition of three diacetylene derivatives (phenyl, biphenyl, and 2,1,3-benzothiadiazole) to Au(tht)Cl and trimethylamine solutions in chloroform. In each case yellow precipitates quickly formed, after which **5.1** was quickly added to each reaction mixture and stirred overnight. Precipitation into methanol allowed for the isolation of yellow and orange solids (**5.2**, **5.3**, and **5.4**) in good yields. Characterisation was obtained by ^{1}H and ^{13}C NMR spectroscopy, and product molecular weights were confirmed by matrix-assisted laser desorption ionisation time-of-flight (MALDI-TOF) mass spectrometry.

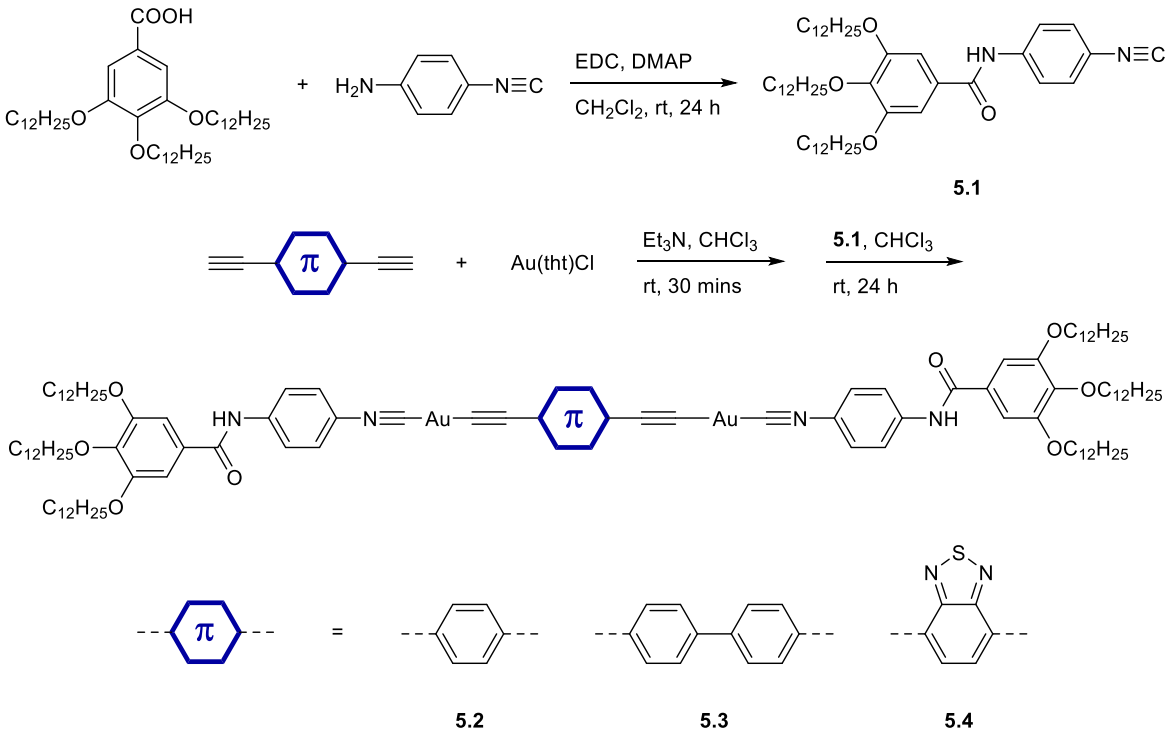

Scheme 5.1. Synthesis of compounds **5.2**, **5.3**, and **5.4**.

5.3.2 Self-Assembly

5.3.2.1 Self-Assembly of **5.2**

Solution-phase self-assembly of **5.2** was initially investigated in chloroform, which afforded monomeric **5.2** as indicated by dynamic light scattering (DLS), which displayed a characteristic peak for well-solvated molecular species (or those with a low degree of aggregation) at <1 nm. In attempts to form self-assembled structures, solutions of **5.2** in a variety of hydrocarbon solvents were prepared (0.5 mg mL^{-1}) by heating to 10 °C below the boiling point of the particular solvent for 10 min (to ensure complete dissolution of the solid). The solutions were then cooled to ambient temperature for 24 h before a drop of each was cast onto carbon-coated copper transmission electron microscopy (TEM) grids. Non-aromatic hydrocarbon solvents were chosen in the expectation that they would favour solvation of the dodecane side-chains over the aromatic core. In all cases surveyed (methylcyclohexane (MCH), *n*-hexanes, cyclohexane, and heptane, Figures A5.10a and A5.11), TEM analysis revealed the presence of aggregated, small particles. Atomic force

microscopy (AFM) data of the small particles in MCH was consistent with collapsed spherical structures (Figure A5.12), with an average height of ~4.1 nm. In addition, significantly less aggregation of the particles was observed on this substrate (carbon-coated mica) compared to on carbon-coated copper TEM grids.

To investigate the self-assembly behaviour of **5.2** in more detail, an aggregated solution of **5.2** in MCH, and a monomeric solution in chloroform (both 0.5 mg mL^{-1}) were studied by UV/Vis absorption spectroscopy (Figure 5.1a). The UV/Vis spectrum of self-assembled **5.2** displayed absorption bands at 215 (λ_{max}) and 313 nm, whilst the spectrum of **5.2** in monomer form displayed strong absorption bands at 307, 321, and 339 nm. Unfortunately, the solvent window of chloroform did not allow for probing of the monomeric state between 200–250 nm. The intense band in the ultraviolet region of the self-assembled sample in MCH is tentatively assigned to metal-to-ligand charge transfer (MLCT),[28] and that at 313 nm to intraligand (IL) absorptions.[29] Monomeric **5.2** displayed low luminescence in solution ($CHCl_3$) which is commonly observed for gold acetylides in a monomeric state. However, **5.2** is highly luminescent in solution in MCH, which indicates the formation of polymeric supramolecular assemblies (Figure 5.1b, λ_{max}: 511 nm).[28] Similar emission spectra have been observed for gold(I) complexes with short Au···Au contacts in the solid state, and the emission has usually involved a $^3(d_\delta^*\text{-}p_\sigma)$ or $^3(d_\sigma^*\text{-}p_\sigma)$ excited state.[30-33]

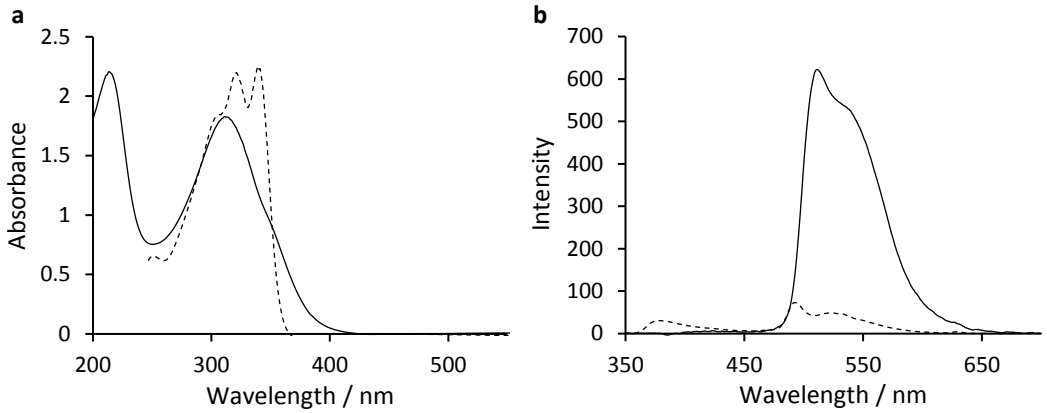

Figure 5.1. a) Overlaid UV/Vis spectra of **5.2** in $CHCl_3$ (dashed line, monomeric) and MCH (solid line, aggregated). b) Overlaid emission spectra of **5.2** in $CHCl_3$ (dashed line, monomeric) and MCH (solid line, aggregated), λ_{ex} = 313 nm.

5.3.2.2 Energy Landscape of **5.2**

As supramolecular polymerisations exploit non-covalent interactions, the self-assembly process is often controlled by the thermodynamics of the system, although application of kinetic control can yield kinetically trapped or metastable states of aggregation.[34] The micelles formed by **5.2** were unaffected by the choice of hydrocarbon solvent (*n*-hexanes, cyclohexane, MCH, heptane), each producing small particles. Furthermore, the addition of up to 20% good solvent (chloroform) to a solution of **5.2** in MCH (v/v, 0.5 mg mL^{-1}) appeared to make no difference to the morphology obtained. Moreover, after heating solutions of **5.2** in MCH to 60–80 °C for 1 h no obvious change was observed by TEM. Sonication of a solution of **5.2** (0.5 mg mL^{-1}, MCH, 24 h) for 30 min at 0 °C appeared to cause fragmentation of the aggregated particles but did not induce a morphological change. Finally, analysis after 3 months by TEM revealed that the small particles were unchanged in MCH. Thus, it is believed that the nanostructures formed by **5.2** represent the thermodynamic equilibrium state i.e. the minimum of the free energy landscape.

Temperature dependent UV/Vis spectrometry was applied to elucidate the formation mechanism of the small aggregates of **5.2** in MCH (at a concentration of 0.5 mg mL^{-1}). Absorption bands at 214 and 313 nm were observed to decrease in intensity upon increasing

temperature, Figure 5.2. Whilst a qualitative difference in spectra could be observed, quantitative analysis proved difficult due to overlap of the monomer and aggregate absorption bands. Regardless, the intensity of the absorption band at 214 nm and that of the minimum at 250 nm were plotted against temperature (Figure 5.2b). Instrumental limits did not allow data collection above 90 °C, thus a complete transformation from aggregated to monomeric species could not be obtained, but by elucidating the gradients throughout, the curves appear to be sigmoidal.[35] This suggests that the formation of the nanostructures of **5.2** in MCH can be described by an isodesmic model, in which each self-assembly step is governed by a single equilibrium constant (comparable to a step-growth polymerisation).

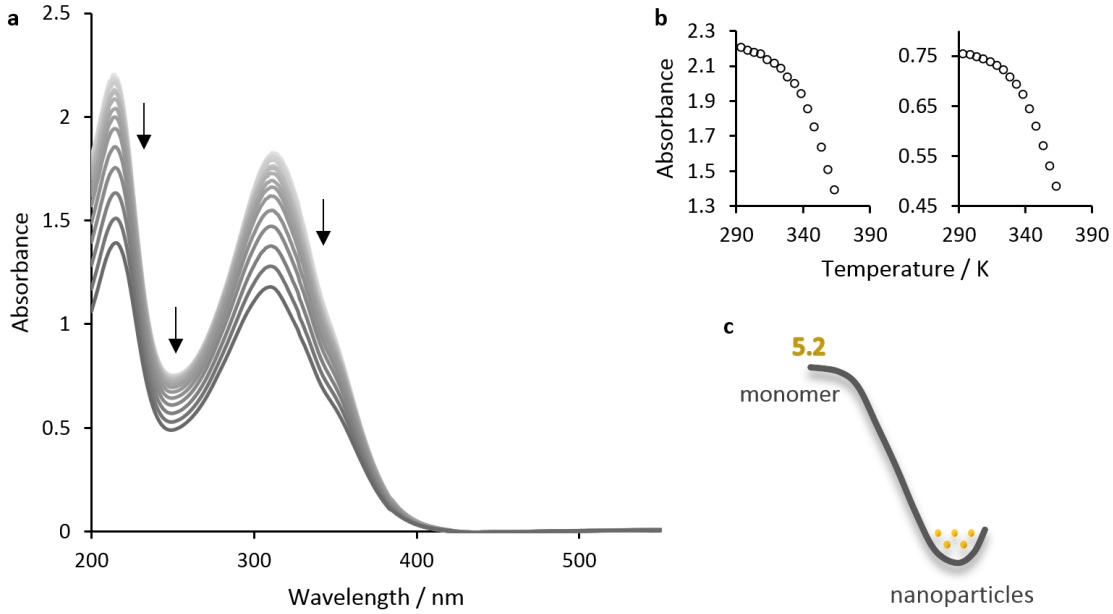

Figure 5.2. a) Temperature-dependent UV/Vis absorption spectra of **5.2** (MCH, 0.5 mg mL^{-1}). b) Absorbance of the band at 214 nm (left) and 250 nm (right) with increasing temperature. c) Energy landscape of **5.2**.

5.3.2.3 Self-Assembly of **5.3**

Next, we explored the effect of a minor modification of the conjugated core of the small molecule, from a phenyl system (**5.2**) to a biphenyl system (**5.3**), on the self-assembly.

Compound **5.3** was suspended in hydrocarbon-based solvents such as *n*-hexanes, heptane, and MCH at a concentration of 0.5 mg mL^{-1}, heated to 10 °C below the solvent boiling point

for 10 min to ensure complete dissolution, then allowed to cool to ambient temperature over 24 h. A drop of each solution was cast onto carbon-coated copper grids for analysis by TEM. This revealed the formation of polydisperse fibre-like micelles in heptane and *n*-hexanes, with longer and more aggregated examples in the latter solvent (Figure A5.13). In MCH, both bundled fibre-like micelles and (potentially spherical) small particles were observed. Thus, we proceeded primarily to employ heptane as a selective solvent. Chloroform was discovered to be a good solvent for **5.3** as analysis by DLS displayed a hydrodynamic radius <1 nm, suggestive of well-solvated molecular species or a low degree of aggregation.

UV/Vis spectroscopic analysis of monomeric **5.3** in chloroform displayed an absorption maximum (λ_{max}) of 328 nm, whilst in the aggregated state (heptane) this band was hypsochromically-shifted (315 nm), alongside the observation of an additional absorption band at 213 nm (λ_{max}) and a weaker absorption shoulder at 371 nm (Figure 5.3a). The appearance of the shoulder suggests the presence of extended conjugation due to Au···Au bonding or π-π stacking.[36] In a similar manner to **5.2**, the highest-energy band is assigned to an MLCT,[28] and the other two to IL absorptions.[29] Compound **5.3** (0.5 mg mL^{-1}) is luminescent in solution in both the monomeric (chloroform, λ_{max}: 388 nm) and aggregated states (heptane, λ_{max}: 544 nm). We assign the emission of monomeric **5.3** to predominantly result from the biphenyl core, while the emission in the visible region for polymeric **5.3** includes excited states containing Au···Au bonding.[17] The stability of the aggregated state was monitored over a 7 day period by UV/Vis spectroscopy (at 20 °C), and no spectral changes were observed. This indicated the persistence of the aggregated species in a heptane solution.

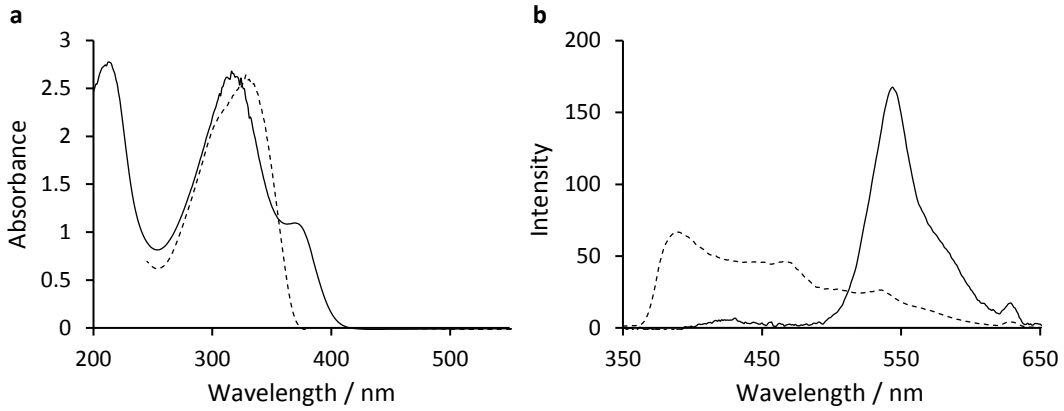

Figure 5.3. a) Overlaid UV/Vis spectra of **5.3** in $CHCl_3$ (dashed line, monomeric) and heptane (solid line, aggregated). b) Overlaid emission spectra of **5.3** in $CHCl_3$ (dashed line, monomeric) and heptane (solid line, aggregated), λ_{ex} = 315 nm.

Atomic force microscopy (AFM) images were collected of **5.3** dropcast from a heptane solution (0.5 mg mL^{-1}) onto carbon coated mica (Figure 5.4). The resulting micrographs displayed highly aggregated, aligned fibrous bundles, although individual fibre-like micelles with narrow widths (~5 nm) could still be detected. By estimation of the diameter of the core section of **5.3** (~4.0 nm, Figure A5.9), we propose that the fibre-like micelles are a single molecule wide. A height image line trace (Figure 5.4b) across multiple fibres showed the structures to be 2.1 nm high.

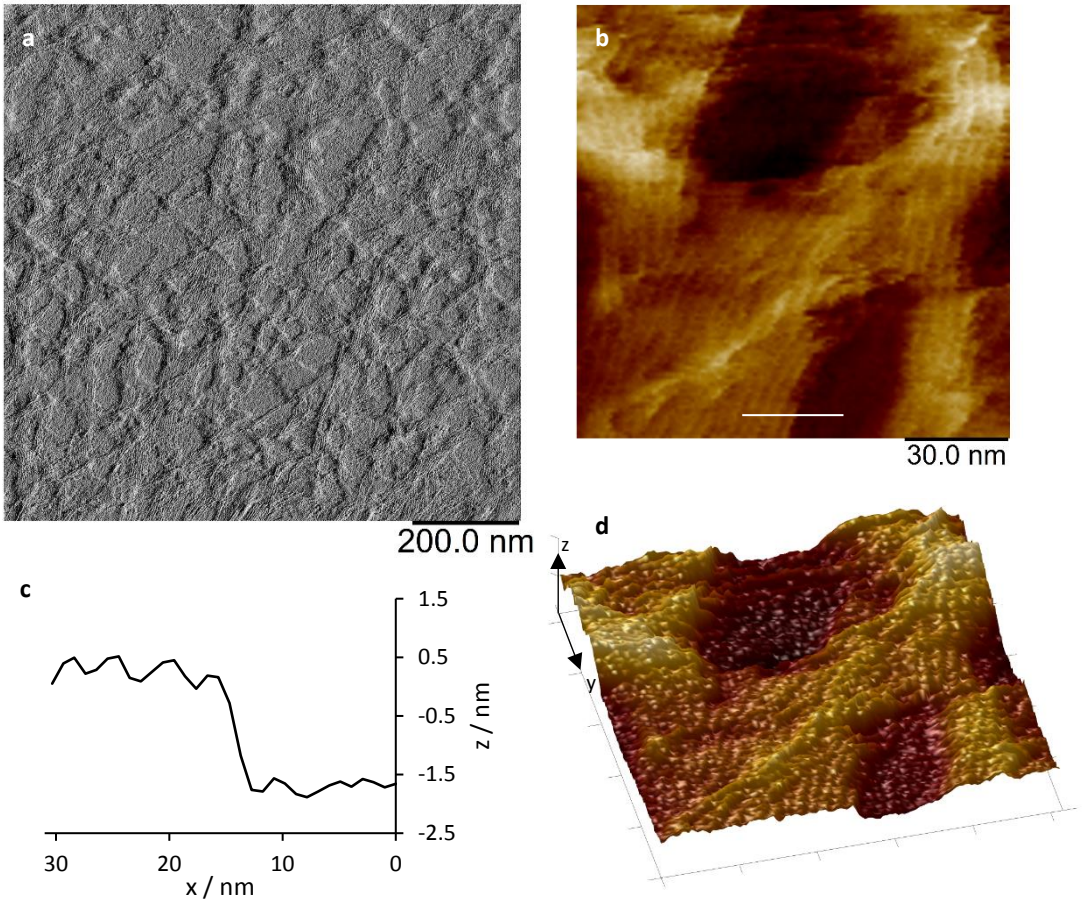

Figure 5.4. a) Large scale AFM force image of aggregated fibres formed by **5.3** in heptane. b) AFM height image of aggregated fibres formed by **5.3** in heptane in the x-y plane; c) height profile of multiple fibres (white line trace in (b)); d) (b) as a 3D projection.

5.3.2.4 Seeded Growth of **5.3**

Living crystallisation-driven self-assembly (CDSA) methods that were originally developed for BCPs with a crystallisable core-forming block have been successfully applied to supramolecular systems.[37-41] The formation of monodisperse fibrous micelles is generally achieved by ultrasonication of long, polydisperse, one-dimensional micelles to form short seed micelles, followed by the addition of further monomer. Thus, we explored the use of such a method to produce fibres of controlled length with this self-assembling supramolecular system. Firstly, short seed micelles were formed by subjecting polydisperse fibres of **5.3** (0.1 mg mL^{-1}, heptane, 24 h) to sonication for 30 min at 0 °C (Figure A5.14a). Note, the use of a lower concentration used here versus Section 5.3.2.3 represents an attempt

to prevent aggregation of fibrous structures and enable more accurate measurements of the individual objects. The average contour length of the seed fibres was determined by TEM: L_n = 43 nm, L_w = 49 nm, polydispersity index (PDI) = 1.16. Additionally, the length distribution of these micelles was monitored over seven days; however, no appreciable differences in L_n or PDI were detected (Figure 5.5a and A5.15), suggesting that the fibrous micelles are kinetically trapped in heptane.

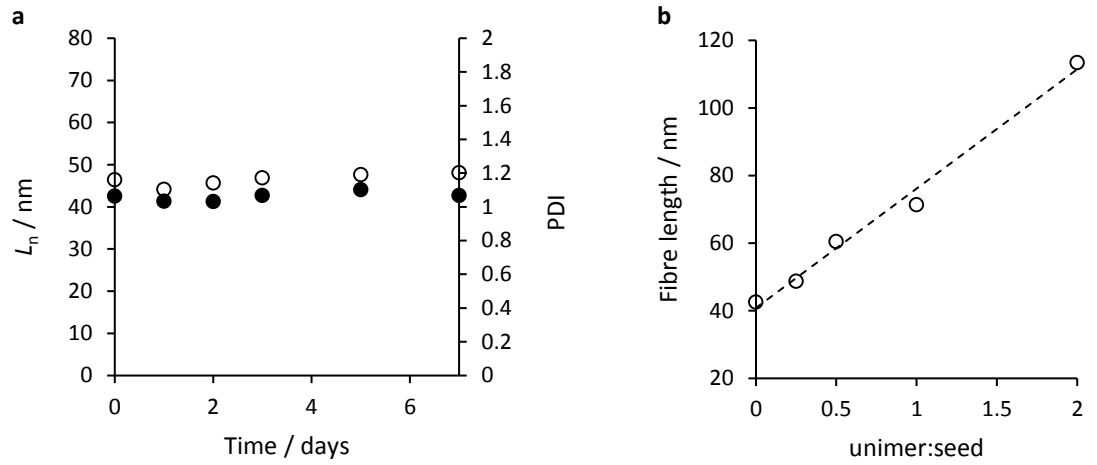

Figure 5.5. a) Time dependence of ● average contour length (L_n), and ○ PDI, of **5.3** seed micelles in heptane (0.1 mg mL^{-1}). b) Linear dependence of average contour length (L_n) on the monomer to seed molar ratio for the seeded growth of **5.3**.

The ability to control the length of fibres was then explored. To a solution containing 10 μg of seed fibres (100 μL, 0.1 mg mL^{-1}) at ambient temperature, monomer in $CHCl_3$ was added (2.5 μg, 5 μg, 10 μg, 20 μg, and 40 μg; various concentrations of monomer solution were used such that the percentage of chloroform added never exceeded 5% v/v) and the solutions aged for 24 h. Analysis by TEM of the resulting solutions revealed that up to a 2:1 monomer:seed molar ratio, linear growth could be observed, (Figure 5.5b, A5.14, and A5.16). Unfortunately, above this ratio, fibre aggregation precluded accurate measurements of contour length.

5.3.2.5 Energy Landscape of **5.3**

The stability of the seed micelles of **5.3** in heptane indicated the kinetically trapped nature of the fibrous structures. Subsequent investigations focussed on the application of heat to overcome the energy barrier preventing the transformation of the kinetically trapped fibres into a thermodynamic energy minimum structure.

Annealing samples of polydisperse fibres for 1 h at temperatures between 60–80 °C did not induce a morphology change, suggesting that the fibres are trapped in a deep kinetic energy well. Indeed, preparing solutions of **5.3** in heptane and directly heating for 1 h at either 80 or 90 °C did not provide the impetus to bypass the fibrous state. Mechanical agitation via stirring or ultrasonication has been applied in other supramolecular systems to accelerate the transformation of systems from a metastable product to the equilibrium state.[42] However, as discussed in Section 5.3.2.4, ultrasonication does not induce a morphological transformation of **5.3**.

Modification of solvent composition by dissolving **5.3** in heptane solutions with increasing good solvent content ($CHCl_3$, 0%–20%, v/v) had some effect, but fibrous structures remained the dominant morphology. TEM micrographs captured after 24 h showed that the length of the fibres formed decreased significantly (Figure 5.6), although this may be due to a decrease in the rate of self-assembly. Interestingly, these structures appeared to aggregate far more than in the absence of good solvent, which is unexpected as better solvation should not induce aggregation. However, this may simply be a sample dependent drying effect.

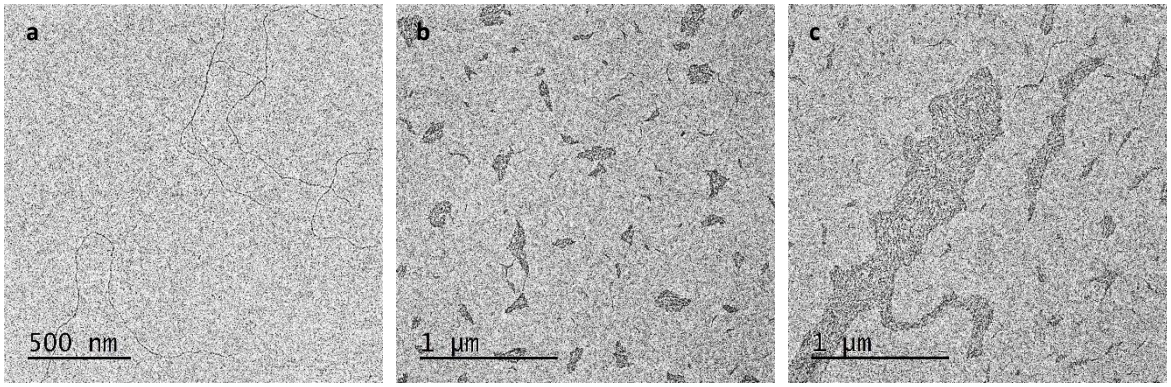

Figure 5.6. TEM images of **5.3** in heptane with: a) 0% $CHCl_3$, b) 10% $CHCl_3$, c) 20% $CHCl_3$. All micrographs acquired from 0.5 mg mL^{-1} solutions, which were heated to 80 °C for 10 min, then cooled to ambient temperature for 24 h.

An energy landscape is proposed for **5.3** in heptane (Figure 5.7b); however, the deep kinetic well in this solvent did not allow for determination of the thermodynamic structure. Although the precise molecular packing is not clear currently, we propose that the fibres observed in heptane occur via face-to-face stacking of **5.3**, stabilised by greater π-π interactions between the extended aromatic core present here compared to in **5.2**. The formation of the fibres fits a cooperative model (elucidated by temperature dependent UV/Vis spectrometry),[35] in which two separate processes occur: a thermodynamically unfavourable nucleation step, and subsequent favourable elongation.

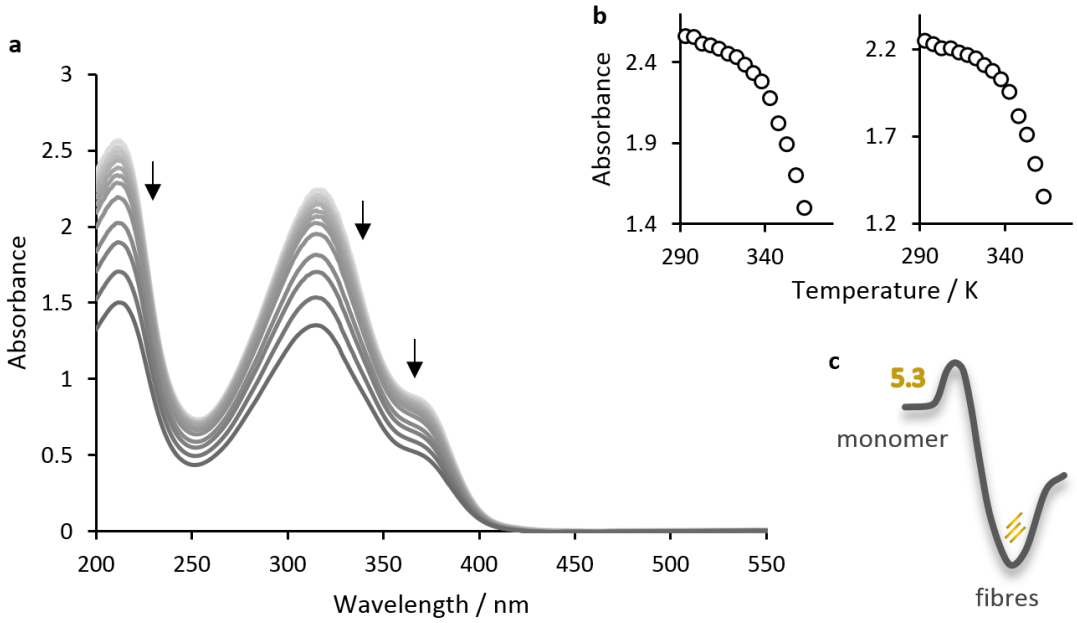

Figure 5.7. a) Temperature-dependent UV/Vis absorption spectra of **5.3** (heptane, 0.5 mg mL^{-1}). b) Absorbance of band at 213 nm (left) and 315 nm (right) with increasing temperature. c) Energy landscape of **5.3**.

5.3.2.6 Self-Assembly of **5.4**

An additional slight modification of the core structure of these gold(I) acetylides, as in compound **5.4**, was found to cause significant differences in the self-assembly behaviour and the energy landscape compared to **5.2** and **5.3**. Use of a 2,1,3-benzothiadiazole moiety ensured that **5.4** contained a larger conjugated core than **5.2**, but in a different steric and electronic manner to **5.3**. When **5.4** was dissolved in hydrocarbon solvents (*n*-hexanes, cyclohexane, MCH, heptane) at 0.5 mg mL^{-1} and heated to 10 °C below each solvent boiling point for 10 min, yellow solutions formed. These were allowed to cool to ambient temperature and aged for 24 h before analysis by TEM. In MCH, long, polydisperse fibre-like micelles with a high degree of bundling were observed, whilst the use of *n*-hexanes, cyclohexane, or heptane yielded mixtures of fibre-like structures and small (potentially spherical) particles (Figure 5.8 and A5.17). Chloroform was evidenced as a good solvent for **5.4** by DLS, in which a hydrodynamic radius <1 nm was measured, indicative of well-solvated molecular species or a low degree of aggregation.

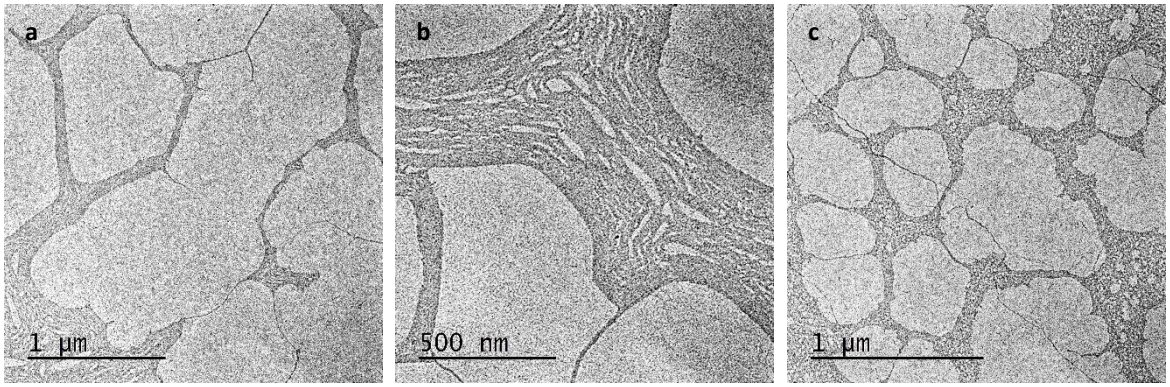

Figure 5.8. TEM images of **5.4**: a) and b) fibres in MCH; c) mixed morphologies in cyclohexane. All micrographs were acquired from 0.5 mg mL^{-1} solutions, which were heated for 10 min to 10 °C below the solvent boiling point and cooled for 24 h before dropcasting.

Due to the formation of fibrous micelles in MCH, this was used primarily as the selective solvent for self-assembly, and the aggregation behaviour was confirmed in solution by UV/Vis absorption spectroscopy. The UV/Vis spectrum of the **5.4** monomer in chloroform displayed an absorption maximum (λ_{max}) of 312 nm with a small lower-energy band at 419 nm that is not present in the spectra of **5.2** or **5.3**, thus likely arises from transitions originating from the benzothiadiazole core section of the molecule (Figure 5.9). The measured λ_{max} of **5.4** in methylcyclohexane occurs at 216 nm, with an additional absorption band at 315 nm. The intense band in the ultraviolet region is tentatively assigned to a metal-to-ligand charge transfer (MLCT),[28] and that at 313 to intraligand (IL) absorptions.[29] A further absorption band centred around 437 nm is bathochromically shifted compared to that of monomeric **5.4**, and is indicative of extended conjugation.[36] This red shift is apparent in the colour change that occurs from green/yellow in chloroform to yellow upon aggregation in MCH (Figure A5.18). In addition, compound **5.4** (concentration: 0.5 mg mL^{-1}) is luminescent in solution in both the unaggregated (in chloroform, λ_{max}: 509 nm) and self-assembled state (in heptane, λ_{max}: 534 nm), and this bathochromic shift is also indicative of aggregation.[36, 43]

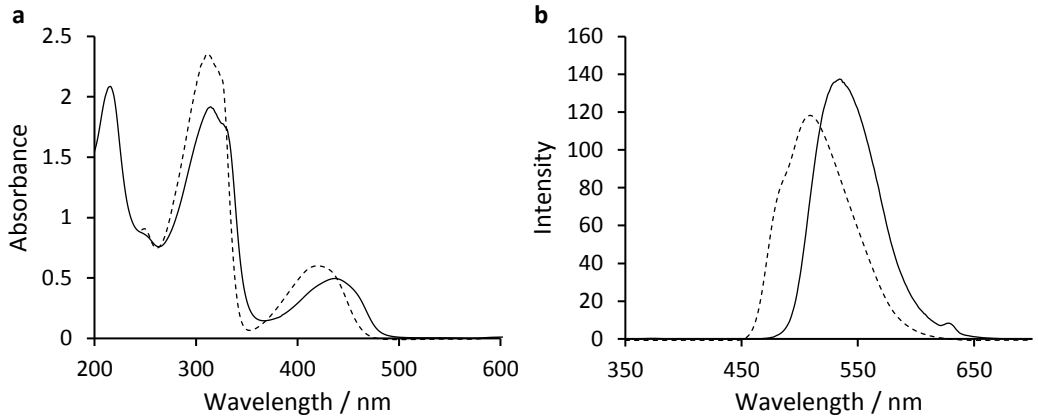

Figure 5.9. a) Overlaid UV/Vis spectra of **5.4** in $CHCl_3$ (dashed line, monomeric) and MCH (solid line, aggregated). b) Overlaid emission spectra of **5.4** in $CHCl_3$ (dashed line, monomeric) and MCH (solid line, aggregated), λ_{ex} = 315 nm.

A sample of **5.4** dropcast from MCH (0.5 mg mL^{-1}) onto carbon coated mica was analysed by AFM, and clearly showed highly aggregated fibrous bundles, as observed for **5.3** (Figure 5.10). The aggregation is believed to be caused during sample preparation, as it differs to that observed by TEM. A height trace measurement across multiple fibre-like micelles evidenced narrow widths (~5 nm) and showed the structures to be ~1.7 nm high. By estimating the diameter of the core section of **5.4** (~3.5 nm, Figure A5.9), we propose that the fibres are a single molecule wide. As with the AFM sample of **5.3**, there appears to be a preferential alignment of the fibres.[44]

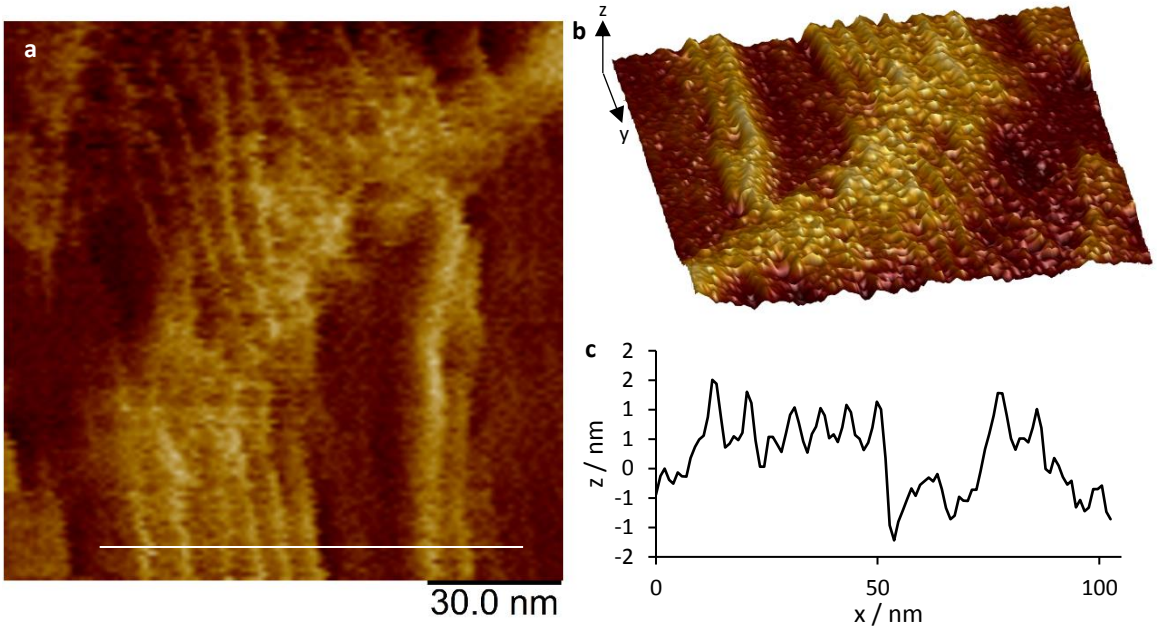

Figure 5.10. AFM height images of aggregated fibres formed by **5.4** in heptane: a) in the x-y plane; b) as a 3D projection. c) Height profile of multiple fibres (white line trace in (a)).

The stability of fibres of **5.4** in MCH was monitored by UV/Vis spectroscopy. No obvious change occurred over 7 days. As a result of the highly aggregated nature of the fibre-like micelles, small morphology changes were difficult to observe by TEM, but when a solution of **5.4** in MCH was analysed after 3 months, the majority of fibres had undergone a morphological transformation into aggregated small particles (similar to those observed for **5.2** in MCH, Figure A5.19a). Due to the slow nature of this transformation, the possibility to form fibre-like structures of controlled length was still believed to be realistic and was therefore investigated.

5.3.2.7 Seeded Growth of **5.4**

In a similar manner to **5.3**, we explored the use of a seeded-growth method to produce fibres of controlled length. Seed micelles were formed by subjecting polydisperse fibres of **5.4** (concentration: 0.5 mg mL^{-1}, MCH, 24 h) to ultrasound for 30 min at 0 °C, Figure 5.11a. The average contour length of the seed fibres was determined by TEM analysis: L_n = 36 nm, L_w = 44 nm, PDI = 1.21 (Figure A5.20). The length distribution of these micelles was then

monitored over a period of time: within 24 h a large number of nanoparticles were apparent by TEM, which increased by 48 h (Figure 5.11b and c, respectively). This, in conjugation with TEM analysis of the polydisperse sample over time suggests that fibres of **5.4** are a kinetically formed product, which later transforms into the thermodynamically stable morphology. It is believed that mechanical agitation by ultrasonication may facilitate this transformation. Unfortunately, the inherent metastability of **5.4** in MCH prevents the use of a seeded growth method to produce fibres of defined length.

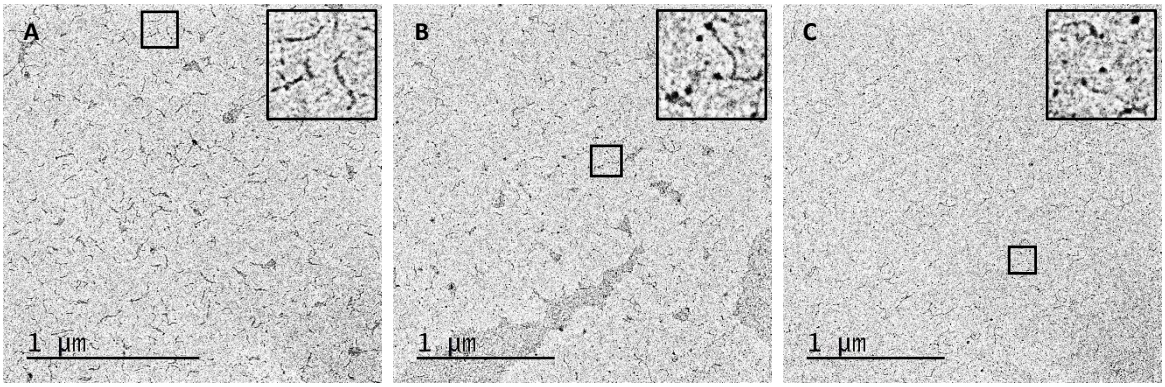

Figure 5.11. TEM micrographs of **5.3** (MCH, 0.5 mg mL^{-1}, aged for 24 h followed by sonication for 30 min): a) seed micelles; b) seed micelles aged for 24 h; c) seed micelles aged for 48 h.

5.3.2.8 Energy Landscape of **5.4**

The change in morphology of **5.4** in MCH from fibrous micelles to small aggregates over a period of days indicates the metastable nature of the former. In addition to aging, increasing the sample sonication time also increased the proportion of micelles undergoing the morphological change. TEM revealed that after sonication for 2 h, a significant proportion of fibre-like micelles of **5.4** had undergone a morphological transformation to small aggregates (Figure A5.19b). When the sonication time was increased to 4 h, even fewer of the micelles retained their original morphology (Figure A5.19c). Comparison of UV/Vis spectra (Figure A5.21) of fibre-like seed micelles (1 h sonication) and the small particles (4 h sonication) revealed a minor red shift of all major absorption bands (~2 nm) upon the

morphological transition. In addition, the band at ~215 nm attributed to an MLCT appeared to become slightly more intense, and that at ~311 nm assigned to IL absorptions marginally less so. The mechanism by which ultrasound induces a morphological transition of **5.4** is still somewhat unclear. However, work on organogelators showed that sonication can have influence on the morphology of supramolecular aggregates, presumably through cleavage of intramolecular hydrogen bonds and π-stacking.[45-49] The morphological change from fibre-like micelles to the potentially spherical structure here should involve molecular rearrangement and it is likely that ultrasonication facilitates this by breaking the intramolecular bonds.

Increasing the content of chloroform to 10% in a solution of **5.4** in MCH (v/v, 0.5 mg mL^{-1}) had little effect after 24 h, and fibre-like micelles were still observed. Upon a further increase to 20% chloroform, similar bundled fibres were observed, but some evidence for a small number of (potentially spherical) small particles in addition to the fibres also emerged (Figure A5.22). If the fibre-like micelles are a stable or metastable morphology in MCH, the addition of good solvent may be allowing the transformation to a thermodynamically stable morphology by partially solvating the core section of **5.4**. Alternatively, the addition of chloroform may modify the energy landscape, and so a smaller kinetic barrier may exist.

The mechanism for the formation of fibre-like micelles of **5.4** in MCH was investigated by temperature dependent UV/Vis spectroscopy. In a similar manner to **5.2** and **5.3**, it was not possible to observe a critical temperature (or lack of) due to instrumental limits at high temperature (Figure 5.12). However, by scrutinising the gradients of the curves, a non-sigmoidal relationship was suggested;[35] thus, a cooperative model may be used to describe the formation of fibre-like micelles of **5.4** in MCH over 24 h.

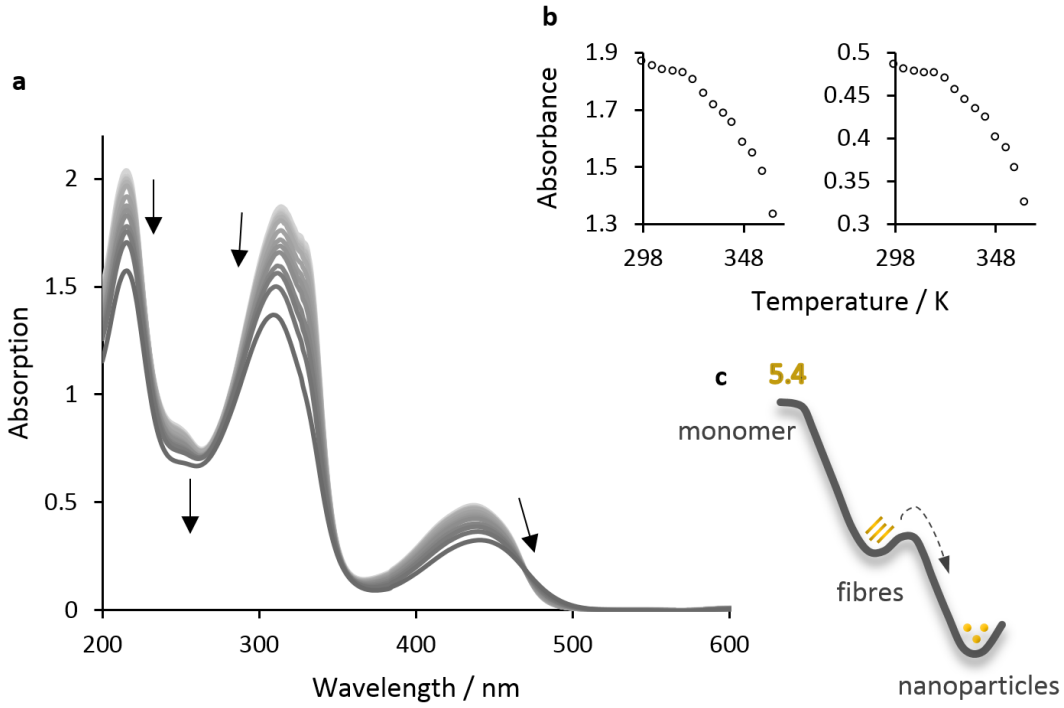

Figure 5.12. a) Temperature-dependent UV/Vis absorption spectra of **5.4** (MCH, 0.5 mg mL^{-1}). b) Absorbance of band at 315 nm (left) and 437 nm (right) with increasing temperature. c) Energy landscape of **5.4**.

5.4 Summary

Three bimetallic gold(I) structures were synthesised with a phenyl (**5.2**), biphenyl (**5.3**), or 2,1,3-benzothiadiazole (**5.4**) core moiety. The behaviour and energy landscape of self-assembly were found to be modulated by these small variances in the core structure, with kinetically trapped fibrous micelles that could undergo seeded-growth to give fibres of defined length observed only for **5.3** in heptane. Metastable fibres were observed for **5.4** in MCH, but as the kinetic energy minimum proved shallow, a morphological transformation into the more thermodynamically stable (potentially spherical) structures prevailed. For the molecule with the smallest aromatic core, only small particles were observed (which AFM suggested may have a spherical morphology). The investigations performed here should provide considerable insight into the self-assembly of gold(I) structures in solution, a significant advance in this area of supramolecular polymer chemistry.

5.5 Experimental

5.5.1 Materials and Equipment

All chemical reagents were purchased from commercial sources (Aldrich, Alfa Aesar, Strem) and were, unless otherwise noted, used without further purification. 4-Isocyanophenylamine,[50] 3,4,5-tris(dodecyloxy)benzoic acid,[51] 4,4'-diethynyl-1,1'-biphenyl,[52] and 4,7-diethynyl-2,1,3-benzothiadiazole[53] were prepared according to reported procedures.

^{1}H NMR spectra were recorded at ambient temperature and are reported relative to external TMS and referenced to the most downfield residual solvent resonance ($CDCl_3$: δ_H 7.26 ppm).

MALDI-TOF MS measurements were performed on a Bruker Ultraflextreme operating in reflector positive mode. Samples were prepared by mixing a 1 mg mL^{-1} solution of sample in a 1:10 ratio with a 20 mg mL^{-1} THF solution of *trans*-2-[3-(4-*tert*-butylphenyl)-2-methyl-2-propenylidene]-malononitrile matrix. 1 μL was transferred to a stainless-steel sample plate and allowed to dry in air.

UV/Vis spectra were recorded using a PerkinElmer Lambda 35 UV/Vis spectrometer using glass cuvettes with a 1 mm path length. Variable temperature was provided by a PerkinElmer PTP-1 Peltier heating system against 15 °C recirculating water. Fluorescence data were obtained from a Perkin Elmer LS 45 Fluorescence Spectrometer.

Carbon films, ~4 nm thick, were deposited onto freshly cleaved mica sheets using a Quorum QT150T ES turbo-pumped sputter/carbon coater. These films were transferred to copper TEM grids (600 mesh) by flotation on water. Samples for imaging were prepared by drop casting 5 μL of the self-assembly solution onto a carbon coated TEM grid placed on filter paper to absorb the excess solution. Bright field TEM micrographs (images) were obtained from a JEOL JEM 1400 microscope operating at 120 kV equipped with a Gatan SC1000 CCD imaging camera. TEM images were analysed using ImageJ, an open source software

package developed at the US National Institute of Health.[54] 100–200 micelles were traced by hand to determine contour lengths that were then used to calculate the number-averaged length (L_n) and weight-average length (L_w) according to Equations 1 and 2 where L = object length and N = number. Fibre length distribution was calculated by L_w/L_n.

$$L_n = \frac{\sum_{i=1}^{n} N_i L_i}{\sum_{i=1}^{n} N_i} \qquad \textbf{Equation 1}$$

$$L_w = \frac{\sum_{i=1}^{n} N_i L_i^{\,2}}{\sum_{i=1}^{n} N_i L_i} \qquad \textbf{Equation 2}$$

AFM height images were taken at ambient temperature in air using a Bruker Multimode VIII atomic force microscope equipped with a ScanAsyst-HR fast scanning module and ScanAsyst-Air-HR probe (tip radius of 2 nm), utilising peak force feedback control. Samples for AFM were drop cast onto freshly cleaved mica sheets coated with 5 nm thick carbon films and allowed to dry in air before imaging.

5.5.2 Synthesis of 3,4,5-Tris(dodecyloxy)-*N*-(4-isocyanide)benzamide (**5.1**)

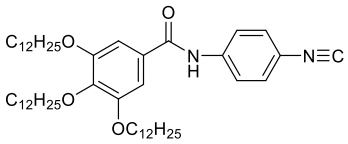

3,4,5-Tris(dodecyloxy)benzoic acid (2.1 g, 3.11 mmol), EDC (656 mg, 3.42 mmol), and DMAP (266 mg, 2.18 mmol) were dissolved in dry CH_2Cl_2 (30 mL), with stirring for 30 min at room temperature. 4-Isocyanophenylamine (354 mg, 3.00 mmol) was then added and the reaction mixture was stirred at room temperature for 24 h. Afterwards, the solution was extracted with a water/brine mixture (1/1, v/v) and the organic layer was dried over $MgSO_4$. The solution was evaporated in vacuo and the crude product was purified by silica gel column chromatography using CH_2Cl_2 as an eluent to yield 3,4,5-tris(dodecyloxy)-*N*-(4-isocyanide)benzamide (**5.1**) as a white solid (90%).

^{1}H NMR (400 MHz, $CDCl_3$): δ (ppm) 7.90 (s, 1H; N*H*), 7.68 (d, *J* = 8.4 Hz, 2H; C_6H_4), 7.37 (d, *J* = 8.4 Hz, 2H; C_6H_4), 7.01 (s, 2H; C_6H_2), 4.01 (m, 6H; OCH_2), 1.87–1.70 (m, 6H; CH_2),

1.47 (m, 6H; C*H*$_2$), 1.40–1.20 (m, 48H; C*H*$_2$), 0.88 (t, *J* = 6.8 Hz, 9H; C*H*$_3$). ^{13}C NMR (400 MHz, $CDCl_3$): δ (ppm) 165.7, 163.8, 153.3, 142.0, 138.9, 129.1, 127.2, 120.5, 105.5, 73.6, 69.6, 31.9, 30.3, 29.7, 29.7, 29.7, 29.6, 29.6, 29.4, 29.4, 26.1, 22.7, 14.1.

5.5.3 General Synthesis of Isocyanide gold(I) Complexes

To a solution of diacetylene derivatives (0.2 mmol) and Au(tht)Cl (0.4 mmol) in 15 mL $CHCl_3$ was added excess Et_3N (200 μL). A yellow precipitate formed quickly, and the solution was stirred for 30 min at room temperature. Isocyanide ligand **5.1** in 10 mL $CHCl_3$ was then added to the reaction quickly, and the mixture stirred for 16 h. After filtration, the product was precipitated by addition of 30 mL MeOH, followed by washing with 30 mL MeOH. Yield: 90–100%.

5.5.3.1 Characterisation of **5.2**

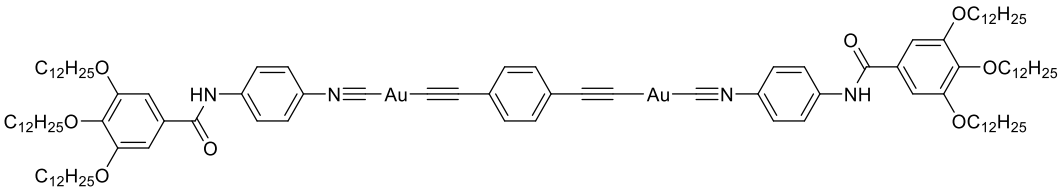

^{1}H NMR (600 MHz, $CDCl_3$): δ (ppm) 8.15 (s, 2H; N*H*), 7.75 (d, *J* = 8.4 Hz, 4H; C$_6$*H*$_4$), 7.46 (d, *J* = 8.4 Hz, 4H; C$_6$*H*$_4$), 7.19 (s, 4H; C$_6$*H*$_4$), 7.07 (s, 4H; C$_6$*H*$_2$), 4.03 (m, 12H; OC*H*$_2$), 1.87–1.70 (m, 12H; C*H*$_2$), 1.47 (m, 12H; C*H*$_2$), 1.40–1.20 (m, 96H; C*H*$_2$), 0.88 (t, *J* = 6.8 Hz, 18H; C*H*$_3$). ^{13}C NMR (500 MHz, $CDCl_3$): δ (ppm) 153.6, 132.3, 128.1, 120.7, 106.1, 77.4, 77.2, 76.9, 73.8, 69.8, 32.1, 32.1, 30.5, 29.9, 29.9, 29.9, 29.8, 29.8, 29.7, 29.6, 29.5, 29.5, 26.2, 22.9, 14.3. MALDI-TOF MS: *m/z* 2069 [M]$^+$, 2082 [M+Na]$^+$, 20108 [M+K]$^+$.

5.5.3.2 Characterisation of **5.3**

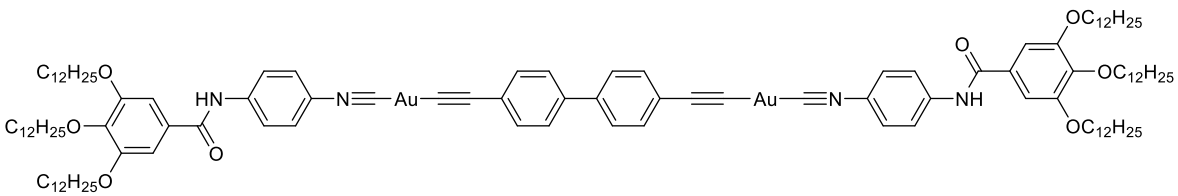

^{1}H NMR (600 MHz, $CDCl_3$): δ (ppm) 8.02 (s, 2H; N*H*), 7.84 (d, *J* = 8.4 Hz, 4H; C$_6$*H*$_4$), 7.55

(m, 12H; C_6H_4), 7.05 (s, 4H; C_6H_2), 4.04 (m, 12H; OCH_2), 1.87–1.70 (m, 12H; CH_2), 1.47 (m, 12H; CH_2), 1.40–1.20 (m, 96H; CH_2), 0.88 (t, J = 6.8 Hz, 18H; CH_3). ^{13}C NMR (150MHz, $CDCl_3$): δ (ppm) 165.7, 155.2, 153.4, 142.1, 140.8, 132.6, 128.9, 127.8, 120.5, 119.5, 117.2, 106.1, 77.3, 77.0, 76.8, 73.6, 69.6, 32.0, 31.9, 30.4, 29.8, 29.8, 29.8, 29.7, 29.7, 29.7, 29.6, 29.4, 29.4, 29.4, 26.1, 26.1, 22.7, 14.1. MALDI-TOF MS: *m/z* 2145 $[M]^+$.

5.5.3.3 Characterisation of **5.4**

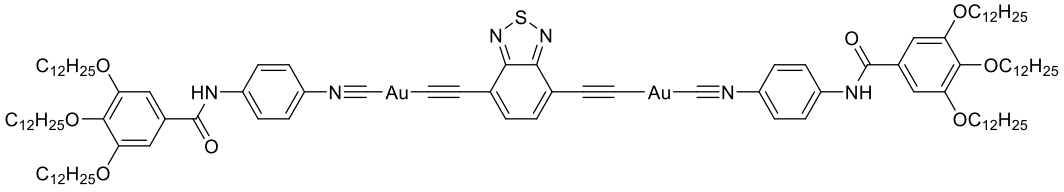

^{1}H NMR (400 MHz, $CDCl_3$): δ (ppm) 7.98 (s, 2H; N*H*), 7.72 (d, J = 8.8 Hz, 4H; C_6H_4), 7.58 (s, 2H; C_6H_2), 7.48 (d, J = 8.8 Hz, 4H; C_6H_4), 7.10 (s, 4H; C_6H_2), 4.07 (m, 12H; OCH_2), 1.90–1.72 (m, 12H; CH_2), 1.50 (m, 12H; CH_2), 1.43–1.21 (m, 96H; CH_2), 0.90 (t, J = 6.8 Hz, 18H; CH_3). ^{13}C NMR (500MHz, $CDCl_3$): δ (ppm) 165.7, 153.4, 142.3, 132.9, 128.7, 128.0, 126.5, 120.6, 106.0, 77.3, 77.0, 76.8, 73.7, 69.6, 32.0, 31.9, 30.3, 29.8, 29.7, 29.7, 29.7, 29.7, 29.6, 29.4, 29.4, 29.4, 26.1, 22.7, 14.1. MALDI-TOF MS: *m/z* 2127 $[M]^+$, 2150 $[M+Na]^+$, 2169 $[M+K]^+$.

5.6 References

1. V. Wing-Wah Yam and E. Chung-Chin Cheng, in *Photochemistry and Photophysics of Coordination Compounds II*, eds. V. Balzani and S. Campagna, Springer Berlin Heidelberg, Berlin, Heidelberg, 2007, pp. 269-309.

2. J. M. López-de-Luzuriaga, in *Modern Supramolecular Gold Chemistry*, ed. A. Laguna, 2009, ch. 6.

3. E. J. Fernández, A. Laguna, J. M. López-de-Luzuriaga, M. Monge, M. Montiel, M. E. Olmos, J. Pérez and M. Rodríguez-Castillo, *Gold Bull.*, 2007, **40**, 172-183.

4. M. J. Calhorda, O. Crespo, M. C. Gimeno, P. G. Jones, A. Laguna, J. M. López-de-Luzuriaga, J. L. Perez, M. A. Ramón and L. F. Veiros, *Inorg. Chem.*, 2000, **39**, 4280-4285.

5. H. Ito, T. Saito, N. Oshima, N. Kitamura, S. Ishizaka, Y. Hinatsu, M. Wakeshima, M. Kato, K. Tsuge and M. Sawamura, *J. Am. Chem. Soc.*, 2008, **130**, 10044-10045.

6. H. Schmidbaur, S. Cronje, B. Djordjevic and O. Schuster, *Chem. Phys.*, 2005, **311**, 151-161.

7. M. B. Brands, J. r. Nitsch and C. l. F. Guerra, *Inorg. Chem.*, 2018, **57**, 2603-2608.

8. H. Schmidbaur, *Gold Bull.*, 2000, **33**, 3-10.

9. H. Schmidbaur and A. Schier, *Chem. Soc. Rev.*, 2012, **41**, 370-412.

10. R. Gavara, A. Pinto, R. Donamaría, M. E. Olmos, J. M. López de Luzuriaga and L. Rodríguez, *Inorg. Chem.*, 2017, **56**, 11946-11955.

11. J. Arcau, V. Andermark, E. Aguiló, A. Gandioso, A. Moro, M. Cetina, J. C. Lima, K. Rissanen, I. Ott and L. Rodríguez, *Dalton Trans.*, 2014, **43**, 4426-4436.

12. E. Aguiló, R. Gavara, C. Baucells, M. Guitart, J. C. Lima, J. Llorca and L. Rodríguez, *Dalton Trans.*, 2016, **45**, 7328-7339.

13. F. K.-W. Hau, T. K.-M. Lee, E. C.-C. Cheng, V. K.-M. Au and V. W.-W. Yam, *Proc. Natl. Acad. Sci. USA*, 2014, **111**, 15900-15905.

14. J. A. Mathews and L. L. Watters, *J. Am. Chem. Soc.*, 1900, **22**, 108-111.

15. G. C. Fortman, A. Poater, J. W. Levell, S. Gaillard, A. M. Z. Slawin, I. D. W. Samuel, L. Cavallo and S. P. Nolan, *Dalton Trans.*, 2010, **39**, 10382-10390.

16. E. Schuh, S. M. Valiahdi, M. A. Jakupec, B. K. Keppler, P. Chiba and F. Mohr, *Dalton Trans.*, 2009, 10841-10845.

17. H.-Y. Chao, W. Lu, Y. Li, M. C. W. Chan, C.-M. Che, K.-K. Cheung and N. Zhu, *J. Am. Chem. Soc.*, 2002, **124**, 14696-14706.

18. T. P. Seifert, A. C. Boukis, T. J. Feuerstein and P. W. Roesky, *J. Organomet. Chem.*, 2018, **867**, 92-97.

19. J. Wu, P. Kroll and H. V. R. Dias, *Inorg. Chem.*, 2009, **48**, 423-425.

20. P. Schulte and U. Behrens, *Chem. Commun.*, 1998, **0**, 1633-1634.

21. M. J. Katz, K. Sakai and D. B. Leznoff, *Chem. Soc. Rev.*, 2008, **37**, 1884-1895.

22. R. J. Puddephatt, *Coord. Chem. Rev.*, 2001, **216-217**, 313-332.

23. W. H. Binder and O. W. Smrzka, *Angew. Chem. Int. Ed.*, 2006, **45**, 7324-7328.

24. J. K.-H. Hui, Z. Yu and M. J. MacLachlan, *Angew. Chem. Int. Ed.*, 2007, **46**, 7980-7983.

25. C. Kulkarni, S. Balasubramanian and S. J. George, *ChemPhysChem*, 2013, **14**, 661-673.

26. T. F. A. De Greef, M. M. J. Smulders, M. Wolffs, A. P. H. J. Schenning, R. P. Sijbesma and E. W. Meijer, *Chem. Rev.*, 2009, **109**, 5687-5754.

27. X. Wang, Y. Han, Y. Liu, G. Zou, Z. Gao and F. Wang, *Angew. Chem.*, 2017, **129**, 12640-12644.

28. R. L. White-Morris, M. Stender, D. S. Tinti, A. L. Balch, D. Rios and S. Attar, *Inorg. Chem.*, 2003, **42**, 3237-3244.

29. K. M.-C. Wong and V. W.-W. Yam, *Acc. Chem. Res.*, 2011, **44**, 424-434.

30. M. J. Irwin, J. J. Vittal and R. J. Puddephatt, *Organometallics*, 1997, **16**, 3541-3547.

31. V. W.-W. Yam and S. W.-K. Choi, *J. Chem. Soc., Dalton Trans.*, 1996, 4227-4232.

32. R. J. Puddephatt, *Chem. Soc. Rev.*, 2008, **37**, 2012-2027.

33. W.-F. Fu, K.-C. Chan, V. M. Miskowski and C.-M. Che, *Angew. Chem. Int. Ed.*, 1999, **38**, 2783-2785.

34. A. Sorrenti, J. Leira-Iglesias, A. J. Markvoort, T. F. A. de Greef and T. M. Hermans, *Chem. Soc. Rev.*, 2017, **46**, 5476-5490.

35. M. M. J. Smulders, M. M. L. Nieuwenhuizen, T. F. A. de Greef, P. van der Schoot, A. P. H. J. Schenning and E. W. Meijer, *Chem. Eur. J.*, 2010, **16**, 362-367.

36. W. J. Hunks, M. C. Jennings and R. J. Puddephatt, *Inorg. Chem.*, 2000, **39**, 2699-2702.

37. M. E. Robinson, D. J. Lunn, A. Nazemi, G. R. Whittell, L. De Cola and I. Manners, *Chem. Commun.*, 2015, **51**, 15921-15924.

38. R. D. Mukhopadhyay and A. Ajayaghosh, *Science*, 2015, **349**, 241-242.

39. S. Ogi, K. Sugiyasu, S. Manna, S. Samitsu and M. Takeuchi, *Nat. Chem.*, 2014, **6**, 188-195.

40. C. Jarrett-Wilkins, X. He, H. E. Symons, R. L. Harniman, C. F. J. Faul and I. Manners, *Chem. Eur. J.*, 2018, **24**, 15556-15565.

41. F. Würthner, *Nat. Chem.*, 2014, **6**, 171.

42. T. Fukui, S. Kawai, S. Fujinuma, Y. Matsushita, T. Yasuda, T. Sakurai, S. Seki, M. Takeuchi and K. Sugiyasu, *Nat. Chem.*, 2016, **9**, 493.

43. S.-K. Yip, E. C.-C. Cheng, L.-H. Yuan, N. Zhu and V. W.-W. Yam, *Angew. Chem. Int. Ed.*, 2004, **43**, 4954-4957.

44. J. B. Gilroy, T. Gädt, G. R. Whittell, L. Chabanne, J. M. Mitchels, R. M. Richardson, M. A. Winnik and I. Manners, *Nat. Chem.*, 2010, **2**, 566-570.

45. M. Zhang, L. Meng, X. Cao, M. Jiang and T. Yi, *Soft Matter*, 2012, **8**, 4494-4498.

46. J. Wu, T. Yi, T. Shu, M. Yu, Z. Zhou, M. Xu, Y. Zhou, H. Zhang, J. Han, F. Li and C. Huang, *Angew. Chem.*, 2008, **120**, 1079-1083.

47. K. Isozaki, H. Takaya and T. Naota, *Angew. Chem.*, 2007, **119**, 2913-2915.

48. J. M. J. Paulusse and R. P. Sijbesma, *Angew. Chem. Int. Ed.*, 2006, **45**, 2334-2337.

49. X. Yu, Q. Liu, J. Wu, M. Zhang, X. Cao, S. Zhang, Q. Wang, L. Chen and T. Yi, *Chem. Eur. J.*, 2010, **16**, 9099-9106.

50. K. Heinze and V. Jacob, *Eur. J. Inorg. Chem.*, 2003, **2003**, 3918-3923.

51. A. Rödle, B. Ritschel, C. Mück-Lichtenfeld, V. Stepanenko and G. Fernández, *Chem. Eur. J.*, 2016, **22**, 15772-15777.

52. M. M. Hansmann, M. Melaimi, D. Munz and G. Bertrand, *J. Am. Chem. Soc.*, 2018, **140**, 2546-2554.

53. Y. Lei, H. Li, W. Gao, M. Liu, J. Chen, J. Ding, X. Huang and H. Wu, *J. Mater. Chem. C*, 2014, **2**, 7402-7410.

54. C. A. Schneider, W. S. Rasband and K. W. Eliceiri, *Nat. Methods*, 2012, **9**, 671.

6 Outlook

In addition to the work outlined within each Chapter of this thesis, some future directions of research are summarised here. These are based on initial results obtained throughout the course of these studies.

6.1 Synthesis of [*n*]Nickelocenophanes for ROP

Chapters 2 and 3 described the synthesis and ring-opening polymerisation (ROP) of [*n*]nickelocenophanes, and their thermodynamic propensity to undergo ring-opening. Currently, the structurally characterised [*n*]nickelocenophane with the largest tilt-angle is the 1,8-naphthalene bridged species ($\alpha = 20.2°$). The formation of this highly strained [3]nickelocenophane from the reaction between naphthalene-1,8-diylbis(cyclopentadienyl-sodium)·THF and hexaaminenickel dichloride is presumably partially due to the rigid structure of the chelating ligand.[1] Dicarba-bridged [2]nickelocenophanes have thus far been elusive with attempts to isolate these species yielding only oligomeric material.[2] Taking inspiration from the synthesis of the naphthalene-bridged [3]nickelocenophane,[1] the analogous [2]nickelocenophane could be synthesised by use of a 1,2-cyclopentadienyl substituted benzyl fly trap ligand and hexaaminenickel dichloride (Scheme 6.1). The predisposition of the ligand to form cyclic structures would presumably help drive the formation of the molecular species, and stabilise it to spontaneous ROP.

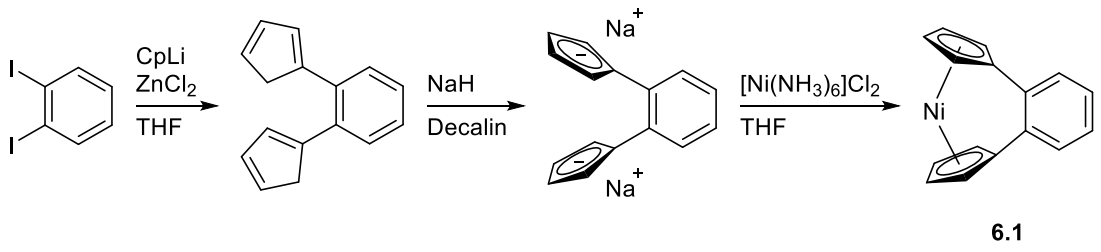

Scheme 6.1. Proposed synthesis of 1,2-benzyl[2]nickelocenophane.

The ROP of [*n*]nickelocenophanes with naphthalene and benzene *ansa* bridges would also be of interest to investigate in the future. The strong chelating effect that drives the formation of the molecular species may in fact leave the highly strained [*n*]nickelocenophanes resistant to ROP. The magnetic properties of polynickelocenes yielded from these species would also be of interest, due to the aromatic linker which may affect the through bond coupling that was found to occur in the polynickelocenes with carbon- and silicon-based spacers in Chapter 2.

6.2 Synthesis and Characterisation of Polycobaltocenes

In addition to the ROP of [*n*]nickelocenophanes, Chapter 2 also explored the magnetic properties of polynickelocenes (containing $S = 1$ centres) and the parent monomers via superconducting quantum interference device (SQUID) magnetometry. The ROP of dicarba[2]cobaltocenophane has previously been reported (Scheme 6.2),[3] but due to the insoluble nature of the resulting polycobaltocene, no characterisation of the neutral polymer was achieved. Poly(cobaltocenylethylene) contains $S = ½$ centres, and regardless of insolubility, its magnetic nature is of interest and thus could still be analysed by a bulk technique such as SQUID magnetometry.

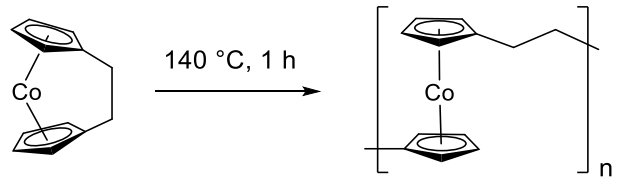

6.2 **6.3**

Scheme 6.2. ROP of **6.2** to yield **6.3**.

In Chapter 2, by incorporating **6.2** into a copolymer with tricarba[3]nickelocenophane, it was possible to achieve some solution characterisation (^{1}H NMR spectroscopy and dynamic light scattering (DLS)) of the cobaltocene-containing polymer. Introduction of solubilising groups, such as *tert*-butyl, onto either the Cp ring or the dicarba *ansa* bridge and subsequent ROP may allow for the first neutral polycobaltocenes that exhibit solubility in organic

solvents. This would allow for solution characterisation of the paramagnetic polymers via NMR, DLS, and electron paramagnetic resonance (EPR).

6.3 Polycondensation Routes to Cobaltocenium Polyelectrolytes

Chapter 4 details initial attempts to yield main-chain cobaltocenium polyelectrolytes via polycondensation routes, alongside the isolation of supramolecular cobaltocenium-containing polymers. Although the polycondensation reactions between 1,1′-dicarboxycobaltocenium hexafluorophosphate and 2,2′-(ethylenedioxy)bis(ethylamine) in aqueous media did yield some oligomeric species, molar masses were limited (max. degree of polymerisation (DP_n) = 12). It was elucidated that the reactions performed in water were hindered by counterion exchange between the cobaltocenium moiety and the coupling reagent, *N*-(3-dimethylaminopropyl)-*N*′-ethylcarbodiimide hydrochloride (EDC) (from hexafluorophosphate to chloride), which was deactivating the cobaltocenium carboxylate groups to further reaction.

Substitution of the counterion of EDC, from chloride to hexafluorophosphate, could be achieved by use of $AgPF_6$ (Scheme 6.3). The resultant species could then be employed as a coupling reagent for future polycondensation reactions, which would thus be unhampered by counterion exchange. As a consequence, high molar mass cobaltocenium polyelectrolytes should be able to form.

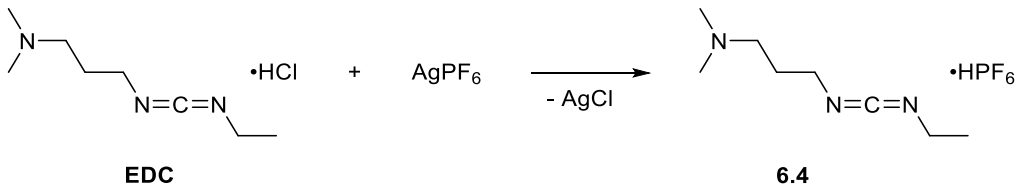

Scheme 6.3. Counterion exchange reaction between EDC and $AgPF_6$.

With an appropriate coupling reagent, the polycondensation (detailed in Scheme 6.4) could realistically prove a general and facile manner in which to synthesise cobaltocenium

polyelectrolytes. In addition, the polymer structure could be easily tuned by use of a variety of diamine linkers.

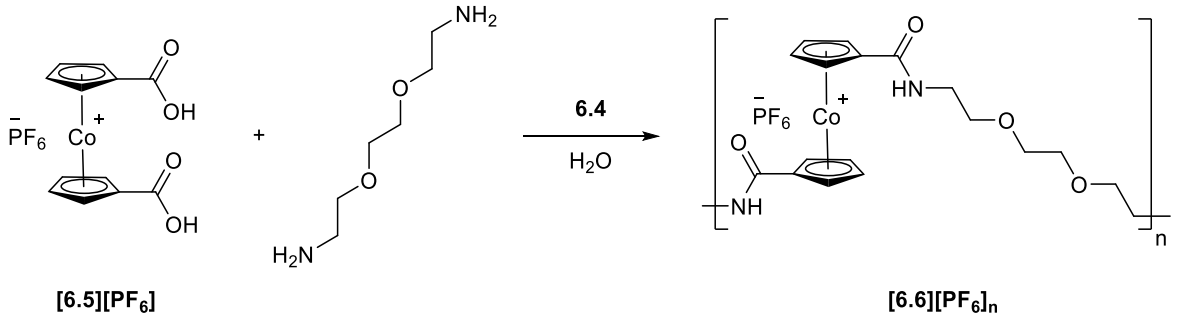

[6.5][PF$_6$] **[6.6][PF$_6$]$_n$**

Scheme 6.4. General reaction between 1,1′-dicarboxycobaltocenium hexafluorophosphate and 2,2′-(ethylenedioxy)bis(ethylamine) in water with the proposed coupling reagent **6.4**.

6.4 Sensing Properties of Gold(I) Supramolecular Polymers

Chapter 5 described the capacity of three bimetallic gold(I) structures (Figure 6.1) to differentiate into fibrous and spherical micelles upon self-assembly, and mechanisms and free energy landscapes of their formation were proposed. The strongly fluorescent nature of complexes **6.7**–**6.9** in the self-assembled state was confirmed by emission spectroscopy, and is common for binuclear and polynuclear gold(I) compounds with close Au···Au contacts when excited by UV light.[4-8]

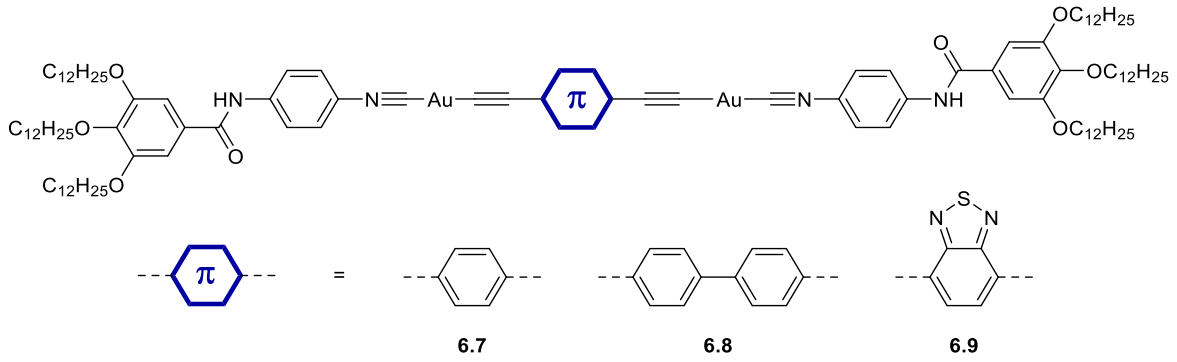

Figure 6.1. Gold(I) bimetallic systems explored in Chapter 5.

There has been significant recent interest in the use of metal organic fluorophores as sensors for gaseous and dissolved oxygen based on their luminescent quenching. Many of the reported systems have been based on transition-metal complexes immobilised in permeable

polymer or sol–gel matrices to allow for easy contact between the oxygen-sensitive compounds and oxygen molecules.

Preliminary studies have revealed that in methylcyclohexane (MCH), **6.8** displays visibly different luminescence under ambient conditions compared to in a nitrogen atmosphere (Figure 6.2). Conversely, in a heptane solution, **6.8** appears to have a yellow/green luminescence under air which does not occur under a nitrogen atmosphere. Future work will involve a detailed investigation into the O_2 sensing properties of **6.8**, in solution in a variety of solvents and as a metallogel (initial investigations of **6.8** in heptane or MCH at 20 mg mL^{-1} have produced metallogels).

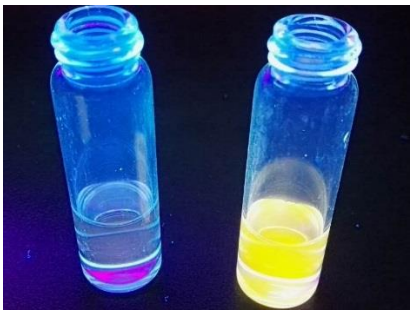

Figure 6.2. Photograph of **6.8** in MCH (0.02 mg mL^{-1}), left: under air, right: immediately after N_2 was bubbled through the solution for ~15 sec.

6.5 References

1. S. Trtica, E. Meyer, M. H. Prosenc, J. Heck, T. Böhnert and D. Görlitz, *Eur. J. Inorg. Chem.*, 2012, 4486-4493.

2. S. Baljak, A. D. Russell, S. C. Binding, M. F. Haddow, D. O'Hare and I. Manners, *J. Am. Chem. Soc.*, 2014, **136**, 5864-5867.

3. U. F. J. Mayer, J. B. Gilroy, D. O'Hare and I. Manners, *J. Am. Chem. Soc.*, 2009, **131**, 10382-10383.

4. R. L. White-Morris, M. Stender, D. S. Tinti, A. L. Balch, D. Rios and S. Attar, *Inorg. Chem.*, 2003, **42**, 3237-3244.

5. M. J. Irwin, J. J. Vittal and R. J. Puddephatt, *Organometallics*, 1997, **16**, 3541-3547.

6. V. W.-W. Yam and S. W.-K. Choi, *J. Chem. Soc., Dalton Trans.*, 1996, 4227-4232.

7. R. J. Puddephatt, *Chem. Soc. Rev.*, 2008, **37**, 2012-2027.

8. W.-F. Fu, K.-C. Chan, V. M. Miskowski and C.-M. Che, *Angew. Chem. Int. Ed.*, 1999, **38**, 2783-2785.

Appendix II

i. Additional Figures on Monomer and Polymer Characterisation

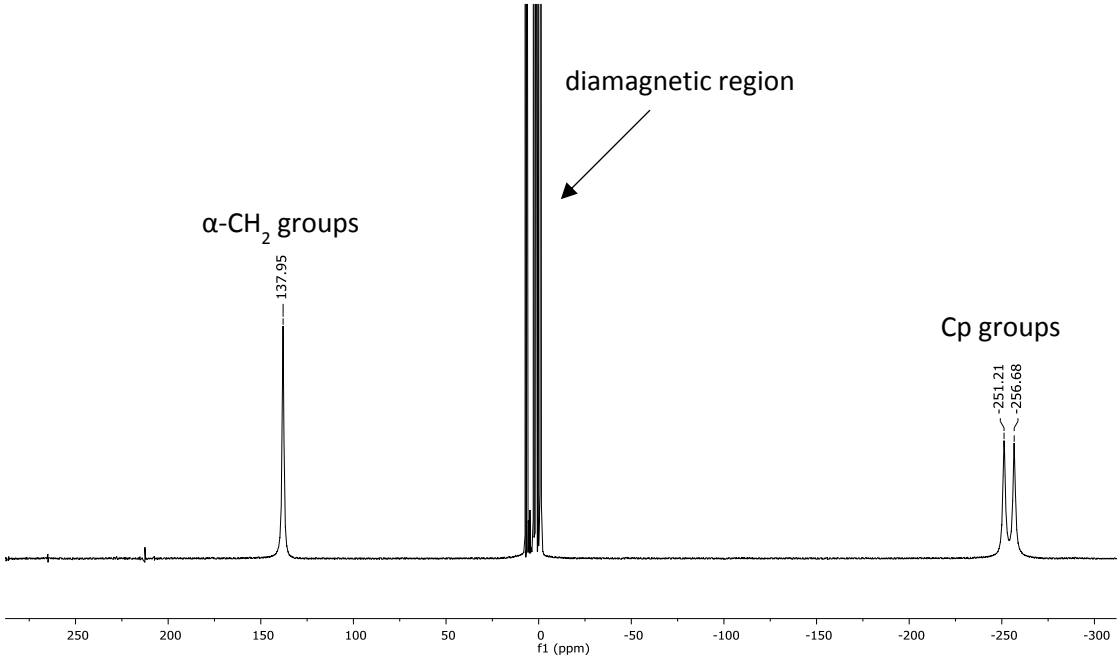

Figure A2.1. ^{1}H NMR spectrum (500 MHz, C_6D_6) of **2.6**.

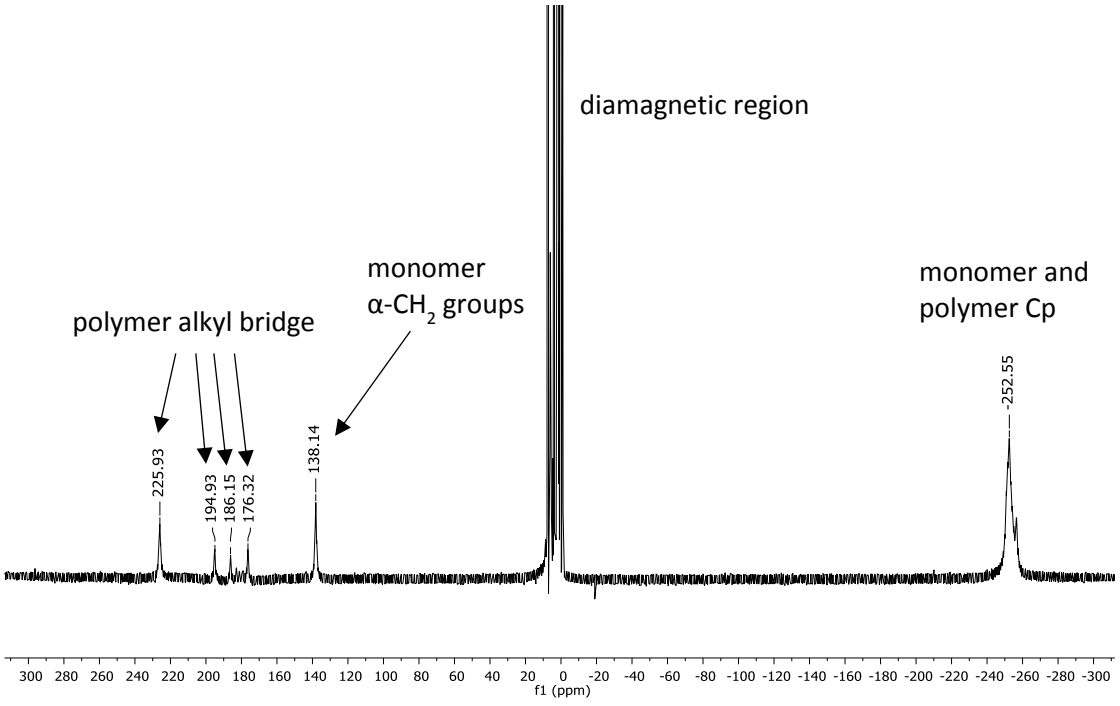

Figure A2.2. ^{1}H NMR spectrum (500 MHz, C_6D_6) of **2.13b**.

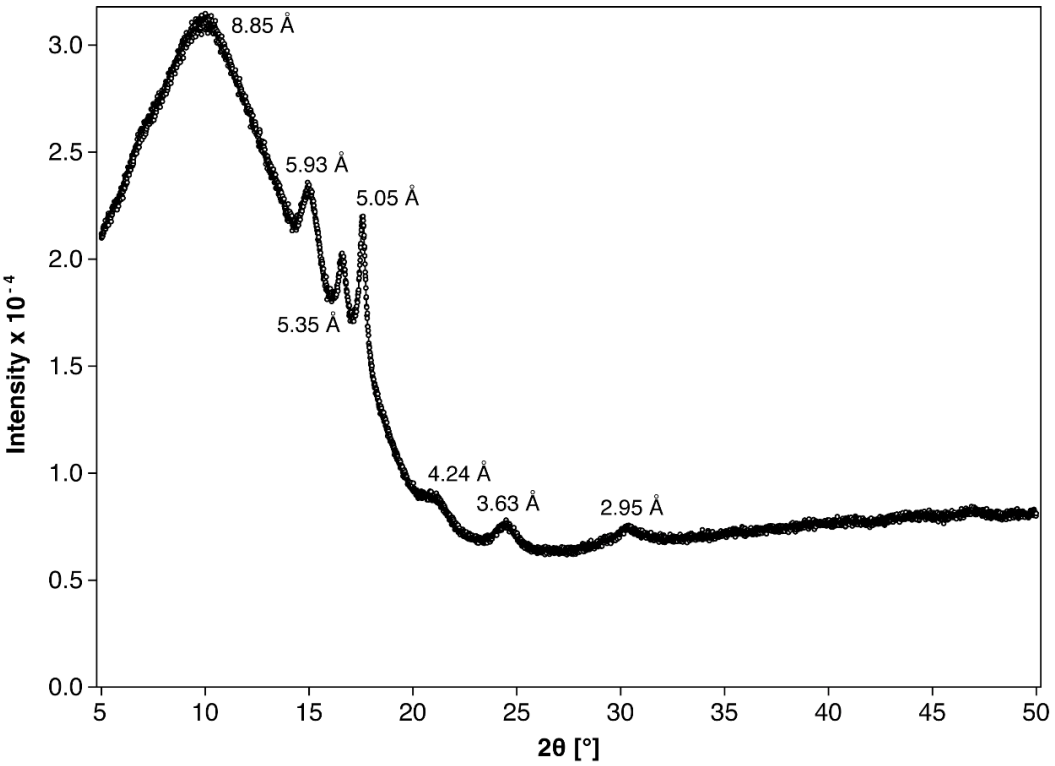

Figure A2.3. WAXS data for insoluble polymer **2.13a**.

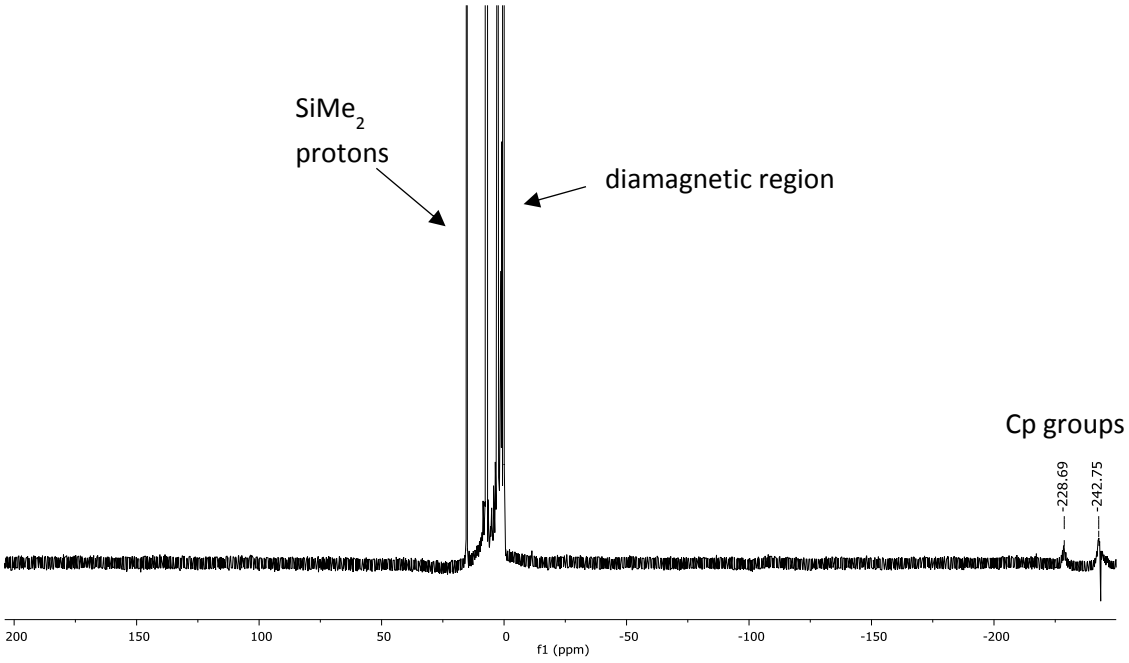

Figure A2.4. ^{1}H NMR spectrum (500 MHz, C_6D_6) of **2.14b** detailing paramagnetic cyclopentadienyl environments.

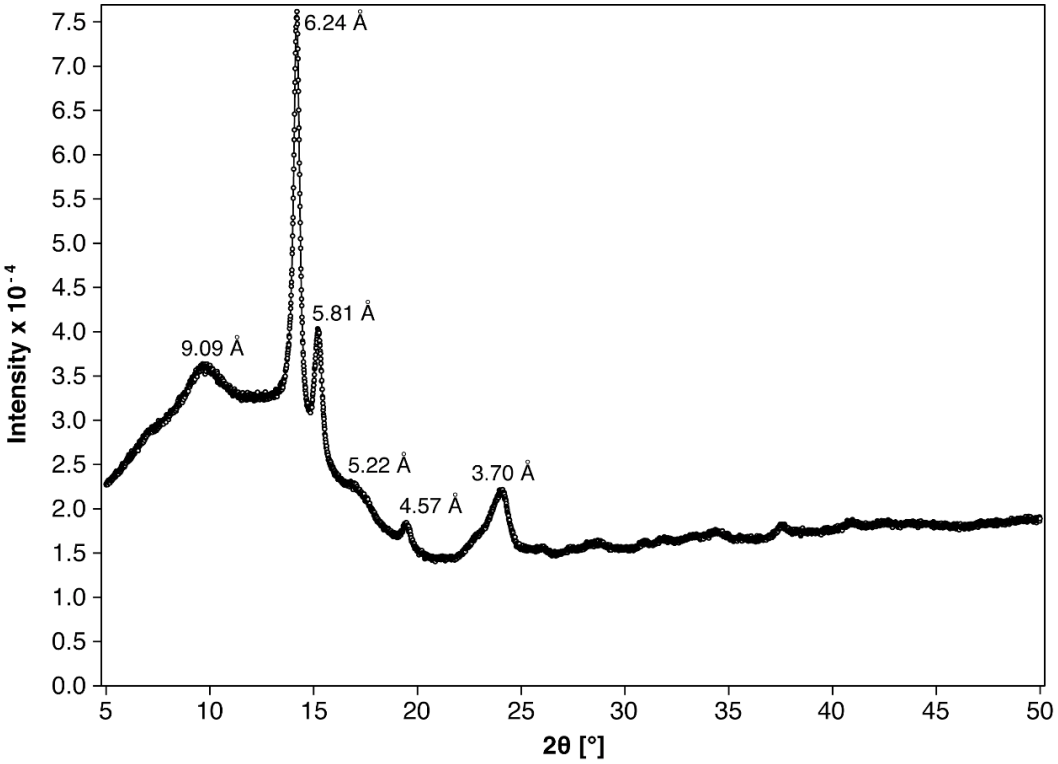

Figure A2.5. WAXS data for insoluble polymer **2.14$_a$**.

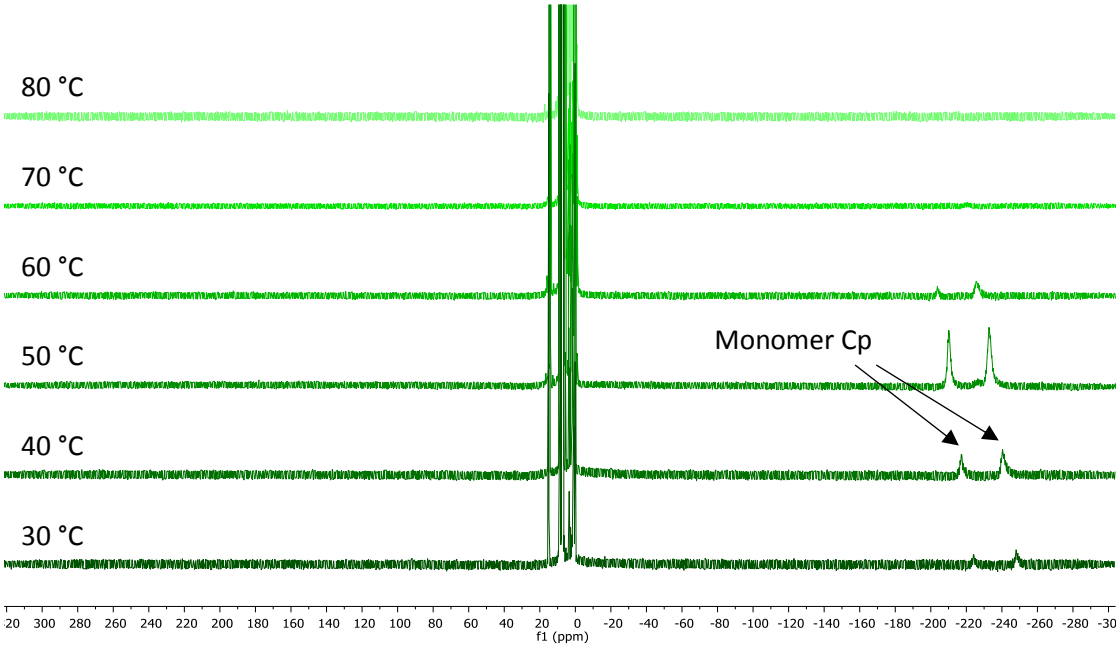

Figure A2.6. Stacked ^{1}H NMR spectra (500 MHz, d_5-pyridine) that show the effect of temperature on the reversible conversion of polymer **2.14$_a$** into monomer **2.10**.

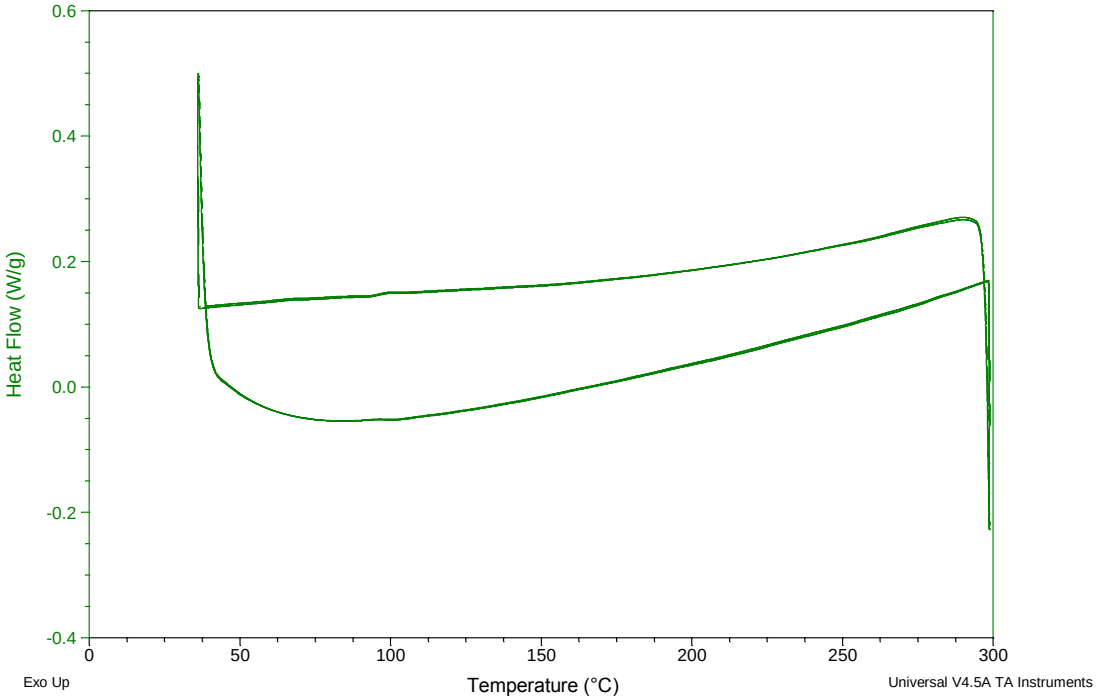

Figure A2.7. DSC thermogram for **2.13a**.

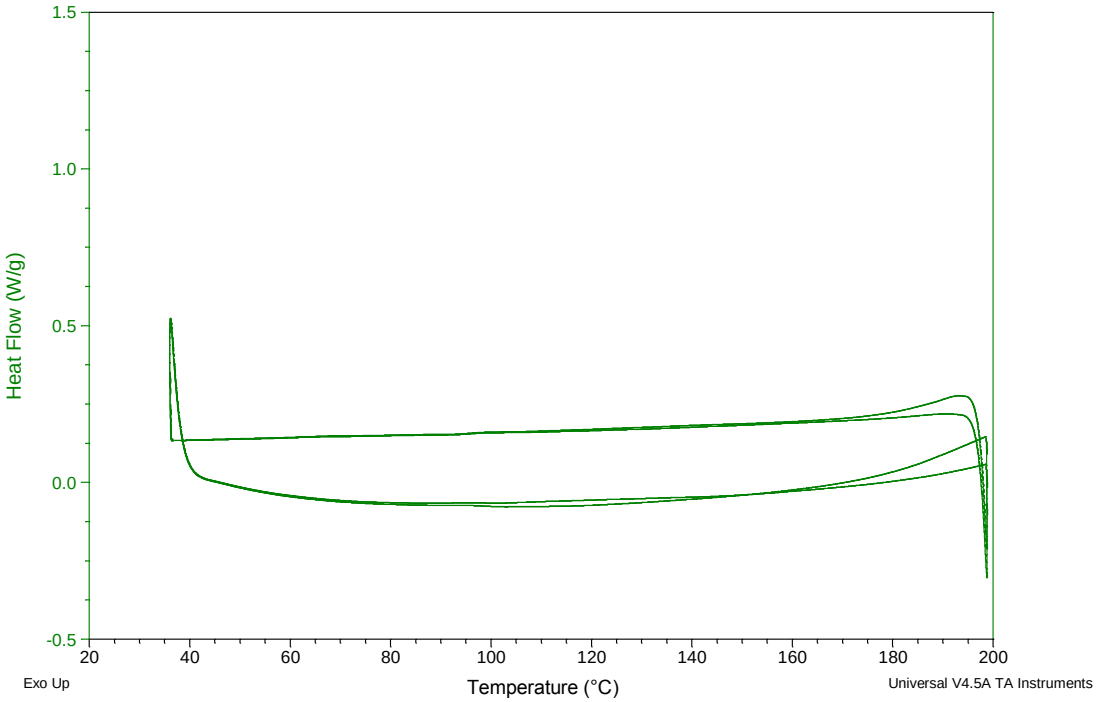

Figure A2.8. DSC thermogram for **2.14a**.

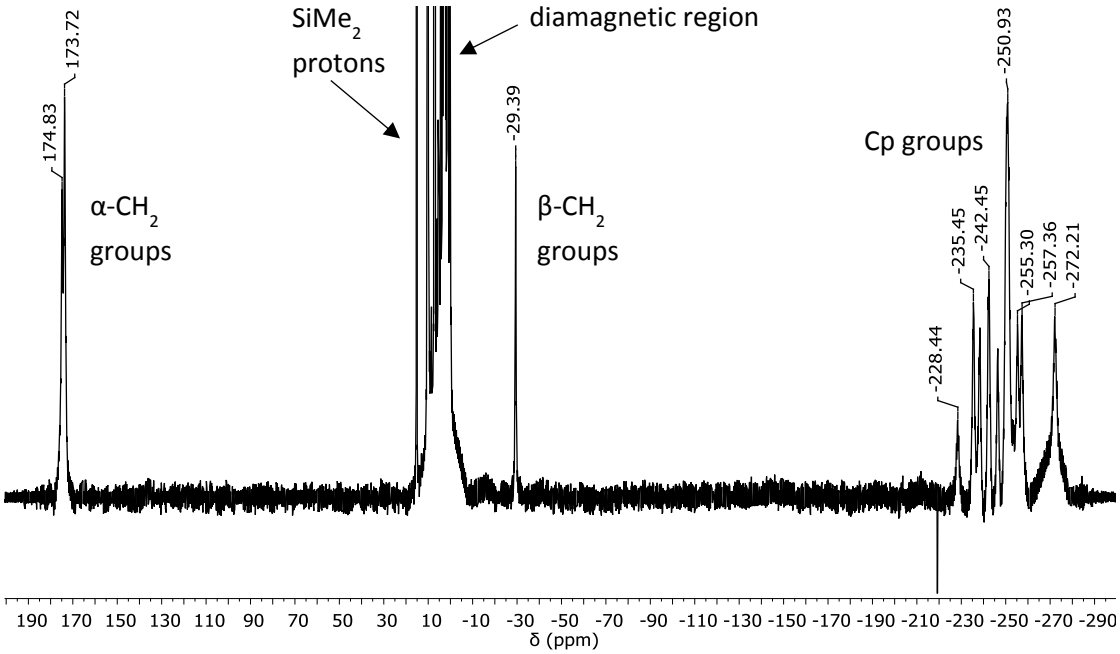

Figure A2.9. ^{1}H NMR spectrum (500 MHz, C_6D_6) of copolymer **2.15**.

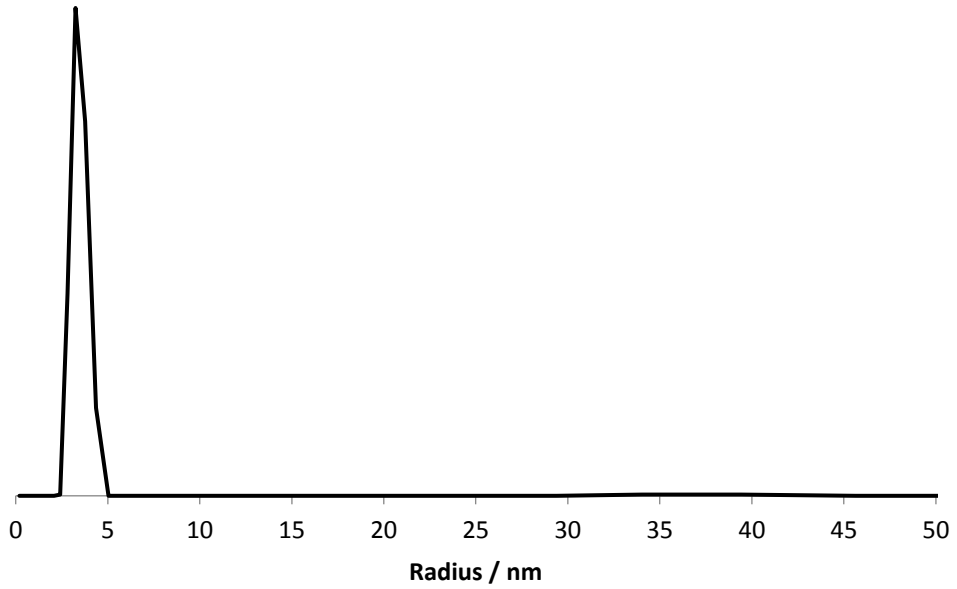

Figure A2.10. DLS size distribution by volume for **2.15** (THF, 20 °C, 1 mg mL^{-1}); R_h = 3.9 nm (σ = 0.43 nm).

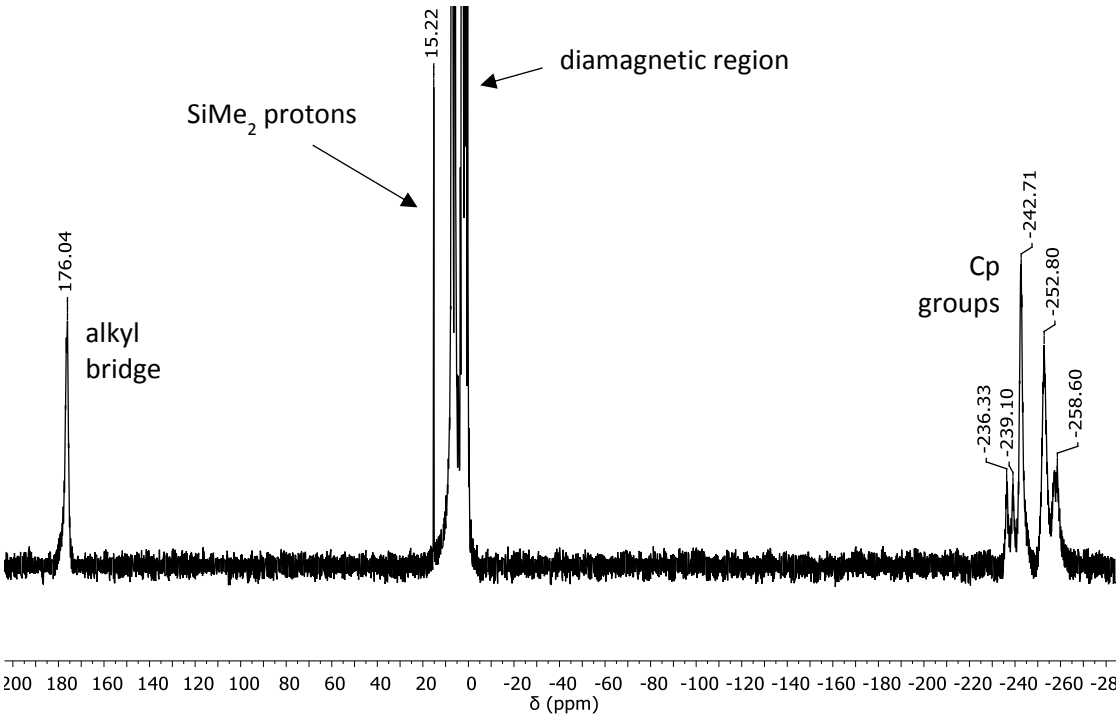

Figure A2.11. ^{1}H NMR spectrum (500 MHz, C_6D_6) of copolymer **2.16b**.

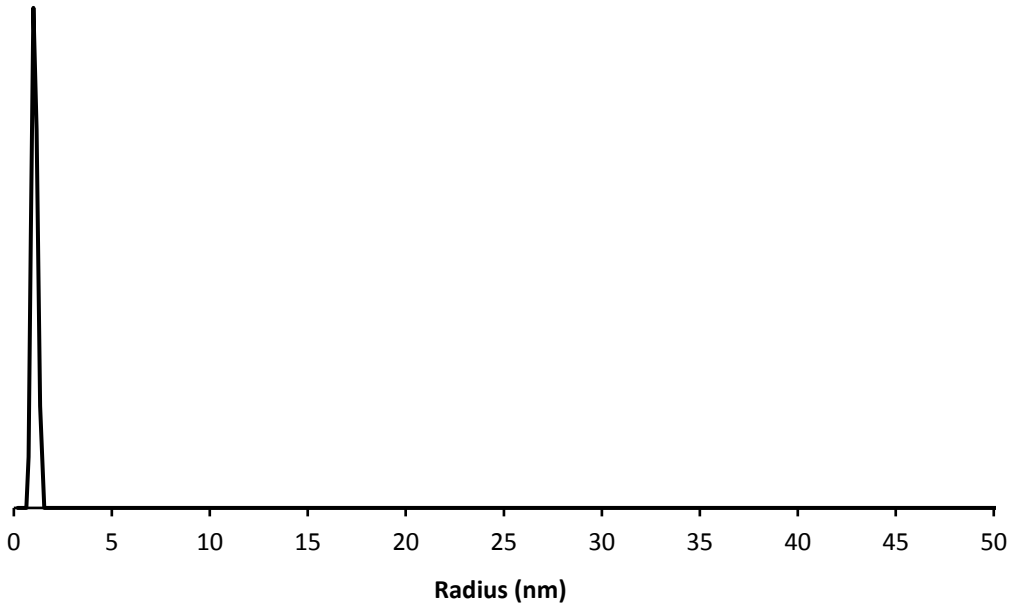

Figure A2.12. DLS size distribution by volume for **2.16b** (THF, 20 °C, 1 mg mL^{-1}); R_h = 1.4 nm (σ = 0.15 nm).

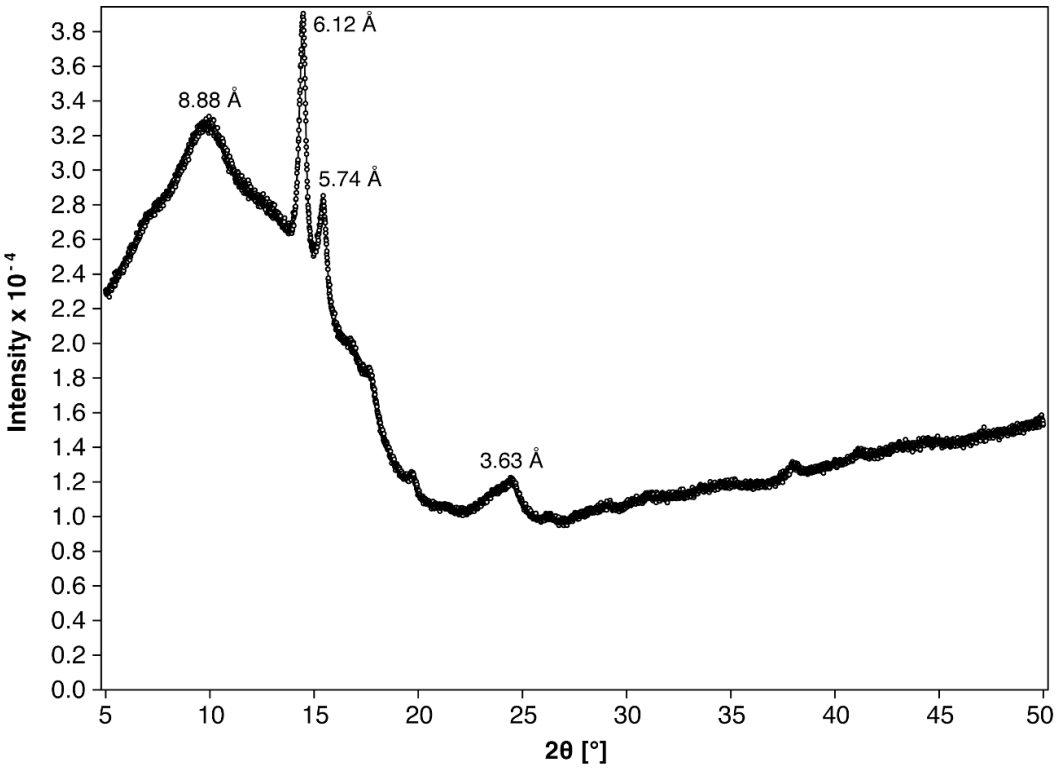

Figure A2.13. WAXS data for insoluble copolymer **2.16a**.

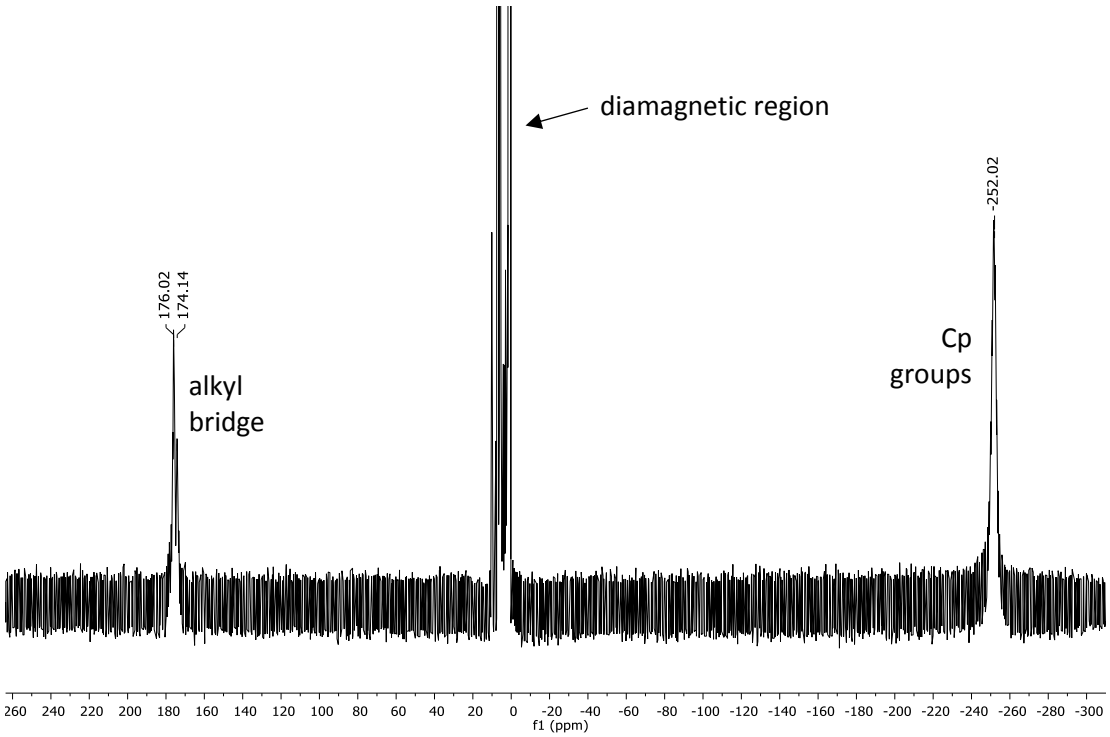

Figure A2.14. ^{1}H NMR spectrum (500 MHz, C_6D_6) of copolymer **2.17b**.

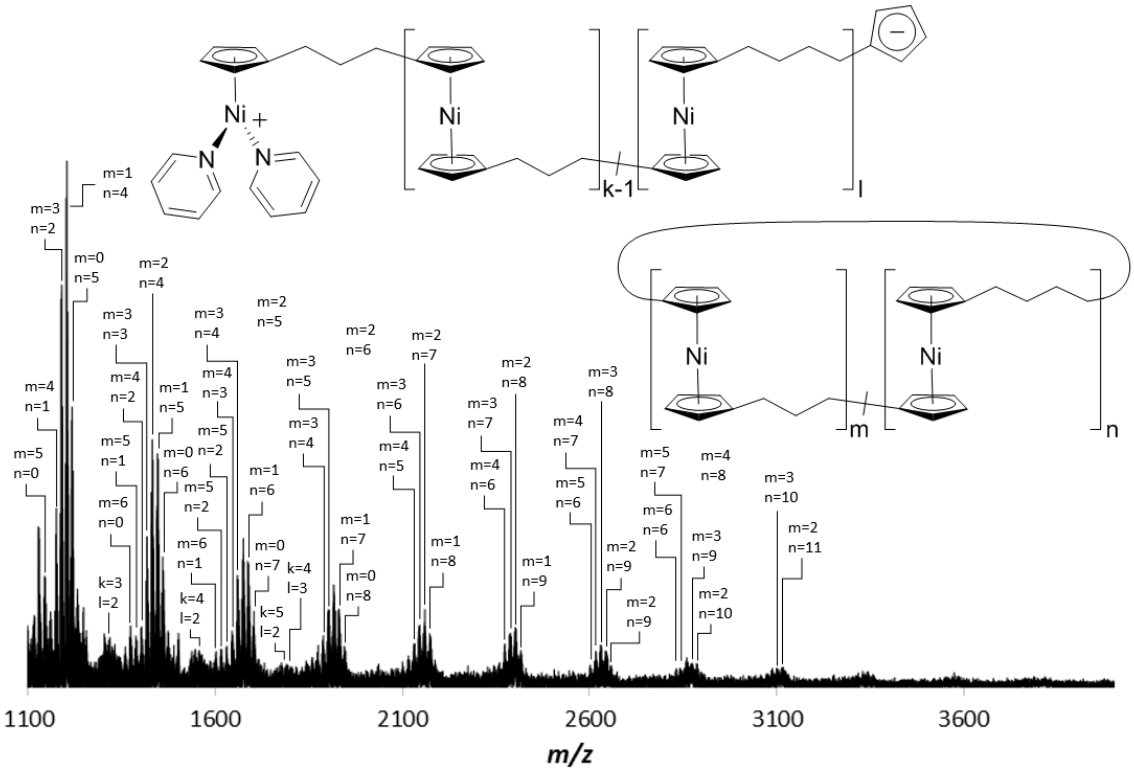

Figure A2.15. MALDI-TOF mass spectrum of copolymer **2.17b**.

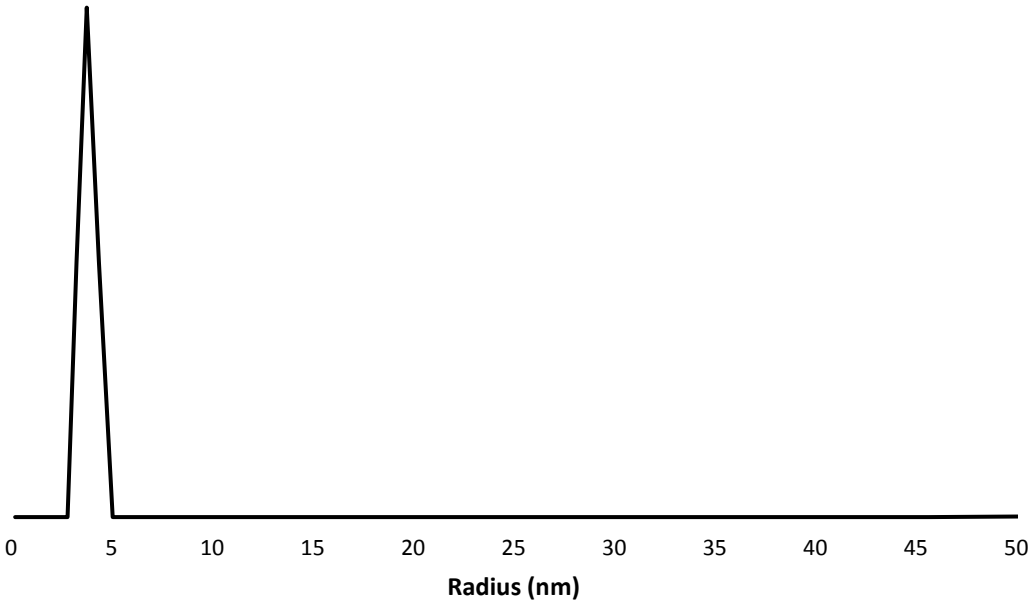

Figure A2.16. DLS size distribution by volume for **2.17b** (toluene, 20 °C, 1 mg mL^{-1}); R_h = 3.8 nm (σ = 0.39 nm).

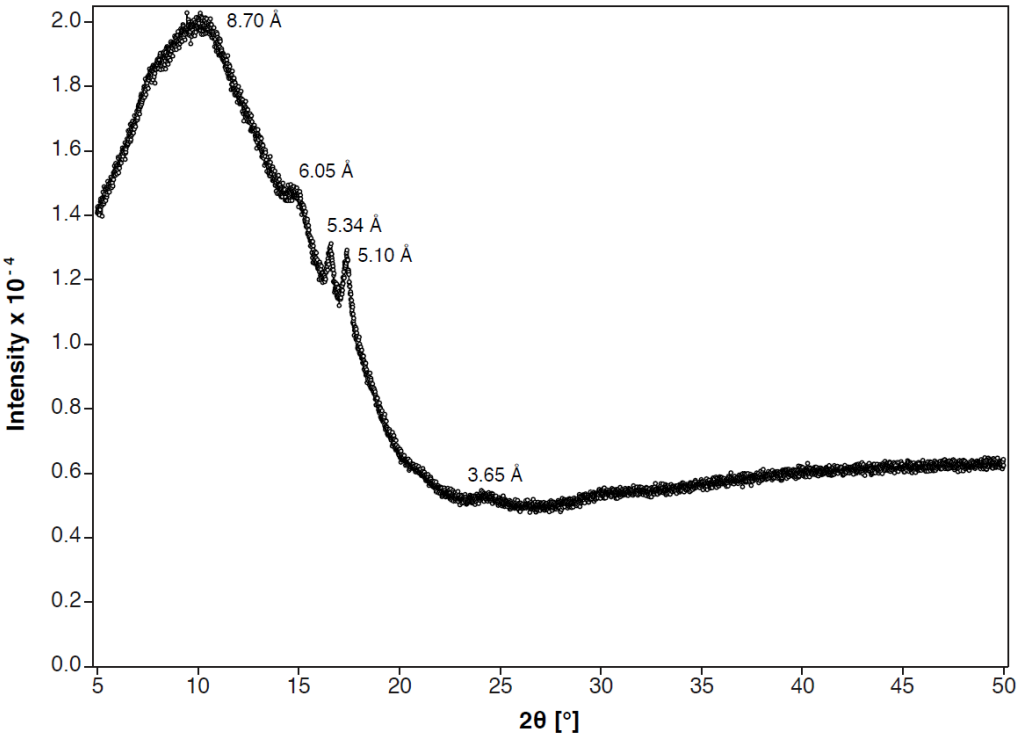

Figure A2.17. WAXS data for insoluble copolymer **2.17a**.

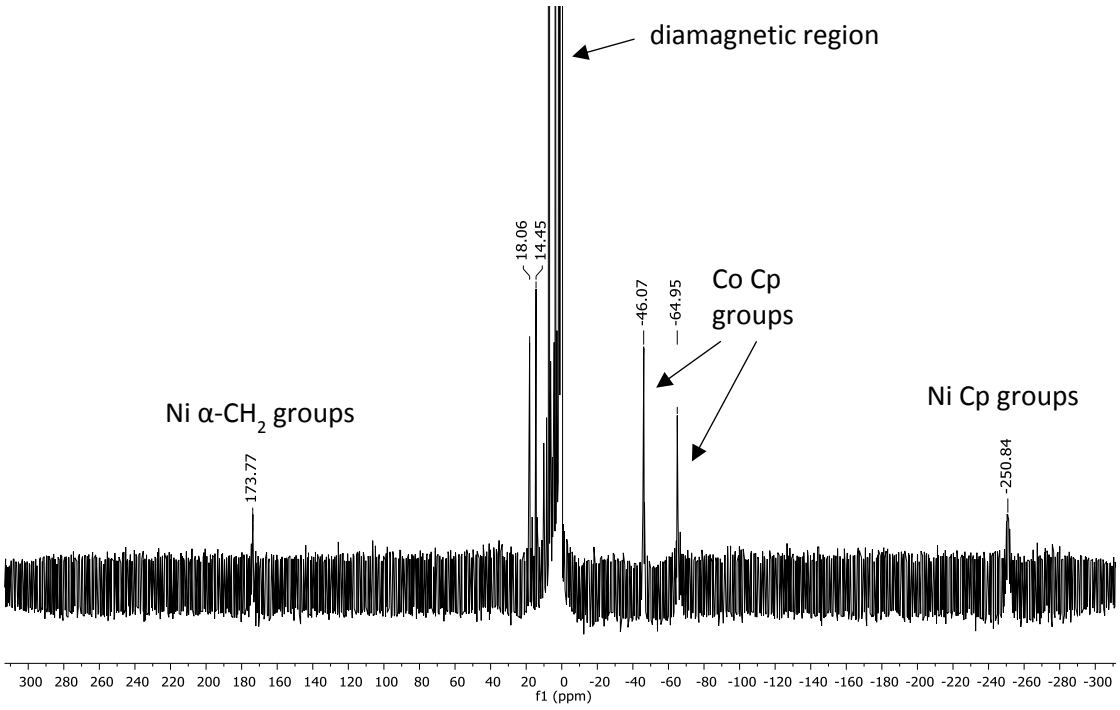

Figure A2.18. ^{1}H NMR spectrum (500 MHz, C_6D_6) of copolymer **2.19b**.

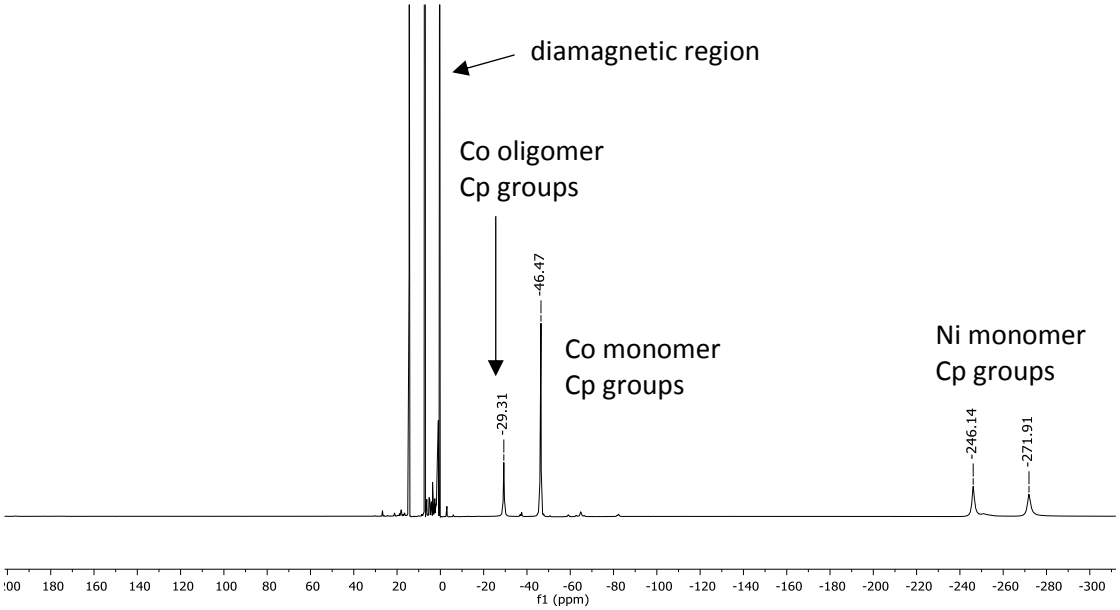

Figure A2.19. ^{1}H NMR spectrum (500 MHz, C_6D_6) of the hexanes soluble supernatant recovered after the precipitation of copolymer **2.19**.

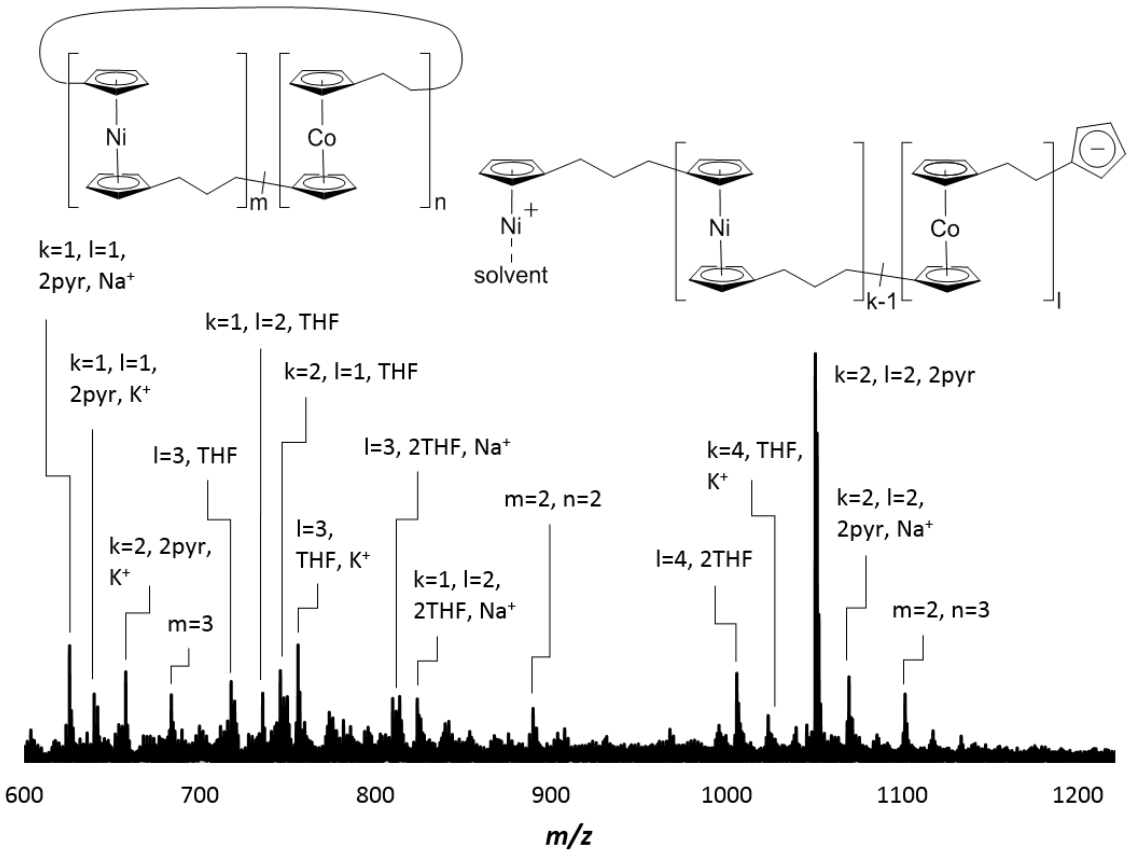

Figure A2.20. MALDI-TOF mass spectrum of copolymer **2.19$_b$**. Pyridine is represented by pyr, and sodium and potassium by their atomic symbols.

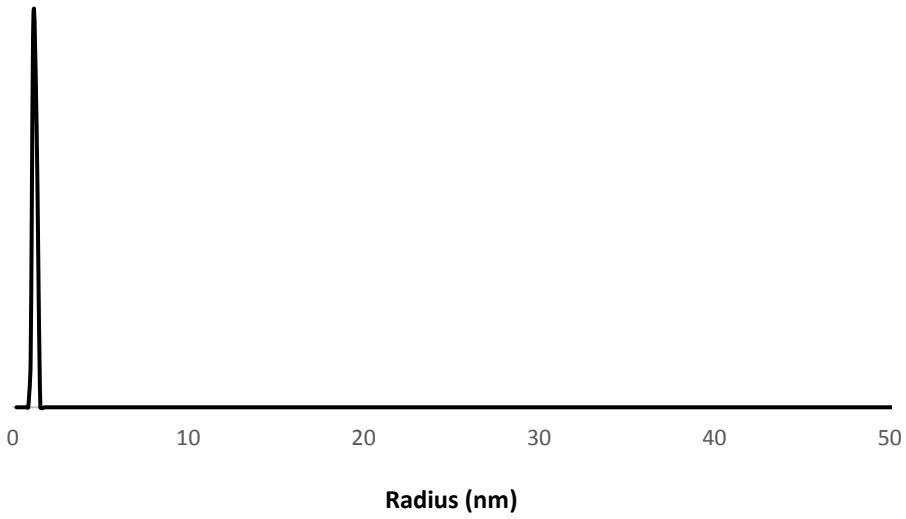

Figure A2.21. DLS size distribution by volume for **2.19b** (toluene, 20 °C, 1 mg mL^{-1}); R_h = 1.2 nm (σ = 0.16 nm).

ii. Additional Figures on Magnetic Measurements

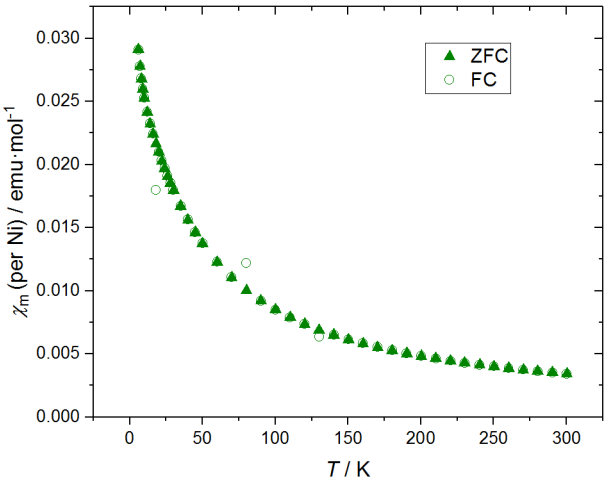

Figure A2.22. Temperature dependence of the field-cooled (FC) and zero-field-cooled (ZFC) magnetic susceptibilities, χ_m, of poly(nickelocenylbutylene) **2.13$_a$** at 0.1 Tesla.

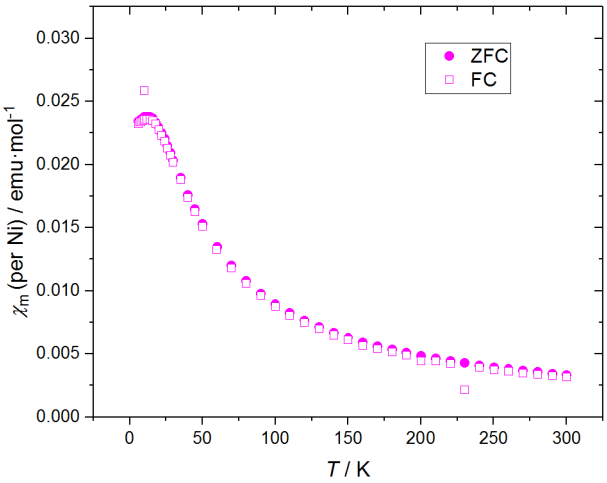

Figure A2.23. Temperature dependence of the field-cooled (FC) and zero-field-cooled (ZFC) magnetic susceptibilities, χ_m, of poly(nickelocenyltetramethyldisilane) **2.14$_a$** at 0.1 Tesla.

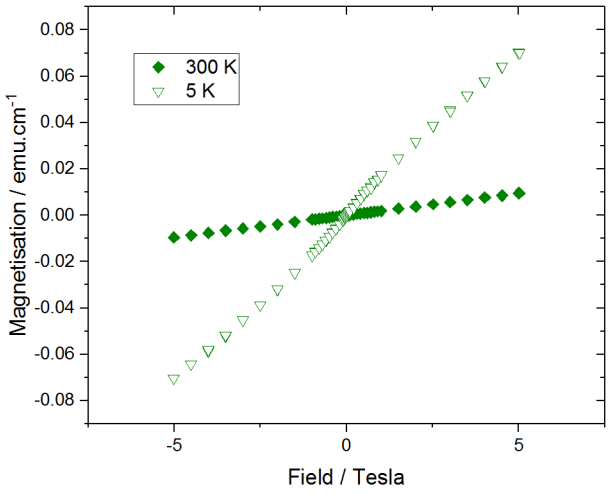

Figure A2.24. Field dependence of the magnetisation for poly(nickelocenylbutylene) **2.13a**.

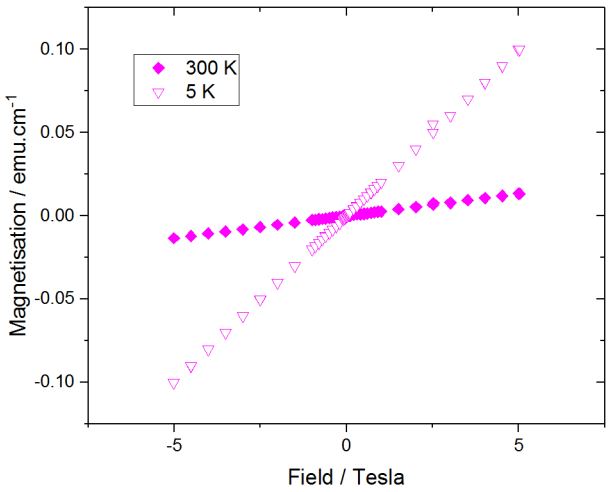

Figure A2.25. Field dependence of the magnetisation for poly(nickelocenyltetramethyldisilane) **2.14a**.

Curie-Weiss Fits

$$\chi_m = \frac{C}{T - \Theta} + \chi_{TIP} \qquad \textbf{Equation A1}$$

$$\mu_{eff} = 2.828\sqrt{C}\,\mu_B \qquad \textbf{Equation A2}$$

$$\hat{H} = \hat{H}_{Zee} + \hat{H}_{ZFS} \qquad \textbf{Equation A3}$$

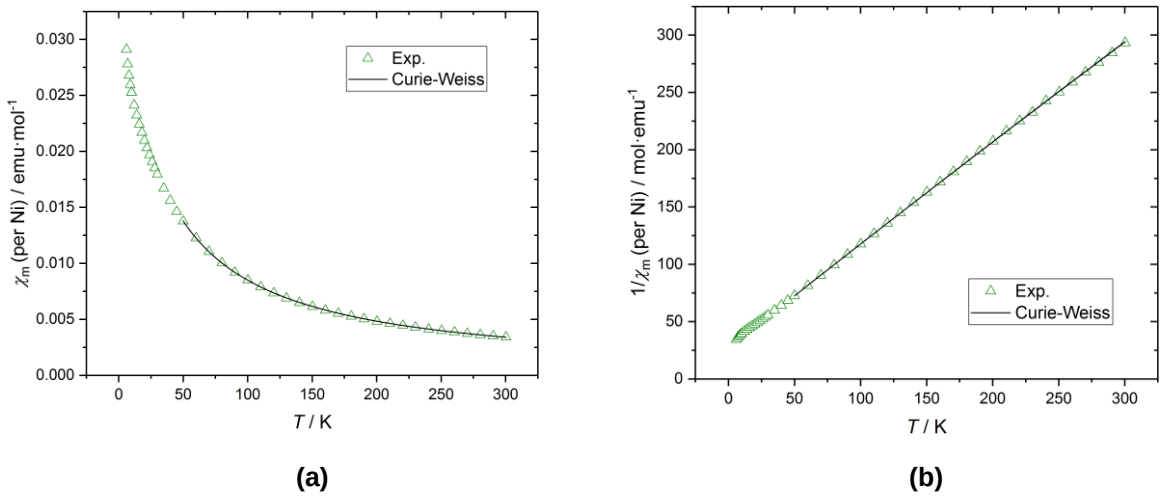

(a) **(b)**

Figure A2.26. Temperature dependence of observed (a) χ_m and (b) χ_m^{-1} per Ni for **2.13a** at 0.1 Tesla. The black lines represent the best fits of the data to Equation A1 in the Curie-Weiss regime (50–300 K) with C = 1.084(6) emu K mol^{-1}, Θ = −29.2(4) K and χ_{TIP} = 109.02×10^{-6} emu mol^{-1}. R^2 = 0.99998.

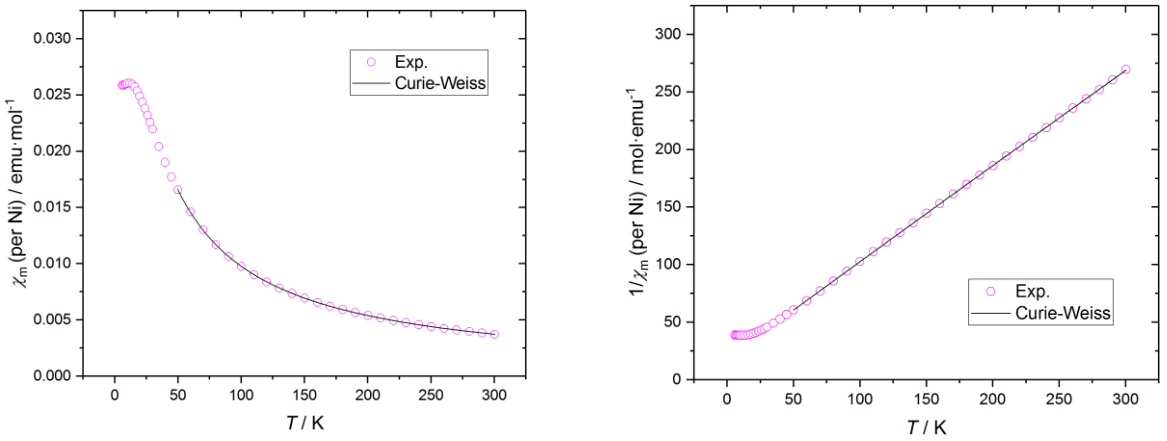

(a) **(b)**

Figure A2.27. Temperature dependence of observed (a) χ_m and (b) χ_m^{-1} per Ni for **2.14a** at 0.1 Tesla. The black lines represent the best fits of the data to Equation A1 in the Curie-Weiss regime (50–300 K) with C = 1.179(7) emu K mol^{-1}, Θ = −21.3(4) K and χ_{TIP} = 53.2×10^{-6}. R^2 = 0.99997.

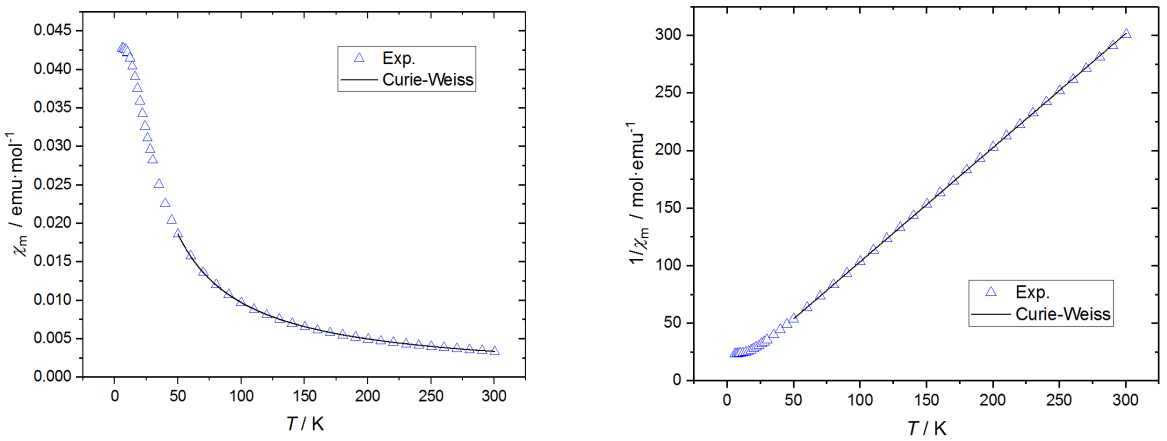

(a) **(b)**

Figure A2.28. Temperature dependence of observed (a) χ_m and (b) χ_m^{-1} per Ni for tricarba[3]nickelocenophane **2.5** at 0.1 Tesla. The black lines represent the best fits of the data to Equation A1 in the Curie-Weiss regime (50–300 K) with C = 1.008(4) emu K mol^{-1}, Θ = −4.2(2) K and χ_{TIP} = 0. R^2 = 0.99998.

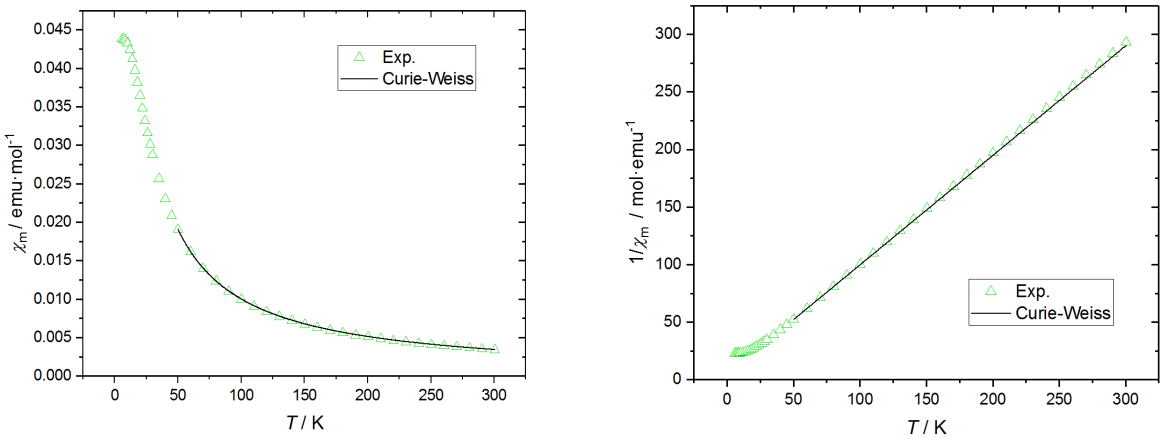

(a) **(b)**

Figure A2.29. Temperature dependence of observed (a) χ_m and (b) χ_m^{-1} per Ni for tetracarba[4]nickelocenophane **2.6** at 0.1 Tesla. The black lines represent the best fits of the data to Equation A1 in the Curie-Weiss regime (50–300 K) with C = 1.052(11) emu K mol^{-1}, Θ = −5.0(5) K and χ_{TIP} = 0. R^2 = 0.99988.

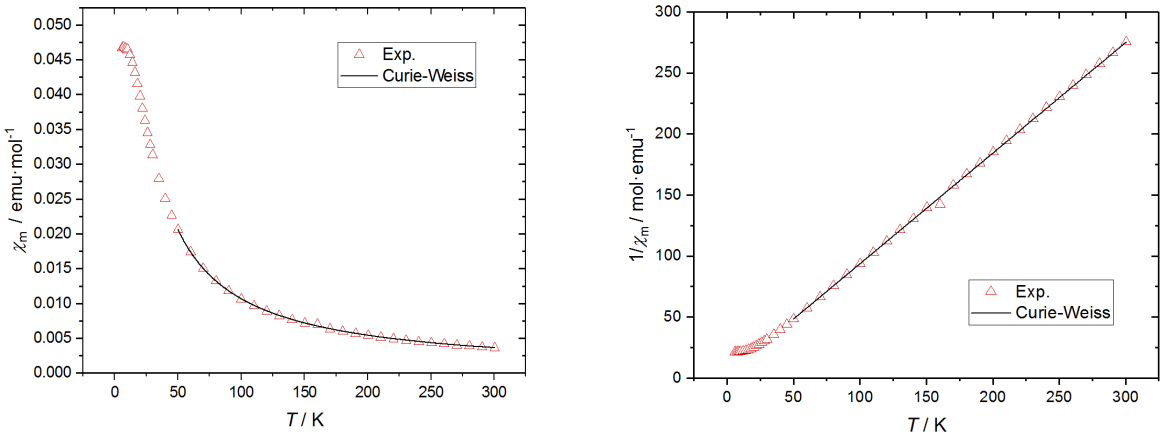

(a) **(b)**

Figure A2.30. Temperature dependence of observed (a) χ_m and (b) χ_m^{-1} per Ni for tetramethyldisila[2]nickelocenophane **2.10** at 0.1 Tesla. The black lines represent the best fits of the data to Equation A1 in the Curie-Weiss regime (50–300 K) with C = 1.103(5) emu K mol^{-1}, Θ = −3.4(2) K and χ_{TIP} = 0. R^2 = 0.99998.

JulX Simulations

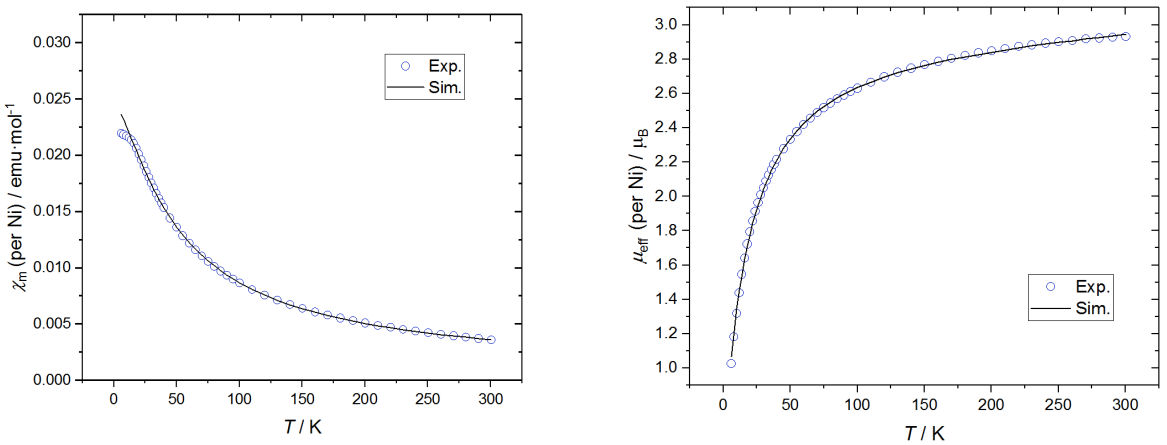

Figure A2.31. Temperature dependence of observed (a) χ_m and (b) μ_{eff} per Ni for **2.12** at 0.1 Tesla.[1] The black lines represent simulated data using the spin Hamiltonian (Equation A3) with g = 2.053, Θ = −23.466 K, χ_{TIP} = 365.8 ×10^{-6} emu mol^{-1} and D = 57.593 cm^{-1} in the temperature range 6–300 K. Summed error on all parameters = 4.595 ×10^{-3}.

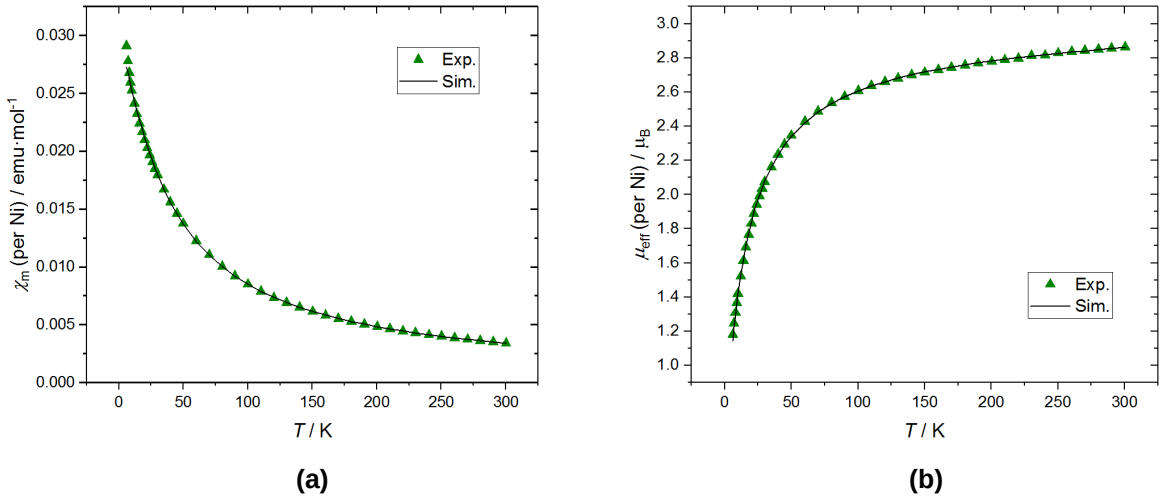

Figure A2.32. Temperature dependence of observed (a) χ_m and (b) μ_{eff} per Ni for **2.13$_a$** at 0.1 Tesla. The black lines represent simulated data using the spin Hamiltonian (Equation A3) with g = 2.054, Θ = −24.978 K, χ_{TIP} = 168.6 ×10^{-6} emu mol^{-1} and D = 42.027 cm^{-1} in the temperature range 6–300 K. Summed error on all parameters = 2.986 ×10^{-3}.

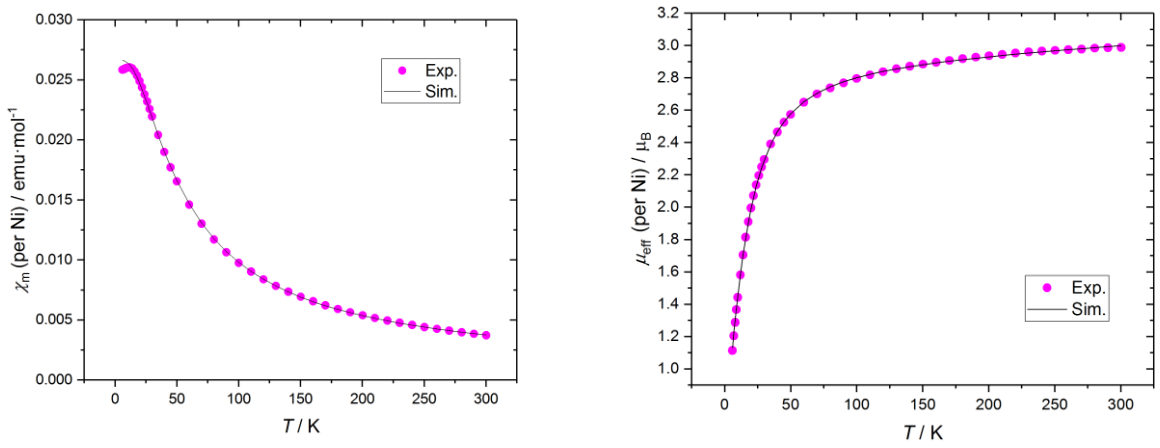

(a) **(b)**

Figure A2.33. Temperature dependence of observed (a) χ_m and (b) μ_{eff} per Ni for **2.14a** at 0.1 Tesla. The black lines represent simulated data using the spin Hamiltonian (Equation A3) with g = 2.045, Θ = −7.026 K, χ_{TIP} = 352.6 ×10^{-6} emu mol^{-1} and D = 55.435 cm^{-1} in the temperature range 6–300 K. Summed error on all parameters = 3.838 ×10^{-3}.

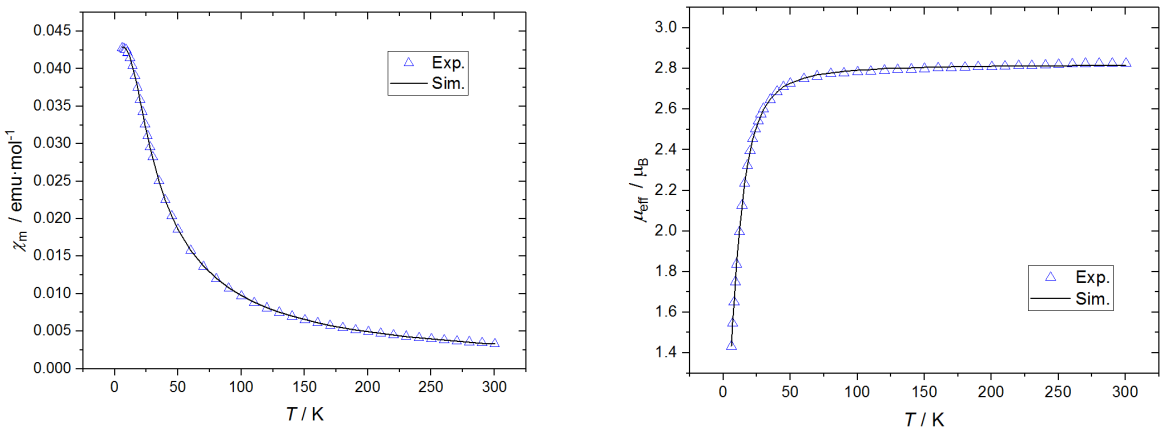

(a) **(b)**

Figure A2.34. Temperature dependence of observed (a) χ_m and (b) μ_{eff} per Ni for tricarba[3]nickelocenophane **2.5** at 0.1 Tesla. The black lines represent simulated data using the spin Hamiltonian (Equation A3) with g = 1.994, Θ = −0.758 K, χ_{TIP} = 0 emu mol^{-1} and D = 32.222 cm^{-1} in the temperature range 6–300 K. Summed error on all parameters = 3.872 ×10^{-3}.

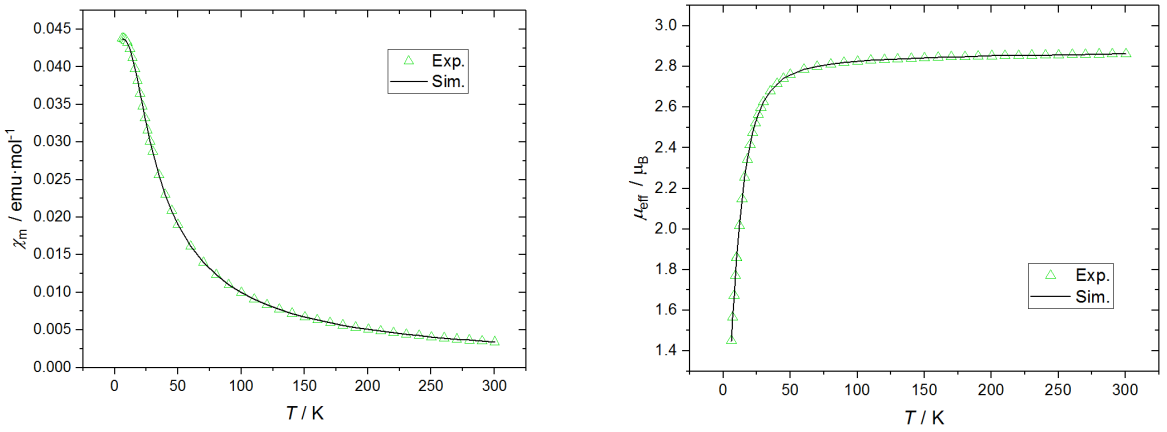

(a) **(b)**

Figure A2.35. Temperature dependence of observed (a) χ_m and (b) μ_{eff} per Ni for tetracarba[4]nickelocenophane **2.6** at 0.1 Tesla. The black lines represent simulated data using the spin Hamiltonian (Equation A3) with g = 2.013, Θ = −0.692 K, χ_{TIP} = 49.0 ×10^{-6} emu mol^{-1} and D = 32.278 cm^{-1} in the temperature range 6–300 K. Summed error on all parameters = 0.6027 ×10^{-3}.

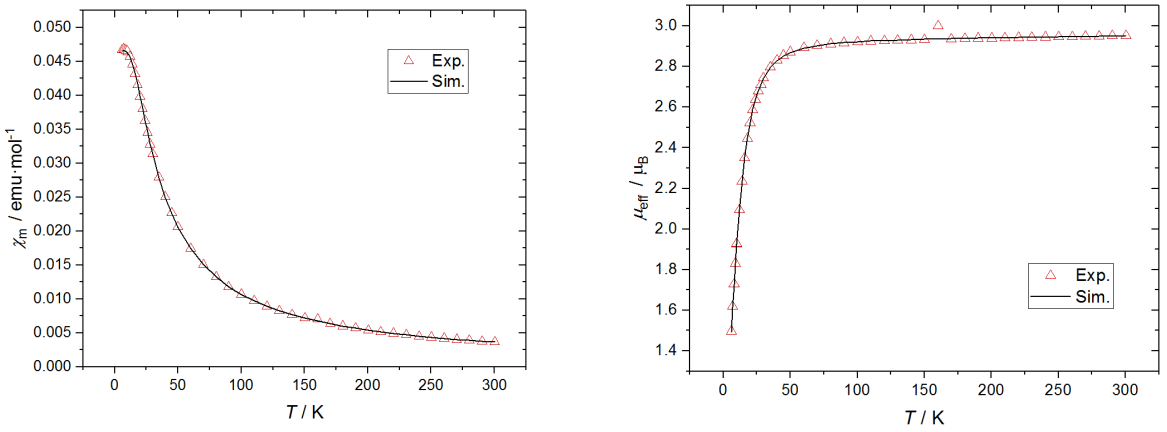

(a) **(b)**

Figure A2.36. Temperature dependence of observed (a) χ_m and (b) μ_{eff} per Ni for tetramethyldisila[2]nickelocenophane **2.10** at 0.1 Tesla. The black lines represent simulated data using the spin Hamiltonian (Equation A3) with g = 2.066, Θ = 0.629 K, χ_{TIP} = 66.4 ×10^{-6} emu mol^{-1} and D = 31.963 cm^{-1} in the temperature range 6–300 K. Summed error on all parameters = 1.306 ×10^{-3}.

iii. Crystallographic Data

Compound	**2.6**
Empirical formula	$C_{14}H_{16}Ni$
Formula weight	242.98
Temperature/K	100.0
Crystal system	orthorhombic
Space group	*Pbca*
a/Å	7.8116(4)
b/Å	11.1074(5)
c/Å	25.3656(11)
α/°	90
β/°	90
γ/°	90
Volume/Å^3	2200.89(18)
Z	8
ρ_{calc}g/cm^3	1.467
μ/mm^{-1}	1.723
F(000)	1024.0
Crystal size/mm^3	0.31×0.16×0.10
Radiation	Mo Kα (λ = 0.71073)
2Θ range for data collection/°	3.212 to 53.556
Index ranges	$-9 \leq h \leq 9$ $-13 \leq k \leq 14$ $-32 \leq l \leq 32$
Reflections collected	15992
Independent reflections	2333 [R_{int} = 0.0827, R_{sigma} = 0.0516]
Data/restraints/parameters	2333/43/154
Goodness-of-fit on F2	1.292
Final R indexes [I>=2σ (I)]	R_1 = 0.0694 wR_2 = 0.1337
Final R indexes [all data]	R_1 = 0.0916 wR_2 = 0.1400
Largest diff. peak/hole/e Å^{-3}	0.49/−1.10
Flack parameter	N/A

iv. References

1. S. Baljak, A. D. Russell, S. C. Binding, M. F. Haddow, D. O'Hare and I. Manners, *J. Am. Chem. Soc.*, 2014, **136**, 5864-5867.

Appendix III

i. Computational Chemistry

DFT Calculations regarding the ring-opening propensity of monomers **3.1**, **3.2**, **3.6**, and **3.13** (Tables A1 and A2) were carried out using Gaussian 09,[1] using the B3LYP functional and the –D2 dispersion correction with keyword iop(3/124=3) of Grimme et al.[2-8] as implemented in Gaussian. For geometry optimisation, the standard Stuttgart/Dresden ECP and associated basis set were used on nickel,[9] and the 6-31G(d) basis set on carbon and hydrogen (with the 5 spherical harmonic d functions on C).[10, 11] This basis set combination is denoted as BS1. Frequency calculations were performed at the same level of theory (B3LYP/BS1) and used to compute zero-point energy and derive gas-phase values for thermal and entropic corrections at 298.15 K. Atomic coordinates are provided in Section iv.

The computed Gibbs energies within Gaussian use standard conditions which correspond to an ideal gas with pressure of 1 atm at 298.15 K. These were converted to Gibbs energies which instead correspond to the solution phase standard state of 1 M, by adding a "free energy correction term" equal to $RTln(V_g/V_s)$ to the free energy of each species. In this equation, R is the ideal gas constant (8.314 J K^{-1} mol^{-1}), T is the absolute temperature (K), V_g is the volume occupied by one mole of ideal gas at 298.15 K, and V_s is the volume occupied by one mole of species in a standard solution of concentration 1 M (i.e. 1 dm^3).

For the basis set correction, a single-point energy was computed, changing the 6-31G(d) basis set of only C and H to the larger 6-311G(d) basis set to obtain improved energy values (this basis set is denoted as BS2). For the solvation correction, the standard IEF-SCRF continuum solvent method was used in single-point calculations with the B3LYP-D2/SDD,6-31G(d) method used for geometry optimisation (BS1), with continuum

parameters designed to describe pyridine solvent (ε = 12.98).[12, 13]

The difference between the vacuum and continuum energy was added to the small basis vacuum free energy:

$$G(BS2) = G(BS1) + (E(BS2) - E(BS1))$$

and also added to the large basis single-point energy:

$$\text{“E(BS2)+SCRF”} = SCRF + (E(BS2) - E(BS1))$$

The difference between the vacuum free energy and vacuum electronic energy was further added to this to yield approximate solvent-phase accurate energies:

$$\text{“E(BS2)+SCRF+G(BS1)”} = SCRF + G(BS2) - E(BS1)$$

Although the continuum energy component cannot be resolved into specific enthalpic or entropic contributions, the small basis vacuum electronic energy (E(BS1) of all species of the tricarba- and tetracarba-bridged systems does not differ significantly from the continuum energy (SCRF), and we can therefore assume that SCRF − E(BS1) = 0. It is unlikely that the enthalpic component within the continuum electronic energy are large enough to alter H(BS2) and significantly, and therefore difference between the vacuum electronic energies of the two basis sets can be added to the sum of electronic and thermal enthalpies to give a rough estimate of the solution phase accurate enthalpy:

$$H(BS2) = H(BS1) + E(BS2) - E(BS1)$$

Conformers of all complexes (**3.1**–**3.1d**, **3.2**–**3.2d**, **3.6**–**3.6c**, **3.13**–**3.13c**) were investigated via molecular mechanics GMMX conformer searches using the MMX forcefield as implemented in PCModel,[14] and where applicable, multiple conformers were optimised in Gaussian (as described above) to confirm the lowest energy structures.

ii. Additional Figures and Schemes

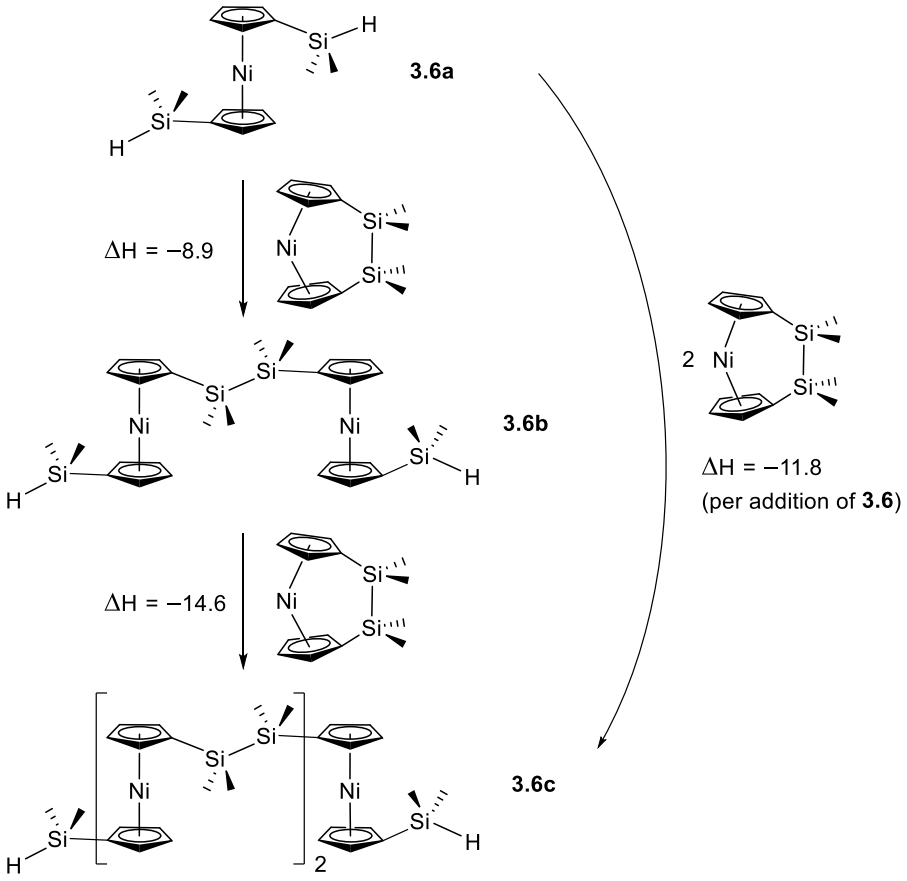

Scheme A3.1. Scheme describing DFT calculations of the ring-opening of monomer **3.6** to form linear oligomeric species and values of enthalpic ring-opening (kJ mol^{-1}).

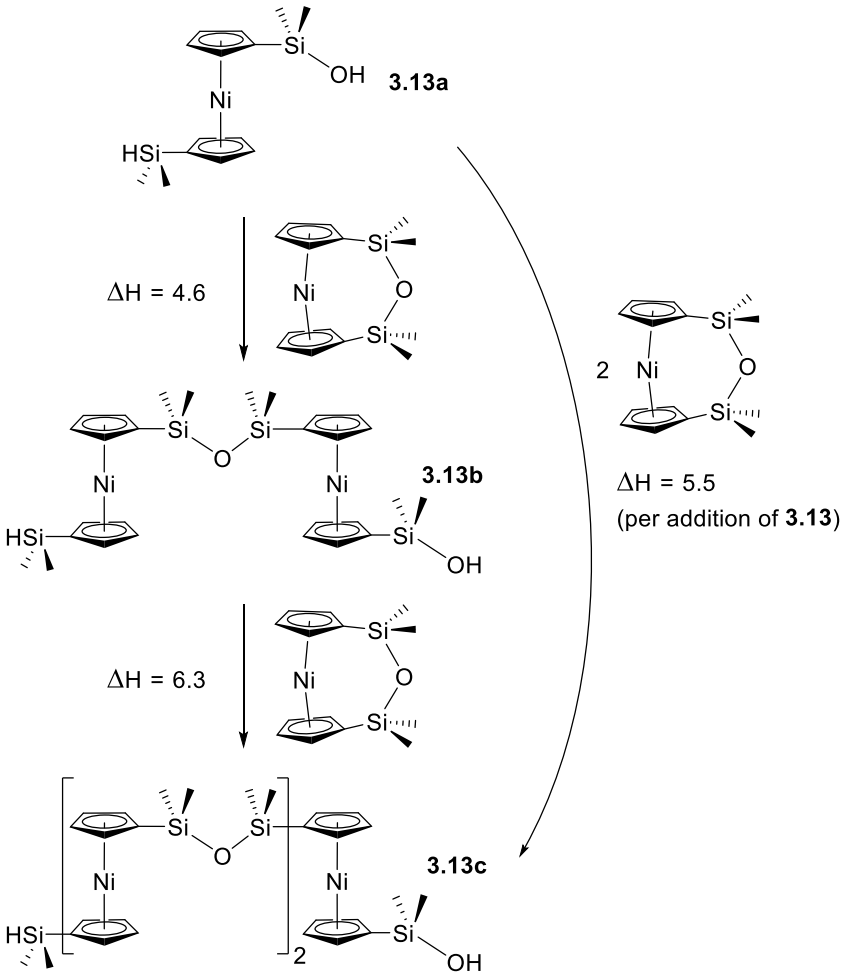

Scheme A3.2. Scheme describing DFT calculations of the ring-opening of monomer **3.13** to form linear oligomeric species and values of enthalpic ring-opening (kJ mol^{-1}).

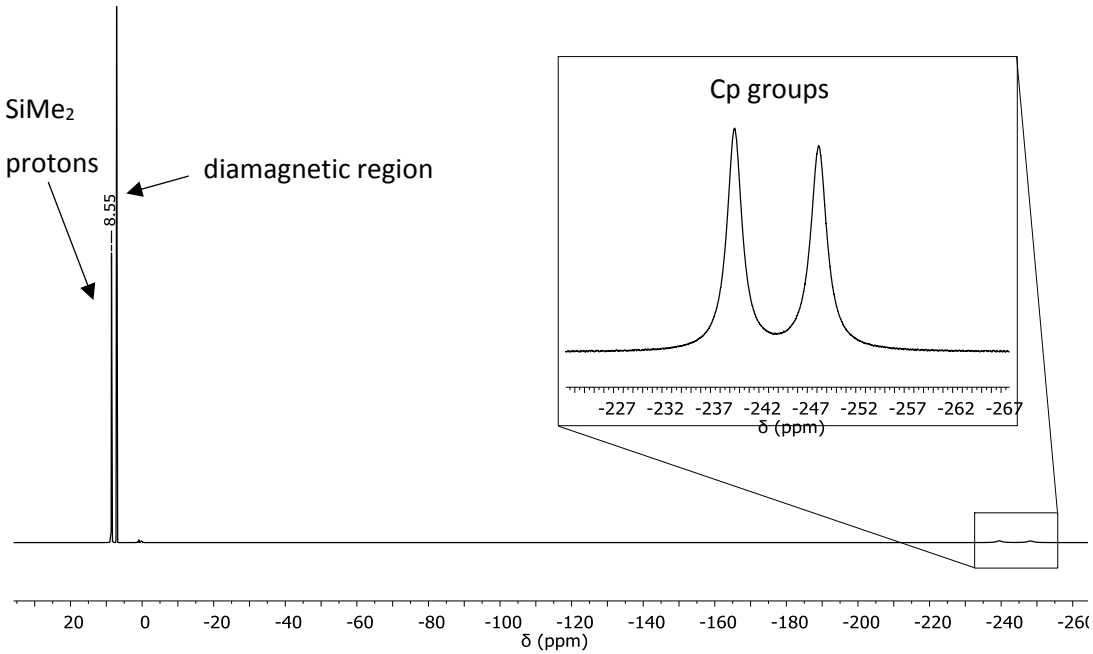

Figure A3.1. ^{1}H NMR spectrum (500 MHz, C_6D_6) of 1,1,3,3-tetramethyldisila-2-oxa[3]nickelocenophane **3.13**.

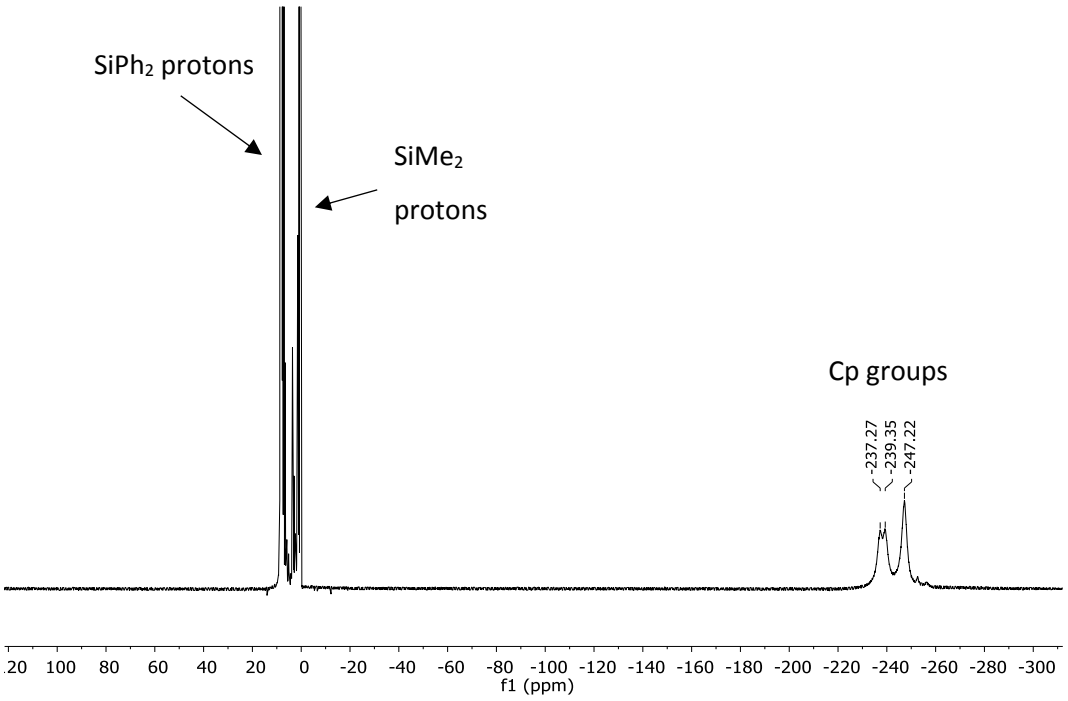

Figure A3.2. ^{1}H NMR spectrum (500 MHz, C_6D_6) of 1,3-dimethyl-1,3-diphenyldisila-2oxane[3]nickelocenophane, **3.14**.

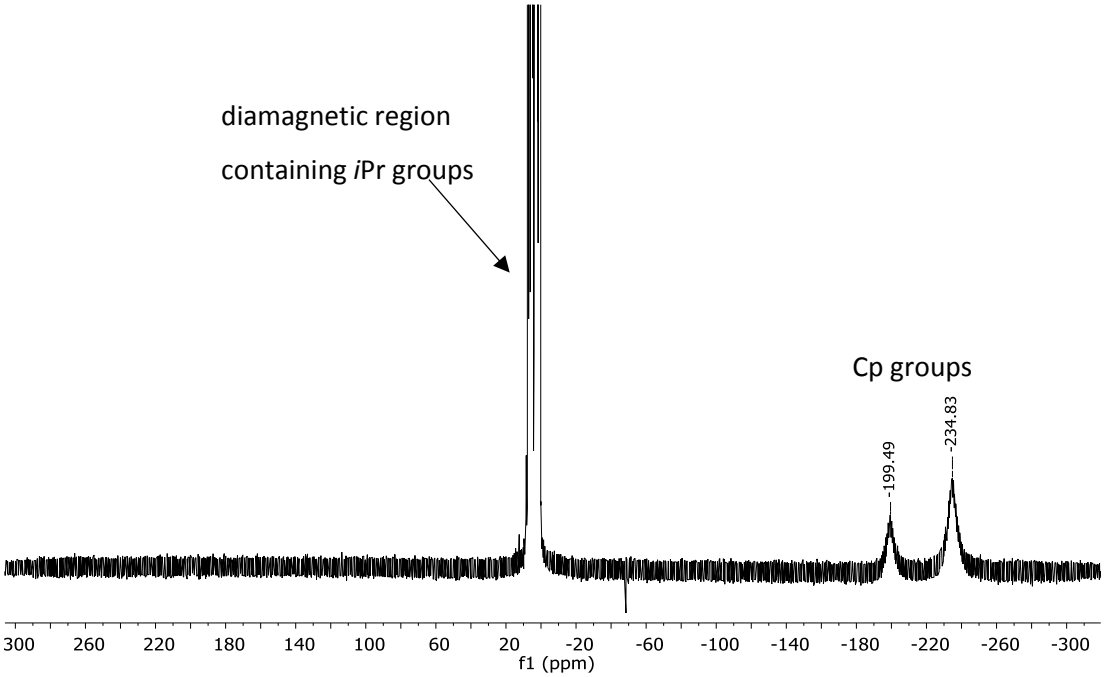

Figure A3.3. ^{1}H NMR spectrum (500 MHz, C_6D_6) of 1,1′,2,2′-bis(tetraisopropyldisiloxa)nickelocene, **3.17**.

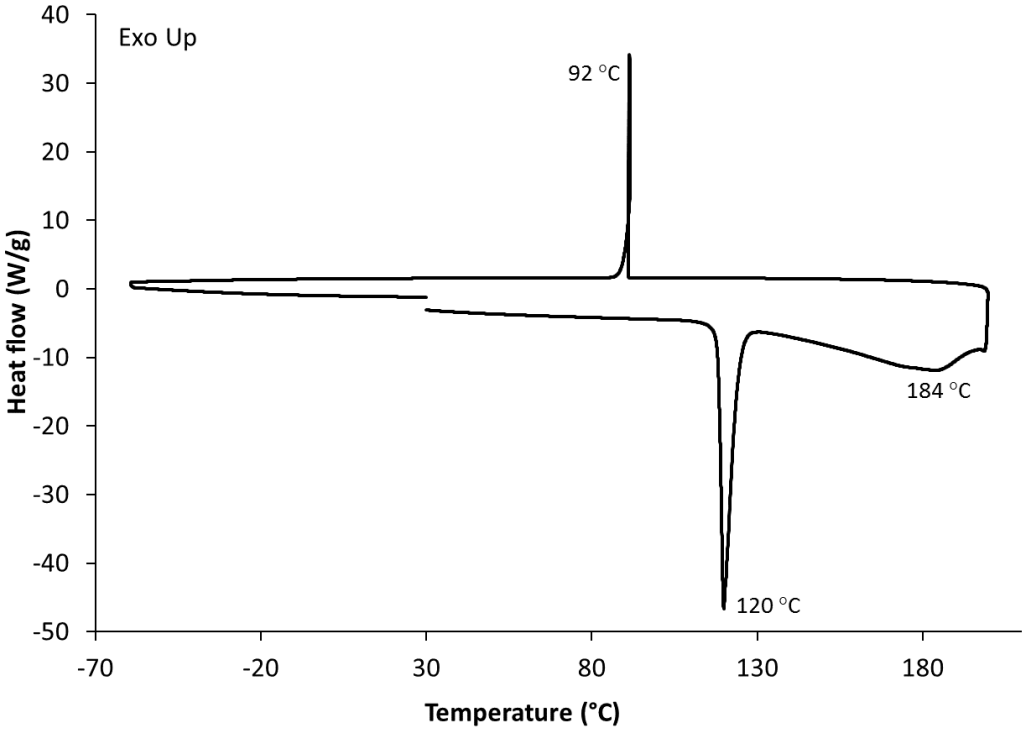

Figure A3.4. DSC thermogram of **3.13** obtained at a scan rate of 10 K min^{-1}.

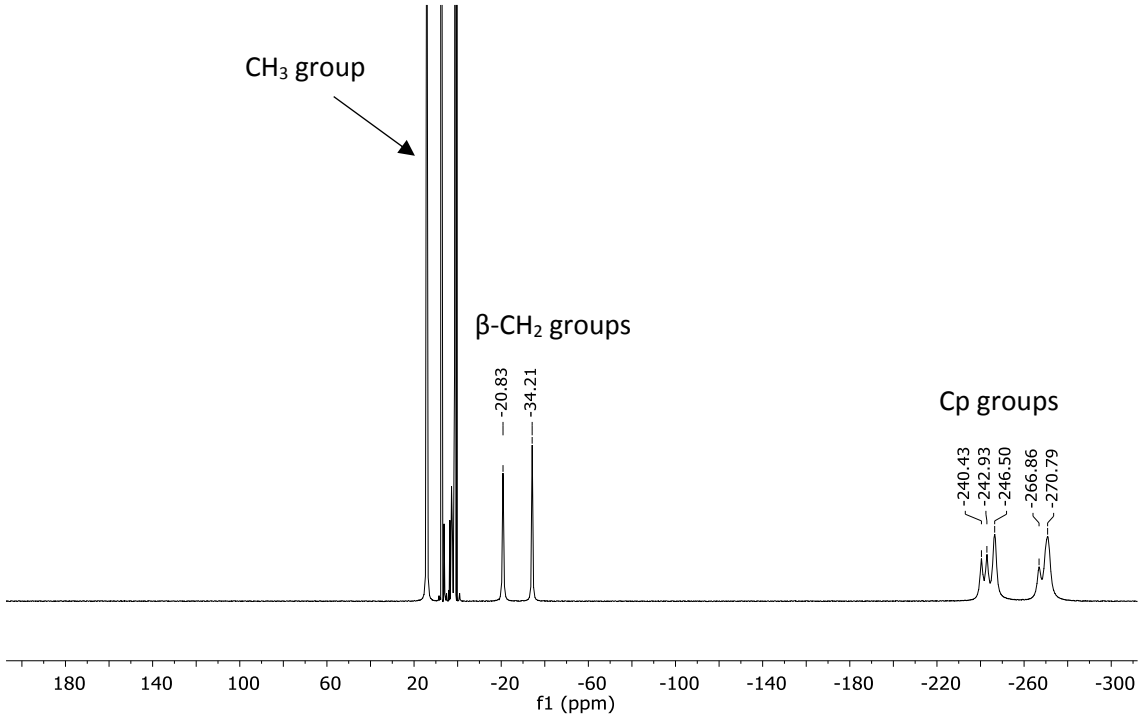

Figure A3.5. ^{1}H NMR spectrum (500 MHz, C_6D_6) of 1-methyltricarba[3]nickelocenophane, **3.15**.

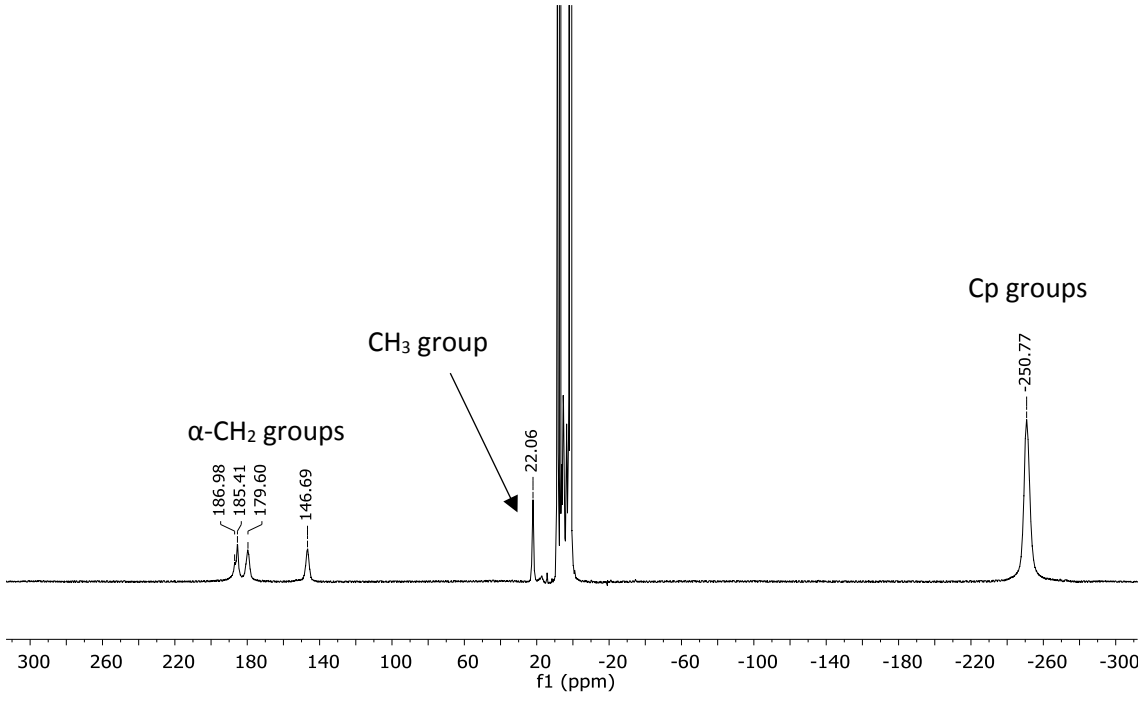

Figure A3.6. ^{1}H NMR spectrum (500 MHz, C_6D_6) of poly(nickelocenyl-1-methyl-propylene), **3.18**.

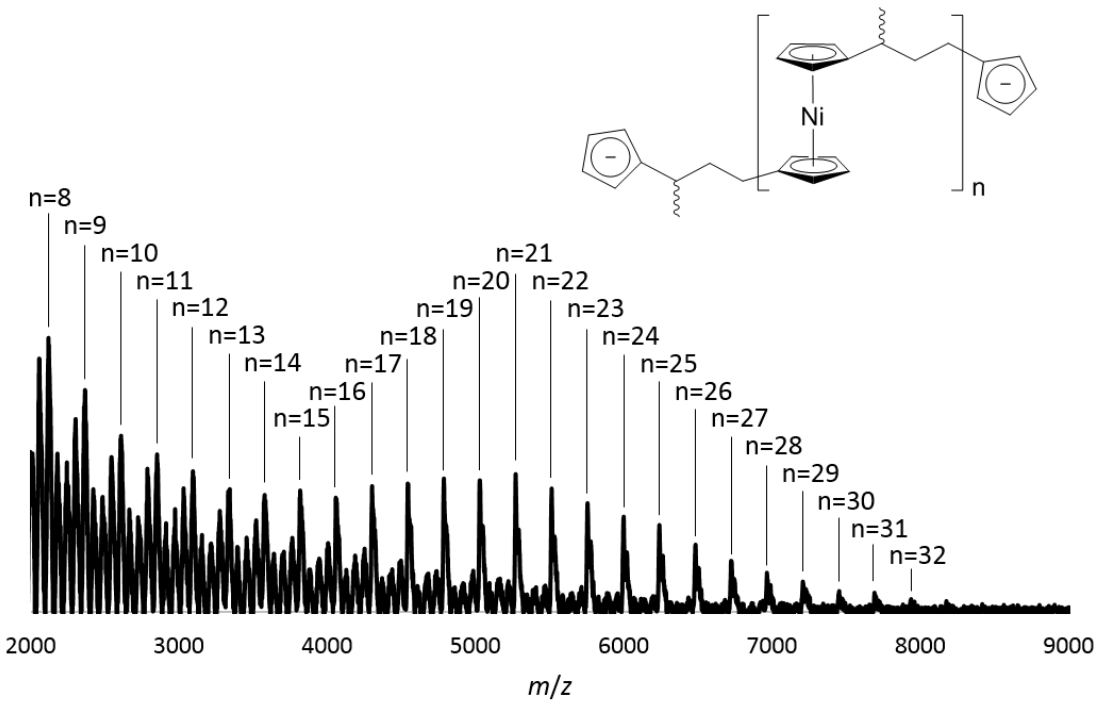

Figure A3.7. MALDI-TOF spectrum of polymer **3.18**.

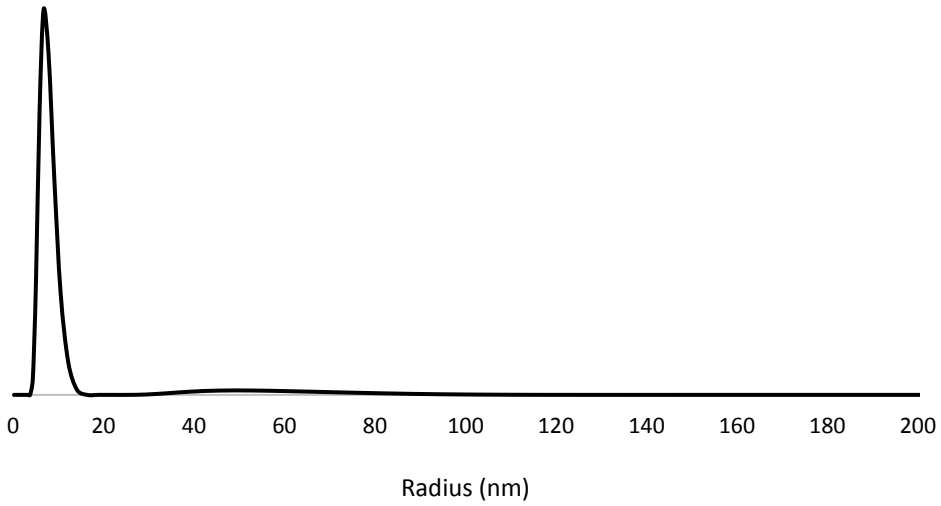

Figure A3.8. DLS size distribution by volume for **3.18**$_a$ (20 °C work up) (toluene, 20 °C, 1 mg mL^{-1}); R_h = 7.42 nm (σ = 1.69 nm).

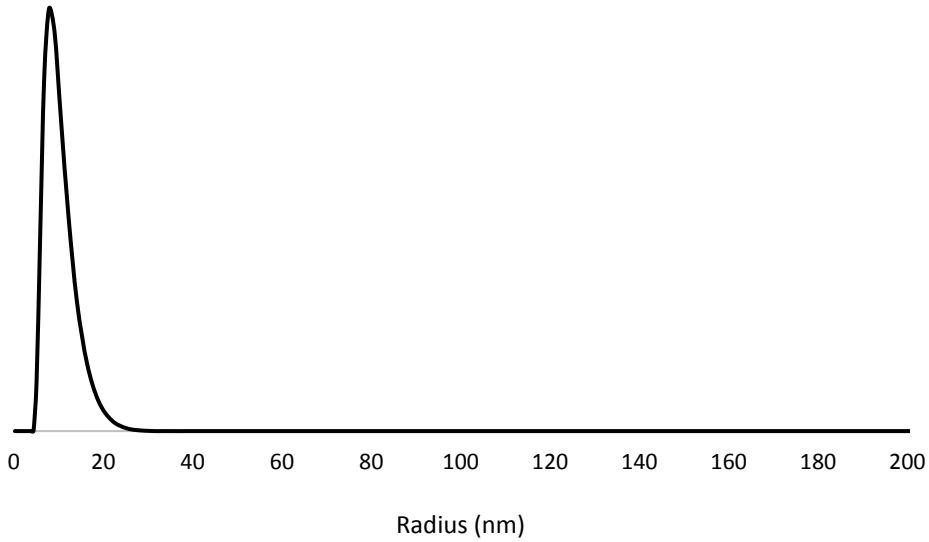

Figure A3.9. DLS size distribution by volume for **3.18$_a$** (−78 °C work up) (toluene, 20 °C, 1 mg mL^{-1}); R_h = 9.35 nm (σ = 3.04 nm).

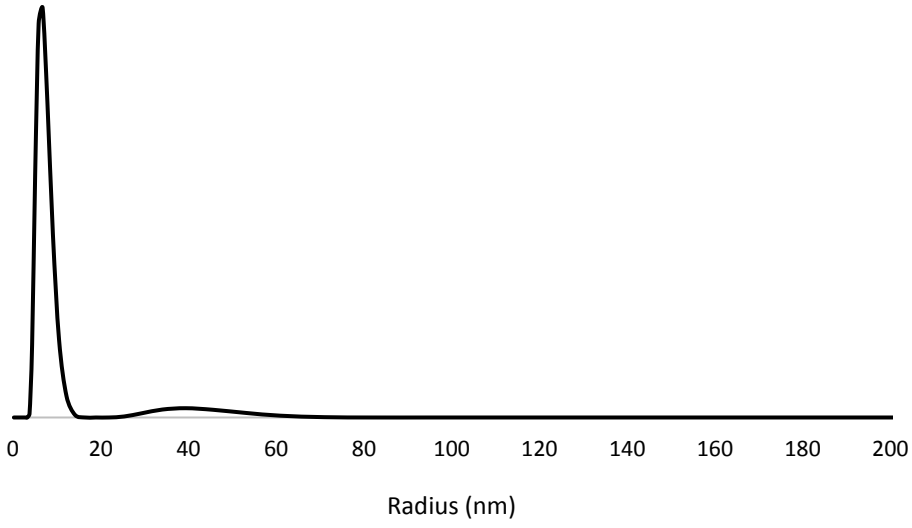

Figure A3.10. DLS size distribution by volume for **3.18$_b$** (−78 °C work up) (toluene, 20 °C, 1 mg mL^{-1}); R_h = 6.90 nm (σ = 1.65 nm).

iii. Crystallographic Data

Compound	**3.13**	**3.14**	**3.15**	**3.17**
Empirical formula	$C_{14}H_{20}NiOSi_2$	$C_{24}H_{24}NiOSi_2$	$C_{14}H_{16}Ni$	$C_{34}H_{62}NiO_2Si_4$
Formula weight	319.19	443.32	242.98	673.9
Temperature/K	100.0	100.01	100.01	200(2)
Crystal system	orthorhombic	Monoclinic	monoclinic	Triclinic
Space group	$P2_12_12_1$	$P2_1/n$	$P2_1/c$	P-1
a/Å	8.3913(2)	9.9885(4)	7.9016(6)	10.1921(17)
b/Å	11.3601(3)	22.3509(9)	9.6856(7)	10.2027(14)
c/Å	15.8756(4)	10.9290(4)	14.8574(11)	10.3527(16)
α/°	90	90	90	83.268(10)
β/°	90	95.756(2)	101.465(5)	83.418(12)
γ/°	90	90	90	62.359(10)
Volume/Å^3	1513.36(7)	2427.62(16)	1114.38(14)	944.9(3)
Z	4	4	4	1
ρ_{calc}g/cm^3	1.401	1.213	1.448	1.184
μ/mm^{-1}	1.426	0.908	1.702	0.667
F(000)	672.0	928.0	512.0	366.0
Crystal size/mm^3	0.20×0.22×0.17	0.22×0.20×0.18	0.369×0.332×0.101	0.527×0.22×0.21
Radiation	MoKα (λ = 0.71073)	MoKα (λ = 0.71073)	MoKα (λ = 0.71073)	MoKα (λ = 0.71073)
2Θ range for data collection/°	4.408 to 53.448	4.486 to 54.962	5.052 to 56.052	3.97 to 51.356
Index ranges	$-10 \le h \le 10$ $-14 \le k \le 14$ $-20 \le l \le 20$	$-9 \le h \le 12$, $-28 \le k \le 28$, $-14 \le l \le 14$	$-10 \le h \le 10$, $-9 \le k \le 12$, $-19 \le l \le 19$	$-12 \le h \le 12$, $-12 \le k \le 12$, $-12 \le l \le 12$
Reflections collected	12207	22709	13870	13275
Independent reflections	3218 [R_{int} = 0.0335, R_{sigma} = 0.0319]	5546 [R_{int} = 0.0328, R_{sigma} = 0.0285]	2697 [R_{int} = 0.0518, R_{sigma} = 0.0412]	3546 [R_{int} = 0.0706, R_{sigma} = 0.0746]
Data/restraints/ parameters	3218/0/168	5546/0/255	2697/808/274	3546/0/196
Goodness-of-fit on F2	1.292	1.044	1.012	1.073
Final R indexes [I>=2σ (I)]	R_1 = 0.0694 wR_2 = 0.1337	R_1 = 0.0288, wR_2 = 0.0699	R_1 = 0.0269, wR_2 = 0.0522	R_1 = 0.0825, wR_2 = 0.2284
Final R indexes [all data]	R_1 = 0.0916 wR_2 = 0.1400	R_1 = 0.0371, wR_2 = 0.0727	R_1 = 0.0460, wR_2 = 0.0575	R_1 = 0.0983, wR_2 = 0.2546
Largest diff. peak/hole/e Å^{-3}	0.49/−1.10	0.41/−0.25	0.32/−0.32	0.88/−1.55
Flack parameter	N/A	N/A	N/A	N/A

iv. Computational Data

Table A3.1. Computed total energies for the different species **3.1**–**3.1d**, **3.2**–**3.2d**, **3.6**–**3.6c**, and **3.13**–**3.13c**. Total energies/enthalpies in atomic units, entropies in kJ mol^{-1}. E(BS1) is the B3LYP-D2/small basis total electronic energy.

	E(BS1)	G(BS1)	H(BS1)	S(BS1)	E(BS2)	SCRF	E(BS2)+SCRF +G(BS1)	H(BS2)
3.1	−674.7486	−674.5548	−674.50	455.12	−674.8572	−674.7520	−674.6668	−674.61
3.1a	−675.9591	−675.7530	−675.69	536.12	−676.0689	−675.9622	−675.8659	−675.80
3.1b	−1350.7160	−1350.3005	−1350.20	871.90	−1350.9335	−1350.7218	−1350.5239	−1350.42
3.1c	−2025.4721	−2024.8423	−2024.71	1163.24	−2025.7966	−2025.4809	−2025.1756	−2025.04
3.1d	−2700.2274	−2699.3858	−2699.22	1480.65	−2700.6591	−2700.2388	−2699.8290	−2699.65
3.2	−714.0608	−713.8405	−713.79	486.94	−714.1780	−714.0640	−713.9609	−713.90
3.2a	−715.2712	−715.0380	−714.97	564.45	−715.3893	−715.2743	−715.1593	−715.09
3.2b	−1429.3401	−1428.8702	−1428.77	921.70	−1429.5748	−1429.3463	−1429.1112	−1429.00
3.2c	−2143.4092	−2142.7028	−2142.56	1281.67	−2143.7605	−2143.4185	−2143.0634	−2142.91
3.2d	−2857.4779	−2856.5325	−2856.35	1620.78	−2857.9455	−2857.4903	−2857.0123	−2856.82
3.6	−1295.51299	−1295.2646	−1295.19	624.23	−1295.6835	−1295.5169	−1295.4390	−1295.36
3.6a	−1296.71351	−1296.4543	−1296.38	685.13	−1296.8849	−1296.7173	−1296.6295	−1296.55
3.6b	−2592.23397	−2591.7095	−2591.58	1178.55	−2592.5739	−2592.2408	−2592.0562	−2591.92
3.6c	−3887.75594	−3886.9645	−3886.78	1655.51	−3888.2649	−3887.7658	−3887.4833	−3887.29
3.13	−1370.84203	−1370.5920	−1370.52	658.06	−1371.0383	−1370.8462	−1370.7925	−1370.71
3.13a	−1372.02675	−1371.7645	−1371.68	727.08	−1372.2247	−1372.0313	−1371.9669	−1371.88
3.13b	−2742.87112	−2742.3398	−2742.20	1234.00	−2743.2632	−2742.8791	−2742.7398	−2742.59
3.13c	−4113.71480	−4112.9130	−4112.72	1728.30	−4114.3010	−4113.7262	−4113.5106	−4113.30

Table A3.2. Computed relative energies, free energies, enthalpies and entropies for the formation of species **3.1b**–**3.1d**, **3.2b**–**3.2d**, **3.6b**–**3.6c**, and **3.13b**–**3.13c**.

	Route	ΔG(BS1)	ΔH(BS1)	ΔS(BS1)	ΔE(BS2)	Δ[E(BS2)+ SCRF+G(BS1)]	ΔH(BS2)
3.1b	**3.1a** + **3.1**	18.8353	−16.61	−119.34	−19.4473	23.2931	−14.20
3.1c	**3.1b** + **3.1**	34.2103	−14.44	−163.79	−15.2284	39.7242	−10.1
	3.1a + 2(**3.1**)	26.5228	−15.53	−141.57	−17.3378	31.5087	−12.15
3.1d	**3.1c** + **3.1**	29.3557	−11.55	−137.71	−13.7703	35.2243	−7.74
	3.1a + 3(**3.1**)	27.4671	−14.2	−140.28	−16.1487	32.7472	−10.68
3.2b	**3.2a** + **3.2**	21.9072	−16.61	−129.68	−19.6011	23.6213	−15.03
3.2c	**3.2b** + **3.2**	20.6732	−17.04	−126.97	−20.1835	22.7186	−15.34
	3.2a + 2(**3.2**)	21.2902	−16.83	−128.33	−19.8923	23.1699	−15.18
3.2d	**3.2c** + **3.2**	28.6521	−15.26	−147.83	−18.3583	31.2559	−12.90
	3.2a + 3(**3.2**)	23.7441	−16.30	−134.83	−19.3810	25.8653	−14.42
3.6b	**3.6a** + **3.6**	24.8477	−14.00	−130.80	−14.5152	32.2189	−8.89
3.6c	**3.6b** + **3.6**	25.2311	−18.51	−147.27	−19.6871	31.4303	−14.61
	3.6a + 2(**3.6**)	25.0394	−16.26	−139.03	−17.1011	31.8246	−11.75
3.13b	**3.13a** + **3.13**	43.9798	−0.92	−151.15	−0.6139	51.5124	4.61
3.13c	**3.13b** + **3.13**	49.3725	0.73	−163.77	1.2239	56.9605	6.26
	3.13a + 2(**3.13**)	46.6761	−0.09	−157.46	0.3050	54.2364	5.44

3.1 E(BS1) = −674.7486 a.u.

	x	y	z
Ni1	−0.000011	0.719506	−0.019905
C1	1.994159	−1.530262	0.623529
C2	1.789456	−0.028344	−1.110605
C3	1.995042	−1.402111	−0.794642
C4	−1.994223	−1.530202	0.623512
C5	−1.788597	−0.233332	1.175762
C6	−1.645634	0.706592	0.108700
C7	−1.789456	−0.028263	−1.110603
C8	−1.995102	−1.402028	−0.794658
C9	1.645663	0.706538	0.108686
C10	1.788588	−0.233376	1.175762
C11	−1.317946	2.174830	0.249877
C12	0.000043	2.650871	−0.411571
C13	1.318035	2.174791	0.249843
H1	2.132231	−2.447055	1.182540
H2	1.723721	0.385835	−2.109554
H3	2.133149	−2.204672	−1.508251
H4	−2.132330	−2.446997	1.182511
H5	−1.718987	0.005281	2.230449
H6	−1.723704	0.385926	−2.109547
H7	−2.133240	−2.204571	−1.508281
H8	1.718986	0.005255	2.230445
H9	−1.290627	2.430271	1.317831
H10	−2.135490	2.770033	−0.181848
H11	0.000025	2.363348	−1.471381
H12	0.000061	3.749064	−0.395017
H13	2.135587	2.769955	−0.181921
H14	1.290760	2.430256	1.317793

3.1a E(BS1) = −675.9591 a.u.

	x	y	z
Ni1	0.238940	−0.370363	−0.180777
C1	−0.731180	−2.066410	0.869310
C2	−1.201376	−0.850828	1.445315
C3	−1.916188	−0.116243	0.449758
C4	−1.866778	−0.888165	−0.750470
C5	−1.141631	−2.087604	−0.492624
C6	2.113759	0.668705	0.519965
C7	2.469439	−0.496043	−0.223544
C8	1.986880	−0.352510	−1.556587
C9	1.322519	0.90246	−1.646307
C10	1.397208	1.527493	−0.367221
C11	−2.657092	1.178299	0.678366
C12	−2.732143	2.110344	−0.537954
C13	2.486924	0.966987	1.945521
H1	−0.149893	−2.828332	1.373376
H2	−1.054833	−0.534234	2.471383
H3	−2.303502	−0.609855	−1.701241
H4	−0.927464	−2.868008	−1.212121
H5	3.014126	−1.347406	0.167275
H6	2.091113	−1.077877	−2.353591
H7	0.833518	1.304473	−2.524758
H8	0.988460	2.496669	−0.107016
H9	−2.192751	1.710940	1.518520
H10	−3.682217	0.945406	1.005719
H11	−1.731206	2.400860	−0.875462
H12	−3.288334	3.022027	−0.292392
H13	−3.242961	1.629940	−1.380125
H14	3.462453	1.469407	2.003209
H15	1.753898	1.625646	2.424278
H16	2.557206	0.051607	2.543520

3.1b E(BS1) = −1350.7160 a.u.

	x	y	z
Ni1	3.516804	−0.447591	0.142872
Ni2	−4.010067	0.655973	−0.175225
C1	4.291803	−2.536815	0.190527
C2	2.920866	−2.567291	0.577713
C3	2.126269	−2.098791	−0.512802
C4	3.027571	−1.772556	−1.572223
C5	4.358625	−2.046346	−1.143628
C6	4.742489	1.444215	0.173727
C7	3.442977	1.731869	−0.343420
C8	2.475518	1.446365	0.662812
C9	3.171521	0.974662	1.812247
C10	4.563926	0.971676	1.509600
C11	0.622055	−2.010716	−0.588580
C12	−0.085528	−1.805641	0.758921
C13	−1.610229	−1.588147	0.627337
C14	−1.971728	−0.306104	−0.079841
C15	−2.369741	−0.162886	−1.443682
C16	−2.531984	1.223958	−1.731249
C17	−2.236372	1.951128	−0.544409
C18	−1.897037	1.011217	0.471160
C19	−6.058234	1.497572	−0.397659
C20	−6.095870	0.122867	−0.769749
C21	−5.747690	−0.668490	0.366227
C22	−5.484077	0.235571	1.439387
C23	−5.678374	1.567973	0.971815
C24	6.056198	1.680203	−0.525105
C25	6.601289	3.103480	−0.302197
C26	−5.737063	−2.170229	0.439168

H1	5.133453	−2.822619	0.808971
H2	2.547667	−2.886132	1.542747
H3	2.738282	−1.383232	−2.541295
H4	5.259796	−1.894747	−1.724441
H5	3.231517	2.100633	−1.340286
H6	1.402324	1.552167	0.561630
H7	2.723246	0.658179	2.745742
H8	5.359060	0.660541	2.176955
H9	0.228934	−2.930569	−1.051262
H10	0.347079	−1.194571	−1.268182
H11	0.087755	−2.678456	1.402495
H12	0.356048	−0.943222	1.273603
H13	−2.046927	−1.593785	1.634700
H14	−2.053447	−2.439653	0.093484
H15	−2.523152	−0.978870	−2.140070
H16	−2.838000	1.646518	−2.679955
H17	−2.281910	3.026613	−0.427103
H18	−1.635138	1.250919	1.495123
H19	−6.261935	2.339206	−1.047737
H20	−6.346170	−0.264055	−1.750481
H21	−5.189123	−0.049694	2.442299
H22	−5.543199	2.472515	1.551258
H23	6.798485	0.952241	−0.172687
H24	5.938566	1.505818	−1.602576
H25	6.762457	3.298342	0.764109
H26	7.556243	3.244535	−0.822432
H27	5.896407	3.855286	−0.674797
H28	−5.497818	−2.618408	−0.531505
H29	−6.718654	−2.558753	0.743911
H30	−5.003543	−2.533901	1.167101

3.1c E(BS1) = −2025.4721 a.u.

	x	**y**	**z**
Ni1	0.341218	3.656328	0.019486
Ni2	4.564241	−2.278690	0.061257
Ni3	−4.639858	−1.834329	0.248645
C1	1.258045	5.469420	0.902418
C2	2.246996	4.443222	0.906033
C3	2.525002	4.070768	−0.444734
C4	1.684142	4.870916	−1.276854
C5	0.909162	5.736295	−0.451485
C6	−1.392128	2.690273	−1.019240
C7	−0.451524	1.691266	−0.631804
C8	−0.366591	1.702009	0.790079
C9	−1.253828	2.707945	1.271895
C10	−1.898709	3.322085	0.156274
C11	3.582678	3.113960	−0.936609
C12	3.844666	1.890930	−0.043474
C13	4.999925	1.028135	−0.570885
C14	5.357620	−0.162973	0.289058
C15	6.437728	−1.064687	0.040722
C16	6.497492	−2.012822	1.102253
C17	5.444550	−1.713937	2.011384
C18	4.742994	−0.578379	1.508615
C19	2.453360	−2.937163	−0.319138
C20	3.212332	−4.063301	0.119936
C21	4.253631	−4.308308	−0.820632
C22	4.148542	−3.332980	−1.851359
C23	3.044604	−2.486955	−1.540678
C24	−2.954975	4.391133	0.213462
C25	1.220464	−2.375722	0.336983
C26	−0.094216	−2.926885	−0.252113
C27	−1.334078	−2.297117	0.413887
C28	−2.638115	−2.763247	−0.177142
C29	−3.221825	−2.309841	−1.399981
C30	−4.433754	−3.026219	−1.620076
C31	−4.611306	−3.926844	−0.531930
C32	−3.507041	−3.763761	0.352697
C33	−5.859870	0.076327	0.183185
C34	−4.678725	0.284879	0.960480
C35	−4.712802	−0.594907	2.081158
C36	−5.910147	−1.361043	2.002909
C37	−6.610590	−0.949778	0.832709
C38	−6.304628	0.856428	−1.029347
C39	−5.211622	1.128193	−2.072692
H1	0.835755	5.947605	1.777271
H2	2.710516	4.021812	1.789061
H3	1.653165	4.828569	−2.359247
H4	0.177536	6.457671	−0.793045
H5	−1.673621	2.938208	−2.035750
H6	0.105484	1.047515	−1.300779
H7	0.266661	1.068302	1.397581
H8	−1.413907	2.969186	2.311189
H9	4.528171	3.668579	−1.049103
H10	3.317817	2.775712	−1.947793
H11	4.083238	2.223653	0.974908
H12	2.928270	1.290920	0.030424
H13	5.892036	1.664874	−0.670413
H14	4.763014	0.695728	−1.592077
H15	7.103913	−1.025625	−0.813087
H16	7.210601	−2.822454	1.193993
H17	5.212427	−2.253394	2.920986
H18	3.887083	−0.110324	1.977440
H19	3.027375	−4.629304	1.025327

H20	5.002965	−5.086995	−0.753549
H21	4.802324	−3.238507	−2.709353
H22	2.702425	−1.645698	−2.132025
H23	−2.943886	5.015236	−0.686839
H24	−3.958991	3.952907	0.295441
H25	−2.816486	5.047009	1.079918
H26	1.214448	−1.281083	0.239394
H27	1.246306	−2.587895	1.414589
H28	−0.119269	−2.729735	−1.331776
H29	−0.122631	−4.018189	−0.137121
H30	−1.318042	−2.524810	1.488604
H31	−1.259332	−1.204422	0.329934
H32	−2.808320	−1.544736	−2.045590
H33	−5.105449	−2.900342	−2.460093
H34	−5.444484	−4.604538	−0.394074
H35	−3.353690	−4.297865	1.283135
H36	−3.885259	0.988439	0.738969
H37	−3.950478	−0.678098	2.845748
H38	−6.223526	−2.130565	2.697231
H39	−7.560173	−1.342778	0.488600
H40	−7.138184	0.325135	−1.506610
H41	−6.719210	1.820342	−0.695635
H42	−4.828266	0.191143	−2.490241
H43	−5.606489	1.733817	−2.896874
H44	−4.363434	1.668466	−1.637280

3.1d E(BS1) = −2700.2274 a.u.

	x	**y**	**z**
Ni1	0.872447	−3.569457	−1.124498
Ni2	6.677169	0.094423	0.570929
Ni3	−1.009033	5.249568	−0.563514
Ni4	−5.746786	−1.522541	0.663172
C1	2.087858	−3.924225	−2.931886
C2	2.978482	−3.480693	−1.912038
C3	2.974309	−4.435787	−0.847352
C4	2.055239	−5.462387	−1.224436
C5	1.513889	−5.155376	−2.505974
C6	−0.406903	−3.185448	0.660701
C7	0.141335	−1.948418	0.207604
C8	−0.355867	−1.707635	−1.104010
C9	−1.207391	−2.795096	−1.454138
C10	−1.249950	−3.713915	−0.362865
C11	3.842266	−4.469858	0.390487
C12	3.599479	−3.388158	1.464744
C13	4.056131	−1.957374	1.096768
C14	5.550982	−1.814026	0.965004
C15	6.464455	−1.573855	2.037790
C16	7.791427	−1.583655	1.521237
C17	7.712030	−1.824330	0.120844
C18	6.335735	−1.963868	−0.220528
C19	5.352931	1.878012	0.218409
C20	6.249238	1.730293	−0.884280
C21	7.584469	1.873957	−0.410032
C22	7.525847	2.107744	0.992931
C23	6.154630	2.107864	1.378400
C24	−2.079744	−4.965123	−0.280090
C25	3.848392	1.891681	0.152732
C26	3.270642	3.303854	−0.073158
C27	1.729978	3.311228	−0.149826
C28	1.163302	4.690929	−0.357131
C29	0.816005	5.627784	0.663668
C30	0.412452	6.846745	0.046452
C31	0.503880	6.672348	−1.363291
C32	0.962158	5.346668	−1.610163
C33	−2.470244	3.654129	0.038491
C34	−2.480090	3.788467	−1.383852
C35	−2.910319	5.105632	−1.715297
C36	−3.168251	5.798634	−0.499271
C37	−2.895249	4.907043	0.577489
C38	−2.164508	2.402409	0.818024
C39	−3.411626	1.527645	1.061859
C40	−3.086143	0.252406	1.854057
C41	−4.260847	−0.648544	2.143432
C42	−4.211915	−2.074057	2.196138
C43	−5.485765	−2.563050	2.604663
C44	−6.338757	−1.440149	2.798660
C45	−5.586856	−0.263539	2.510126
C46	−7.228435	−0.897066	−0.939460
C47	−5.899922	−0.564243	−1.344733
C48	−5.136966	−1.762792	−1.451307
C49	−5.988751	−2.848379	−1.102835
C50	−7.271799	−2.315755	−0.785357
C51	−8.373342	0.077131	−0.811804
C52	−9.399128	−0.257236	0.279308
H1	1.878465	−3.409626	−3.861354
H2	3.570673	−2.575666	−1.952603
H3	1.828483	−6.341224	−0.632077
H4	0.792513	−5.748097	−3.054060
H5	−0.219813	−3.650766	1.621202
H6	0.823687	−1.313567	0.757563
H7	−0.113763	−0.860647	−1.733666
H8	−1.724056	−2.919389	−2.398606
H9	4.898180	−4.430513	0.089072
H10	3.702911	−5.449228	0.865041

H11	2.530923	−3.364825	1.712936
H12	4.129792	−3.691360	2.377355
H13	3.561425	−1.641677	0.171078
H14	3.698986	−1.276916	1.881194
H15	6.186673	−1.407389	3.071998
H16	8.697811	−1.416190	2.089422
H17	8.547026	−1.876364	−0.566441
H18	5.946877	−2.151151	−1.214105
H19	5.956308	1.539164	−1.909964
H20	8.484524	1.799994	−1.007383
H21	8.373230	2.243718	1.653113
H22	5.776845	2.256700	2.383194
H23	−1.626904	−5.703677	0.390450
H24	−3.085208	−4.745619	0.104585
H25	−2.202520	−5.433689	−1.262827
H26	3.430081	1.481158	1.082213
H27	3.506050	1.232545	−0.657202
H28	3.598108	3.966302	0.738486
H29	3.683803	3.724190	−0.999174
H30	1.324389	2.876822	0.774290
H31	1.410905	2.650297	−0.967811
H32	0.854158	5.437181	1.729836
H33	0.079479	7.740694	0.558599
H34	0.251024	7.409396	−2.115120
H35	1.130238	4.903707	−2.584806
H36	−2.202349	3.014135	−2.089339
H37	−3.006914	5.512062	−2.714311
H38	−3.493807	6.827312	−0.407940
H39	−2.989010	5.136855	1.632402
H40	−1.411991	1.805510	0.285070
H41	−1.720025	2.667007	1.787393
H42	−3.858475	1.255806	0.097912
H43	−4.164295	2.122539	1.595525
H44	−2.321032	−0.322678	1.315768
H45	−2.621526	0.545822	2.809707
H46	−3.339982	−2.672481	1.959539
H47	−5.762396	−3.602749	2.727741
H48	−7.377762	−1.473321	3.101382
H49	−5.959188	0.751708	2.569337
H50	−5.542652	0.438513	−1.546810
H51	−4.090170	−1.832199	−1.718406
H52	−5.708800	−3.893792	−1.065133
H53	−8.133006	−2.894428	−0.475367
H54	−8.896640	0.135831	−1.778840
H55	−7.966848	1.081204	−0.634305
H56	−9.862086	−1.235906	0.109093
H57	−10.201812	0.488656	0.296457
H58	−8.929508	−0.276898	1.268805

3.2 E(BS1) = −714.0608 a.u.

	x	**y**	**z**
Ni1	−0.026880	0.781974	0.000955
C1	1.882136	−0.422612	−0.004418
C2	1.895621	0.519507	−1.080079
C3	1.842632	1.835360	−0.536874
C4	1.787037	1.719429	0.881125
C5	1.810919	0.332082	1.204966
C6	−1.964774	1.705248	0.535653
C7	−1.899312	1.592976	−0.882233
C8	−1.827385	0.207121	−1.205496
C9	−1.848907	−0.550320	0.004135
C10	−1.928622	0.388954	1.079411
C11	−1.818589	−2.053876	0.140818
C12	−0.451185	−2.645732	0.554486
C13	0.631184	−2.608711	−0.554554
C14	1.954797	−1.924695	−0.140804
H1	1.947869	0.270206	−2.133467
H2	1.840830	2.758565	−1.102685
H3	1.734420	2.538458	1.587311
H4	1.781577	−0.086727	2.203938
H5	−2.027682	2.626586	1.101016
H6	−1.900542	2.413454	−1.588712
H7	−1.768236	−0.209191	−2.204231
H8	−1.964589	0.137060	2.132828
H9	−2.134875	−2.510630	−0.806273
H10	−2.566641	−2.352289	0.887749
H11	−0.098288	−2.106370	1.442818
H12	−0.607590	−3.684105	0.873835
H13	0.242179	−2.094473	−1.442715
H14	0.858045	−3.633969	−0.873993
H15	2.721623	−2.171643	−0.887467
H16	2.301240	−2.358574	0.806489

3.2a E(BS1) = −715.2712 a.u.

	x	**y**	**z**
Ni1	−0.000047	0.000096	0.423210
C1	−0.912214	−1.742386	1.455192
C2	−1.891809	−0.712267	1.371279
C3	−2.174414	−0.455730	−0.005250
C4	−1.345659	−1.332536	−0.769004
C5	−0.571954	−2.126112	0.127771
C6	1.345766	1.332442	−0.769099
C7	0.572132	2.126181	0.127580
C8	0.912311	1.742533	1.455037

C9	1.891778	0.712296	1.371238
C10	2.174391	0.455620	−0.005251
C11	−3.224451	0.496866	−0.521879
C12	−2.923296	1.119473	−1.891341
C13	3.224317	−0.497161	−0.521762
C14	2.923303	−1.119550	−1.891352
H1	−0.488314	−2.147128	2.365647
H2	−2.353647	−0.204116	2.209768
H3	−1.309690	−1.389353	−1.849595
H4	0.152680	−2.880067	−0.152748
H5	1.309833	1.389165	−1.849695
H6	−0.152384	2.880217	−0.153025
H7	0.488440	2.147415	2.365442
H8	2.353517	0.204156	2.209786
H9	−3.375781	1.294836	0.216729
H10	−4.185997	−0.036026	−0.582983
H11	−1.989288	1.691554	−1.868813
H12	−3.730976	1.795307	−2.194041
H13	−2.827269	0.352514	−2.668256
H14	4.185998	0.035518	−0.582606
H15	3.375318	−1.295245	0.216789
H16	2.827680	−0.352489	−2.668217
H17	3.730859	−1.795587	−2.193927
H18	1.989125	−1.691365	−1.869099

3.2b E(BS1) = −1429.3401 a.u.

	x	**y**	**z**
Ni1	4.232197	−0.406122	−0.133971
Ni2	−4.420792	−0.127734	−0.405009
C1	−5.475858	−2.033935	−0.836504
C2	−4.148021	−2.133558	−1.342267
C3	−3.231140	−2.043995	−0.250778
C4	−4.011745	−1.872083	0.933422
C5	−5.391269	−1.869983	0.574030
C6	−4.041004	1.886999	0.526597
C7	−3.202885	1.729799	−0.619849
C8	−4.028275	1.583486	−1.772249
C9	−5.384717	1.644733	−1.346857
C10	−5.391159	1.828082	0.065955
C11	−1.734311	−2.204989	−0.351551
C12	−0.918809	−1.474298	0.725717
C13	0.594227	−1.663516	0.558718
C14	1.406657	−0.972559	1.664530
C15	2.904398	−1.117957	1.554520
C16	3.635216	−2.228471	1.033689
C17	5.027464	−1.985628	1.216822
C18	5.170985	−0.719836	1.849715
C19	3.865737	−0.184221	2.050154
C20	5.064977	−0.470626	−2.196114
C21	5.501176	0.740440	−1.584718
C22	4.356630	1.538600	−1.281670
C23	3.210680	0.797878	−1.704974
C24	3.644861	−0.434874	−2.273303
C25	4.336498	2.936718	−0.714707
C26	5.443428	3.244350	0.302521
C27	−3.588685	2.163512	1.937140
C28	−3.443768	3.668673	2.229842
H1	−6.385238	−2.057886	−1.423706
H2	−3.871999	−2.262515	−2.382233
H3	−3.623822	−1.766278	1.938689
H4	−6.224840	−1.747819	1.254277
H5	−2.119315	1.728347	−0.610139
H6	−3.684300	1.436624	−2.788423
H7	−6.257064	1.547606	−1.980928
H8	−6.271807	1.905020	0.692731
H9	−1.403730	−1.870942	−1.344716
H10	−1.489221	−3.278158	−0.304194
H11	−1.163350	−0.403525	0.699559
H12	−1.218381	−1.834603	1.719776
H13	0.910681	−1.275996	−0.419341
H14	0.823146	−2.738347	0.552999
H15	1.151209	0.095962	1.687203
H16	1.081351	−1.374867	2.637294
H17	3.206213	−3.108327	0.571205
H18	5.832769	−2.641518	0.910843
H19	6.104904	−0.240085	2.113838
H20	3.632149	0.767621	2.512655
H21	5.702377	−1.281240	−2.526429
H22	6.530906	1.005853	−1.380569
H23	2.183472	1.131952	−1.617247
H24	3.007321	−1.211421	−2.676970
H25	3.356967	3.119264	−0.253847
H26	4.412678	3.656376	−1.544403
H27	5.381230	2.575394	1.167892
H28	5.362220	4.276604	0.661249
H29	6.439023	3.127173	−0.140254
H30	−4.302936	1.727319	2.647574
H31	−2.627001	1.667689	2.122254
H32	−4.397897	4.188557	2.087947
H33	−3.113886	3.837931	3.261782
H34	−2.710874	4.129750	1.558086

3.2c E(BS1) = −2143.4092 a.u.

x	**y**	**z**

Ni1	−0.002877	−2.508744	0.346278	H3	6.047153	3.185215	−1.397775
Ni2	−8.010691	0.822152	0.051379	H4	8.487852	4.021102	−0.604316
Ni3	7.782878	1.243394	0.008802	H5	8.096936	0.311435	−2.786865
C1	7.977716	3.016236	1.331489	H6	6.523916	−1.150461	−1.156037
C2	6.811907	2.301760	1.732470	H7	7.818048	−1.445595	1.197694
C3	5.881481	2.299635	0.648458	H8	10.18474	−0.167475	1.005390
C4	6.495538	3.010910	−0.426746	H9	11.23858	1.616994	−0.832875
C5	7.781949	3.457443	−0.007364	H10	10.38632	1.831815	−2.355231
C6	9.539344	0.336704	−1.076827	H11	12.12157	−0.610350	−1.633718
C7	8.335673	0.012728	−1.772875	H12	12.58396	0.703815	−2.733133
C8	7.504387	−0.761308	−0.912394	H13	11.26059	−0.397173	−3.164719
C9	8.187573	−0.918752	0.326943	H14	3.795684	2.514780	1.053576
C10	9.436527	−0.241263	0.225055	H15	4.157541	1.598600	−0.396162
C11	10.72732	1.073734	−1.638160	H16	4.570716	0.597754	2.477748
C12	11.73371	0.138213	−2.333840	H17	4.940704	−0.325533	1.028671
C13	4.476187	1.751134	0.644084	H18	2.160311	0.731748	1.786110
C14	4.271508	0.447022	1.431094	H19	2.514730	−0.212348	0.346625
C15	2.821426	−0.051298	1.389167	H20	2.910781	−1.172850	3.227938
C16	2.612692	−1.350738	2.182331	H21	3.301866	−2.119028	1.805552
C17	1.207934	−1.900498	2.163028	H22	1.560172	−4.105728	2.283866
C18	0.856473	−3.282170	2.252986	H23	−1.128638	−4.314575	2.362617
C19	−0.562699	−3.393614	2.299969	H24	−2.153349	−1.818028	2.233801
C20	−1.102546	−2.078545	2.229957	H25	−0.103816	−0.085666	2.071000
C21	−0.014410	−1.162320	2.142375	H26	2.196822	−2.322885	−1.582664
C22	1.126288	−2.483201	−1.558785	H27	0.299166	−0.406493	−1.706150
C23	0.123671	−1.472241	−1.617976	H28	−1.702887	−4.259514	−1.360347
C24	−1.161045	−2.093886	−1.555840	H29	0.947400	−4.707110	−1.363012
C25	−0.936188	−3.499616	−1.442600	H30	−2.382028	−0.360160	−1.292265
C26	0.467991	−3.739876	−1.447068	H31	−2.713311	−1.258043	−2.760086
C27	−2.483673	−1.379631	−1.689352	H32	−3.460626	−2.204517	0.055168
C28	−3.678050	−2.069126	−1.013087	H33	−3.805011	−3.077424	−1.431364
C29	−4.988215	−1.288461	−1.177961	H34	−4.876588	−0.283327	−0.748989
C30	−6.186121	−1.989551	−0.518566	H35	−5.189858	−1.145488	−2.248750
C31	−7.507831	−1.272321	−0.641480	H36	−5.967694	−2.153864	0.545541
C32	−7.984486	−0.507029	−1.749283	H37	−6.285638	−2.994731	−0.958616
C33	−9.324220	−0.100929	−1.480573	H38	−7.424603	−0.271262	−2.645446
C34	−9.686785	−0.608501	−0.201451	H39	−9.949424	0.497695	−2.131216
C35	−8.567631	−1.321949	0.315027	H40	−10.636404	−0.463187	0.298043
C36	−7.609205	1.916297	1.948259	H41	−8.521071	−1.825039	1.273705
C37	−8.561326	2.660720	1.194770	H42	−7.777391	1.461860	2.916587
C38	−7.955249	3.071692	−0.031505	H43	−9.580368	2.875315	1.494617
C39	−6.620039	2.565726	−0.026021	H44	−5.894986	2.702174	−0.819800
C40	−6.405011	1.856700	1.191458	H45	−5.491716	1.354267	1.484380
C41	−8.574499	3.949846	−1.087742	H46	−8.147970	3.703132	−2.068682
C42	−8.366087	5.450527	−0.810381	H47	−9.650490	3.743730	−1.157463
H1	8.861772	3.179694	1.935096	H48	−7.299025	5.696616	−0.768531
H2	6.660550	1.839101	2.699654	H49	−8.826252	6.062415	−1.595341

H50	−8.811291	5.736915	0.149093

3.2d E(BS1) = −2857.4779 a.u.

	x	y	z
Ni1	4.524297	2.667765	0.170898
Ni2	11.05295	−3.116328	−0.251227
Ni3	−3.978948	4.242365	−0.470313
Ni4	−11.341484	−3.390411	0.186045
C1	10.77666	−4.578026	−1.901988
C2	9.885846	−3.491416	−2.135963
C3	8.951590	−3.424593	−1.057453
C4	9.288616	−4.475495	−0.151256
C5	10.40657	−5.190168	−0.671679
C6	12.80718	−2.990789	1.175896
C7	11.70995	−2.251053	1.711041
C8	11.39057	−1.192823	0.811175
C9	12.28544	−1.272528	−0.292722
C10	13.15038	−2.381733	−0.069994
C11	13.54064	−4.141276	1.820796
C12	12.69646	−5.001314	2.770141
C13	7.759915	−2.508365	−0.930728
C14	7.968138	−1.074342	−1.443052
C15	6.711133	−0.205364	−1.308303
C16	6.932289	1.239189	−1.784003
C17	5.733437	2.149355	−1.682754
C18	5.780984	3.556908	−1.444431
C19	4.459919	4.082541	−1.529375
C20	3.580664	2.998915	−1.810242
C21	4.363457	1.811339	−1.900198
C22	5.163121	1.604446	2.008185
C23	3.778789	1.340860	1.795639
C24	3.056653	2.568989	1.893587
C25	4.015545	3.594646	2.155426
C26	5.309066	3.002671	2.228501
C27	1.555426	2.707300	1.830158
C28	1.036735	4.043024	1.275356
C29	−0.495120	4.116038	1.232796
C30	−1.010720	5.452695	0.676305
C31	−2.510986	5.592657	0.602587
C32	−3.477954	5.105214	1.534156
C33	−4.768327	5.557507	1.131565
C34	−4.611123	6.326043	−0.056129
C35	−3.224857	6.341103	−0.382483
C36	−3.897954	3.312469	−2.491850
C37	−5.234312	3.214930	−2.009580
C38	−5.238732	2.410568	−0.829403
C39	−3.887091	2.017930	−0.588270
C40	−3.061759	2.570119	−1.610716
C41	−6.449096	1.983604	−0.041501
C42	−7.059440	0.660703	−0.549395
C43	−10.114104	−1.530336	0.522791
C44	−11.468649	−1.161922	0.261836
C45	−12.296567	−1.709861	1.284040
C46	−11.458503	−2.425518	2.185767
C47	−10.118560	−2.316327	1.715355
C48	−10.697650	−4.546422	−1.588842
C49	−12.095644	−4.295362	−1.703828
C50	−12.770687	−4.946340	−0.626805
C51	−11.769247	−5.591629	0.161116
C52	−10.496138	−5.349691	−0.431323
C53	−8.294158	0.222768	0.247498
C54	−8.902559	−1.100546	−0.261705
C55	−14.266348	−5.005469	−0.436605
C56	−14.734618	−5.082611	1.022498
H1	11.60059	−4.872712	−2.539822
H2	9.914820	−2.828424	−2.991537
H3	8.767990	−4.694777	0.773547
H4	10.89246	−6.040331	−0.209959
H5	11.20263	−2.456658	2.644975
H6	10.60451	−0.460941	0.946277
H7	12.29574	−0.619227	−1.156080
H8	13.94208	−2.713135	−0.731659
H9	14.40113	−3.742983	2.380332
H10	13.96875	−4.777277	1.034933
H11	12.30782	−4.410740	3.607522
H12	13.29802	−5.814170	3.191872
H13	11.84123	−5.444411	2.248029
H14	6.912467	−2.953225	−1.476623
H15	7.447410	−2.473506	0.121837
H16	8.277269	−1.100083	−2.497249
H17	8.797996	−0.612516	−0.891502
H18	5.893825	−0.662809	−1.883102
H19	6.380226	−0.193059	−0.261076
H20	7.269173	1.212207	−2.832700
H21	7.764196	1.681043	−1.218568
H22	6.680161	4.126316	−1.240703
H23	4.175358	5.117891	−1.390704
H24	2.506227	3.061266	−1.928247
H25	3.978746	0.819529	−2.101642
H26	5.961220	0.873214	1.997606
H27	3.337266	0.370606	1.600787
H28	3.799618	4.648854	2.275155
H29	6.239460	3.527890	2.404802
H30	1.146047	1.883128	1.229882

H31	1.143348	2.568223	2.842501
H32	1.441025	4.197317	0.265715
H33	1.419695	4.870104	1.889336
H34	−0.887409	3.293661	0.619274
H35	−0.892412	3.960311	2.245497
H36	−0.588778	5.612945	−0.325322
H37	−0.608640	6.266824	1.300390
H38	−3.269236	4.494973	2.403962
H39	−5.702533	5.342208	1.635028
H40	−5.404470	6.799587	−0.620736
H41	−2.776935	6.840559	−1.233584
H42	−3.573452	3.868094	−3.362713
H43	−6.105985	3.679392	−2.455632
H44	−3.550731	1.403849	0.238793
H45	−1.988950	2.453350	−1.697414
H46	−6.182379	1.869051	1.017988
H47	−7.215924	2.768911	−0.084037
H48	−6.293248	−0.126206	−0.507216
H49	−7.323817	0.772859	−1.610317
H50	−11.806296	−0.567943	−0.579357
H51	−13.372092	−1.607834	1.355592
H52	−11.782565	−2.969727	3.063928
H53	−9.244982	−2.760069	2.178319
H54	−9.926373	−4.179506	−2.254318
H55	−12.575347	−3.712098	−2.481038
H56	−11.944905	−6.168790	1.060277
H57	−9.543128	−5.701325	−0.056174
H58	−8.030036	0.110641	1.308483
H59	−9.060918	1.009076	0.204976
H60	−8.134160	−1.884511	−0.219503
H61	−9.168294	−0.985052	−1.321234
H62	−14.721565	−4.131524	−0.920505
H63	−14.657730	−5.880940	−0.977539
H64	−14.395061	−4.210685	1.592256
H65	−15.828410	−5.122026	1.075930
H66	−14.348188	−5.978846	1.520885

3.6 E(BS1) = −1295.5130 a.u.

	x	**y**	**z**
Ni	1.528636	0.000002	0.000036
Si	−1.678730	1.199556	0.000018
Si	−1.678720	−1.199560	−2.3E−05
C	0.999105	1.818343	1.146033
C	0.137464	1.719530	0.000198
C	0.998751	1.817900	−1.145960
C	2.345451	1.967099	−0.712700
C	2.345663	1.967380	0.712286
C	0.998754	−1.817950	1.145925
C	2.345665	−1.967350	−0.712330
C	0.999109	−1.818290	−1.146070
C	0.137467	−1.719530	−0.000230
C	2.345456	−1.967130	0.712662
C	−2.531400	1.903606	1.547709
C	−2.530770	1.903333	−1.548150
C	−2.530730	−1.903330	1.548165
C	−2.531420	−1.903610	−1.547700
H	0.678577	1.767835	2.179896
H	0.677805	1.767050	−2.179670
H	3.214590	2.067406	−1.351140
H	3.214996	2.067949	1.350418
H	0.677808	−1.767150	2.179643
H	3.214999	−2.067880	−1.350460
H	0.678581	−1.767730	−2.179930
H	3.214594	−2.067470	1.351096
H	−2.065110	1.542355	2.471844
H	−2.482480	2.999414	1.555114
H	−3.588690	1.613962	1.580685
H	−2.064890	1.541032	−2.472080
H	−3.588300	1.614532	−1.580840
H	−2.480970	2.999097	−1.556380
H	−2.064840	−1.541030	2.472085
H	−3.588270	−1.614530	1.580873
H	−2.480940	−2.999100	1.556394
H	−2.06516	−1.54236	−2.47184
H	−2.48249	−2.99942	−1.5551
H	−3.58872	−1.61398	−1.58065

3.6a E(BS1) = −1296.7135 a.u.

	x	**y**	**z**
Ni	−0.01191	0.252517	0.500013
Si	−3.50385	−0.61795	−0.16381
Si	3.322925	−0.1411	−0.97279
C	−0.72414	2.373342	0.564781
C	−1.78243	1.513612	0.962902
C	−2.12395	0.646305	−0.13008
C	−1.24084	0.999754	−1.20613
C	−0.38755	2.053768	−0.78282
C	2.034684	−0.63292	0.29239
C	1.05177	−1.67058	0.15202
C	0.317545	−1.7861	1.362908
C	0.8297	−0.82007	2.27678
C	1.877198	−0.11693	1.62379
C	−3.0825	−2.03613	−1.34329
C	−5.14264	0.182873	−0.67392

C	3.862709	1.654392	−0.71681
C	4.827828	−1.28738	−0.88256
H	−0.24529	3.124338	1.181203
H	−2.24924	1.502736	1.940934
H	−1.21648	0.529399	−2.18202
H	0.390859	2.519699	−1.37433
H	0.888161	−2.26173	−0.74138
H	−0.49984	−2.47094	1.552485
H	0.469639	−0.64037	3.282329
H	2.454412	0.691056	2.057807
H	−3.6627	−1.15556	1.221821
H	−2.94181	−1.67172	−2.3683
H	−3.88806	−2.77967	−1.36599
H	−2.16095	−2.54594	−1.04121
H	−5.08282	0.595275	−1.68837
H	−5.40941	1.003293	0.002194
H	−5.96148	−0.54688	−0.65544
H	2.713195	−0.28698	−2.32952
H	4.308051	1.797716	0.275353
H	4.614244	1.946255	−1.45994
H	3.016082	2.344295	−0.8051
H	5.319293	−1.22019	0.095574
H	4.53812	−2.33327	−1.03631
H	5.568109	−1.02839	−1.64958

3.6b E(BS1) = −2592.2340 a.u.

	x	**y**	**z**
Ni	3.982668	−0.00328	−1.05851
Ni	−4.41225	−0.58579	0.153514
Si	0.561234	−0.49925	0.308805
Si	−1.04769	−2.23696	0.169229
Si	−4.48745	3.088712	0.10091
Si	5.997879	0.986568	1.854717
C	4.09728	−2.23102	−1.04339
C	3.211917	−1.8179	−0.01017
C	2.091016	−1.13201	−0.59004
C	2.319401	−1.13813	−2.00848
C	3.54164	−1.80899	−2.28571
C	5.341188	1.324883	0.13557
C	5.96843	1.009834	−1.11744
C	5.176431	1.523365	−2.17897
C	4.041855	2.166399	−1.60515
C	4.14215	2.044084	−0.19319
C	−2.69115	−1.79478	0.98481
C	−3.88394	−2.5969	0.952192
C	−4.86723	−2.01452	1.796571
C	−4.30711	−0.83424	2.365053
C	−2.98148	−0.70118	1.868194
C	−4.71014	−0.44415	−2.05659
C	−4.02563	0.716507	−1.60562
C	−4.87048	1.440398	−0.69666
C	−6.08875	0.685813	−0.60457
C	−5.99135	−0.46308	−1.43368
C	−0.03376	1.102246	−0.52669
C	1.020372	−0.13999	2.11928
C	−1.33968	−2.71161	−1.65088
C	−0.34809	−3.76898	1.060897
C	−5.43351	3.293733	1.726884
C	−4.9027	4.51693	−1.07175
C	7.144409	2.382857	2.423278
C	6.916882	−0.6665	1.919817
H	5.036197	−2.75428	−0.90968
H	3.362562	−1.98713	1.049195
H	1.669001	−0.6924	−2.75174
H	3.983048	−1.95348	−3.26429
H	6.892317	0.456414	−1.2383
H	5.385592	1.423773	−3.23708
H	3.23702	2.644528	−2.14974
H	3.424947	2.426622	0.523467
H	−4.01627	−3.50397	0.373894
H	−5.86972	−2.3896	1.963291
H	−4.80778	−0.15378	3.042713
H	−2.30276	0.105829	2.116161
H	−4.32075	−1.19304	−2.7349
H	−3.02267	1.007145	−1.89424
H	−6.94263	0.941317	0.011877
H	−6.74705	−1.22984	−1.55301
H	−3.01972	3.133576	0.379065
H	−0.224	0.950042	−1.59608
H	0.722955	1.89086	−0.43397
H	−0.96254	1.468844	−0.07474
H	1.373398	−1.042	2.632922
H	0.15787	0.237071	2.681486
H	1.817407	0.611051	2.181907
H	−1.76114	−1.87776	−2.2233
H	−2.03607	−3.55596	−1.73129
H	−0.39841	−3.00874	−2.12844
H	−0.20575	−3.58031	2.13134
H	0.620586	−4.06204	0.638033
H	−1.02987	−4.62326	0.964189
H	−6.51781	3.254119	1.566144
H	−5.2049	4.261124	2.189792
H	−5.17255	2.507903	2.444455
H	−5.97288	4.534182	−1.31107

H	−4.35377	4.425864	−2.01612
H	−4.64232	5.484008	−0.62418
H	4.826637	0.940105	2.781496
H	8.022021	2.465452	1.770666
H	6.628182	3.349608	2.40748
H	7.50138	2.209331	3.445924
H	7.765486	−0.67699	1.224695
H	7.312199	−0.85553	2.925003
H	6.257383	−1.5001	1.654154

3.6c E(BS1) = −3887.7559 a.u.

	x	**y**	**z**
Ni	6.626435	−1.91237	0.241785
Ni	0.402267	3.945541	0.075255
Ni	−7.40885	−1.12791	−0.14297
Si	4.240086	0.807378	−0.53825
Si	4.073364	3.106229	0.021218
Si	−2.42302	1.568769	−0.57808
Si	−4.4309	0.98027	0.536618
Si	−9.49994	−4.1205	0.207583
Si	9.391798	−4.26577	−0.25233
C	8.104679	−0.27063	0.571917
C	7.144632	0.165601	−0.38108
C	5.84563	0.193923	0.231598
C	6.042437	−0.23858	1.588023
C	7.41958	−0.52179	1.796217
C	7.558219	−3.89121	−0.24645
C	6.635019	−4.06246	0.840781
C	5.326255	−3.73258	0.399111
C	5.412669	−3.35076	−0.97147
C	6.774447	−3.44605	−1.36435
C	2.539397	3.945012	−0.68755
C	2.119956	5.290021	−0.40311
C	1.02161	5.628511	−1.23829
C	0.730393	4.496296	−2.05289
C	1.655008	3.47052	−1.71392
C	0.054358	3.416123	2.207634
C	−0.32737	2.308282	1.401181
C	−1.41969	2.692873	0.551427
C	−1.69025	4.069636	0.861047
C	−0.7935	4.510514	1.871333
C	−5.36923	−0.26178	−0.52262
C	−5.2757	−1.69378	−0.45799
C	−6.0516	−2.26389	−1.5038
C	−6.64353	−1.19546	−2.23811
C	−6.22748	0.024551	−1.63915
C	−9.15811	−0.01215	0.702063
C	−9.63386	−1.15673	0.008825
C	−9.1234	−2.34001	0.643454
C	−8.32078	−1.88386	1.743398
C	−8.34333	−0.46414	1.780765
C	2.793235	−0.20655	0.16637
C	4.331051	0.555998	−2.42212
C	4.103655	3.299061	1.914863
C	5.600997	4.007774	−0.67498
C	−2.83836	2.462231	−2.20633
C	−1.41224	0.007367	−0.97062
C	−5.50233	2.530635	0.7984
C	−4.03576	0.194603	2.222266
C	−11.0223	−4.73905	1.149573
C	−9.77136	−4.32156	−1.65482
C	10.16329	−3.89984	1.436722
C	9.712211	−6.07085	−0.72807
H	9.164208	−0.40579	0.392814
H	7.360298	0.423687	−1.41096
H	5.263114	−0.34372	2.333518
H	7.865154	−0.8832	2.714968
H	6.89512	−4.37954	1.843942
H	4.426251	−3.74834	1.00143
H	4.588692	−3.03036	−1.59689
H	7.163471	−3.20941	−2.34775
H	2.568542	5.94512	0.334571
H	0.486514	6.570383	−1.24045
H	−0.06408	4.42573	−2.78513
H	1.682964	2.485381	−2.16366
H	0.858003	3.432709	2.933103
H	0.138254	1.330621	1.4202
H	−2.45082	4.682275	0.390842
H	−0.7458	5.507238	2.292769
H	−4.71272	−2.25417	0.278679
H	−6.18425	−3.32163	−1.69508
H	−7.30653	−1.29509	−3.08882
H	−6.52268	1.014158	−1.96754
H	−9.36174	1.020239	0.44562
H	−10.2696	−1.13716	−0.8686
H	−7.77487	−2.52217	2.428209
H	−7.82182	0.163812	2.492468
H	−8.32748	−4.94671	0.627824
H	2.738209	−0.12331	1.258417
H	2.909062	−1.26908	−0.07988
H	1.833237	0.133195	−0.2391
H	5.175445	1.099476	−2.86194
H	3.421079	0.913563	−2.918
H	4.453846	−0.50574	−2.66889

H	3.251108	2.797683	2.386828
H	4.071007	4.35659	2.206378
H	5.02181	2.866875	2.330484
H	5.621492	3.975578	−1.77045
H	6.529367	3.555024	−0.30612
H	5.599573	5.063703	−0.37664
H	−3.32903	3.426796	−2.02981
H	−3.51313	1.853881	−2.82075
H	−1.93052	2.653571	−2.79122
H	−1.1133	−0.52548	−0.06033
H	−0.5012	0.255609	−1.52929
H	−2.00137	−0.6881	−1.58
H	−5.80347	2.982543	−0.15419
H	−4.95397	3.291275	1.367052
H	−6.4163	2.286669	1.35348
H	−3.45582	−0.72972	2.114792
H	−4.95333	−0.05101	2.771006
H	−3.44549	0.882197	2.839327
H	−11.9164	−4.16496	0.8779
H	−10.8836	−4.64311	2.232586
H	−11.2212	−5.79508	0.928989
H	−10.6136	−3.71086	−2.00294
H	−9.99567	−5.36499	−1.90662
H	−8.88412	−4.02137	−2.22332
H	10.02627	−3.39363	−1.28687
H	9.701764	−4.50754	2.224909
H	11.23648	−4.12486	1.433766
H	10.04031	−2.84668	1.712592
H	9.268487	−6.75833	0.002254
H	9.280361	−6.30472	−1.70796
H	10.78772	−6.28142	−0.77678

3.13 E(BS1) = −1370.8420 a.u.

	x	**y**	**z**
Ni	−1.53384	−0.00062	−7.7E−05
Si	1.62109	−1.61167	0.000126
Si	1.619727	1.612856	0.000035
O	2.040169	0.000762	0.000573
C	−2.45984	−1.91274	−0.71312
C	−1.1085	−1.85423	−1.14677
C	−0.24334	−1.81217	0.000073
C	−1.10876	−1.85411	1.146739
C	−2.46001	−1.91269	0.712782
C	−2.46142	1.910931	0.713138
C	−1.11005	1.853041	1.146772
C	−0.24486	1.811776	−0.0001
C	−1.11032	1.853573	−1.14674
C	−2.46159	1.911264	−0.71275
C	2.347428	−2.39868	1.550367
C	2.347403	−2.39774	−1.55062
C	2.345591	2.399537	−1.5506
C	2.345331	2.400383	1.550363
H	−3.33507	−1.94692	−1.35032
H	−0.78343	−1.82976	−2.18008
H	−0.78388	−1.82964	2.180105
H	−3.33538	−1.94675	1.349797
H	−3.33666	1.944469	1.350365
H	−0.78495	1.828676	2.180073
H	−0.78547	1.829488	−2.18013
H	−3.33697	1.944999	−1.34975
H	1.930866	−1.95345	2.461872
H	3.434093	−2.25624	1.583133
H	2.146615	−3.47639	1.582444
H	1.931823	−1.95098	−2.46182
H	2.145571	−3.47522	−1.58411
H	3.434229	−2.25631	−1.58259
H	1.930631	1.952318	−2.46186
H	3.432563	2.259188	−1.58235
H	2.142694	3.476809	−1.58419
H	1.929803	1.954114	2.461828
H	2.142939	3.477781	1.582996
H	3.432223	2.259537	1.58264

3.13a E(BS1) = −1372.0268 a.u.

	x	**y**	**z**
Ni	2.059119	−0.39462	−0.05418
Si	−1.25504	1.15339	0.120316
Si	−3.96492	−0.44926	−0.34228
O	−2.8652	0.718477	0.092442
C	1.01224	−2.30524	0.466675
C	0.287949	−1.2161	1.019191
C	−0.17932	−0.36889	−0.04446
C	0.281908	−0.97727	−1.26249
C	1.008394	−2.15669	−0.95122
C	3.03663	1.613574	0.071433
C	3.428056	0.844312	1.204631
C	4.143885	−0.29436	0.736586
C	4.194155	−0.22915	−0.68534
C	3.509422	0.949824	−1.0968
C	−0.94469	2.001	1.77318
C	−0.94826	2.332552	−1.31797
C	−5.6709	0.344816	−0.36551
C	−3.90155	−1.89586	0.862293
H	1.497963	−3.09748	1.023118

H	0.124878	−1.04485	2.076541
H	0.110682	−0.59305	−2.26087
H	1.489329	−2.81711	−1.66236
H	2.476001	2.539411	0.09421
H	3.213908	1.080282	2.239414
H	4.568181	−1.07694	1.352929
H	4.66275	−0.954	−1.33906
H	3.368414	1.280433	−2.11811
H	−3.6404	−0.94932	−1.71365
H	−1.12249	1.316862	2.611373
H	−1.61778	2.857182	1.899892
H	0.086226	2.366136	1.851168
H	−1.11976	1.839819	−2.28256
H	0.079046	2.715832	−1.31656
H	−1.62938	3.190006	−1.26162
H	−5.94212	0.726851	0.625933
H	−6.43812	−0.37864	−0.66855
H	−5.70598	1.185288	−1.06801
H	−4.17258	−1.58025	1.877167
H	−2.89464	−2.32735	0.90234
H	−4.59594	−2.69038	0.561158

3.13b E(BS1) = −2742.8711 a.u.

	x	**y**	**z**
Ni	2.747313	2.627062	−0.18168
Ni	−1.35277	−1.9154	0.302333
Si	4.019967	−0.80996	−0.65973
Si	2.12955	−2.94418	0.846024
Si	−4.4341	−0.30035	−0.90859
Si	−5.8049	2.172436	0.560334
O	2.781979	−1.60054	0.119304
O	−5.37617	1.034109	−0.57162
C	3.07172	2.842865	−2.37927
C	4.007837	1.901774	−1.87191
C	3.298244	0.774587	−1.33375
C	1.903764	1.054939	−1.52499
C	1.764475	2.317421	−2.16158
C	2.650545	2.454128	2.041034
C	3.820322	3.190166	1.693921
C	3.409322	4.383809	1.035326
C	1.986601	4.385253	0.974286
C	1.517014	3.19359	1.596581
C	0.444944	−3.23437	0.089705
C	−0.63938	−3.99272	0.650453
C	−1.70719	−4.04369	−0.28493
C	−1.30505	−3.31673	−1.44358
C	0.007416	−2.82416	−1.21458
C	−1.68774	−0.74056	2.172257
C	−2.94608	−0.99467	1.565772
C	−2.98431	−0.36937	0.272439
C	−1.71034	0.275886	0.110418
C	−0.91813	0.049167	1.26753
C	−7.41924	2.96289	0.003739
C	5.429872	−0.45867	0.543764
C	4.66068	−1.87612	−2.0814
C	1.982344	−2.63932	2.700748
C	3.237746	−4.44375	0.54224
C	−3.83258	−0.10687	−2.68279
C	−5.50872	−1.83731	−0.71816
C	−4.44009	3.457208	0.746266
H	3.308147	3.798996	−2.82999
H	5.084615	2.025141	−1.88369
H	1.095232	0.40567	−1.21373
H	0.832477	2.805482	−2.41946
H	2.627925	1.496613	2.54601
H	4.842356	2.891065	1.889357
H	4.064114	5.150617	0.640749
H	1.369759	5.153685	0.525402
H	0.481412	2.897617	1.70455
H	−0.65122	−4.44488	1.635333
H	−2.66204	−4.53333	−0.13707
H	−1.89971	−3.15805	−2.3348
H	0.584967	−2.22391	−1.90699
H	−1.36258	−1.10153	3.140213
H	−3.74543	−1.57934	2.005104
H	−1.39809	0.838709	−0.76086
H	0.099524	0.387424	1.415958
H	−6.01987	1.502515	1.879746
H	−7.30222	3.460567	−0.96632
H	−8.21107	2.212253	−0.09991
H	−7.7605	3.713198	0.727898
H	5.074745	0.105712	1.413248
H	5.888074	−1.38788	0.904413
H	6.220287	0.132476	0.063655
H	3.854352	−2.13037	−2.77941
H	5.432939	−1.34393	−2.65099
H	5.100917	−2.81311	−1.71883
H	1.390527	−1.74069	2.907357
H	1.495764	−3.48301	3.206582
H	2.970357	−2.50595	3.157861
H	3.344277	−4.65039	−0.52892
H	4.241491	−4.29399	0.959741
H	2.814623	−5.3414	1.010187
H	−3.18768	0.773112	−2.79206

H	−3.26255	−0.98262	−3.01483
H	−4.68223	0.022017	−3.36369
H	−5.8669	−1.95057	0.31215
H	−6.39033	−1.77142	−1.36682
H	−4.96076	−2.74917	−0.98416
H	−4.28068	4.005719	−0.19013
H	−4.68781	4.188227	1.526172
H	−3.49232	2.979855	1.021353

3.13c E(BS1) = −4113.7148 a.u.

	x	**y**	**z**
Ni	5.672344	−3.05204	0.245975
Ni	1.720405	3.738925	1.094981
Ni	−4.61825	−2.44487	0.817209
Si	4.984547	−0.16982	−1.90941
Si	3.468986	2.690946	−2.06341
Si	−0.23492	0.655436	1.584844
Si	−3.35099	0.636561	2.341082
Si	−6.44507	−1.29838	−2.19559
Si	−6.07273	1.791292	−2.8609
O	3.900815	1.089628	−1.99812
O	−1.80626	0.199977	1.903305
O	−5.95184	0.293673	−2.15172
C	4.575843	−1.91754	1.833808
C	5.173556	−0.99118	0.937914
C	4.615197	−1.17351	−0.37467
C	3.660848	−2.24058	−0.25094
C	3.636296	−2.69426	1.094543
C	7.159597	−4.50022	1.067917
C	6.249293	−5.2096	0.233166
C	6.375651	−4.69926	−1.09011
C	7.365086	−3.67441	−1.07323
C	7.849192	−3.55098	0.260795
C	3.465707	3.358664	−0.31183
C	3.63063	2.595302	0.892953
C	3.72611	3.482273	1.999673
C	3.618236	4.813894	1.5015
C	3.456003	4.736888	0.091764
C	−0.00536	4.771227	2.083055
C	0.071385	3.439536	2.569438
C	−0.12681	2.522819	1.480344
C	−0.32606	3.338732	0.313661
C	−0.25133	4.709217	0.680362
C	−4.34916	−0.93858	2.453049
C	−5.75002	−1.09491	2.175366
C	−6.13665	−2.43255	2.460187
C	−4.98128	−3.12999	2.918947
C	−3.8923	−2.2183	2.914393
C	−3.90735	−4.09793	−0.49775
C	−5.18424	−3.67449	−0.95478
C	−5.10249	−2.30414	−1.37935
C	−3.74117	−1.90382	−1.16566
C	−3.01163	−2.99658	−0.62651
C	4.743867	−1.22604	−3.4515
C	6.740741	0.515898	−1.82153
C	4.722818	3.673572	−3.07931
C	1.784007	2.77887	−2.90171
C	0.250126	−0.12641	−0.05761
C	0.846162	0.012673	2.988423
C	−4.11345	1.792963	1.061082
C	−3.29328	1.498353	4.021349
C	−6.66373	−1.842	−3.99108
C	−8.08565	−1.48723	−1.28343
C	−4.34233	2.453705	−3.19272
C	−7.0407	2.949633	−1.73591
H	4.807297	−2.02908	2.886009
H	5.937984	−0.26978	1.201107
H	3.058951	−2.64113	−1.05771
H	3.026364	−3.49886	1.486504
H	7.296534	−4.65032	2.131439
H	5.572416	−5.99248	0.551361
H	5.81273	−5.02653	−1.95505
H	7.689456	−3.08959	−1.92456
H	8.604185	−2.85434	0.6027
H	3.679746	1.514654	0.944335
H	3.846636	3.198666	3.038057
H	3.639033	5.720966	2.0932
H	3.344176	5.588468	−0.56955
H	0.12548	5.673688	2.667681
H	0.26663	3.16024	3.597974
H	−0.50079	2.969396	−0.68906
H	−0.34696	5.556291	0.012044
H	−6.40593	−0.31862	1.799542
H	−7.12679	−2.85278	2.332844
H	−4.93756	−4.17616	3.19679
H	−2.87221	−2.45224	3.193956
H	−3.66498	−5.07536	−0.0986
H	−6.07697	−4.28907	−0.97025
H	−3.34216	−0.9183	−1.36911
H	−1.96754	−2.98526	−0.33992
H	−6.80156	1.66027	−4.16081
H	5.429265	−2.08164	−3.46662
H	3.720239	−1.61442	−3.5109
H	4.922751	−0.63387	−4.35709

H	7.48241	−0.28998	−1.76844	H	−4.27874	1.27918	0.10753
H	6.969121	1.123202	−2.70558	H	−4.30027	1.767638	4.363311
H	6.877575	1.153188	−0.93947	H	−2.8476	0.847756	4.783213
H	4.446122	4.734587	−3.12727	H	−2.69795	2.41858	3.970645
H	5.726242	3.614997	−2.6423	H	−6.96633	−2.89527	−4.04494
H	4.7782	3.300892	−4.10959	H	−7.4314	−1.2477	−4.50165
H	1.383898	3.800326	−2.89638	H	−5.72854	−1.73864	−4.55372
H	1.852743	2.449796	−3.94587	H	−8.38389	−2.54171	−1.22218
H	1.062853	2.130602	−2.39287	H	−8.01556	−1.10218	−0.26001
H	1.300914	0.059445	−0.30829	H	−8.89122	−0.94652	−1.79557
H	0.10566	−1.21282	−0.01408	H	−4.38499	3.434629	−3.68256
H	−0.36856	0.253134	−0.87997	H	−3.77882	2.56872	−2.25913
H	1.910846	0.173231	2.782132	H	−3.7781	1.777974	−3.84587
H	0.606408	0.501666	3.940379	H	−6.53597	3.072662	−0.77047
H	0.691799	−1.0646	3.123702	H	−7.14517	3.942713	−2.19084
H	−5.08289	2.176318	1.405024	H	−8.04837	2.564265	−1.54125
H	−3.46033	2.655787	0.882534				

v. References

1. M. J. Frisch, G. W. Trucks, H. B. Schlegel, G. E. Scuseria, M. A. Robb, J. R. Cheeseman, G. Scalmani, V. Barone, B. Mennucci, G. A. Petersson, H. Nakatsuji, M. Caricato, X. Li, H. P. Hratchian, A. F. Izmaylov, J. Bloino, G. Zheng, J. L. Sonnenburg, M. Hada, M. Ehara, K. Toyota, R. Fukuda, J. Hasegawa, M. Ishida, T. Nakajima, Y. Honda, O. Kitao, H. Nakai, T. Vreven, J. A. Montgomery Jr., J. E. Peralta, F. Ogliaro, M. Bearpark, J. J. Heyd, E. Brothers, K. N. Kudin, V. N. Staroverov, T. Keith, R. Kobayashi, J. Normand, K. Raghavachari, A. Rendell, J. C. Burant, S. S. Iyengar, J. Tomasi, M. Cossi, N. Rega, J. M. Millam, M. Klene, J. E. Knox, J. B. Cross, V. Bakken, C. Adamo, J. Jaramillo, R. Gomperts, R. E. Stratmann, O. Yazyev, A. J. Austin, R. Cammi, C. Pomelli, J. W. Ochterski, R. L. Martin, K. Morokuma, V. G. Zakrzewski, G. A. Voth, P. Salvador, J. J. Dannenberg, S. Dapprich, A. D. Daniels, O. Farkas, J. B. Foresman, J. V. Ortiz, J. Cioslowski and D. L. Fox, *Gaussian 09, Revision B.01*, Wallingford CT, 2010.

2. S. H. Vosko, L. Wilk and M. Nusair, *Can. J. Phys.*, 1980, **58**, 1200.

3. A. D. Becke, *Phys. Rev. A*, 1988, **38**, 3098.

4. J. C. Slater, *Quantum Theory of Molecules and Solids*, McGraw-Hill, 1974.

5. B. Miehlich, A. Savin, H. Stoll and H. Preuss, *Chem. Phys. Lett.*, 1989, **157**, 200-206.

6. C. Lee, W. Yang and R. G. Parr, *Phys. Rev. B*, 1988, **37**, 785-789.

7. A. D. Becke, *J. Chem. Phys.*, 1993, **98**, 5648-5652.

8. S. Grimme, S. Ehrlich and L. Goerigk, *J. Comput. Chem.*, 2011, **32**, 1456-1465.

9. A. Bergner, M. Dolg, W. Küchle, H. Stoll and H. Preuß, *Mol. Phys.*, 1993, **80**, 1431-1441.

10. M. J. Frisch, J. A. Pople and J. S. Binkley, *J. Chem. Phys.*, 1984, **80**, 3265-3269.

11. P. C. Hariharan and J. A. Pople, *Theor. Chem. Acc.*, 1973, **28**, 213-222.

12. B. Marten, K. Kim, C. Cortis, R. A. Friesner, R. B. Murphy, M. N. Ringnalda, D. Sitkoff and B. Honig, *J. Phys. Chem*, 1996, **100**, 11775-11788.

13. D. J. Tannor, B. Marten, R. Murphy, R. A. Friesner, D. Sitkoff, A. Nicholls, B. Honig, M. Ringnalda and W. A. Goddard III, *J. Am. Chem. Soc.*, 1994, **116**, 11875-11882.

14. A. Berenbaum, M. Ginzburg-Margau, N. Coombs, A. J. Lough, A. Safa-Sefat, J. E. Greedan, G. A. Ozin and I. Manners, *Adv. Mater.*, 2003, **15**, 51-55.

Appendix IV

i. Materials

Transformation of Competent Cells

Three plasmids containing NDM-1 (1 µL), KPC-3 (0.5 µL), or CTX-M-15 (0.5 µL) carried on the pOPIN F vector were added to competent soluBL21 *E.coli* cells (3×50 µl) and cooled to 0 °C for 30 min, then heat-shocked (42 °C, 30 sec) and added to an SOC solution (500 µL). Cells were incubated at 37 °C for 1.5 h, then centrifuged. The resuspended pellets were streaked onto carbenicillin plates (LB agar) and allowed to incubate at 37 °C for 16 h. The surviving cells contained plasmid inserts.

Large Scale Expression and Purification

A colony expressing CTX-M-15 was looped into LB broth (50 mL), to which carbenicillin was added (50 µg mL^{-1}). This was agitated for 16 h at 37 °C, before 5 mL was added to 6×500 mL auto-induction terrific broth containing 250 µL carbenicillin. After incubation at 37 °C for 6 h and at 18 °C for 16 h, cells were centrifuged. The dried pellet was resuspended in 35 mL RB and a Protease Inhibitor Cocktail tablet (Roche) was added. Cells were homogenised in 100 mL buffer and lysozyme was added, then passed through a cell disrupter and centrifuged. 200 µL imidazole was added to the supernatant with washed Ni-NTA agarose beads and rotated for 1.5 h. The beads were centrifuged, then, along with 10 mL supernatant, were washed through a column with WB1 and WB2 sequentially. EB was passed through the column, collected, and concentrated in a 10 kDa molecular weight cut off concentrator. DB was added to lower the imidazole concentration to 20 mM. 3C protease was added and left overnight. This was concentrated further and added to Ni-NTA beads before being passed through a column again. This was concentrated once more to reach an appropriate concentration for kinetic experiments and loaded onto Superdex 75 column equilibrated with PBS. Peak fractions were run on an SDS-PAGE gel then pooled and

concentrated. The concentration of purified protein was determined (using Thermo scientific nanodrop lite). This was repeated using a colony expressing KPC-3. The experiment for NDM-1 was performed in the same way but required different buffers containing Zinc and TCEP (Table A4.1).

Production of Competent Cells

E.coli ATCC 25922 glycerol stock cells were streaked onto an LB plate and incubated for 16 h. A single colony was looped into 10 mL LB broth and agitated for 16 h. 1 mL of the resultant broth was added to LB broth (49 mL) and allowed to grow until an OD of 0.4–0.6 was reached, when it was centrifuged. The pellet was resuspended in 50 mL cold Mili-Q water and was pelleted again. This step was repeated once more with Mili-Q water and with cold 10% glycerol twice before being resuspended in 500 µL 10% glycerol. 0.5 µL of each insert (CTX-M-15, KPC-3, and NDM-1 carried on the pSU18 vector) was added to 50 µL of this resuspension in 4 chilled electroporation cuvettes. After electroporation, 500 µL of pre-warmed SOC media was added to each cuvette. These were incubated for 1.5 h, then centrifuged. The pellets were resuspended and incubated overnight on 30 mg mL^{-1} chloramphenicol plates. A colony from each plate was looped into 50 mL nutrient broth (chloramphenicol concentration: 30 mg mL^{-1}) and incubated for 16 h.

Minimum Inhibitory Concentration Determination

Glycerol stocks of each insert (control, NDM-1, KPC-3, CTX-M-15) were plated on 30 mg mL^{-1} chloramphenicol plates and grown for 16 h. Cells from the plates were diluted in PBS until an absorbance of 0.010 OD at 600 nm was reached. 150 µL of a 10% dilution of Mueller-Hinton (MH, containing 30 µg mL^{-1} chloramphenicol) was plated into three rows of wells of a 96 well plate. 300 µL of meropenem (128 mg L^{-1}) in MH (and chloramphenicol) was added to the final column wells and serial diluted across the wells. Diluted cells (10 µL) were added to the wells, and the plates incubated for 16 h at 37 °C. Absorbance was measured at 600 nm. Experiments were repeated with a serial dilution of cephalothin,

cefaclor, **[4.2][NO_3]$_n$**, and a mix of polymer and each antibiotic (128 mg L^{-1} polymer and 128 mg L^{-1} antibiotic).

Table A4.1. Description of buffers (all buffer reagents sourced from Sigma Aldrich).

Buffer	Contents
Resuspension Buffer (RB)	50 mM TRIS pH 8, 400 mM NaCl
Wash Buffer 1 (WB1)	50 mM Hepes pH 7.5, 400 mM NaCl, 10 mM Imidazole
Wash Buffer 2 (WB2)	50 mM Hepes pH 7.5, 200 mM NaCl, 20 mM Imidazole
Elution Buffer (EB)	50 mM Hepes pH 7.5, 150 mM NaCl, 400 mM Imidazole
Dialysing Buffer (DB)	50 mM Hepes pH 7.5, 150 mM NaCl
Resuspension Buffer + Zinc	50 mM TRIS pH 8, 400 mM NaCl, 100 µM $ZnCl_2$
Wash Buffer 1 + Zinc	50 mM Hepes pH 7.5, 400 mM NaCl, 10 mM Imidazole, 1 mM TCEP, 100 µM $ZnCl_2$
Wash Buffer 2 + Zinc	50 mM Hepes pH 7.5, 200 mM NaCl, 20 mM Imidazole, 1 mM TCEP, 100 µM $ZnCl_2$
Elution Buffer + Zinc	50 mM Hepes pH 7.5, 150 mM NaCl, 400 mM Imidazole, 1 mM TCEP, 100 µM $ZnCl_2$
Dialysing Buffer + Zinc	50 mM Hepes pH 7.5, 150 mM NaCl, 1 mM TCEP, 100 µM $ZnCl_2$
Kinetics Buffer (KB)	5 mM Hepes pH 7.5

Table A4.2. Descriptions of media.

Media	Contents
LB agar	1% tryptone; 0.5% yeast extract; 1% NaCl 1.5% agar to pH7
LB broth	1% tryptone; 0.5% yeast extract; 1% NaCl to pH7
SOC media	2% tryptone; 0.5% yeast extract; 10 mM NaCl; 2.5 mM KCl; 10 mM $MgCl_2$; 20 mM glucose
Autoinduction terrific broth	0.5% glycerol; 0.25% aspartate; 0.05% glucose; 0.2% α-lactose; 25 m Na_2HPO_4; 25 mM KH_2PO_4; 50 mM NH_4Cl; 5 mM Na_2SO_4; 2 mM $MgSO_4$
2xYT media	1.6% tryptone; 1% yeast extract; 0.5% NaCl to pH 6.8
Mueller Hinton	1.7% agar, 0.15% starch, 0.2% beef extract, 1.75% casein hydrolysate

Table A4.3. Bacterial strains and vectors.

Name	Genotype	Supplier	Vector	Vector supplier	β-lactamase
SoluBL21	SoluBL21™ Strain: F- ompT hsdSB (rB - mB -) gal dcm (DE3)	Genlantis	pOPIN F	Addgene	CTX-M-15 KPC-3 NDM-1
ATCC	ATCC™ Strain: 25922	ATCC	pSU18	Addgene	CTX-M-15 KPC-3 NDM-1 Control (empty)

ii. Additional Tables

Table A4.4. Minimum inhibitory concentrations (MIC)s (mg L^{-1}) of **[4.2][NO_3]$_n$** and β-lactam antibiotics against β-lactamase expressing *E. coli*.

Recombinant	**[4.2][NO_3]$_n$**	Meropenem	Cephalothin	Cefaclor
Control	16	<0.25	8	2–4
CTX-M-15	16	<0.25	>128	>128
KPC-3	16	0.25	>128	>128
NDM-1	16	16–32	>128	>128

Table A4.5. MICs (mg L^{-1}) of **[4.2][NO_3]$_n$** co-administration upon β-lactam antibiotic susceptibility of β-lactamase expressing *E. coli*. All samples were administered with Co^+:antibiotic 1:1 molar ratios.

Recombinant	Meropenem + **[4.2][NO_3]$_n$**	Cephalothin + **[4.2][NO_3]$_n$**	Cefaclor + **[4.2][NO_3]$_n$**
Control	<0.25	4–8	2–8
CTX-M-15	<0.25	16	16
KPC-3	0.25–0.5	16	16
NDM-1	16	16	16

Table A4.6. Specific conditions for the attempted syntheses of **[4.4][PF$_6$]$_n$** in organic solvents.*

Reaction	Solvent	Coupling reagent	Reaction time / h	Temperature / °C
4.3.2a†	MeCN	DIC (no base)	48	60
4.3.2b	MeCN	DIC	48	60
4.3.2c	MeCN	DIC	72	60
4.3.2d	MeCN	DIC (1.5 eq.)	72	60
4.3.2e	MeCN	DIC (10 eq.)	72	60
4.3.2f	MeCN	HATU	72	60
4.3.2g	DMF	DIC	72	60
4.3.2h	MeCN : H_2O (5 : 1)	DIC	72	60
4.3.2i	MeCN	DIC	168	40
4.3.2j	MeCN	DIC	168	60

*General conditions: **[4.3][PF$_6$]** (50 mg, 118 mmol) was dissolved in acetonitrile (1 mL), to which DIPEA (41.3 μL, 237 mmol) and coupling reagent (2.05 equiv., 243 mmol) were added. The brown mixture was stirred at a specified temperature for 1 h, before 2,2′-(ethylenedioxy)bis(ethylamine) (17.3 μL, 118 mmol) was added. The reaction was then stirred at this temperature for 48–168 h.

†No base (DIPEA) was added to this reaction.

iii. Additional Figures

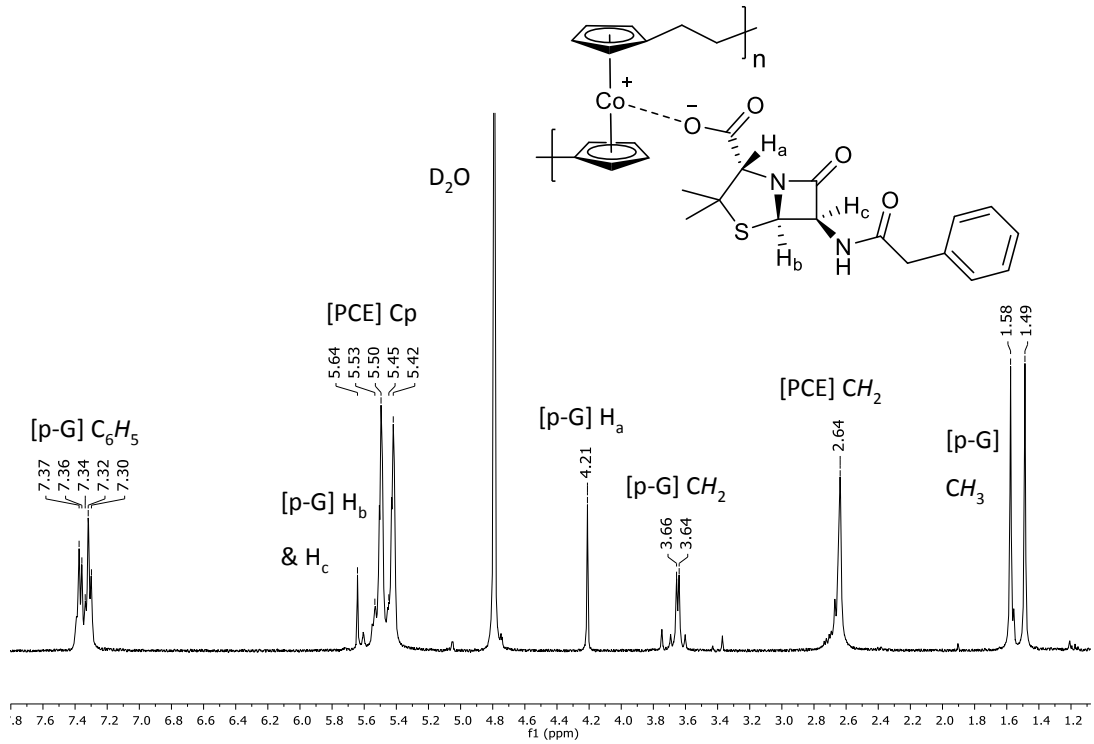

Figure A4.1. ^{1}H NMR spectrum (400 MHz, D_2O) of the bioconjugate **[4.2][penicillin-G]$_n$**.

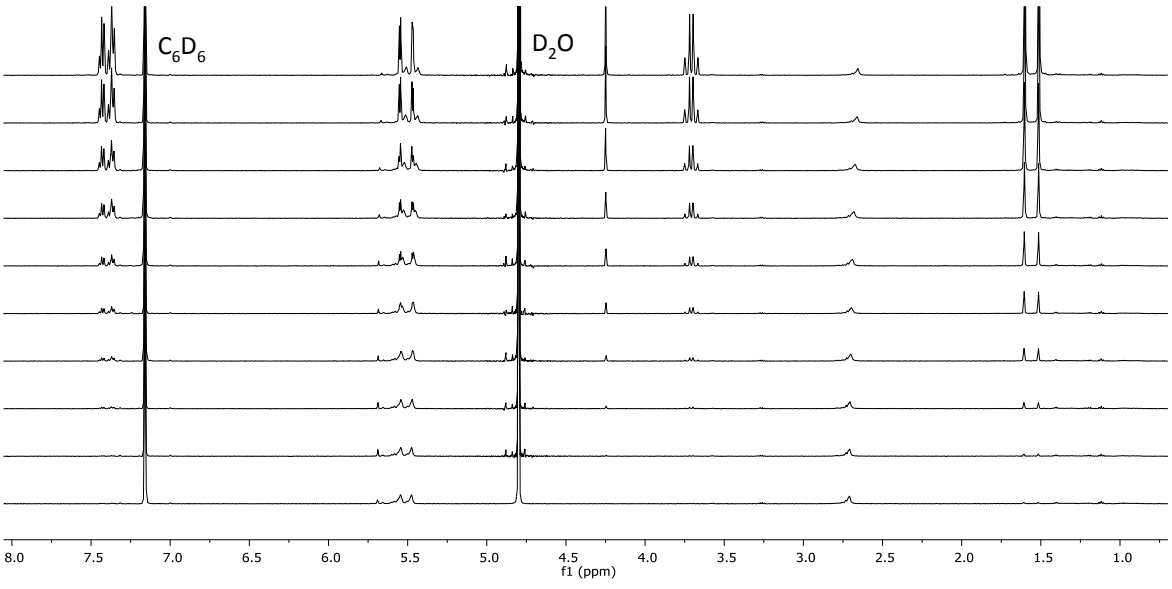

Figure A4.2. Stacked ^{1}H NMR spectra (500 MHz, D_2O) displaying the titration of sodium penicillin-G into **[4.2][Cl]$_n$** (up: increasing sodium penicillin-G).

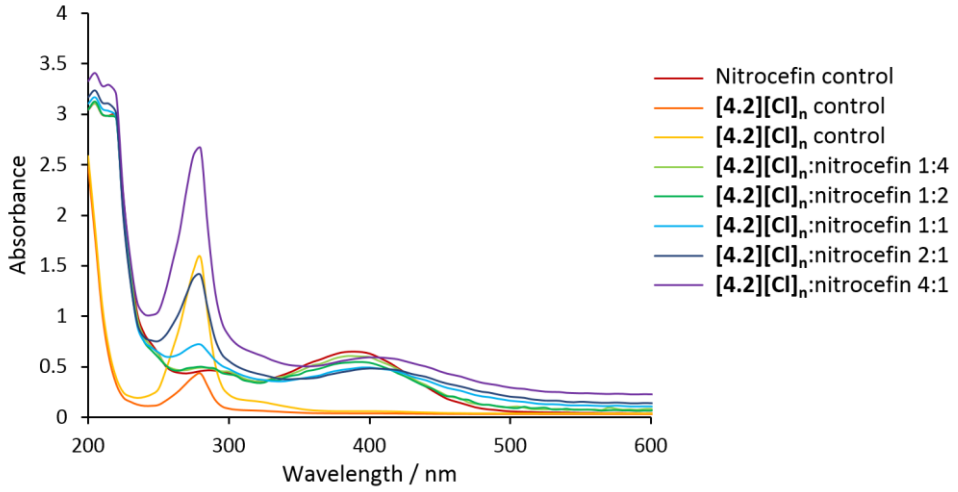

Figure A4.3. UV/Vis spectra of **[4.2][Cl]$_n$**/nitrocefin bioconjugates prior to addition of β-lactamase enzyme KPC-3.

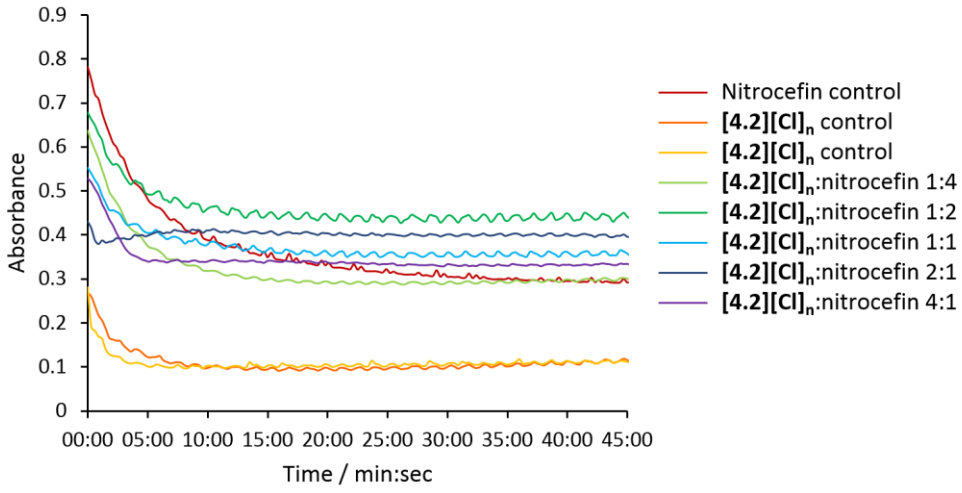

Figure A4.4. Steady-state kinetics for β-lactamase-catalysed nitrocefin hydrolysis in the presence of **[4.2][Cl]$_n$**. KPC-3 enzyme was added to (pre-incubated) mixtures of **[4.2][Cl]$_n$** and nitrocefin. Absorbance at 395 nm was measured thrice for each mixture over 45 min and averaged.

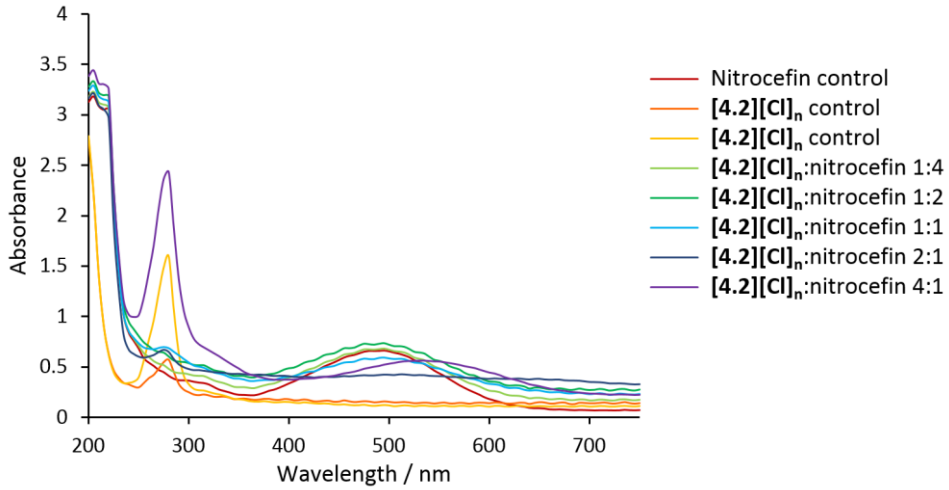

Figure A4.5. UV/Vis spectra of **[4.2][Cl]$_n$**/nitrocefin bioconjugates 45 min after addition of β-lactamase enzyme KPC-3.

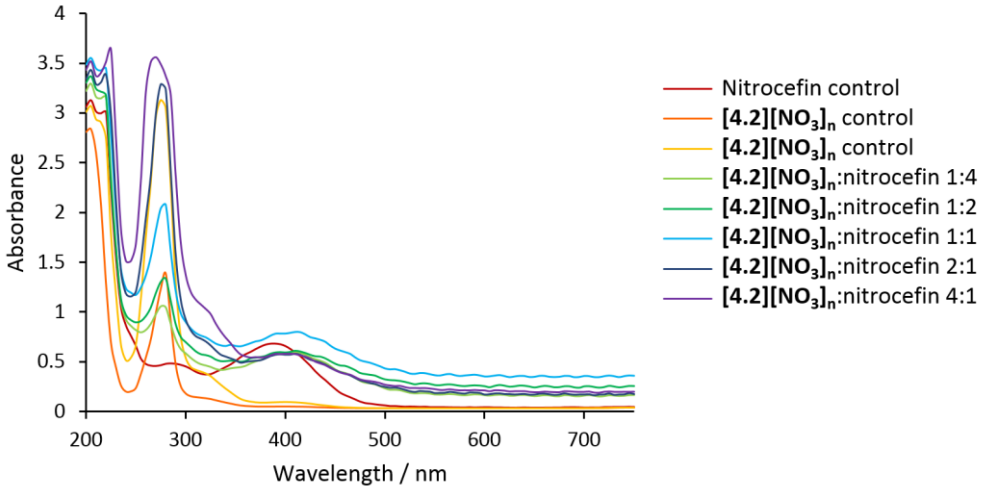

Figure A4.6. UV/Vis spectra of **[4.2][NO$_3$]$_n$**/nitrocefin bioconjugates prior to addition of β-lactamase enzyme KPC-3.

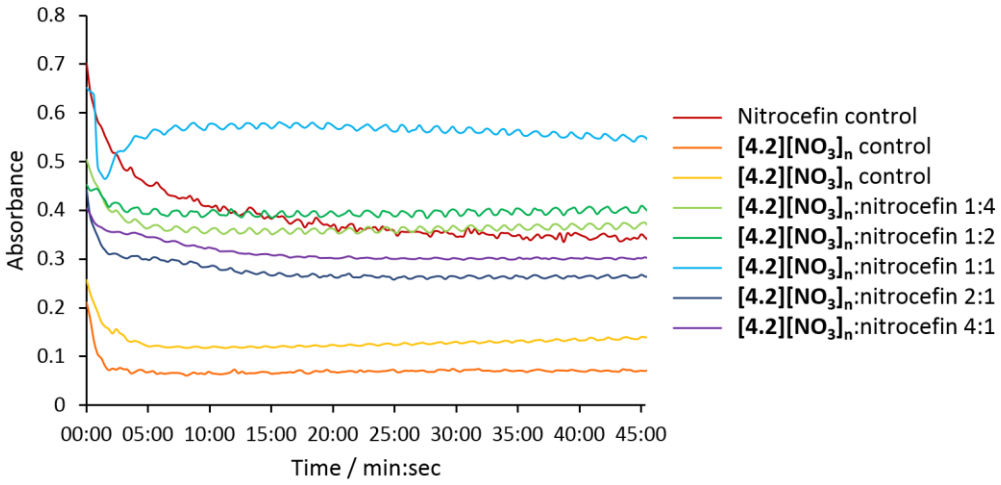

Figure A4.7. Steady-state kinetics for β-lactamase-catalysed nitrocefin hydrolysis in the presence of **[4.2][NO$_3$]$_n$**. KPC-3 enzyme was added to (pre-incubated) mixtures of **[4.2][NO$_3$]$_n$** and nitrocefin. Absorbance at 395 nm was measured thrice for each mixture over 45 min and averaged.

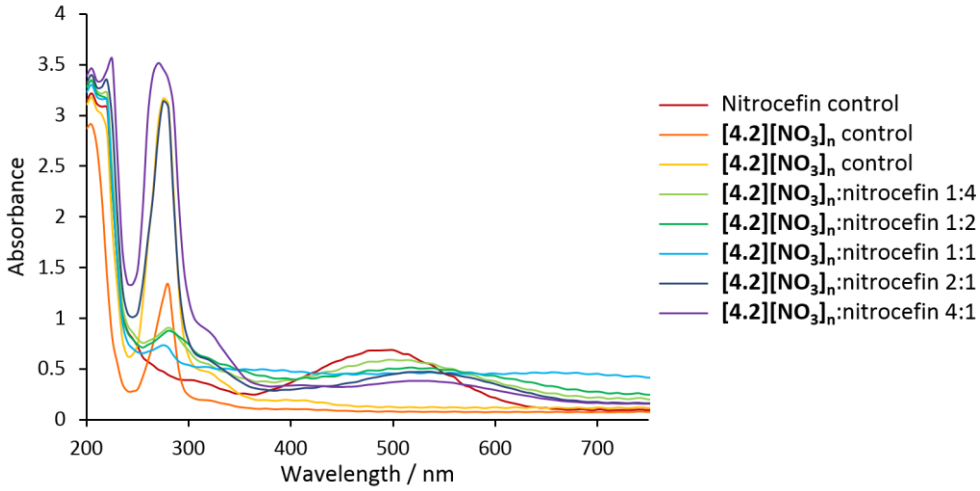

Figure A4.8. UV/Vis spectra of **[4.2][NO$_3$]$_n$**/nitrocefin bioconjugates 45 min after addition of β-lactamase enzyme KPC-3.

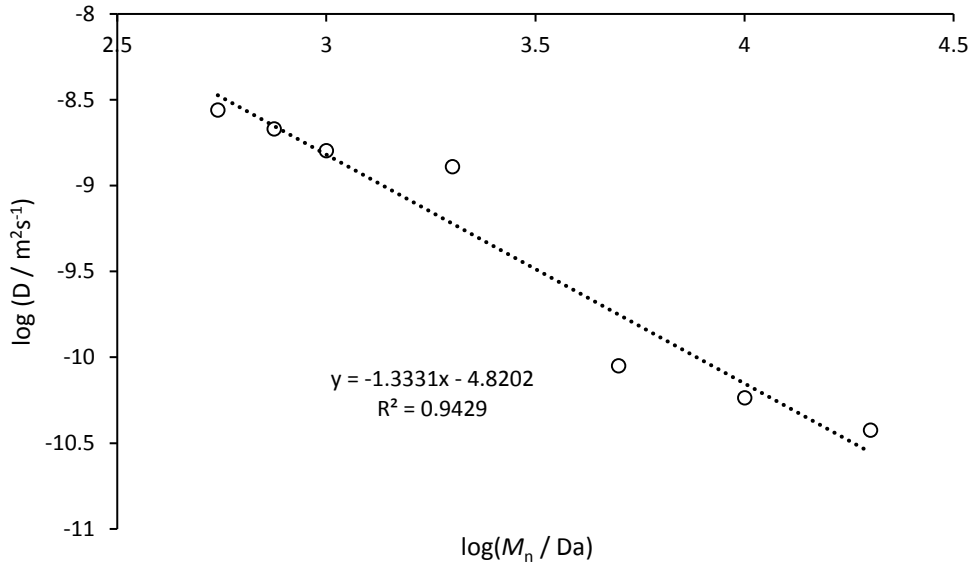

Figure A4.9. A log-log plot of diffusion vs M_n for a series of poly(ethylene glycol) samples in D_2O. It provides a linear relationship that can be used to calculate molecular weights from diffusion coefficients.

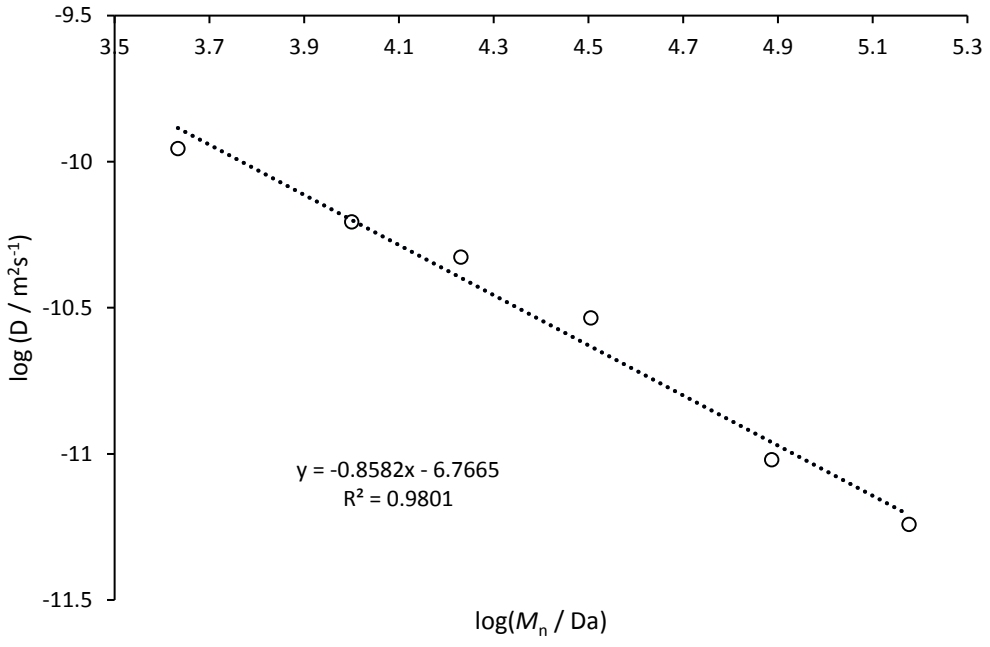

Figure A4.10. A log-log plot of diffusion vs M_n for a series of poly(sodium 4-styrenesulfonate) samples in D_2O. It provides a linear relationship that can be used to calculate molecular weights from diffusion coefficients.

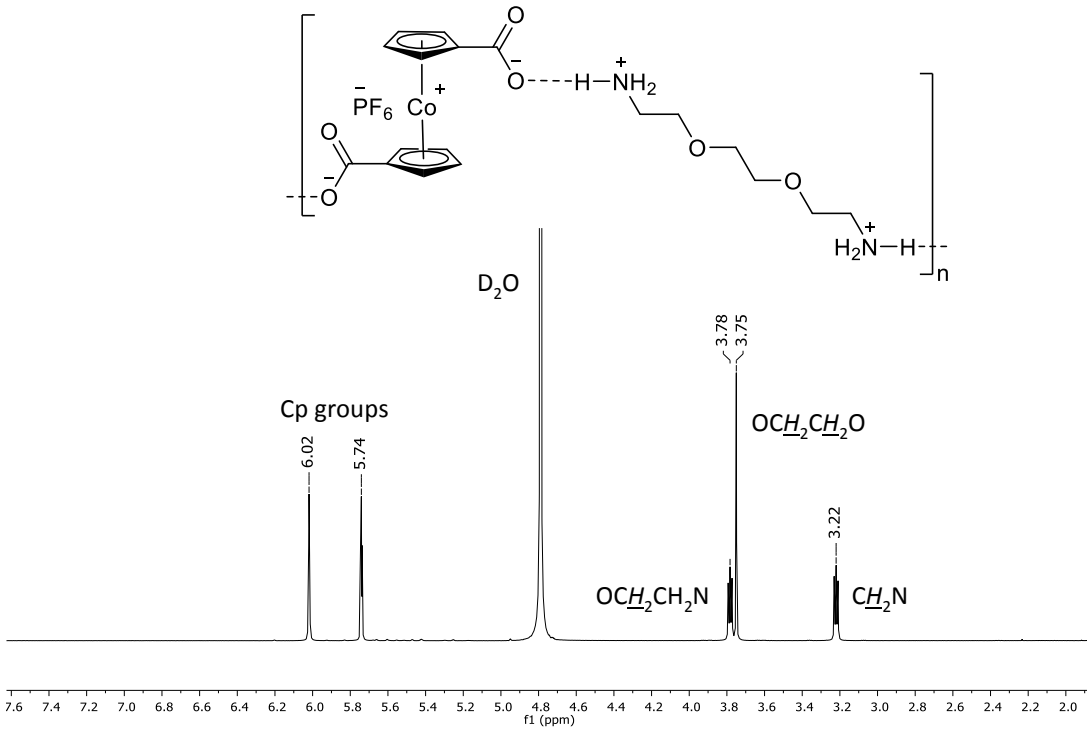

Figure A4.11. ^{1}H NMR spectrum (500 MHz, D_2O) of coordination polymer **4.5**.

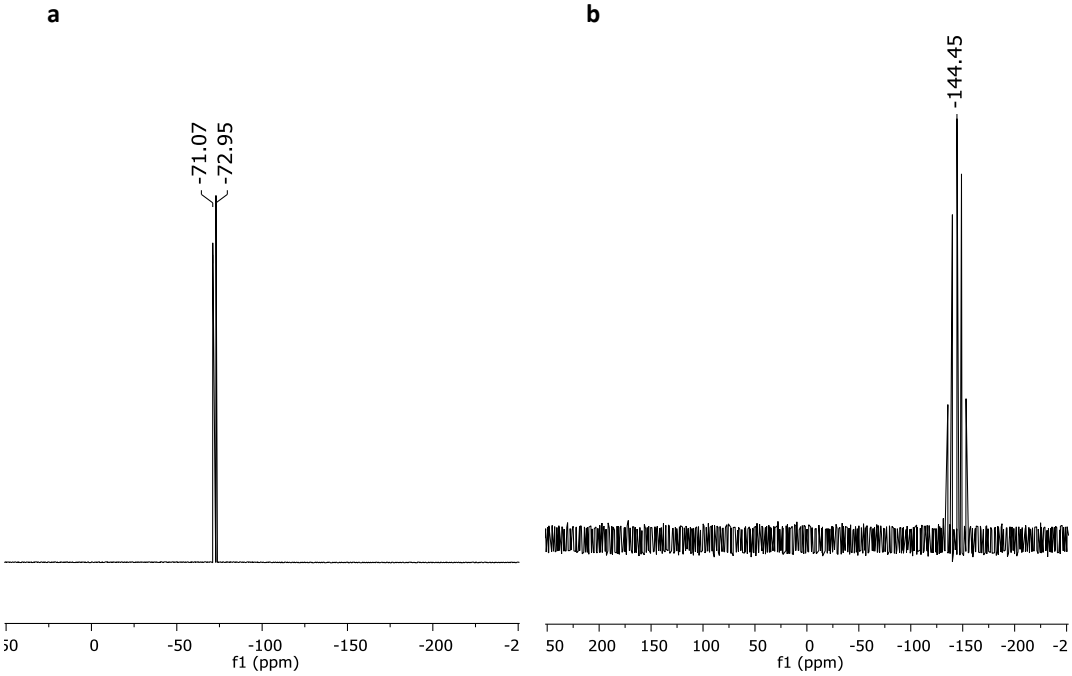

Figure A4.12. ^{19}F (a) and ^{31}P (b) NMR spectra (400 MHz, D_2O) of coordination polymer **4.5**.

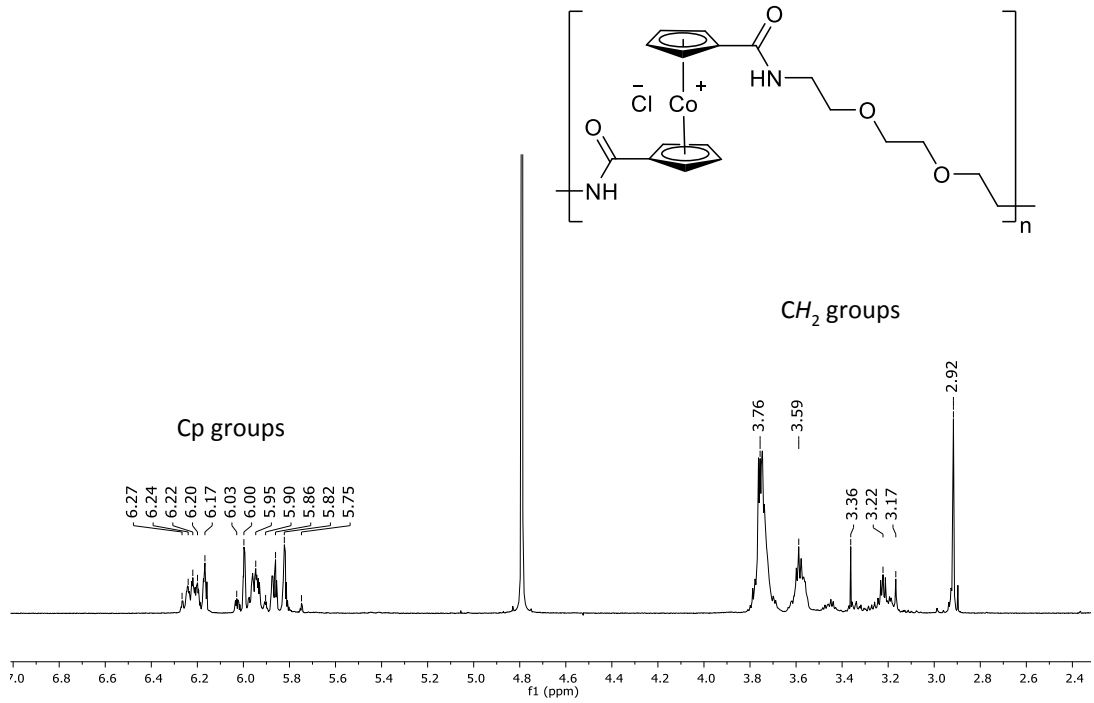

Figure A4.13. ^{1}H NMR spectrum (500 MHz, D_2O) of the oligomeric product **[4.4][Cl]$_n$** from reaction 4.3.3g.

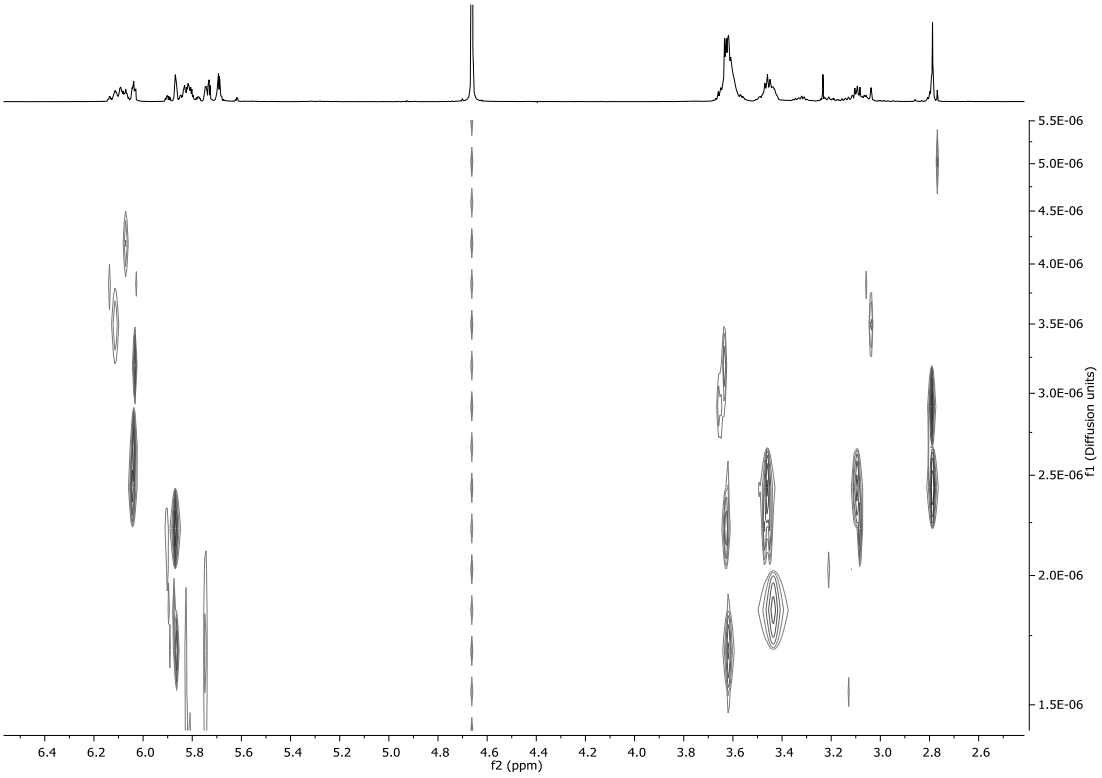

Figure A4.14. DOSY spectrum (500 MHz, D_2O) of the oligomeric product **[4.4][Cl]$_n$** from reaction 4.3.3g.

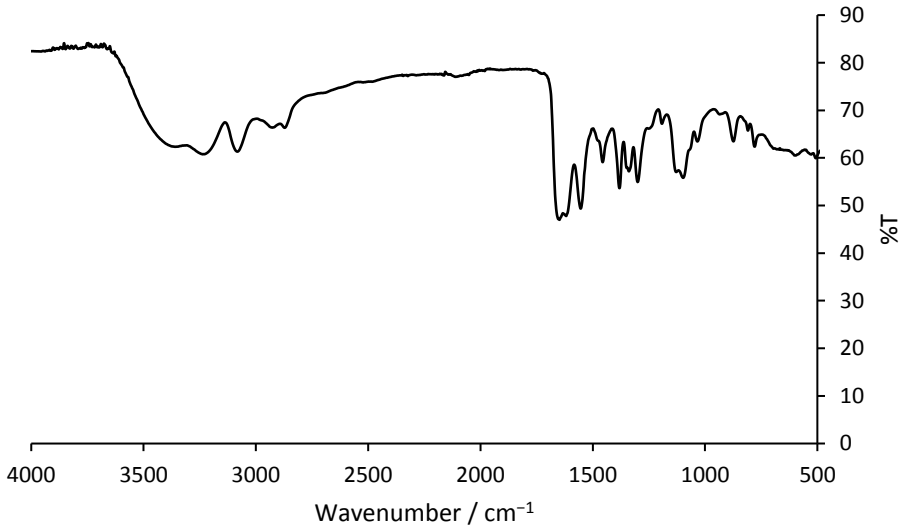

Figure A4.15. IR spectrum for the oligomeric product **[4.4][Cl]$_n$** from reaction 4.3.3g.

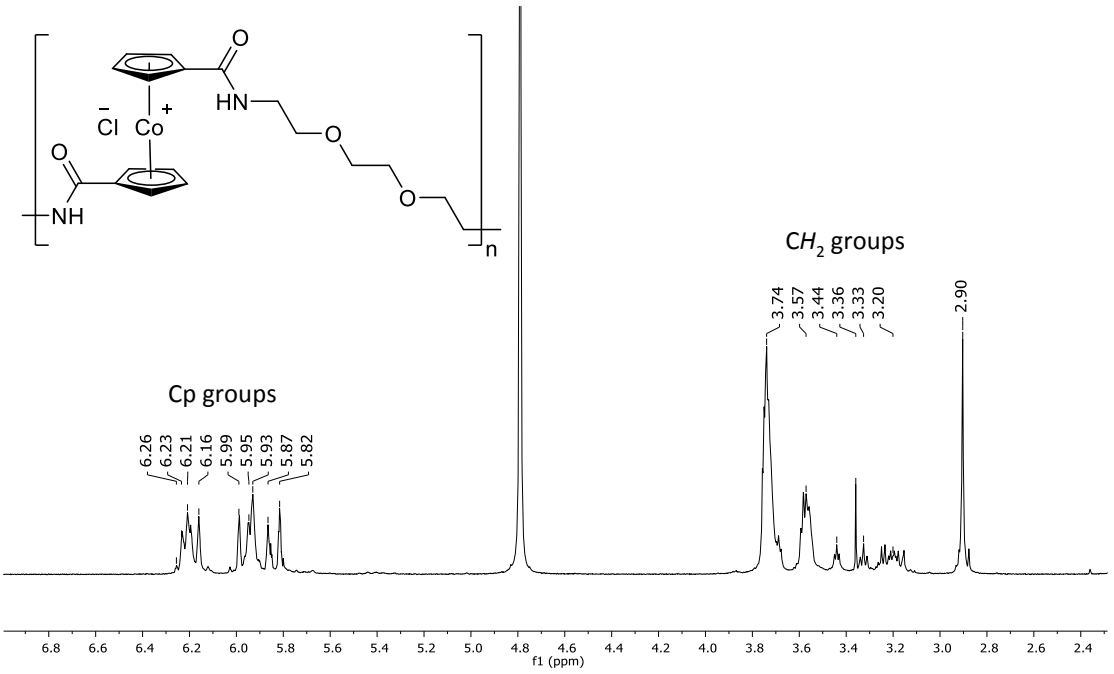

Figure A4.16. ^{1}H NMR spectrum (500 MHz, D_2O) of the oligomeric product **[4.4][Cl]$_n$** from reaction 4.3.3i.

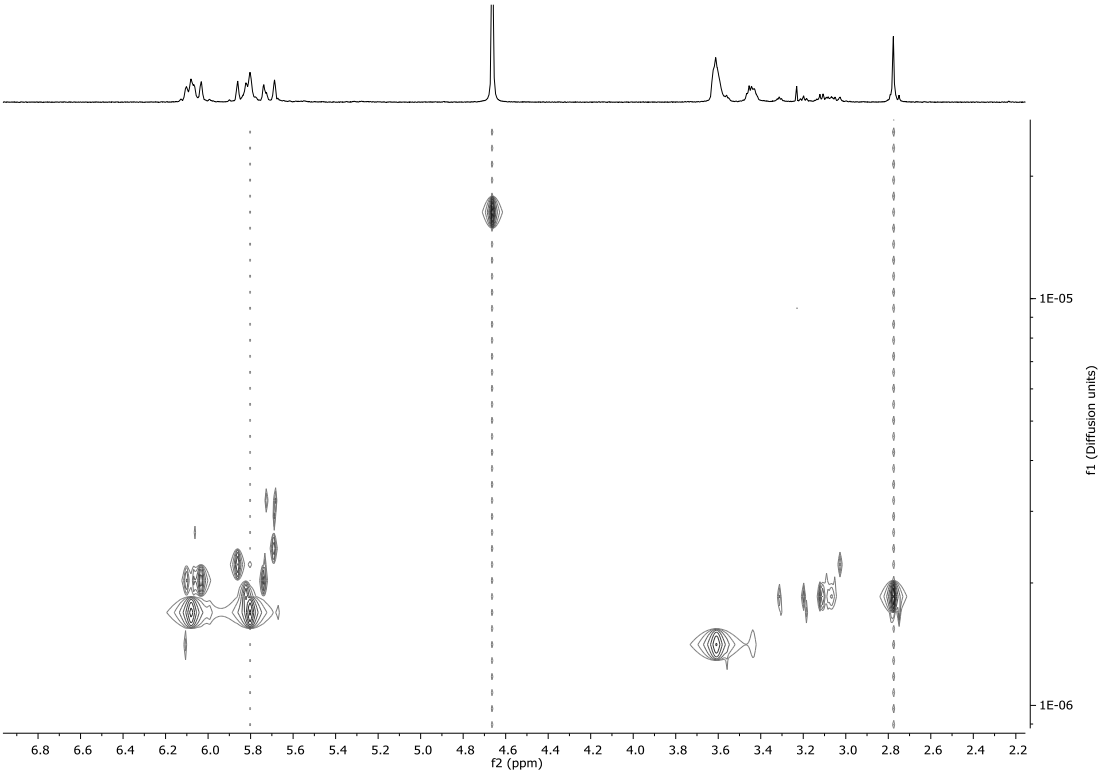

Figure A4.17. DOSY spectrum (500 MHz, D_2O) of the oligomeric product **[4.4][Cl]$_n$** from reaction 4.3.3i.

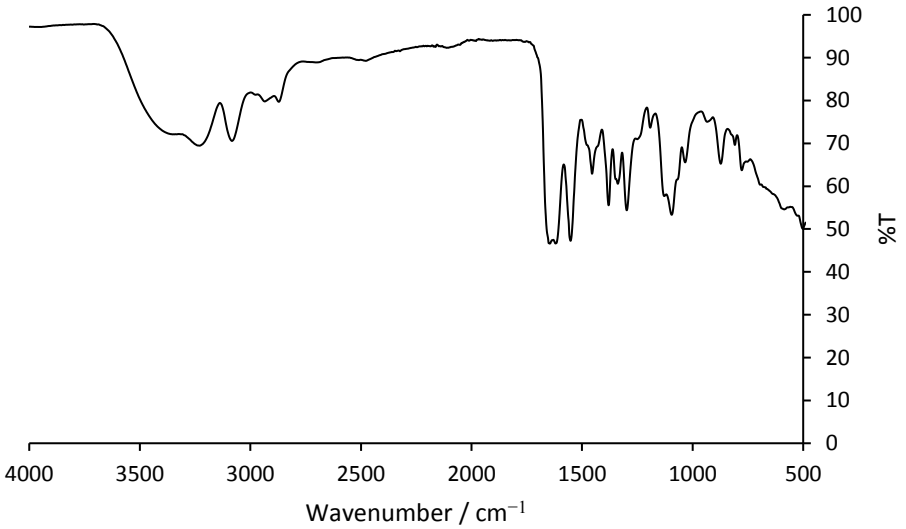

Figure A4.18. IR spectrum for the oligomeric product **[4.4][Cl]$_n$** from reaction 4.3.3i.

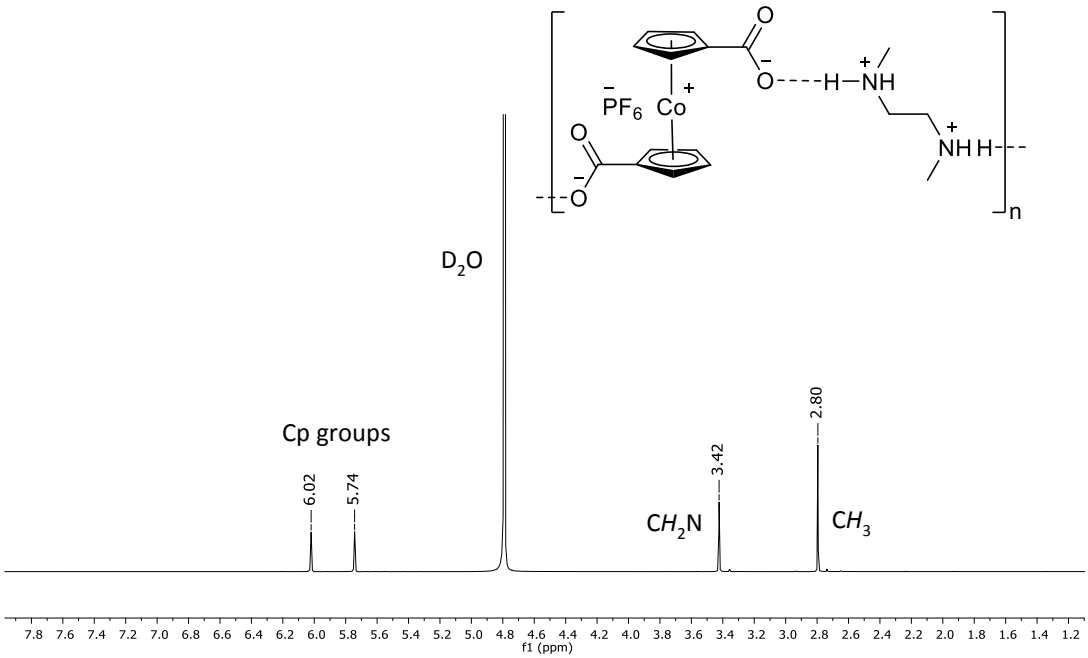

Figure A4.19. ^{1}H NMR spectrum (500 MHz, D_2O) of coordination polymer **4.6**.

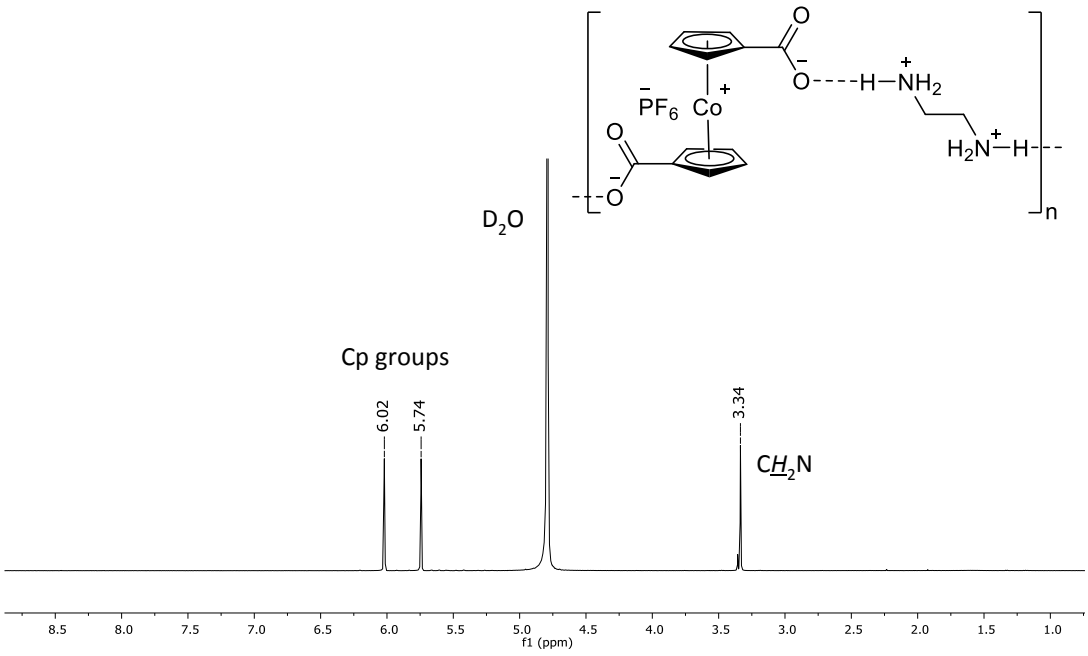

Figure A4.20. ^{1}H NMR spectrum (500 MHz, D_2O) of coordination polymer **4.7**.

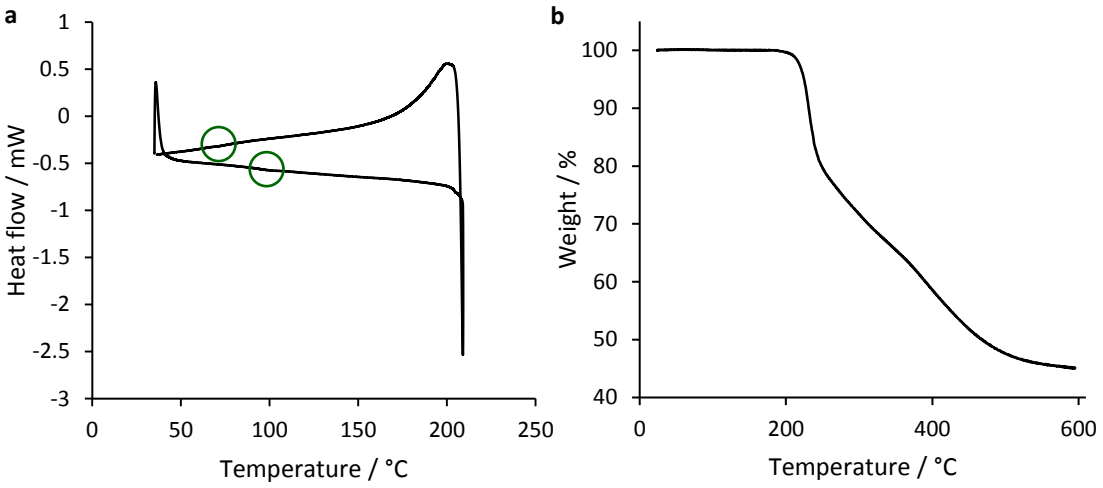

Figure A4.21. a) Differential scanning calorimetry performed on a sample of **4.5** between 35 –210 °C. b) TGA trace for **4.5** showing significant mass loss after ~210 °C.

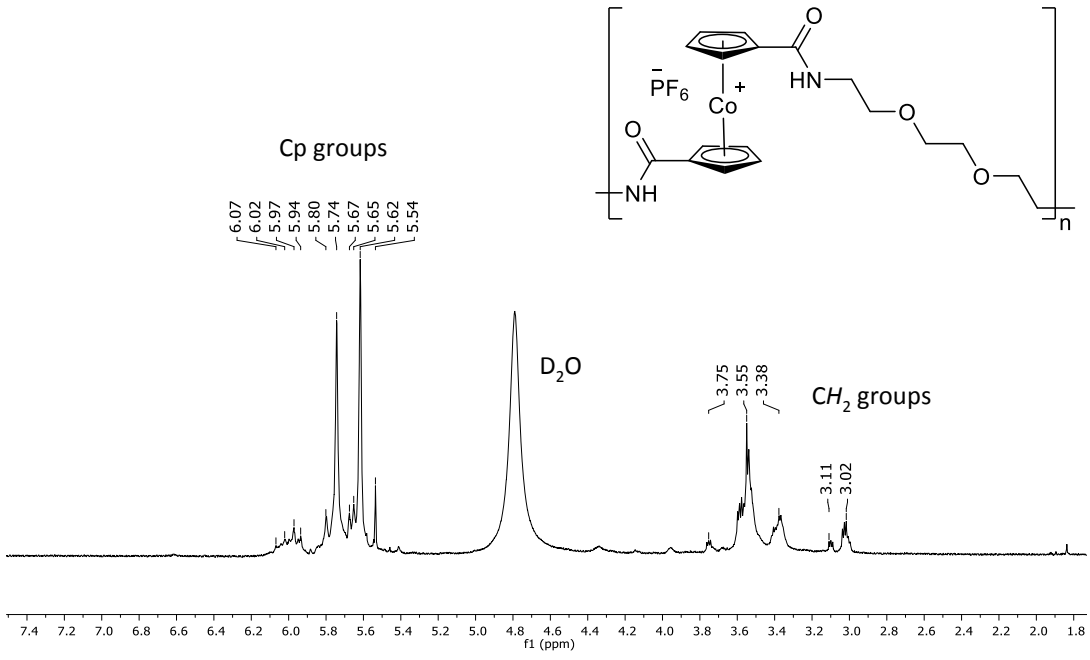

Figure A4.22. ^{1}H NMR spectrum (500 MHz, D_2O) of the oligomeric product **[4.4][PF$_6$]$_n$** from reaction 4.3.4c.

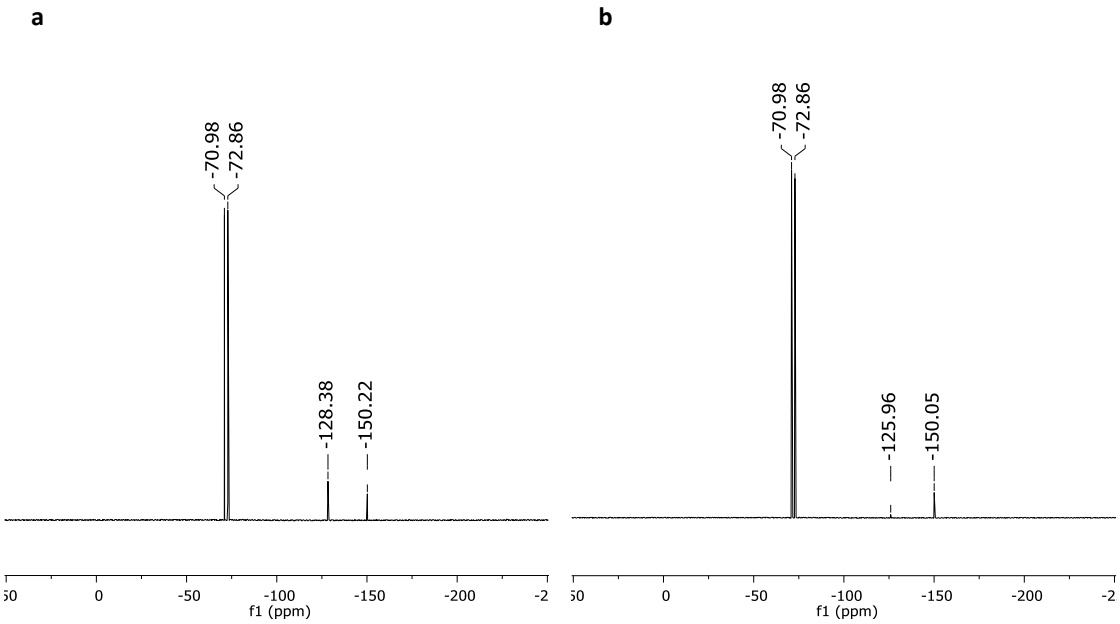

Figure A4.23. ^{19}F NMR spectra for oligomeric **[4.4][PF$_6$]$_n$** resulting from: a) reaction 4.3.4b, b) reaction 4.3.4c.

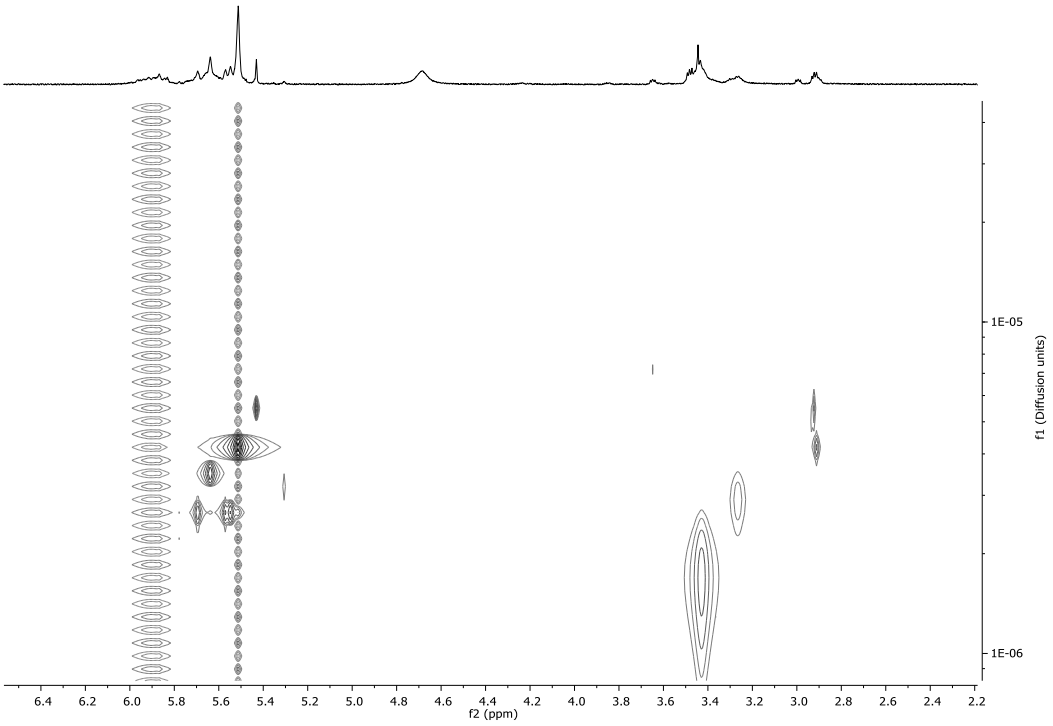

Figure A4.24. DOSY spectrum (500 MHz, D_2O) of the oligomeric product **[4.4][PF$_6$]$_n$** from reaction 4.3.4c.

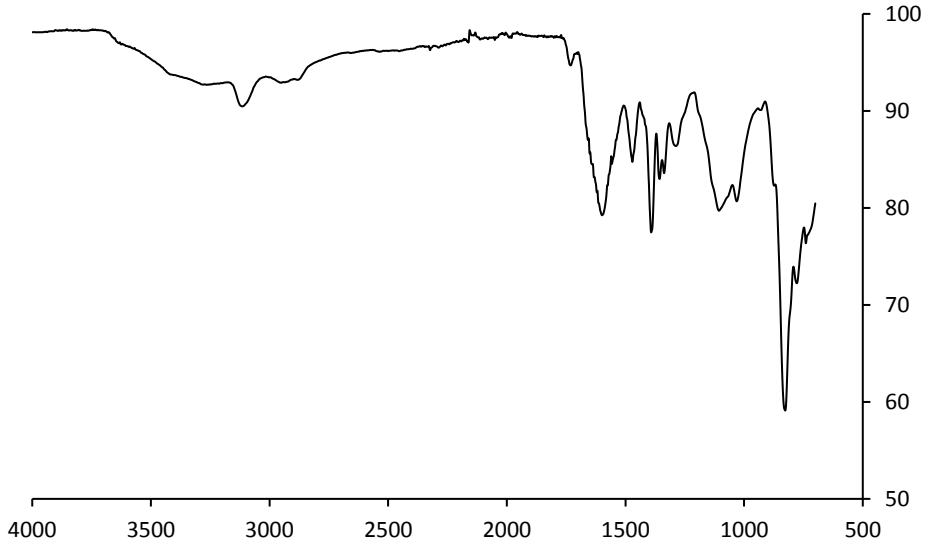

Figure A4.25. IR spectrum for the oligomeric product **[4.4][PF_6]$_n$** from reaction 4.3.4c.

iv. Crystallographic Data

Compound	**4.5**	**4.6**	**4.7**
Empirical formula	$C_{18}H_{26}CoF_6N_2O_6P$	$C_{16}H_{22}CoF_6N_2O_4P$	$C_{14}H_{18}CoF_6N_2O_4P$
Formula weight	570.31	510.25	482.2
Temperature/K	100	99.97	99.99
Crystal system	triclinic	orthorhombic	triclinic
Space group	*P*-1	*Fddd*	*P*-1
a/Å	7.1911(10)	14.0236(15)	7.5351(7)
b/Å	12.3695(16)	18.5854(18)	7.9526(7)
c/Å	12.7371(17)	31.221(3)	15.1395(13)
α/°	93.951(4)	90	78.332(2)
β/°	102.916(4)	90	76.171(3)
γ/°	91.584(4)	90	79.713(3)
Volume/Å^3	1100.6(3)	8137.3(14)	854.58(13)
Z	2	16	2
ρ_{calc}g/cm^3	1.7208	1.666	1.874
μ/mm^{-1}	0.943	1.002	1.187
F(000)	585.3	4160	488.0
Crystal size/mm^3	0.393×0.336×0.23	0.629×0.411×0.195	0.329×0.187×0.138
Radiation	MoKα (λ = 0.71073)	MoKα (λ = 0.71073)	MoKα (λ = 0.71073)
2Θ range for data collection/°	3.3 to 53.52	3.866 to 50.684	5.28 to 55.162
Index ranges	$-9 \le h \le 9$, $-15 \le k \le 15$, $-16 \le l \le 15$	$-14 \le h \le 16$, $-22 \le k \le 22$, $-37 \le l \le 37$	$-9 \le h \le 8$, $-10 \le k \le 10$, $-19 \le l \le 19$
Reflections collected	14584	23184	12232
Independent reflections	4633 [R_{int} = 0.0758, R_{sigma} = 0.1017]	1868 [R_{int} = 0.0910, R_{sigma} = 0.0403]	3956 [R_{int} = 0.0550, R_{sigma} = 0.0728]
Data/restraints/ parameters	4633/0/309	1868/22/156	3956/0/255
Goodness-of-fit on F2	1.019	1.069	1.021
Final R indexes [I>=2σ (I)]	R_1 = 0.0521, wR_2 = 0.1040	R_1 = 0.0373, wR_2 = 0.0757	R_1 = 0.0494, wR_2 = 0.1115
Final R indexes [all data]	R_1 = 0.1017, wR_2 = 0.1231	R_1 = 0.0704, wR_2 = 0.0871	R_1 = 0.0781, wR_2 = 0.1231
Largest diff. peak/hole/e Å^{-3}	1.01/−1.01	0.30/−0.34	1.05/−0.67
Flack parameter	N/A	N/A	N/A

Appendix V

i. Additional Synthetic Figures

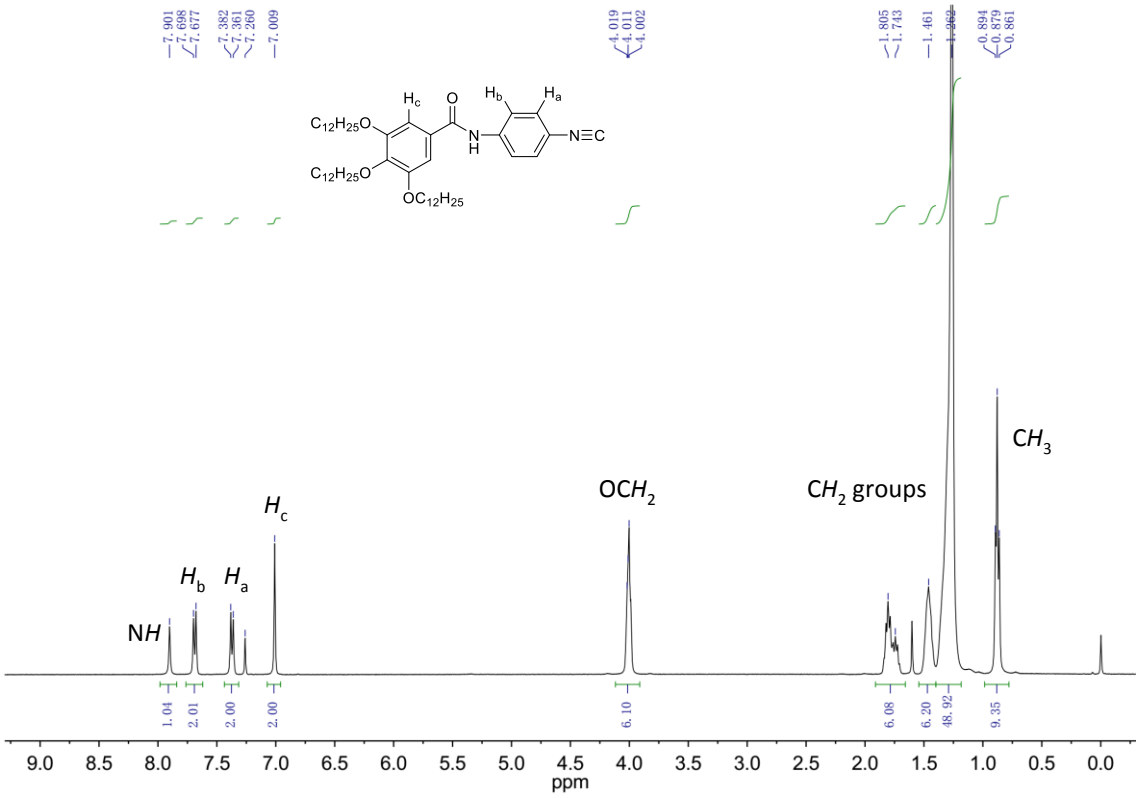

Figure A5.1. ^{1}H NMR spectrum (400 MHz, $CDCl_3$) of isocyanide ligand **5.1**.

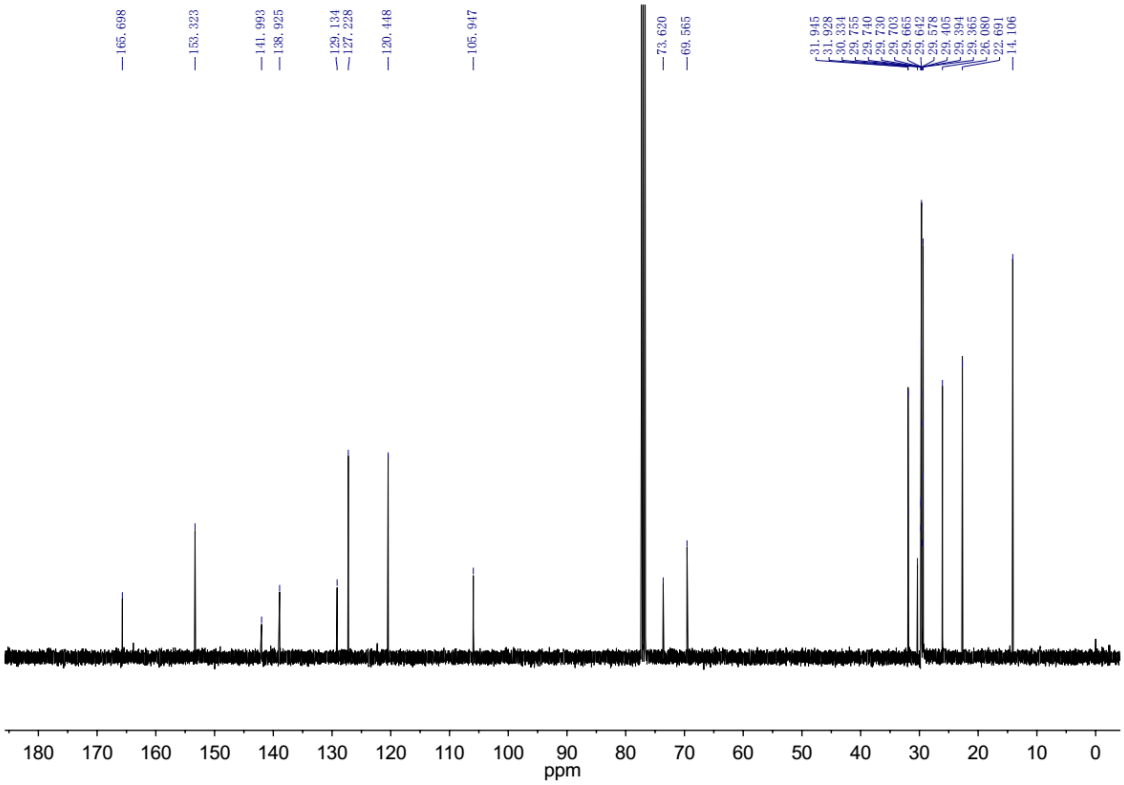

Figure A5.2. ^{13}C NMR spectrum (400 MHz, $CDCl_3$) of isocyanide ligand **5.1**.

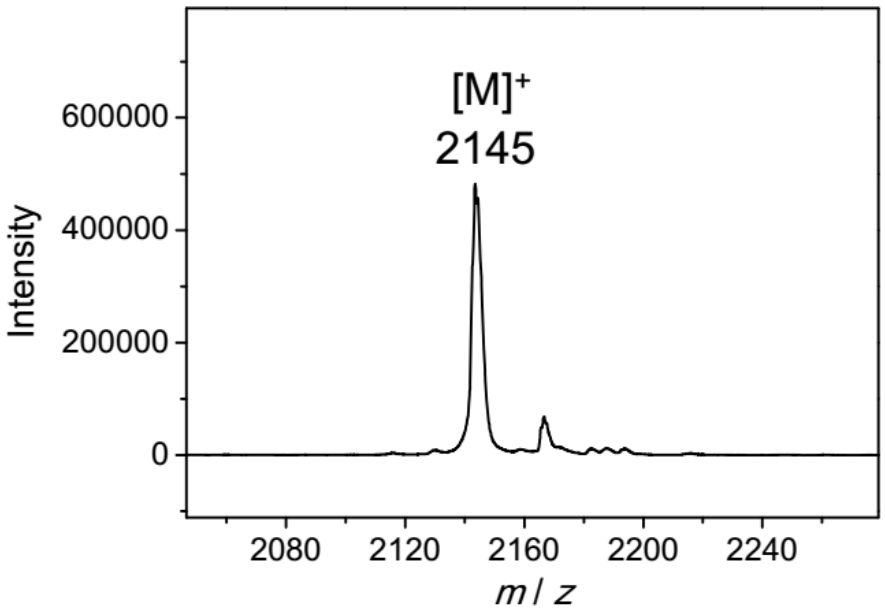

Figure A5.3. MALDI-TOF mass spectra of **5.2**.

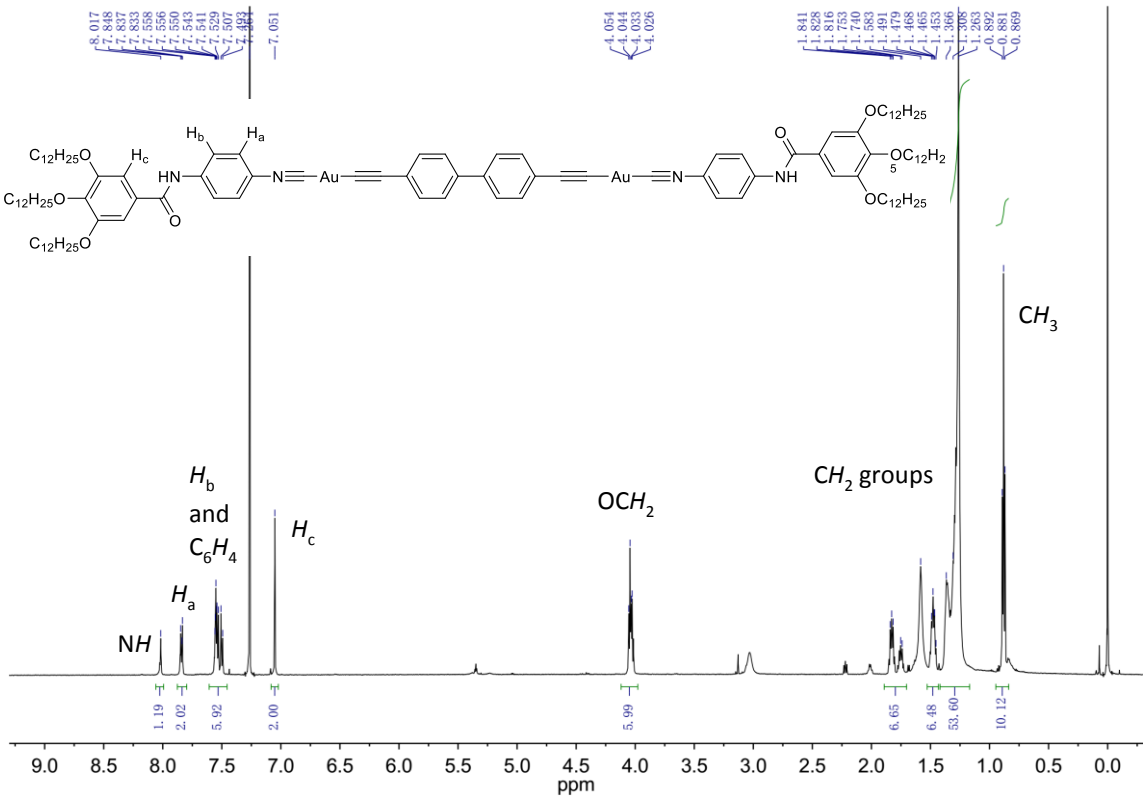

Figure A5.4. ^{1}H NMR spectrum (600 MHz, $CDCl_3$) of **5.2**.

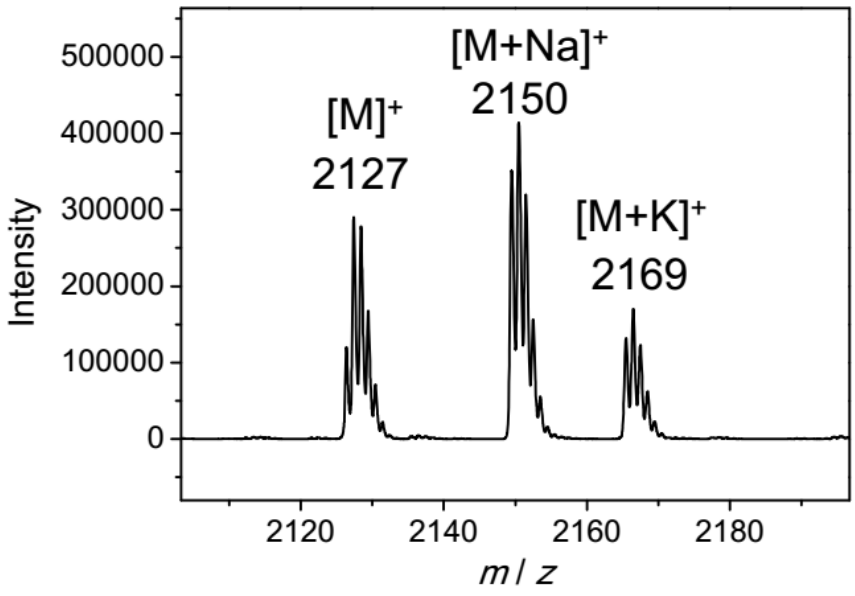

Figure A5.5. MALDI-TOF mass spectra of **5.3**.

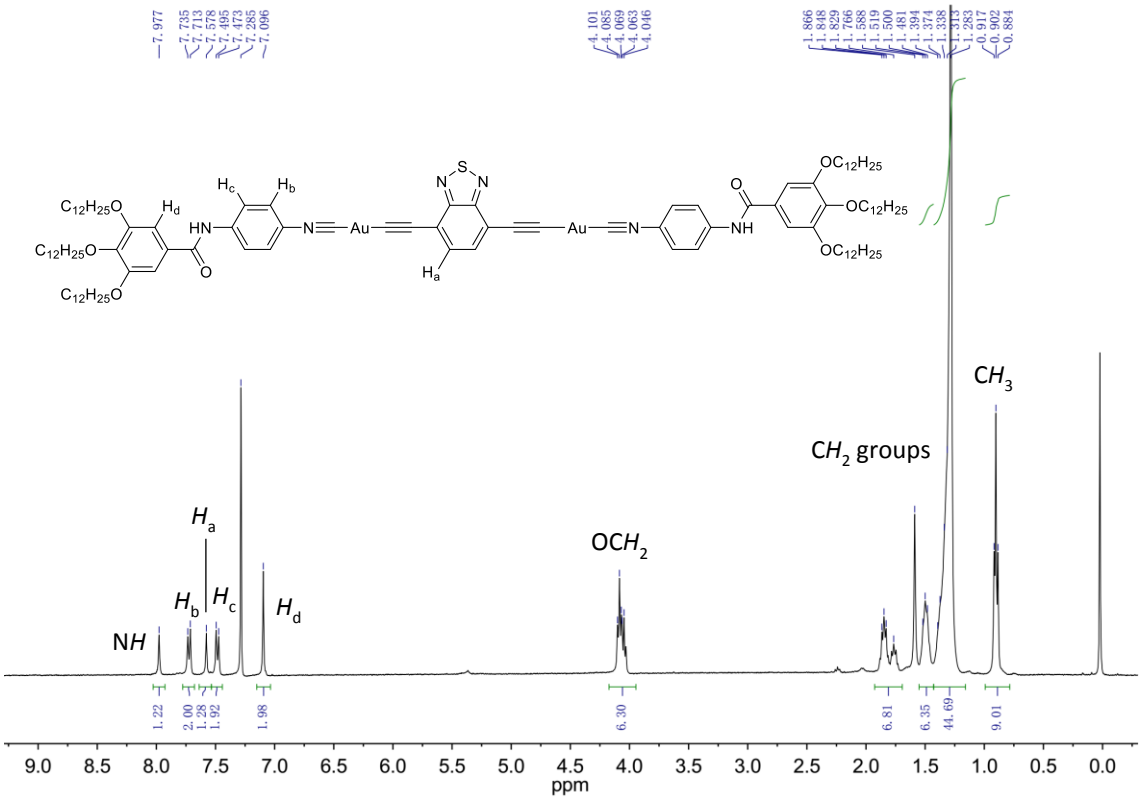

Figure A5.6. ^{1}H NMR spectrum (600 MHz, $CDCl_3$) of **5.3**.

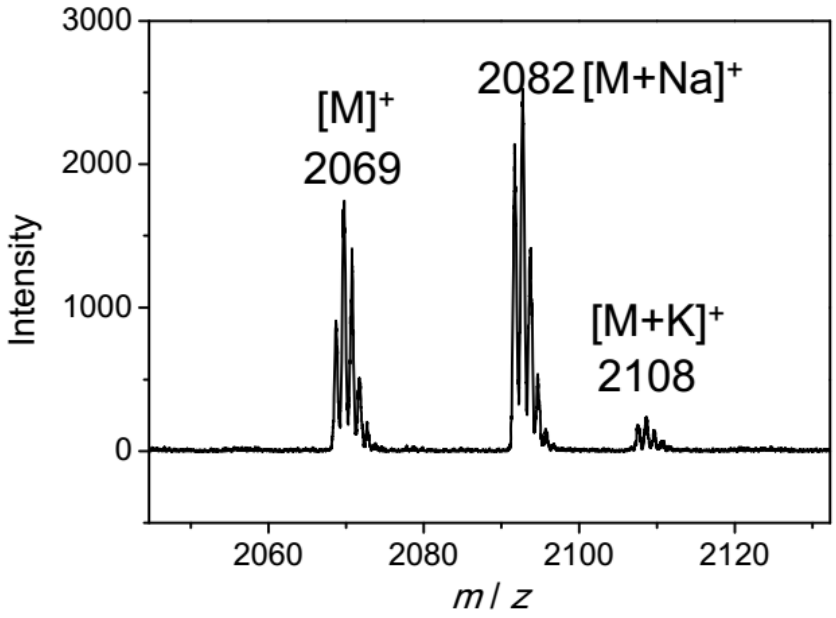

Figure A5.7. MALDI-TOF mass spectra of **5.4**.

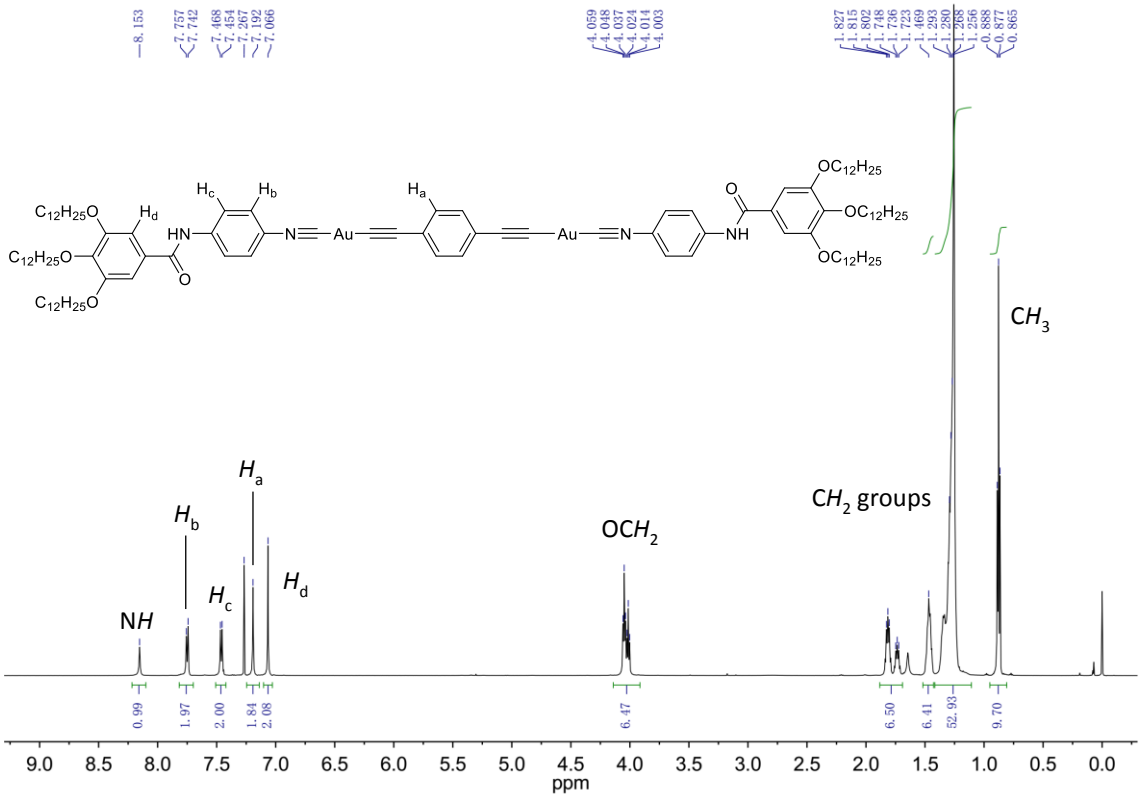

Figure A5.8. ^{1}H NMR spectrum (600 MHz, $CDCl_3$) of **5.4**.

ii. Additional Self-Assembly Information

To generate an estimate of the diameter of the core section of **5.3**, the distance between the N1 of one amide to N4 of the other was calculated from known bond distances as 3.51 nm. If the outer phenyl moieties were accounted for in a planar model, the maximum distance from C to C (Figure A5.9) was calculated to be 4.48 nm. An analogous process was followed for **5.4**: N↔N 3.05 nm**,** C↔C 4.02 nm.

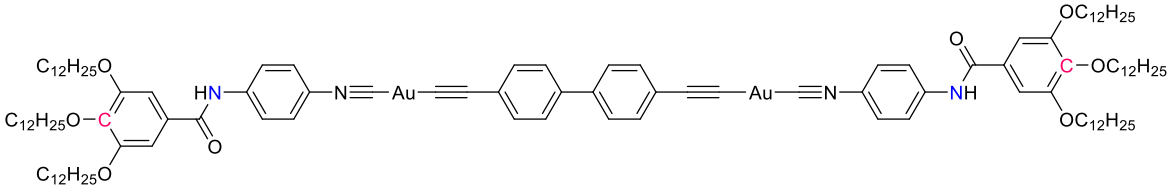

Figure A5.9. Compound **5.3** with coloured pairs of atoms between which the distance of the core section was estimated.

iii. Additional Self-Assembly Figures

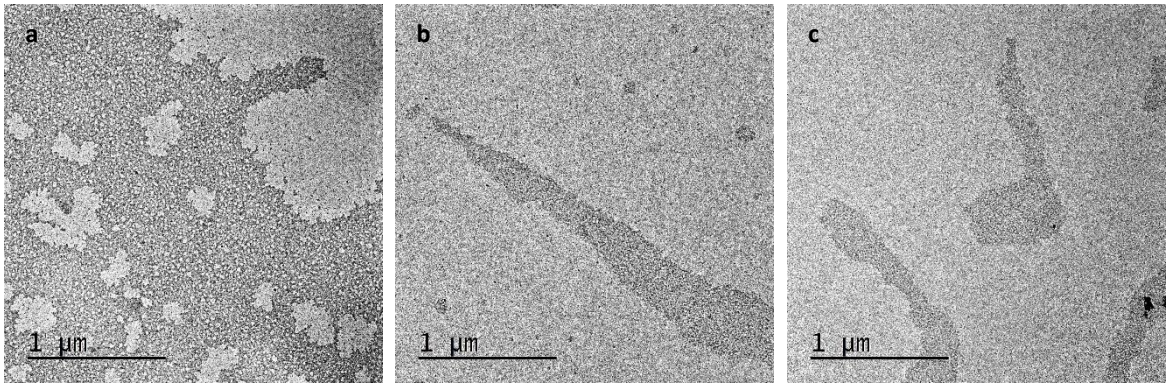

Figure A5.10. TEM images of solutions of **5.2** in methylcyclohexane (MCH) (0.5 mg mL^{-1}, 24 h) containing v/v: a) 0% $CHCl_3$, b) 10% $CHCl_3$, c) 20% $CHCl_3$.

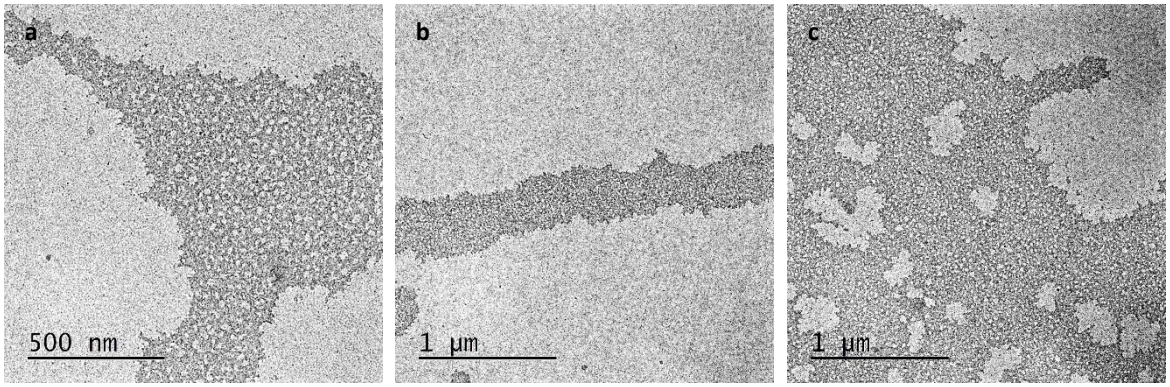

Figure A5.11. TEM images of solutions of **5.2** (0.5 mg mL^{-1}, 24 h) in: a) *n*-hexanes, b) cyclohexane, c) heptane.

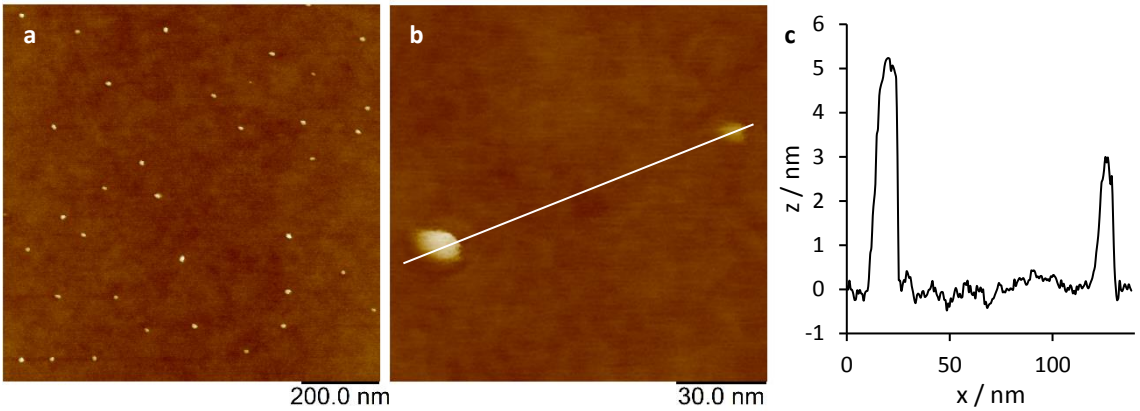

Figure A5.12. a) and b) AFM height images of spheres formed by **5.2** in MCH. c) Height profile of two spheres (white line trace in (b)).

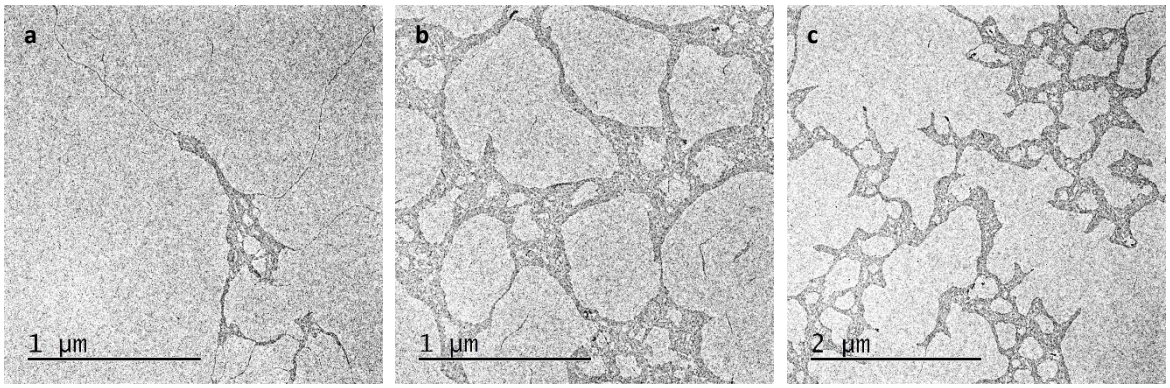

Figure A5.13. TEM images of **5.3** (0.5 mg mL^{-1}, 24 h) in: a) *n*-hexanes, b) cyclohexane, c) MCH.

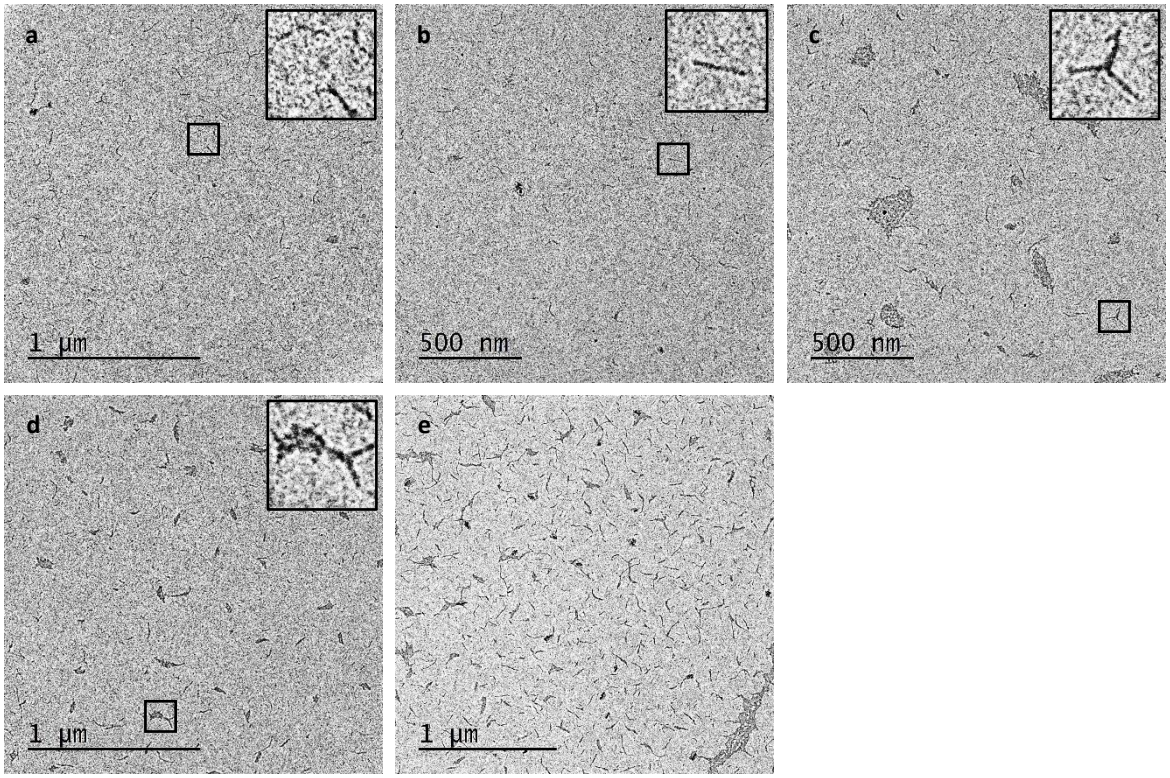

Figure A5.14. TEM images of a) seed micelles of **5.3**. TEM images of fibre-like micelles (b–e) after addition of: b) 0.25, c) 0.5, d) 1, e) 2 eq. of **5.3** unimer to seed micelles.

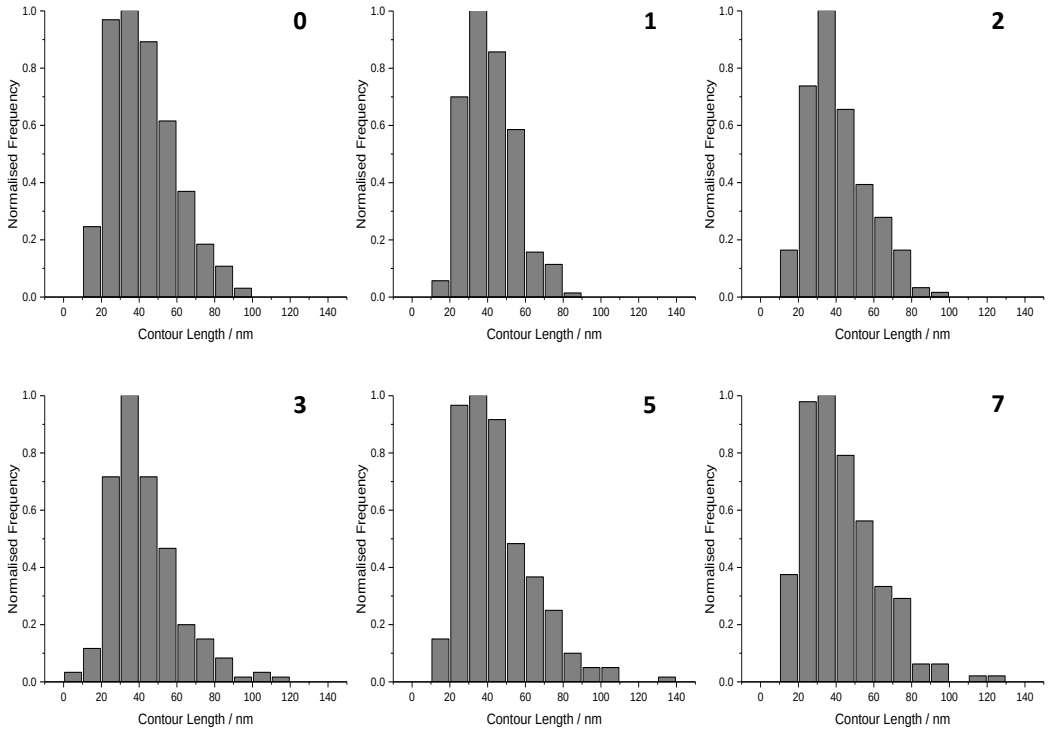

Figure A5.15. Histogram plots of the contour length of **5.3** seed micelles, where the number in bold indicates the number of days after sonication.

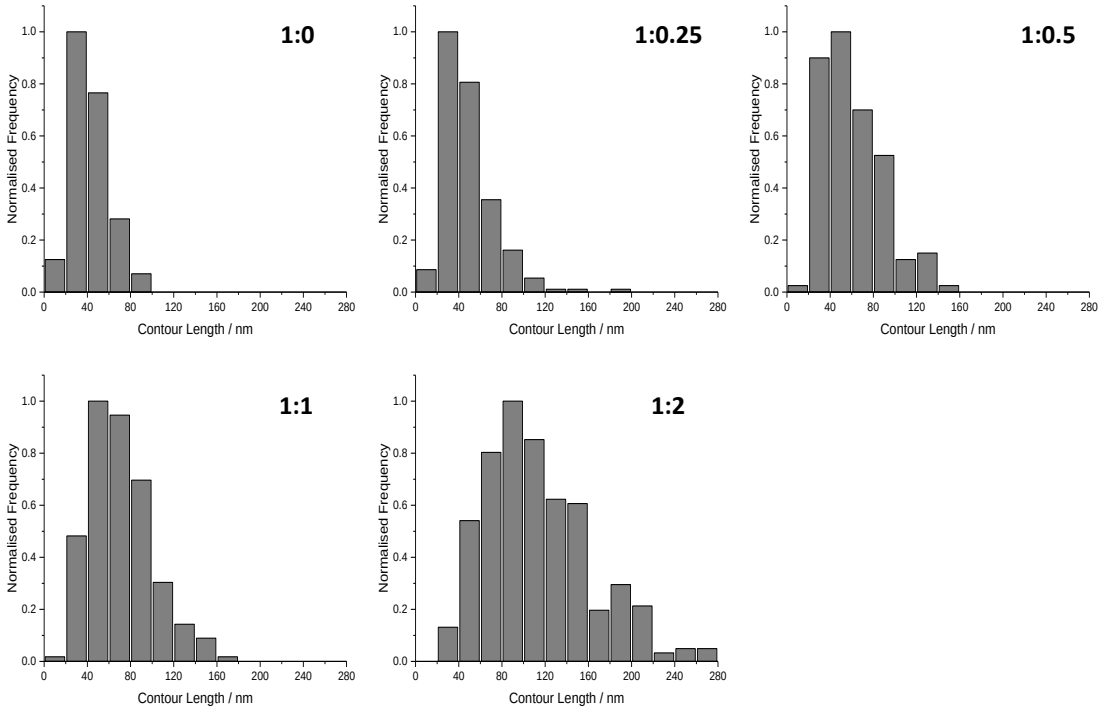

Figure A5.16. Histogram plots of micelle contour length after addition of **5.3** unimer to seed micelles, where the number in bold indicates the ratio of seed micelles to unimer.

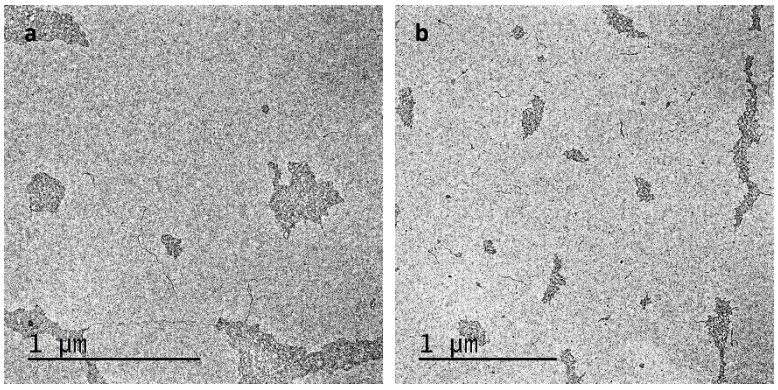

Figure A5.17. TEM images of **5.4** (0.5 mg mL^{-1}, 24 h) in: a) *n*-hexanes, b) heptane.

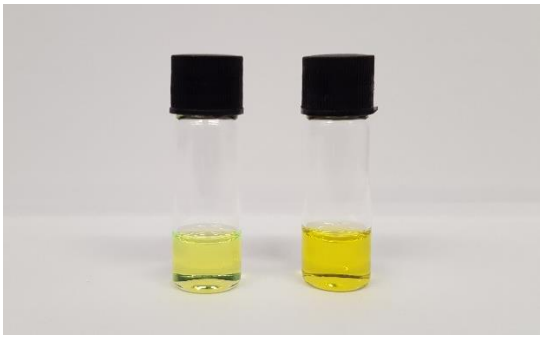

Figure A5.18. Compound **5.4** in the unimeric (chloroform, left) and aggregated (MCH, right) states.

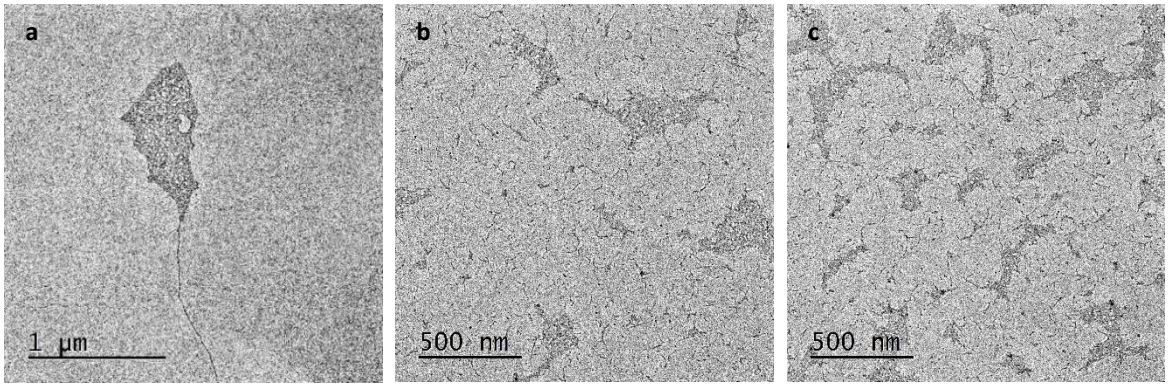

Figure A5.19. TEM image (a) of a solution of **5.4** (MCH, 0.5 mg mL^{-1}) aged for 3 months before dropcasting. TEM images of solutions of **5.4** (MCH, 0.5 mg mL^{-1}, 24 h) following ultrasonication for: b) 2 h, c) 4 h.

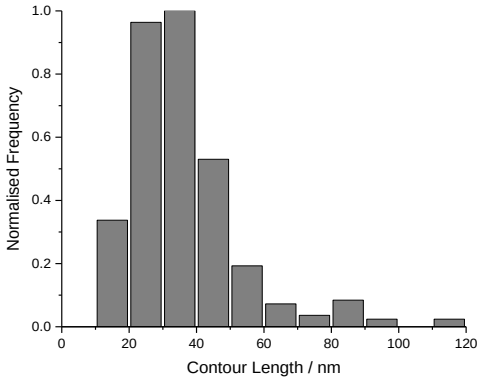

Figure A5.20. Histogram plot of the contour length of **5.4** seed micelles immediately after sonication.

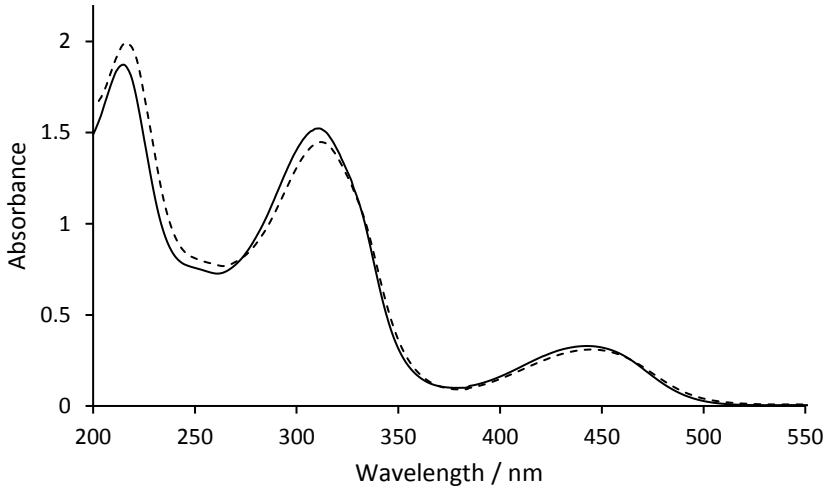

Figure A5.21. Overlaid UV/Vis spectra of **5.4** in MCH (0.5 mg mL^{-1}) after: 1 h (solid line, seed fibres), and 4 h (dashed line, spheres).

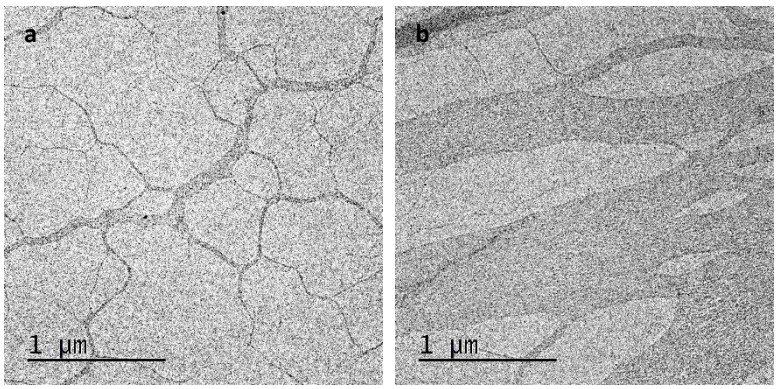

Figure A5.22. TEM images of solutions of **5.4** in MCH (0.5 mg mL^{-1}, 24 h) containing v/v: a) 10% $CHCl_3$, b) 20% $CHCl_3$.